3-22-2019

Piezoelectric Sensor Crack Detection on Airframe Systems

Kevin J. Lin

Piezoelectric Sensor Crack Detection on Airframe Systems

THESIS

Kevin J. Lin, 2nd Lt, USAF

AFIT-ENC-MS-19-M-001

DEPARTMENT OF THE AIR FORCE
AIR UNIVERSITY

AIR FORCE INSTITUTE OF TECHNOLOGY

Wright-Patterson Air Force Base, Ohio

AFIT-ENC-MS-19-M-001

Piezoelectric Sensor Crack Detection on Airframe Systems

THESIS

Presented to the Faculty

Department of Mathematics and Statistics

Graduate School of Engineering and Management

Air Force Institute of Technology

Air University

Air Education and Training Command

in Partial Fulfillment of the Requirements for the

Degree of Master of Science in Applied Mathematics

Kevin J. Lin, B.A.,M.S.

2nd Lt, USAF

March 21, 2019

AFIT-ENC-MS-19-M-001

Piezoelectric Sensor Crack Detection on Airframe Systems

THESIS

Kevin J. Lin, B.A.,M.S.
2nd Lt, USAF

Committee Membership:

Richard P. Uber, PhD
Chair

Christine Schubert M. Kabban, PhD
Member

Mark E. Oxley, PhD
Member

AFIT-ENC-MS-19-M-001

Abstract

In 2008, the Department of Defense published a guidebook for a methodology named Condition-Based Maintenance Plus (CBM+) which capabilities include improving productivity, shortening maintenance cycles, lowering costs, and increasing availability and reliability. This push replaces existing inspection criteria, often conducted as non-destructive testing (NDT), with structural health monitoring (SHM) systems. The SHM system addressed utilizes guided Lamb waves generated by piezoelectric wafer active sensors (PWAS) to detect the existence, size, and location of damage from through-thickness cracks around a rivet hole. The SHM field lacks an experiment testing how small changes in receiver sensor distances affect damage detection. In addition, prior research has shown that transmitter and receiver PWAS angles significantly affected the received signal. Experiments here used existing damage detection metrics to establish thresholds for detection. Tests with two transmitter angles $\theta = 9°, 27°$ and three receiver distances, linearly incremented by 5mm, illustrated that damage detection capabilities significantly changed as the receiver distances were incremented at both 50mm and 1000mm transmitter distances. For 1000mm, the PWAS was able to detect the damage at certain geometries. This work validates of the PWAS detection capabilities for small changes and motivates further pursuits for varying PWAS geometries for long distances.

Acknowledgements

Lt Lin would like to extend absolute gratitude to his dear advisor, Captain Richard Uber, for his unwavering support and trust in Lt Lin's work. Captain Uber and Dr. Christine Schubert Kabban's efforts allowed Lt Lin to be able to present at two major conferences and co-author his first academic paper on works that supports his thesis. Lt Lin would also like to personally thank Dr. Alan Lair, AFIT's Mathematics and Statistics chair, for his willingness to devote departmental resources in support of Lt Lin's academic work. Additionally, Md Yeasin Bhuiyan acted as Lt Lin's liaison between the mathematical and engineering worlds, answering questions and greatly assisting introducing this mathematician into the world of mechanical engineering. Lt Connor Crandall for validation of the programs used and generating data sets for analysis. Finally, Lt Lin would like to thank his family and close friends for their unconditional love and support.

Kevin J. Lin

Table of Contents

Page

Page

List of Figures

List of Tables

List of Symbols

Piezoelectric Sensor Crack Detection on Airframe Systems

I. Introduction

1.1 Motivation

The United States Air Force is tasked with maintaining mission readiness on an aging fleet of airframes, many of which are beyond their design life and will remain in service for an extended period. Current practices of maintenance for these crafts are routine or schedule-based maintenance which means that even if the airframe does not require the costly maintenance, it will undergo maintenance procedures once the end of a specific time cycle is reached. The inspection and maintenance costs accounts for more than 27% [13] of the total life-cycle cost of an aircraft. Furthermore, current nondestructive evaluation (NDE) methods are reactive, focusing on fixing an aircraft once a problem has occurred. Many of these fixes require costly scaffolding of the airframe, grounding it while workers try to find sources of the damage. This places leadership at a difficult decision crossroad: Should the USAF regularly ground a fleet of aircraft that might be at risk for damage and sacrifice capability and productivity? Or should the USAF try to fly the plane as long as possible and only check it when the need arises, risking catastrophic failure and loss?

The field of Structural Health Monitoring (SHM) offers a new possibility where airframes undergo maintenance as needed, or condition-based maintenance, and provides airmen key information to predict damage before it becomes problematic. In SHM, the airframe is constantly monitored in real-time and grounded only when the structural health of the system is severely compromised. A current approach in

the field of SHM is the use of piezoelectric wafer active sensor (PWAS) which has advantages over detection systems including being smaller, lighter, inexpensive, and flexible in geometry [19]. Additionally, it can be bonded onto a surface, mounted inside structures, or embedded in materials as needed. This technology is already being slowly integrated into the aerospace industry and research. The Laboratory for Active Materials and Smart Structures (LAMSS) at the University of South Carolina and the Department of Mechanical and Aerospace Engineering at the University of Florida are just some of the current locations where the PWAS has been implemented fully in SHM pursuits. Work done by Ting Dong and Nam Kim at the Department of Mechanical and Aerospace Engineering in the University of Florida using cost-benefit analysis has shown that the PWAS sensor is the most promising sensor for aircraft SHM [8]. Per plane, the cost saving due to reducing maintenance downtime and labor is about $5 million over the lifetime of the aircraft. Considering that the USAF has over 5,000 airframes, there is a potential to save a significant amount of cost.

1.2 Review of Essential Concepts

For determining damage location, we need to be able to obtain information about the displacement of a wave generated by the PWAS. Before we state our problem and research objectives, we must first establish groundwork for determining this PWAS wave displacement. Additionally, as a reference, the table below in Table 1 defines variables used.

The PWAS acts as an electromechanical resonator when excited by an alternating electric voltage. In elastic, isotropic, infinite media, mechanical disturbances propagate as bulk elastic waves [16]. These waves exist as either longitudinal or pressure (P-waves) and transverse or shear (S-waves) shown in Figure 1. Furthermore, the shear waves can also be separated into shear horizontal (SH) or shear vertical (SV)

Table 1. Variable Definitions and Relations.

Variable	Definition	Equivalent Expression
ω	Frequency	
ξ	Wavenumber (spatial frequency)	
f	Input signal	
Ω	Domain: Infinitely thin plate	
$\mathbf{u}$	Displacement Vector	
E	Young modulus of elasticity	
G	Shear modulus	
ν	Poisson ratio	
λ	Lamé's first constant	$\lambda = \frac{2G\nu}{1-2\nu}$
μ	Lamé's second constant	$\mu = G = \frac{E}{2(1+\nu)}$
c	Wave speed	
c_p	Pressure wave speed	$\sqrt{\frac{1-\nu}{(1+\nu)(1-2\nu)}\frac{E}{\rho}} = \sqrt{\frac{\lambda+2\mu}{\rho}}$
c_s	Shear wave speed	$\sqrt{\frac{G}{\rho}} = \sqrt{\frac{1}{2(1+\nu)}\frac{E}{\rho}} = \sqrt{\frac{\mu}{\rho}}$
$\mathbf{d}$	Motion unit vector	
$\mathbf{p}$	Propagation unit vector	
l	Crack length	
a	PWAS radius	
d	Half of Plate thickness ($2d$ is the plate thickness)	
$sigma$	Stress vector	
ε	Strain vector	

waves shown in Figure 2.

Elastic Waves in An Unbounded Medium.

The displacement of a plane wave, $\mathbf{u}$ with direction of motion, unit vector $\mathbf{d}$, direction of propagation, unit vector $\mathbf{p}$, wave speed, c, and position vector, $\mathbf{x}$, is given by [1]:

$$\mathbf{u} = f(\mathbf{x} \cdot \mathbf{p} - ct)\mathbf{d} \tag{1}$$

Assuming no body forces and a homogeneous, isotropic, linearly elastic medium, the displacement vector components follow this system of PDEs [1]:

$$\mu\nabla^2\mathbf{u} + (\lambda + \mu)\nabla(\nabla \cdot \mathbf{u}) = \rho\ddot{\mathbf{u}} \tag{2}$$

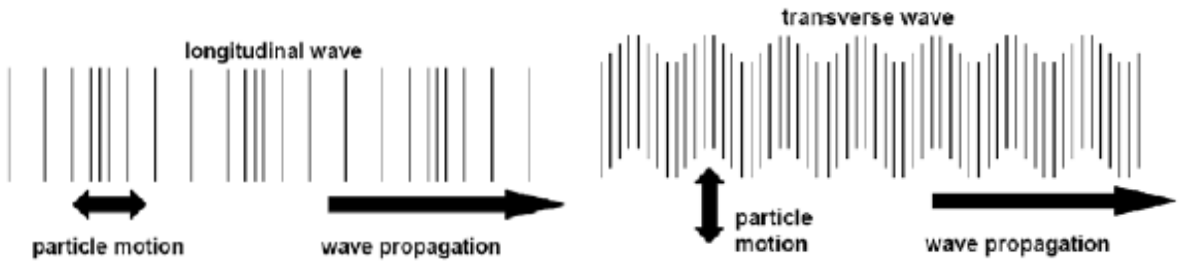

(a) P(Pressure) Wave.

(b) S(Shear) Wave.

Figure 1. Particle Motion in Pressure and Shear Waves. [5]

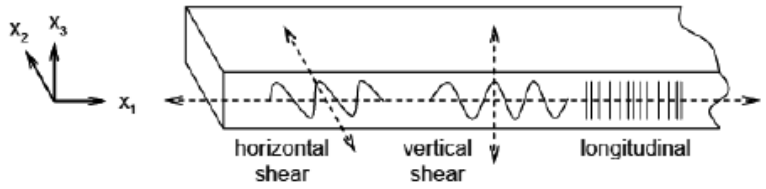

Figure 2. Shear Horizontal and Vertical Waves. [5]

where λ and μ are Lamé constants. Lamé constants define Hooke's law in 3D given by the equation [1]:

$$\sigma = 2\mu\varepsilon + \lambda \text{tr}(\varepsilon) I \tag{3}$$

where σ is the stress, ε is the strain tensor, I is the identity matrix, and $\text{tr}(\cdot)$ is the trace function.

Inserting our plane displacement equation, Equation (1), into our PDE, Equation (2), and simplifying, we get

$$(\mu - \rho c^2)\mathbf{d} + (\lambda + \mu)(\mathbf{p} \cdot \mathbf{d})\mathbf{p} = 0. \tag{4}$$

Since $\mathbf{d}$ and $\mathbf{p}$ are two different unit vectors, we have two cases where Equation (4) is satisfied. Either $\mathbf{d} = \mathbf{p}$, or $\mathbf{p} \cdot \mathbf{d} = 0$ (orthogonality).

Case 1: $\mathbf{d} = \mathbf{p}$.

Since $\mathbf{d} = \mathbf{p}$, $\mathbf{d} \cdot \mathbf{p} = \pm 1$ and we have

$$c = c_p = \left(\frac{\lambda + 2\mu}{\rho} \right)^{1/2}.$$

This gives the governing equation for the pressure wave, or P-Wave, speed. Observe that the motion is parallel to the direction of the propagating wave, a longitudinal wave.

Solutions for the wave equation here are given by:

$$u(x, y, t) = f(y) J_0(\eta_p x) e^{-i\omega t},$$

$$f(y) = A_1 \sin \eta_p y + A_2 \cos \eta_p y,$$

$$\eta_p^2 = \frac{\omega^2}{c_p^2} - \xi_p^2,$$

where ξ is the wavenumber (spatial frequency), c_p is the pressure wave speed, and ω is the frequency.

Case 2: $\mathbf{p} \cdot \mathbf{d} = 0$.

Since $\mathbf{d}$ is a nonzero vector, we have

$$c = c_s = \left(\frac{\mu}{\rho} \right)^{1/2}.$$

This gives the governing equation for the shear wave, or S-wave, speed. Observe that the motion is normal to the direction of the propagating wave, a transverse wave.

Solutions for the wave equation here are given by:

$$u(x, y, t) = h(y)J_1(\eta_s x)e^{-i\omega t},$$

$$h(y) = B_1 \sin \eta_s y + B_2 \cos \eta_s y,$$

$$\eta_s^2 = \frac{\omega^2}{c_s^2} - \xi_s^2,$$

where ξ is the wavenumber (spatial frequency), c_s is the shear wave speed, and ω is the frequency.

Shear-Horizontal Plate Waves.

Shear-Horizontal (SH) waves travel parallel to the wave front, i.e. perpendicular to the direction of wave propagation. Thus, waves are z-invariant and only depend on x and y.

Using properties of stress-displacement relations, circumferential motion, and axial symmetry, the general solution to the wave equation is given as [10]:

$$u_z(x, y, t) = C_1 \sin \eta y + C_2 \cos \eta y)e^{i(\xi x - \omega t)}, \tag{5}$$

where C_1 and C_2 are constants, ω is the frequency, and

$$\eta^2 = \frac{\omega^2}{c_s^2} - \xi_s^2.$$

.

Shear-Vertical Waves.

Shear-Vertical (SV) Waves have the same wave equation as shown in Equation 5 and same wave speed for shear-horizontal plate waves except that the motion is vertical instead of horizontal.

1.3 Lamb Waves

Lamb waves are guided plates waves traveling between two parallel free surfaces such as the upper and lower surfaces of a plate. They exist in two states: symmetric and antisymmetric. There exists modes corresponding to the wave solutions denoted by S0, S1, ... for symmetric modes, and A0, A1, ... for antisymmetric modes. Let the thickness of a plate be $2d$, the product of the frequency ω and the thickness d has a direct relation to the amount of modes present. As shown in Figure 3, when ωd is small, we only see the zero order modes. However, the higher the ωd value is, the larger the number of Lamb wave modes that can simultaneously exist. This means if we want to use one of these modes specifically for detection, we have an upper bound for our frequency (d, here the thickness of the plate is kept constant). If ωd is greater than 1500 kHz·mm, we start to see higher order symmetric modes and if ωd is greater than 1000 kHz·mm, we start to see higher order antisymmetric modes.

Upon activation, the PWAS expands which generates a force from the beam onto the PWAS and an equal and opposite from the PWAS onto the beam. This force then excites the beam which propagates as an axial force excitation and a flexural (bending) moment excitation. By using a high frequency harmonic signal to electrically excite it, the PWAS will induce elastic waves in the beam structure that travel horizontally, reflect at the beam boundaries, and set the beam structure into sustained oscillation (high frequency vibration). PWAS transducers generate Lamb waves in the structural material by converting the electrical energy into the acoustic energy of ultrasonic wave propagation.

The symmetric and antisymmetric Lamb wave modes are derived from the following four equations: [19]

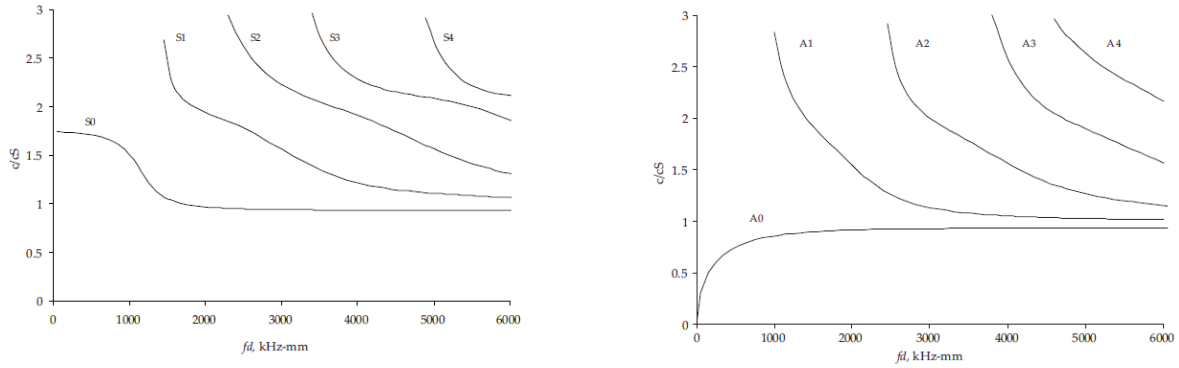

Figure 3. Symmetric and Antisymmetric Lamb wave speed dispersion curves (c_s is the shear wave speed, d is the half thickness of the plate. [10])

$\sigma_{yy}(z = d) = 0$:

$$(\xi^2 - \eta_s^2)(A_1 \sin \eta_p d + A_2 \cos \eta_p d) + 2\xi(B_1 \eta_s \cos \eta_s d - B_2 \eta_s \sin \eta_s d) = 0 \qquad (6)$$

$\sigma_{yy}(z = -d) = 0$:

$$(\xi^2 - \eta_s^2)(-A_1 \sin \eta_p d + A_2 \cos \eta_p d) + 2\xi(B_1 \eta_s \cos \eta_s d + B_2 \eta_s \sin \eta_s d) = 0 \qquad (7)$$

$\sigma_{xy}(z = d) = 0$:

$$2\xi(A_1 \eta_p \cos \eta_p d - A_2 \eta_p \sin \eta_p d) + (\xi^2 - \eta_s^2)(B_1 \sin \eta_s d + B_2 \cos \eta_s d) = 0 \qquad (8)$$

$\sigma_{xy}(z = -d) = 0$:

$$2\xi(A_1 \eta_p \cos \eta_p d + A_2 \eta_p \sin \eta_p d) + (\xi^2 - \eta_s^2)(-B_1 \sin \eta_s d + B_2 \cos \eta_s d) = 0 \qquad (9)$$

where

$$\eta_p^2 = \frac{\omega^2}{c_p^2} - \xi^2, \quad \eta_s^2 = \frac{\omega^2}{c_s^2} - \xi^2,$$

and where ξ is the wavenumber (spatial frequency), c_p is the pressure wave speed, c_s

is the shear wave speed, and ω is the frequency, and d is half the plate thickness.

This can be further reduced to two equations. One for symmetric motion and another for antisymmetric motion.

Symmetric Motion.

By adding Equations (6) and (7) and subtracting Equations (8) and (9), we have

$$A_2(\xi^2 - \eta_s^2)\cos\eta_p d + B_1 2\xi\eta_s \cos\eta_s d = 0$$

$$-A_2 2\xi\eta_p \sin\eta_p d + B_1(\xi^2 - \eta_s^2)\sin\eta_s d = 0.$$

These equations can be represented in the matrix form:

$$\begin{bmatrix} (\xi^2 - \eta_s^2)\cos\eta_p d & 2\xi\eta_s\cos\eta_s d \\ -2\xi\eta_p\sin\eta_p d & (\xi^2 - \eta_s^2)\sin\eta_s d \end{bmatrix} \begin{bmatrix} A_2 \\ B_1 \end{bmatrix} = \begin{bmatrix} 0 \\ 0 \end{bmatrix}. \tag{10}$$

Solutions for these equations exist if the determinant of the matrix in Equation (10) is zero which is equivalent to solving the Rayleigh-Lamb equation for symmetric modes:

$$\frac{\tan\eta_p d}{\tan\eta_s d} = -\frac{(\xi^2 - \eta_s^2)^2}{4\xi^2\eta_p\eta_s}. \tag{11}$$

Numerical solutions for Equation (11) yield the symmetric eigenvalues ξ_0^S, ξ_1^S, ξ_2^S, ... which are the wave numbers of the symmetric Lamb wave modes. For each eigenvalue, the solution is

$$A_2 = -2\xi\eta_s\cos\eta_s d$$

$$B_1 = (\xi^2 - \eta_s^2)\cos\eta_p d.$$

Antisymmetric Motion.

By subtracting Equations (6) and (7) and adding Equations (8) and (9), we have

$$A_1(\xi^2 - \eta_s^2)\sin\eta_p d + B_2 2\xi\eta_s \sin\eta_s d = 0$$

$$A_1 2\xi\eta_p \cos\eta_p d + B_2(\xi^2 - \eta_s^2)\cos\eta_s d = 0.$$

These equations can be represented in the matrix form:

$$\begin{bmatrix} (\xi^2 - \eta_s^2)\cos\eta_p d & 2\xi\eta_s \cos\eta_s d \\ -2\xi\eta_p \sin\eta_p d & (\xi^2 - \eta_s^2)\sin\eta_s d \end{bmatrix} \begin{bmatrix} A_1 \\ B_2 \end{bmatrix} = \begin{bmatrix} 0 \\ 0 \end{bmatrix}. \tag{12}$$

Much like the symmetric case, solutions exist if the determinant of the matrix in Equation (12) is zero which is equivalent to solving the Rayleigh-Lamb equation for antisymmetric modes:

$$\frac{\tan\eta_p d}{\tan\eta_s d} = -\frac{4\xi^2\eta_p\eta_s}{(\xi^2 - \eta_s^2)^2}. \tag{13}$$

Numerical solutions for Equation (13) yield the antisymmetric eigenvalues ξ_0^A, ξ_1^A, ξ_2^A which are the wave numbers of the antisymmetric Lamb wave modes. For each eigenvalue, the solution is

$$A_1 = 2\xi\eta_s \sin\eta_s d$$

$$B_2 = (\xi^2 - \eta_s^2)\sin\eta_p d.$$

Lamb Wave Group Velocity.

To assist in calculation of the approximate time incident and reflected signals should arrive at the receiving PWAS, we need a representation of the speed at which

these signals travel. This is given by the Lamb Wave Group Velocity, c_g given by

$$c_g = c^2 \left(c - fd \frac{\partial c}{\partial (fd)} \right)^{-1} \tag{14}$$

where c is the phase velocity.

1.4 Strain-Displacement Relation

With this background of Lamb wave modes, we now focus on the strain-displacement relation in order to find the Lamb wave displacement. The strain-displacement relations for a Lamb wave are:

$$\varepsilon_{xx} = \frac{\partial u_x}{\partial x}, \tag{15}$$

$$\varepsilon_{yy} = \frac{1}{x} \frac{\partial u_y}{\partial y} + \frac{u_x}{x}, \tag{16}$$

$$\varepsilon_{xy} = \frac{1}{2} \left(\frac{1}{x} \frac{\partial u_x}{\partial y} + \frac{\partial u_y}{\partial y} - \frac{u_y}{x} \right). \tag{17}$$

Our Lamb wave is going to be generated by a uniform electric field which gives us the following assumptions

$$u_y = 0, \frac{\partial u_x}{\partial y} = 0, \frac{\partial u_y}{\partial y} = 0.$$

This reduces Equations (15) - (17) to the following:

$$\varepsilon_{xx} = \frac{du_x}{dx}$$
$$\varepsilon_{yy} = \frac{u_x}{x}$$
$$\varepsilon_{xy} = 0.$$

This yields the wave equation

$$\frac{d^2u_x}{dx^2} + \frac{1}{x}\frac{du_x}{dx} - \frac{u_x}{x^2} = -\frac{\omega^2}{c_p^2}u_x.$$

Setting the wavenumber $\xi = \frac{\omega}{c_p}$, we have

$$x^2\frac{d^2u_x}{dx^2} + x\frac{du_x}{dx} + (x^2\xi^2 - 1)u_x = 0.$$

For simplicity, let us set $z = \xi x$. We now have

$$z^2\frac{d^2u_x}{dz^2} + z\frac{du_x}{dz} + (z^2 - 1)u_x = 0. \tag{18}$$

Equation (18) is Bessel's Equation which we will solve using a power series expansion. Let $u_x = \sum_{k=0}^{\infty} a_k z^{x+k}$ and define $a_0 \neq 0$.

Inserting u_x into (18) gives

$$\sum_{k=0}^{\infty} a_k(x+k)(x+k-1)z^{x+k} + \sum_{k=0}^{\infty} a_k(x+k)z^{x+k} + \sum_{k=0}^{\infty} a_k z^{x+k+2} - \sum_{k=0}^{\infty} a_k z^{x+k} = 0. \tag{19}$$

When $k = 0$,

$\implies a_0(x)(x-1)z^x + a_0(x)z^x + a_0z^{x+2} - a_0z^x$

$= a_0(x^2-1)z^x + a_0z^{x+2}.$

When $k = 1$,

$\implies a_1(x+1)(x)z^{x+1} + a_1(x+1)z^{x+1} + a_1z^{x+3} - a_1z^{x+1}$

$= a_1\left[(x+1)^2 - 1\right]z^{x+1} + a_1z^{x+3}.$

For simplicity, we pull out the terms for $k = 0$ and $k = 1$ values. Equation (19) is now:

$$a_0(x^2-1)z^x + a_1((x+1)^2-1)z^{x+1} + \sum_{k=2}^{\infty}\left[a_k\left[(x+k)^2-1\right] + a_{k-2}\right]z^{x+k} = 0. \quad (20)$$

Equation (20) implies the following three other equations

$$a_0(x^2-1) = 0 \quad (21)$$

$$a_1\left[(x+1)^2-1\right] = 0 \quad (22)$$

$$a_k\left[(x+k)^2-1\right] + a_{k-2} = 0. \quad (23)$$

Equation (21) implies that $x = \pm 1$.

When $x = 1$,

$$a_1\left[(x+1)^2-1\right] = 0 \implies a_1 = 0$$

$$a_k\left[(k+1)^2-1\right] + a_{k-2} = 0$$

$$a_k = -\frac{1}{k(k+2)}a_{k-2}.$$

Since $a_1 = 0, a_3, a_5, a_7, \cdots = 0$.

Looking at only the even terms, let $k = 2n$. Then,

$$
\begin{aligned}
a_{2n} &= -\frac{1}{2n(2n+2)} a_{2n-2} \\
a_{2n} &= -\frac{1}{2^2 n(n+1)} a_{2(n-1)} \\
a_2 &= -\frac{1}{2^2(1)(2)} a_0 \\
a_4 &= -\frac{1}{2^2(2)(3)} a_2 = \frac{1}{2^4(1)(2)(2)(3)} a_0 \\
a_6 &= -\frac{1}{2^2(3)(4)} a_4 = \frac{1}{2^6(1)(2)(2)(3)(3)(4)} a_0
\end{aligned}
$$

Recalling $u_x = \sum_{k=0}^{\infty} a_k z^{x+k}$, we have

$$u_x = a_0 \sum_{k=0}^{\infty} \frac{(-1)^k}{2^{2k} k!(k+1)!} z^{2k+1}.$$

$u_x = a_0 J_1(z)$ where $J_1(z)$ is the Bessel function of order 1 [19].

We now have a representation for Lamb wave displacement which is crucial in our goal towards damage detection.

Modal Analysis.

Now that we have a representation of displacement, a further step would be to consider the wave modes since we are sending an incident wave throughout the material. This requires first some understanding of axial and flexural plate waves.

Axial Plate Waves.

The equation of motion for an axial plate wave is expressed as

$$u(r,t) = AH_1^{(1)}(\gamma r)e^{-i\omega t} + BH_1^{(2)}(\gamma r)e^{-i\omega t}, \tag{24}$$

where H_1 denotes the Hankel function of order 1. Equation (24) is in this form since these two Hankel functions of the first and second order are two linearly independent solutions to Bessel's equation from Equation 18.

Asymptotic behavior of the Hankel function of order 1 at extrema is

$$H_1^{(1)}(x) \xrightarrow{x\to\infty} \sqrt{\frac{2}{\pi x}}e^{i(x-3\pi/4)}, \tag{25}$$

$$H_1^{(2)}(x) \xrightarrow{x\to\infty} \sqrt{\frac{2}{\pi x}}e^{-i(x-3\pi/4)}. \tag{26}$$

Substituting Equations (25) and (26) into Equation (24) gives

$$u(r,t)|_{r\to\infty} = e^{-i(x-3\pi/4)}\sqrt{2/\pi\gamma r}\left[Ae^{i(\gamma r-i\omega)} + Be^{i(-\gamma r-i\omega)}\right].$$

Since we our only interested in the axial wave propagating outward (diverging wave), we retain only the $H_1^{(1)}$ term ($B = 0$). The general solution for the circular-crested axial plate waves emanating from a source at the origin is then

$$u_r(r,t) = AH_1^{(1)}(\gamma r)e^{-i\omega t}.$$

Flexural Plate Waves.

The equation of motion for a flexural plate is expressed as

$$\hat{w} = A_1H_0^{(1)}(x) + A_2H_0^{(2)}(x) + A_3I_0(x) + A_4K_0(x). \tag{27}$$

For the pristine plate with no damage, the third and fourth terms can be discarded since they do not lead to propagating waves [10]. Similar to the axial plate wave approach, we now focus on the asymptotic behavior of the Hankel function of order 1 at extrema.

$$H_0^{(1)}(x) \xrightarrow{x\to\infty} \sqrt{\frac{2}{\pi x}} e^{i(x-\pi/4)} \tag{28}$$

$$H_0^{(2)}(x) \xrightarrow{x\to\infty} \sqrt{\frac{2}{\pi x}} e^{-i(x-\pi/4)}. \tag{29}$$

Substituting Equations (28) and (29) into Equation (27) gives

$$w(r,t)|_{r\to\infty} = e^{-i(x-1\pi/4)}\sqrt{2/\pi\gamma r}\left[A_1 e^{i(\gamma r - i\omega)} + A_2 e^{i(-\gamma r - i\omega)}\right].$$

Once again, we're only concerned with the diverging wave and discard the second terms. The general solution for the circular-crested flexural plate waves emanating from a source at the origin is then

$$w(r,t) = AH_0^{(1)}(\gamma r)e^{-i\omega t}.$$

Linear Elastic Fracture Mechanics Principles.

Finally, since this work focuses on crack formation, it is important to establish a basis of how cracks are formed. This is illustrated in the concept of stress intensity factors.

Stress intensity factors for a crack have the general expression

$$K(\sigma, l) = C\sigma\sqrt{\pi l}, \tag{30}$$

where σ is the applied stress, l is the crack length, and C depends on the geometry and distribution of the system. Thus, stress intensity does not just grow with stress but

also with crack length. At a critical stress intensity K_c, the crack grows uncontrollably (usually this is when the crack becomes visible). K_c is an intrinsic property of the material. In order for a fracture to occur, the local stress intensity must exceed the value of K_c. The K_c is also another way to quantitatively express a material's resistance to brittle fracture when a crack is present. For aluminum, the K_c ranges from 14-28 MPa$\cdot m^{1/2}$

1.5 Problem Statement

The domain Ω is assumed to be an infinite thin plate of thickness $2d$, with a single full-thickness hole radius R centered at the origin. One crack with length L extends in a straight line radially from the edge of the hole. Given input signal $f(x_0, y_0, z_0, t_0)$ determine received signal $u(x_1, y_1, d, t)$ subject to PDE governing elastic motion in Equation 31.

$$\mu\nabla^2\mathbf{u} + (\lambda + \mu)\nabla(\nabla \cdot \mathbf{u}) = \rho\ddot{\mathbf{u}} \tag{31}$$

with free boundary (no stress) conditions at $z = \pm d$:

$$\sigma_{zz} = \sigma_{zy} = \sigma_{zx} = 0$$

where λ and μ are Lamé's first and second constants respectively and ρ is the mass density.

The motivation for our research is to be able to detect damage within a reasonable radius location. Thus, our main goal is to answer the questions about how PWAS responds to significant changes in transmitter distance and how does PWAS respond to varying the transmitter angle and receiver distance simultaneously.

1.6 Research Objective

Our objectives are to create data sets for a receiver PWAS for differing system geometries, extract a net signal representing the damage from the data sets, and perform data analysis on established damage index metrics to draw conclusions about the PWAS detection capabilities.

Researchers in LAMSS in South Carolina have created a program in MATLAB called WaveFormRevealer2D [19] that analytically creates data sets of out-of-plane displacements of the S0 mode for PWAS sensors. With this program, we can adjust transmitter distance, transmitter angle, and receiver distance in order to assess the affect these changes have on the PWAS detection capabilities. By extracting the net signal for damage from the data sets and performing appropriate data analysis, we can have analytical results that can be compared with potential live experiments to see if our detection capabilities shown through WaveFormRevealer2D actually reflect true detection capabilities for the same initial conditions.

1.7 Research Contribution

This thesis serves to demonstrate to the SHM community that PWAS sensors are sensitive to comparatively small changes in system geometry. These changes will be in the form of incrementing the received sensor distance a fixed amount and determining if these changes produce significantly different results for our damage detection. From an application standpoint, a recent SAF/AQ-directed, 45-day sprint review team was tasked with developing strategies to improve aircraft availability with a strong focus on Condition Based Maintenance Plus (CBM+). CBM+ is the application and integration of appropriate processes, technologies, and knowledge-based capabilities to achieve the target availability, reliability, and operation and support costs of DoD systems and components across their life cycle [7]. Proponents

of CBM+ have included the Chief Analyst of the Air Force and commanders at various MAJCOMs indicating that this technology is not only being considered from a technological standpoint but also being implemented in the cultural and operational standpoint.

Additionally, interactions with researchers at the Air Force Research Laboratory (AFRL) have demonstrated that although there has been extensive research done in relation to PWAS arrays and different geometries, there has not been any experiments run where both the transmitter angle and receiver distances are changed. As a further step, in contrast with current research illustrating how effective a PWAS is under ideal conditions, we will purposely put the PWAS in a geometry where it might not be ideal and detection may be difficult to achieve by increasing the transmitter and receiver sensor distances past most live experimental conditions. Therefore, this work demonstrates explicitly to the current SHM community the flexibility of the PWAS, instilling confidence in current applications and motivating future PWAS tests.

1.8 Investigative Questions

The structural health monitoring field has much to gain in the field of predictive approaches to damage. Some initial investigative questions are how does the PWAS detection capabilities change with different geometries? At what distance ranges do the PWAS detection capabilities drop below a certain threshold? Do small changes in the receiver distance have an impact on the PWAS detection even at these long distances?

1.9 Thesis Overview

By establishing the core equations and theory behind wave propagation and crack formation, we are now able to explore current approaches to justify our experimental

motivation and understand where our results showing PWAS detection capabilities at varying geometries fits in to the rest of the research area. For this thesis, Chapter 2 provides a solid foundation of supporting literature in the Air Force and SHM field, Chapter 3 focuses on the process and approach to creating experiments that will rigorously test the PWAS's capabilities, Chapter 4 presents results and data analysis, and Chapter 5 closes with connecting this project with Air Force application and potential future works.

II. Literature Review

2.1 Overview

According to the Department of Defense's (DoD) released information about CBM, titled CBM+, CBM+ is the application and integration of appropriate processes, technologies, and knowledge-based capabilities to achieve the target availability, reliability, and operation and support costs of DoD systems and components across their life cycle [7]. At its core, CBM+ is maintenance performed based on evidence of need, integrating reliability centered maintenance (RCM) analysis with those enabling processes, technologies, and capabilities that enhance the readiness and maintenance effectiveness of DoD systems and components. CBM+ uses a systems engineering approach to collect data, enable analysis, and support the decision-making processes for system acquisition, modernization, sustainment, and operations. This push in the Air Force has garnered support from upper leadership[14].

PWAS Justification.

Ting Dong and Nam H. Kim of the SmartDATA Lab at the University of Florida published a paper in *Aerospace* analyzing the capability of SHM focused sensors: piezoelectric wafer active sensor (PWAS), fiber Bragg grating (FBG), and comparative vacuum monitoring (CVM)[8]. Capabilities for each of the sensors were assessed using a cost-benefit analysis. Factors considered in the study included detection range, detectable damage size, and installed weight. After determining the PWAS was most promising, Dong and Kim performed a case study of inspecting the fuselage of a Boeing 737NG (the most popular model used in civilian aviation) and compared the sensor's performance with traditional non-destructive testing methods. The main reason for using sensors is to transition from schedule-based maintenance to condition-

based maintenance (CBM). In CBM, the health status of the aircraft is continuously monitored and maintenance is only requested when the system's safety is threatened. One of the most significant advantages of CBM is that the SHM system used not only detect damage, but also predict where damage will happen based on previous data. Overall, this approach has the potential to reduce aircraft downtime and, through that reduce revenue/lethality loss due to maintenance times.

Schedule-Based Maintenance Procedures.

Depending on the structural health of the aircraft, different maintenance procedures are used when an airframe reaches a certain value in a metric such as flight hours or time in service. For example, current US Air Force (USAF) maintenance practices call for inspection at time intervals corresponding to half the anticipated life of the component [6]. Inspections range from the most basic cursory "walk around" of the aircraft, visually inspecting for damage, to full scale maintenance, where key components of the aircraft are removed to rigorously inspect the internal structures. Inspection intervals are determined by the detection of the NDE techniques and the anticipated crack growth [6]. For tests done in the University of Florida, Dong and Kim focus on a "C-Check" which is the first check where internal parts are required to be removed, the first time where maintenance time significantly increases. Although this C-Check is used for commercial airliners, this check is similar to the extensive checks the USAF does on its fleet. The C-check is required at every 2800 flight cycles in a maintenance hanger and takes about four days by 20 technicians (640 personnel-hours)[8]. Then, the aircraft is checked with a detailed visual inspection (DVI) which is a comprehensive and intensive method of detecting damage including dents, corrosions, and cracks. Tools used here include magnifying lenses and flashlights. Cracks around 0.5in are usually detected. This means that even if the crack is visible, there

is an element of human error where the inspector does not detect it. The DVI usually takes one week by two inspectors (80 personnel hours). Any damage observed, even if it does not affect the safety of the system, must be repaired which can be very costly if the damage is not covered in the aircraft repair manual. In these cases, the part must be custom manufactured, incurring an increase in money and time as the part is made. Additionally, removing and re-installing internal components increases the risk of damaging the system unnecessarily and incurring additional costs. Just one C-check takes around three weeks and 1000 personnel hours. This means three weeks of no revenue for the aircraft, potentially costing aircraft companies millions of potential revenue. For the Air Force, a C-Check would mean three weeks of the airframe being out of service. If the airframe was used in a combat environment, the impact of this downtime could significantly affect overall force capability including jeopardizing the lives of troops on the ground.

Condition-Based Maintenance.

Currently, CBM is not the primary maintenance approach in industry and in the Air Force but early results do show promise. The most important similarity between schedule and condition-based maintenance is that repairs will be treated exactly the same. Therefore, the savings in time and personnel-hours is reliant on the maintenance itself and not what processes are needed after the maintenance is complete. This means that CBM has the largest potential for improvement on new aircraft. Since SBM relies on a firm maintenance schedule, many new aircraft are grounded early in their life to perform maintenance when none is really needed. This is especially concerning since this is also the time when the aircraft should be most efficient and, thus, most profitable. CBM in this case can skip several schedule maintenances because there is no considerable damage. Additionally, even if damage is detected,

CBM can allow maintainers crucial information about whether the damage is significant enough to warrant repairs. The damage, if determined not critical, will be constantly monitored and fixed at the time in which it passes the safety threshold. Such practice would reduce the number of repairs and number of maintenances in general.

Piezoelectric Wafer Active Sensor.

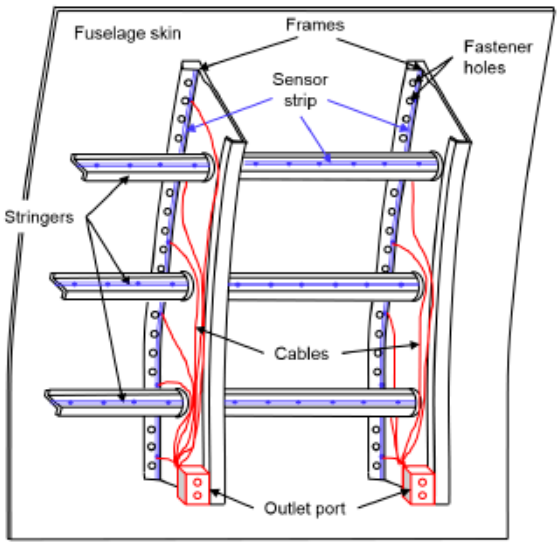

Figure 4. PWAS Network (SMART Layer) on Fuselage. [8]

PWAS mechanisms are based upon ultrasonic wave theory [10] where each PWAS is able to act as both an actuator and a receiver. Detection of damage relies upon sending a incident elastic wave through the material and comparing that to the received wave. Damage will act as a separate point source and scatter the incident wave. By comparing the incident and scattered waves, information about the damage location and geometry can be obtained. PWAS configurations include pulse-echo where the PWAS is both the source and receiver, pitch-catch where one PWAS is the source and one is the receiver, and phased array where multiple sensors in the pulse-

echo configuration are placed in a line. For the phased array method, the sensors are set to specific time delay so that all the incident waves will arrive at the same time. By superimposing the signals, the damage can be located with a relatively high signal-to-noise ratio and resolution. However, this method falls apart when the damage is close to sensor [19]. Lamb waves are the main focus for PWAS analysis due to their long range and little amplitude loss. For any given frequency, at least two Lamb wave modes exist and single mode waves are crucial for damage detection. Finally, as expected, the detection range for PWAS is limited and a large number of sensors will be required. Although the Lamb waves have a long range with little amplitude loss, the most limiting part of detection for the PWAS is being able to discern between a damaged signal and noise. As the distance increases, the damage could be indistinguishable from the noise. One solution to this problem of a limited detection range is to attach the PWAS to a circuit called a SMART Layer which can be further connected to create a SMART Suitcase which has shown promising results, detecting cracks 0.2in small with the same level of uncertainty as conventional non-destructive testing (NDT) methods [8]. This SMART Suitcase is composed of multiple SMART layers shown in Figure 4. These layers are able to connect to an array of PWAS sensors and actuate the sensors one-by-one to detect and verify the presence of damage. Because data is received by a large number of sensors, Dong and Kim were able to compare the signals from each sensor to obtain the location of the damage.

Fiber Bragg Grating Sensor.

Fiber Bragg Grating (FBG) sensors use a series of parallel lines with different refractive indices on the core of optical fiber shown in Figure 5. When damage occurs, the spacing between the gratings changes. A broadband light is then shown

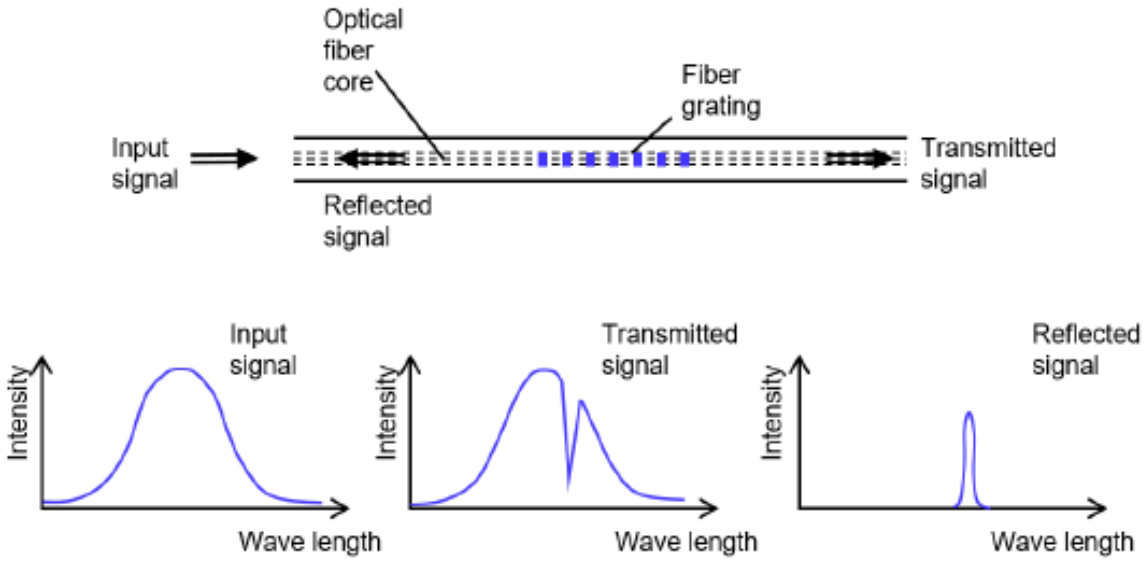

Figure 5. Fiber Bragg Grating Sensor. [8]

through the grating and specific wavelengths are reflected depending on the spacing. The shift in the reflected wavelength provides information on the damage. Strengths of the FBG sensors over the PWAS include a smaller size (a single optical fiber can incorporate up to 2,000 FGB sensors [8]), weight, and safety from electromagnetic interference. FBG sensors are also able to detect bare visible impact damage (BVID) in composite panels which is the main source of composite delamination. This is especially important since BVIDs deteriorate the mechanical strength of composite structures but cannot be seen from the surface. However, the FBG suffers from poor range as it depends on strain measurement and is not as useful for attempting to locate damage at an unknown location. Additionally, FBG is useless on the ground, where most maintenance occurs, since all the strains disappear when the system is at rest.

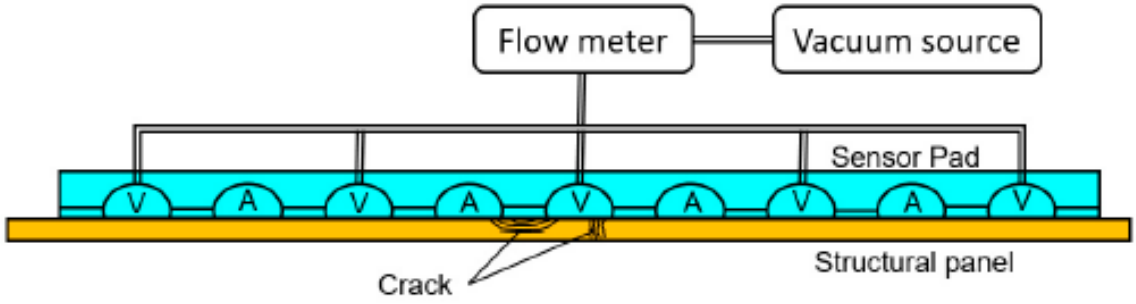

Figure 6. Comparative Vacuum Monitoring Sensor. [8]

Comparative Vacuum Monitoring Sensor.

CVM sensors use a pattern of alternative vacuum and atmospheric pressure galleries depicted in Figure 6. In the absence of damage, the vacuum galleries should retain their low pressure. Once a crack is formed, it can make a channel between the vacuum and atmospheric galleries. By recording the extent of the increase in pressure in the vacuum galleries, the size of the crack can be determined. The CVM system includes a sensor pad, a flowmeter measuring pressure, and a pump to maintain the low pressure in the vacuum galleries. Sandia National Laboratory found that the 0.02in cracks could be detected with a probability of 90% and confidence interval of 95%. Some significant advantages are that these sensors seem far more accurate than the previously introduced ones and that the sensor pad is made of very lightweight polymer. However, the major drawback is that CVM has no range in its detection: it only detects damage directly below the sensor. Like the FBG sensor, it seems that the CVM sensor is a great choice for known hotspot locations but a poor choice for finding damage at unknown locations.

Limitations of Different Approaches.

For a PWAS system where the sensors are 10in away from each other, Dong and Kim estimated that it would take 9988 sensors to fully cover the entire Boeing 737NG

fuselage [8]. Each SMART Suitcase can connect up to 30 sensors which means 333 connection ports are needed for the full fuselage. Each port takes about 30mins to connect the SMART Suitcase, activate the sensor, collect data from the sensor, and analyze the data for damage information. This means that the whole process would take around 167hrs. Although this seems like a large number, this is a significant improvement in time over the 3 weeks and 1000 personnel hours the SBM approach currently requires. Dong and Kim then performed a cost-benefit analysis to see if this network of PWAS sensors was financially reasonable. The 10,000 PWAS grid cost along with the lost revenue from decreased cargo loads totalled a little more than $50 million while the benefit would be a little more than $5 million [8]. The main factors that increased the cost was the immense weight from all the sensors. In the Air Force, this extra weight means that more fuel would be needed to maintain the same flight capabilities. Consequently, the increase in fuel consumption would decrease the range of the airframe before needing a refuel. Finally, the reliability of the sensors was assumed that all 10,000 sensors would be maintained in good condition during the life of the aircraft.

It is important to note that Dong and Kim's study relied upon data from the civilian sector. The Boeing 737NG may be the most popular model for civilian aircraft, but from a military standpoint, may not be the most appropriate model to model the Air Force's typical airframe. This difference rests mostly on the different missions of the two sectors. In the civilian sector, the main goal is transportation while in the military sector, the main goal is overall force lethality. For combat aircraft, especially fighters, the strain on the material may be far higher which would make the FBG sensor an appropriate choice. In addition, radar jammars or other systems that produce a strong electromagnetic signature can cause serious problems in the PWAS's performance since a non-uniform electric field would cause the underlying equations

for damage detection to no longer be accurate. Thus, in very specific cases, the FBG sensors could be used jointly with a PWAS as a check when conditions are not ideal.

However, these different sectors also share similarities in their goals. The use of sensors to detect/predict cracks is invaluable to both in the interest of safety and revenue. Furthermore, much of the Air Force is comprised of transport aircraft, carrying troops and equipment to and from operational areas. Therefore, it is safe to say that although this study focuses on civilian aircraft, we can extend Dong and Kim's conclusion to military aircraft and say that the PWAS sensor is the most promising sensor for detecting and, thus, predicting cracks.

As shown in the above analysis, we can see that the continuous health monitoring aspect of CBM is merely in its infancy since the financial costs and weight make it impractical to constantly monitor an airframe. Additionally, the data processing requires operators to activate sensors one-by-one, collect all data, and then process it to identify damage sizes and location. Ultimately, this process would take 3-4 days on average which is far longer than the typical 30min window for maintenance between each flight [8].

2.2 CAFA Approach Justification

For an analytical solution for damage detection, a common approach is to model a 3-D system, add appropriate loading forces and boundary conditions, and mesh it with small uniform elements using a method called finite element modeling (FEM). This process allows researchers to accurately assess the effects different stresses and forces have on the 3-D system before attempting to perform any live tests. However, one of the limitations of a full FEM is how costly it is in terms of runtime especially when the elements used to mesh the 3-D system have to be very fine. Using small uniform elements to mesh a model with a small crack requires the elements to be ex-

tremely small, in order to accurately account for the crack, and, therefore, the mesh to be very fine [11, 8, 19]. Although this full FEM models the crack with a great deal of accuracy, analysis performed has the potential to take a significant amount of time since the FEM software must account for each of these elements in its calculations. Yanfeng Shen and Victor Giurgiutiu from LAMSS at the University of South Carolina published an article in *Ultrasonics* [21] providing the groundwork and justification of not attempting to perform a full FEM approach to the damage detection problem. Shen and Giurgiutiu noted that many researches in the SHM field [11] have developed analytical models using Kirchhoff, Mindlin, Kane-Mindlin plate theory, and 3-D elasticity solution and exact Lamb mode solutions. For numerical methods, they acknowledged the finite, boundary, and spectral element methods along with a finite difference methods. Analytical methods, in general, are accurate, efficient, and produce results quite quickly for works with simple parameters. However, the main limitation is that these same methods fall apart when they try to analyze complex damage geometries. The solution for this case is usually to apply a numerical solution which is more costly due to usually discretizing the analyzed domain and performing a time marching procedure. Shen and Giurgiutiu balanced the strengths of both methods through the Combined Analytical FEM Approach (CAFA) [19].

CAFA Overview.

CAFA uses exact analytical expressions for Lamb wave generation, propagation, damage interaction, and detection while storing a 3-D wave-damage interaction coefficient (WDIC) calculated numerically for a local FEM with non-reflective boundaries (NRB). The CAFA process is shown in Figure 7. The middle step shows the separation in the work: The WDIC's are first calculated in a Local FEM Harmonic Analysis where they are then used to account for the scattering from the damage

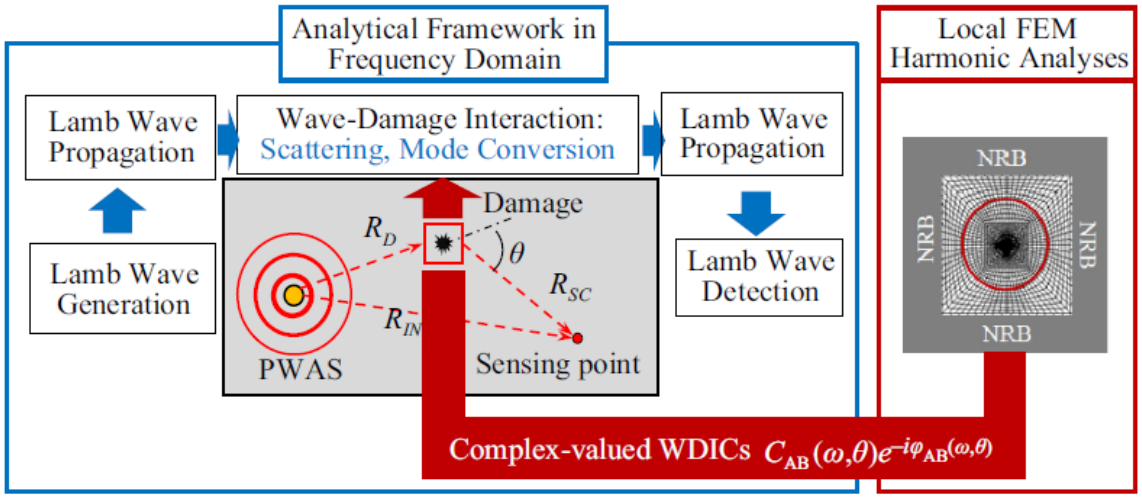

Figure 7. CAFA Method.

source (the damage acts as another wave source) and calculate the sensing signal. This is demonstrated through the following 7 step process [19].

1. Perform Fourier transform of the time-domain excitation signal $V_T(t)$ to obtain the frequency domain excitation spectrum, $\tilde{V}_T(\omega)$

2. Calculate structure transfer function.

$$G^S(\omega, r) = -\pi i \frac{a^2 \kappa_{PWAS}(\omega)}{2\mu} \sum_{\xi^S} \frac{J_1(\xi^S a) N_S(\xi^S)}{D'_S(\xi)} H_1^{(1)}(\xi^S r) \tag{32}$$

$$G^A(\omega, r) = -\pi i \frac{a^2 \kappa_{PWAS}(\omega)}{2\mu} \sum_{\xi^A} \frac{J_1(\xi^S a) N_S(\xi^A)}{D'_A(\xi)} H_1^{(1)}(\xi^A r) \tag{33}$$

3. Multiply structure transfer function (Equations (32) and (33))by the frequency-domain excitation signal from the PWAS to the sensing location (R_{IN}) to obtain the direct incident waves. Perform the same operation from the PWAS to the damage location (R_D) to obtain the interrogating waves. For the direct incident

waves we have:

$$U_{IN}(\omega, R_{IN}) = \tilde{V}_T(\omega)[G^S(\omega, R_{IN}) + G^A(\omega, R_{IN})] \tag{34}$$

$$U_D(\omega, R_D) = \tilde{V}_T(\omega)[G^S(\omega, R_D) + G^A(\omega, R_D)] \tag{35}$$

4. Obtain scattering waves source at the damage location by modifying incident waves with pre-calculated WDICs

$$u_N^S = C_{SS}(\omega, \theta)e^{-i\varphi_{SS}(\omega,\theta)}u_D^S + C_{AS}(\omega, \theta)e^{-i\varphi_{AS}(\omega,\theta)}u_D^A \tag{36}$$

$$u_N^A = C_{SA}(\omega, \theta)e^{-i\varphi_{SA}(\omega,\theta)}u_D^S + C_{AA}(\omega, \theta)e^{-i\varphi_{AA}(\omega,\theta)}u_D^A \tag{37}$$

$$u_N^{SH} = C_{SSH}(\omega, \theta)e^{-i\varphi_{SSH}(\omega,\theta)}u_D^S + C_{ASH}(\omega, \theta)e^{-i\varphi_{ASH}(\omega,\theta)}u_D^A \tag{38}$$

The transfer function is calculated from the amplitude relationship between the incident and scattered waves in the WDICs:

$$u_{SC}^S = u_N^S H_1^{(1)}(\xi^S R_{SC}) \tag{39}$$

$$u_{SC}^A = u_N^A A_1^{(1)}(\xi^A R_{SC}) \tag{40}$$

$$u_{SC}^{SH} = u_N^{SH} H_0^{(1)}(\xi^{SH} R_{SC}) \tag{41}$$

5. Sum the direct incident waves and the scattered waves to get the total wave field for in-plane displacement:

$$u_{TOTAL} = u_{IN}^S + u_{IN}^A + u_{SC}^S + u_{SC}^A + u_{SC}^{SH} \tag{42}$$

6. Convert in-plane wave motion to out-of-plane wave motion using the mode

shape component ratio:

$$u_z^S = u_r^S \frac{U_r^S(\omega, d)}{U_r^S(\omega, d)} \tag{43}$$

$$u_z^A = u_r^S \frac{U_r^A(\omega, d)}{U_r^A(\omega, d)} \tag{44}$$

$$u_z^{SH} = u_r^S \frac{U_r^{SH}(\omega, d)}{U_r^{SH}(\omega, d)} \tag{45}$$

7. Perform Inverse Fourier transform to obtain the time domain sensing signal

FEM Approach and WDIC Calculation.

Not surprisingly, the scattered wave field is obtained by the subtraction of the incident waves from the total waves [10, 19]. Recent research on local FEM techniques allow for the extraction of scattering information of any Lamb modes from the damage [12]. For the radial and tangential directions, scattering is given by.

$$u_{SC}^{S0} = \frac{u_r^T + u_r^B}{2} \tag{46}$$

$$u_{SC}^{A0} = \frac{u_r^T - u_r^B}{2} \tag{47}$$

$$u_{SC}^{SH0} = \frac{u_\theta^T + u_\theta^B}{2} \tag{48}$$

From here, the relationship between the incident waves arriving at the damage and the scattered waves received on the sensing boundary is:

$$u_{IN}^A e^{-i\varphi_{IN}^A} \cdot C_{AB}(\omega, \theta) e^{-i\varphi_{AB}(\omega,\theta)} \cdot H_m^{(1)}(\xi^B r) = u_{SC}^B(\theta) e^{-i\varphi_{SC}^B(\theta)} \tag{49}$$

where $u_{IN}^A e^{-i\varphi_{IN}^A}$ is the A mode incident wave recorded, $C_{AB}(\omega, \theta) e^{-i\varphi_{AB}(\omega,\theta)}$ is the WDIC with the mode conversion from A to B, direction dependency, amplitude ratio, and phase relationship information, and $H_m^{(1)}(\xi^B r)$ is the outward propagating 2-D

wave field of the scattered wave mode B. As before, m = 1 for Lamb waves and m = 0 for shear waves. Finally, $u^B_{SC}(\theta)e^{-i\varphi^B_{SC}(\theta)}$ is the resulting scattered waves recorded on the sensing boundary with scatter angle, amplitude, and phase information.

Now we rearrange Equation (49) and solve for the WDIC:

$$C_{AB}(\omega,\theta)e^{-i\varphi_{AB}(\omega,\theta)} = \frac{u^B_{SC}(\theta)}{u^A_{IN}}\frac{1}{H^{(1)}_m(\xi^B r)}e^{-i\Delta\varphi_{AB}(\theta)} \tag{50}$$

where $\Delta\varphi_{AB}(\theta) = \varphi^B_{SC}(\theta) - \varphi^A_{IN}$. This can be further simplified to:

$$C_{AB}(\omega,\theta) = \left|\frac{u^B_{SC}(\theta)}{u^A_{IN}}\frac{1}{H^{(1)}_m(\xi^B r)}\right| \tag{51}$$

$$\varphi_{AB}(\omega,\theta) = \Delta\varphi_{AB}(\theta) - \left[\angle\frac{1}{H^{(1)}_m(\xi^B r)} - \frac{1}{H^{(1)}_m(0^+)}\right] \tag{52}$$

Here $\angle\frac{1}{H^{(1)}_m(\xi^B r)} - \frac{1}{H^{(1)}_m(0^+)}$ is the phase of the propagating wave.

Performing the experiment with the scanning laser Doppler vibrometer (SLDV) and comparing the results with our Full FEM Approach and CAFA approach gives the following graph:

We see here in Figure 8 that CAFA results follow the Full FEM and Experimental values closely with the only significant differences being slight deviations in phase and amplitude. The main advantage of CAFA is that the entire structure does not need to be meshed which significantly reduces computation time. Shen and Giurgiutiu noted that the Full Scale FEM Model took around 20 hours while the CAFA took around 2-3 hours [3]. Additionally, the Full FEM approach requires a re-model and re-run for any changes in parameters including PWAS size, sensor location, wave frequency, and different waveforms. The CAFA approach, however, only requires the modification of the parameters and takes significantly less time to check each one. Finally, the data size of the conventional Full 3-D FEM simulation can reach several hundred gigabytes

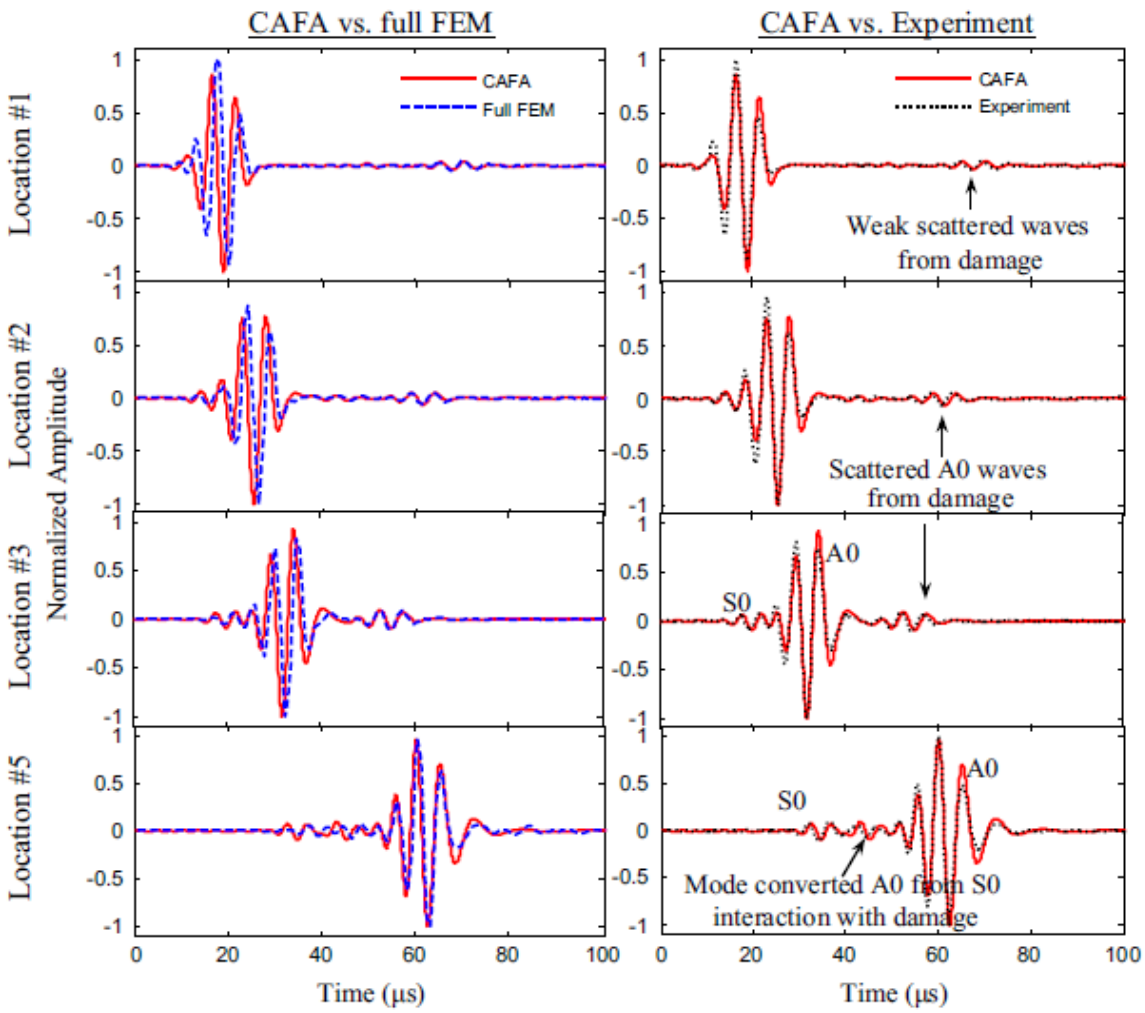

Figure 8. CAFA Versus FEM and Experiment. [3]

while the 2-D CAFA only consumes several hundred megabytes.

Limitations of CAFA Approach.

Shen and Giurgiutiu used a SLDV which only measures the out-of-plane velocity of the wave field meaning that the shear horizontal waves cannot be captured because they have no out-of-plane motion [19, 20]. Additionally, the entire study depended on analysis of the only the fundamental plate guided waves modes (S0, A0, and SH0). Shen and Giurgiutiu have explicitly stated in multiple occurrences throughout the

paper that this same methodology will not work for higher order modes and a different approach must be utilized. Finally, this study assumes negligible noise/unaccounted interference.

2.3 Introduction of Crack Geometry Considerations

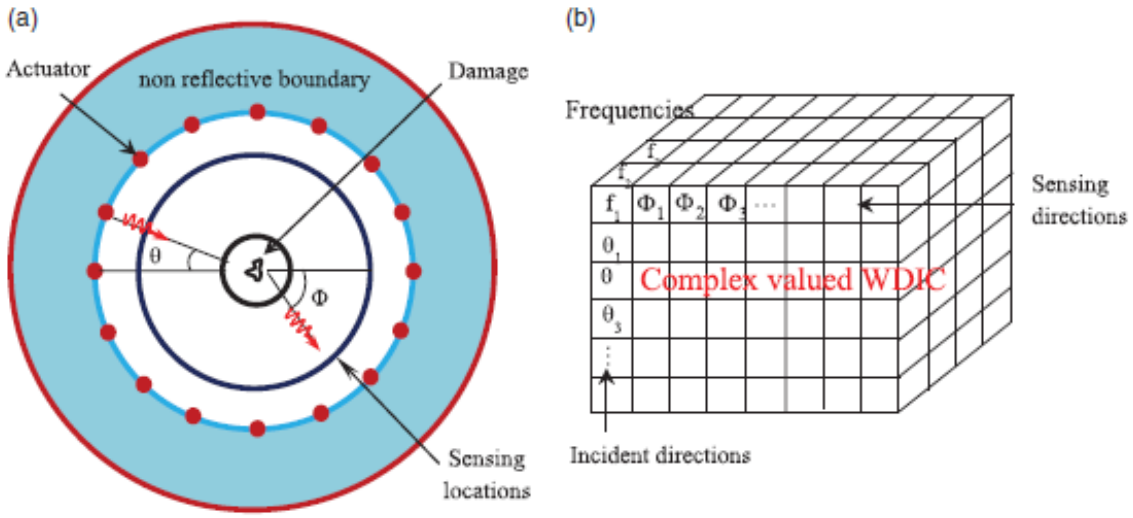

Figure 9. Wave Damage Interaction Coefficient Scatter Cubes.

Md Yeasin Bhuiyan, Yanfeng Shen, and Victor Giurgiutiu investigated using WDIC to account for Lamb waves scattering from different directions [2, 3]. Bhuiyan, et al. used a butterfly cracked rivet hole as the damage source and analyzed it using local FEM. This paper continues the idea presented in the previous paper of CAFA, where the analytical method is used everywhere except for a small area close to the damage source which is analyzed using a local FEM method. When Lamb waves encounter the damage source, they are scattered and experience mode conversion. This produces the shear horizontal waves in the scattered weaves. The symmetric and antisymmetric fundamental Lamb wave nodes impact the damage from multiple directions, creating corresponding WDICs. From there Bhuiyan, et al. performed har-

monic analysis over the fundamental frequency domain and formed complex-valued "scatter cubes" of WDICs. Each scatter cube stores the relative amplitude and phase of the scattered waves which help inform about ideal sensor locations.

WDIC for Pristine Plate.

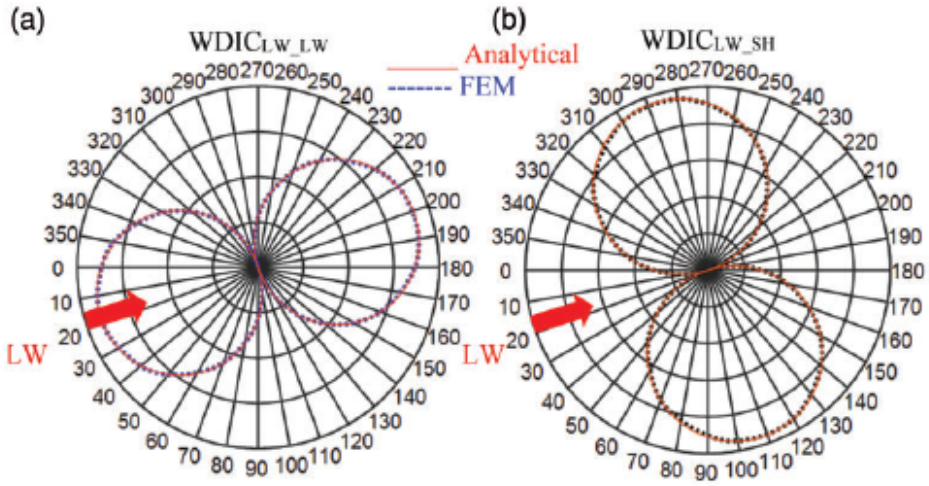

Figure 10. Wave Damage Interaction Coefficient for Pristine Plate.

As a preliminary work, Bhuiyan, et al. created a WDIC for a pristine plate [2, 3, 10]. For the pristine plate, the WDIC only depends on the azimuthal direction ϕ for a given frequency and sensing circle. Therefore, we see that the polar plots of the WDICs show that Lamb waves are guided forward and backward while the shear horizontal waves are guided transversely. As expected, these plots are symmetric with one merely being a 90° rotation of the other.

Local FEM Approach.

The local FEM Approach is performed on a small size (40mm x 40mm) 3-D FE model for each incident Lamb Wave shown in Figure 11. On all sides, there is a 20mm wide non-reflective boundary (NRB) to enforce the simplifying assumption

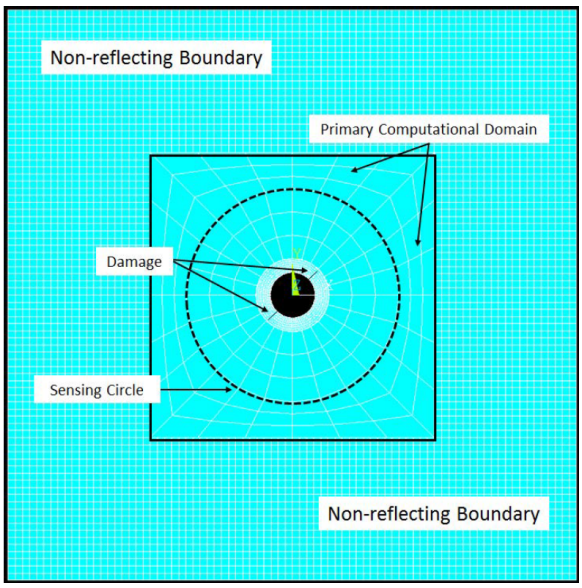

Figure 11. FEM Computational Domain.

of no interference from reflections [3, 10]. Lamb wave excitation appears through elemental nodal forces in the following equation:

$$F_{ix}^{e} = \int_{0}^{L_e} \sigma_{xx}^{e}(s) N_i^e(s)\ ds \tag{53}$$

$$F_{iy}^{e} = \int_{0}^{L_e} \sigma_{xy}^{e}(s) N_i^e(s)\ ds \tag{54}$$

where e represents the element, L_e is the element size, F_{ix}^{e} and F_{iy}^{e} are the nodal forces in the x and y directions, i is the element node number, and $N_i^e(s)$ is the shape function of the element type. Figure 12 shows this Lamb wave excitation as a loading force in red entering the primary computational domain from Figure 11. From our general Lamb wave equations, the stress mode shapes are given by:

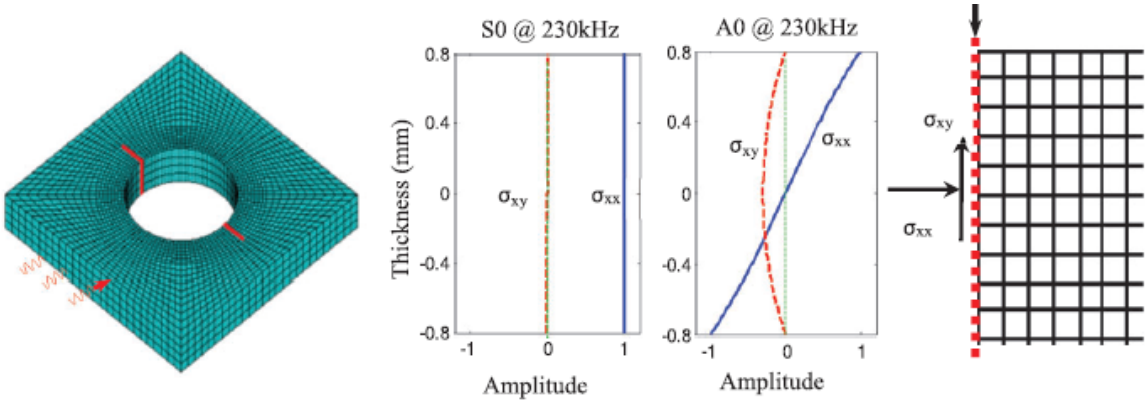

Figure 12. Finite Element Model Approach.

Symmetric modes

$$\sigma_{xx}^{S}(x,y,t) = C^{S}2\mu\xi\eta_{S}[(\xi^{2}+\eta_{S}^{2}-2\eta_{P}^{2})\cos\eta_{S}d\cos\eta_{P}y-(\xi^{2}-\eta_{S}^{2})\cos\eta_{P}d\cos\eta_{S}y]e^{i(\xi x-\omega t)}$$

$$\sigma_{yy}^{S}(x,y,t) = -C^{S}2\mu\xi\eta_{S}(\xi^{2}-\eta_{S}^{2})(\cos\eta_{S}d\cos\eta_{P}y-\cos\eta_{P}d\cos\eta_{S}y)e^{i(\xi x-\omega t)}$$

$$\sigma_{xy}^{S}(x,y,t) = iC^{S}2\mu[4\xi^{2}\eta_{P}\eta_{S}\cos\eta_{S}d\sin\eta_{P}y+(\xi^{2}-\eta_{S}^{2})^{2}\cos\eta_{P}d\sin\eta_{S}y]e^{i(\xi x-\omega t)}$$

Antisymmetric modes

$$\sigma_{xx}^{A}(x,y,t) = -C^{A}2\mu\xi\eta_{S}[(\xi^{2}+\eta_{S}^{2}-2\eta_{P}^{2})\sin\eta_{S}d\sin\eta_{P}y-(\xi^{2}-\eta_{S}^{2})\sin\eta_{P}d\sin\eta_{S}y]e^{i(\xi x-\omega t)}$$

$$\sigma_{yy}^{A}(x,y,t) = C^{A}2\mu\xi\eta_{S}(\xi^{2}-\eta_{S}^{2})(\sin\eta_{S}d\sin\eta_{P}y-\sin\eta_{P}d\sin\eta_{S}y)e^{i(\xi x-\omega t)}$$

$$\sigma_{xy}^{A}(x,y,t) = iC^{A}2\mu[4\xi^{2}\eta_{P}\eta_{S}\sin\eta_{S}d\cos\eta_{P}y+(\xi^{2}-\eta_{S}^{2})^{2}\sin\eta_{P}d\cos\eta_{S}y]e^{i(\xi x-\omega t)}$$

The crack is model as a discontinuity at the adjacent pair of nodes along the cracks. Bhuiyan, et al. used a crack length of 1.6mm on each side of the rivet hole which represents a crack forming from fatigue and a rivet hole length of 6.4mm. From the polar plots and preliminary work with the pristine plate, it is apparent that the rivet hole cracks is symmetric in terms of the direction of the incident wave about

the line of cracks and the line perpendicular to it. Therefore, the FE analyses are performed just for the 0 to 90° angles of the incident waves.

The local model of the plate is meshed with a 0.4mm mesh size using eight-node SOLID 45 structural elements while the COMBIN14 spring-damper elements are used to model the NRB. For materials, an aircraft grade aluminum 2024-T3 of 1.6mm thickness is used. To accurately capture the stresses near the damage source, finer meshes were used while relatively coarser meshes were used on less important areas.

FE simulations were done for three separate cases:

1. Butterfly cracked rivet hole
2. Rivet hole only
3. Pristine plate (No crack or hole)

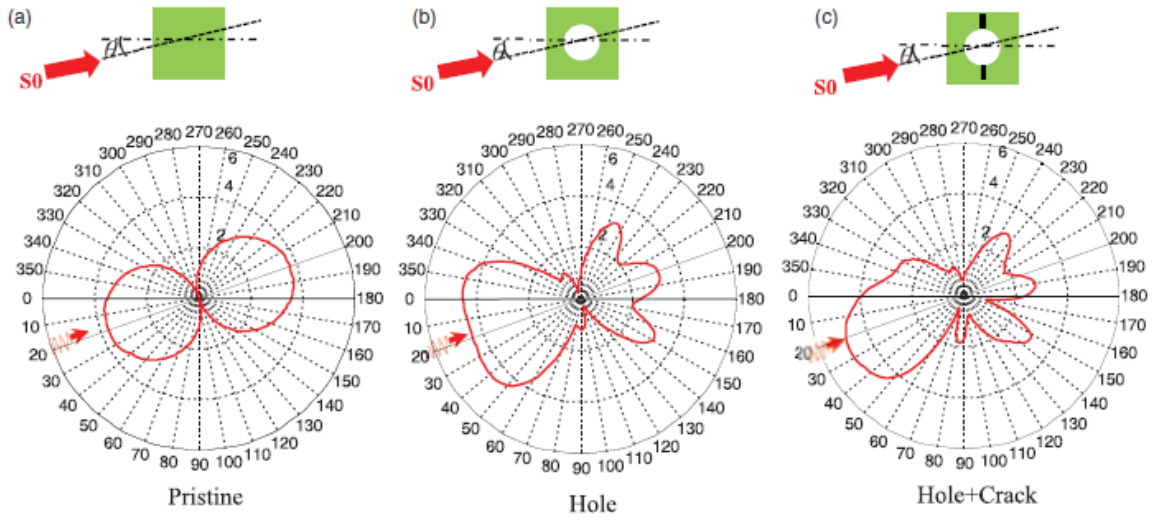

Figure 13. Polar plots for Pristine, Rivet Hole Only, and Rivet Hole with Butterfly Crack.

We see here that symmetry is maintained through the pristine and rivet hole only experiments. For the rivet hole, we can see that at certain directions, the scattered

wave amplitude is higher than the other directions. From observation, we can see that these values would be around 150, 200, and 245° on the opposite side of the incident wave and around 45 and 355° on the same side of the incident wave. With the crack introduce, symmetry is lost and there is a clear difference in amplitude in specific directions. We can see that it seems that there may be other modes present as there is zero amplitude received on 70, 100, and 165°, a property that occurs when higher modes are present. The maximum amplitude for the crack seems to be very close to the same direction as the incident wave, almost indicating that maybe a direct reflection occurred on the discontinuity created by the crack.

Limitations.

All data and output from this study has not been verified by a live experiment and, thus, there is no concrete proof that this same results will be obtained using experimental methods. Additionally, this paper did not address any of the possibly present higher modes in the structure which may have been the reason behind the increase in the number of directions where the peak amplitude was zero. Therefore, future work should be done to test whether or not high modes had an impact on this work.

RAPID Approach.

Researchers at the Intelligent Automation, Inc. have also approached this same problem for SHM using PWAS sensors (Called PZT on their paper) [24] [25]. However, they utilized a different approach called reconstruction algorithm for probabilistic inspection of defects (RAPID) which seemed to show good performance for defect detection, size estimation and localization on aircraft wing structures. Additionally, this paper was able to obtain an E-2 surveillance airplane wing section from the

US Navy for the study. This wing, being of varying thickness, does not allow the conventional uniform-thickness plate model and, thus, is a relatively novel addition to the the SHM field that usually relies so heavily on that assumption.

Zhao et al. used a full circular array around the defect with 8 PWAS sensors with radius around 10in as shown [24] [25]. In their experiment, the sensor stake turns generating ultrasonic signals while the rest are receivers. For example, when disc 1 is sending a signal, sensors 28 are in the reception mode; then disc 2 is transmitting signals and sensors 1, 38 are listening, and so on.

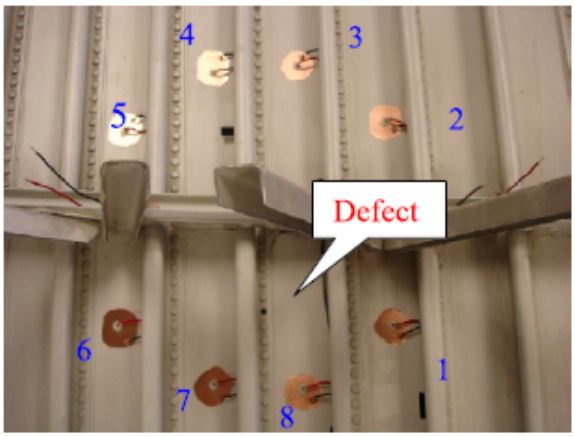

Figure 14. PWAS Array.

The RAPID approach uses a Bayesian correlation analysis technique by measuring differences in the guided wave signals between the damaged and undamaged conditions [24] [25]. New signals are compared with reference data to determine whether or not damage has occurred. Geometry of where the damage is located is determined by observing which sensors had the largest change from the reference data. Four conditions were studied, i.e., (a) the normal, defect-free condition; (b) a rivet was driven out of the wing panel and then put back in to simulate a loose rivet; (c) a 1 mm notch was machined in the loose-rivet hole to simulate a small crack; and (d) the rivet crack was increased to 3 mm.

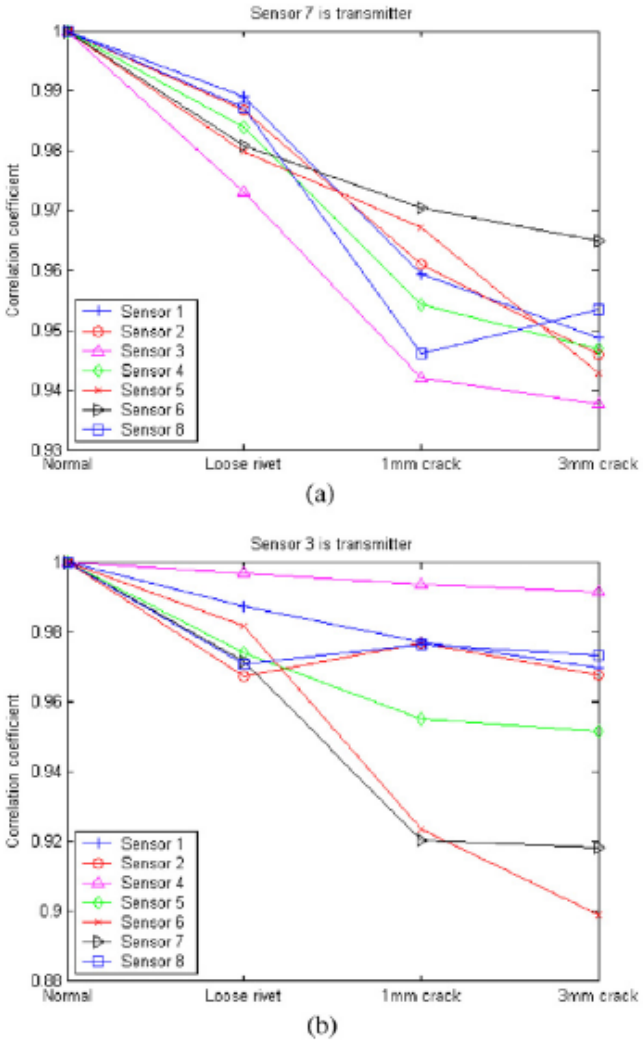

Figure 15. Damage Impact on Correlation for Sensors.

We can see that the correlation sharply decreases for all receiving sensors in the first case, indicating that the damage most likely happened near sensor 7 (the transmitter). This is because the scattered wave would be more prominent the closer the transmitter is to the damage and, since the change in correlation indicates the impact of a damage source, the larger the impact, the closer the transmitter to the damage. This is far less obvious on the second case where there seems to be a mixture of correlation changes but the concept still holds. Sensor 4 seemed to detect almost no change while sensors 6 and 7 have a large decrease in correlation. This indicates that

the damage probably was close to these two sensors but far from sensor 4. Looking at the array configuration, this is definitely a possible outcome.

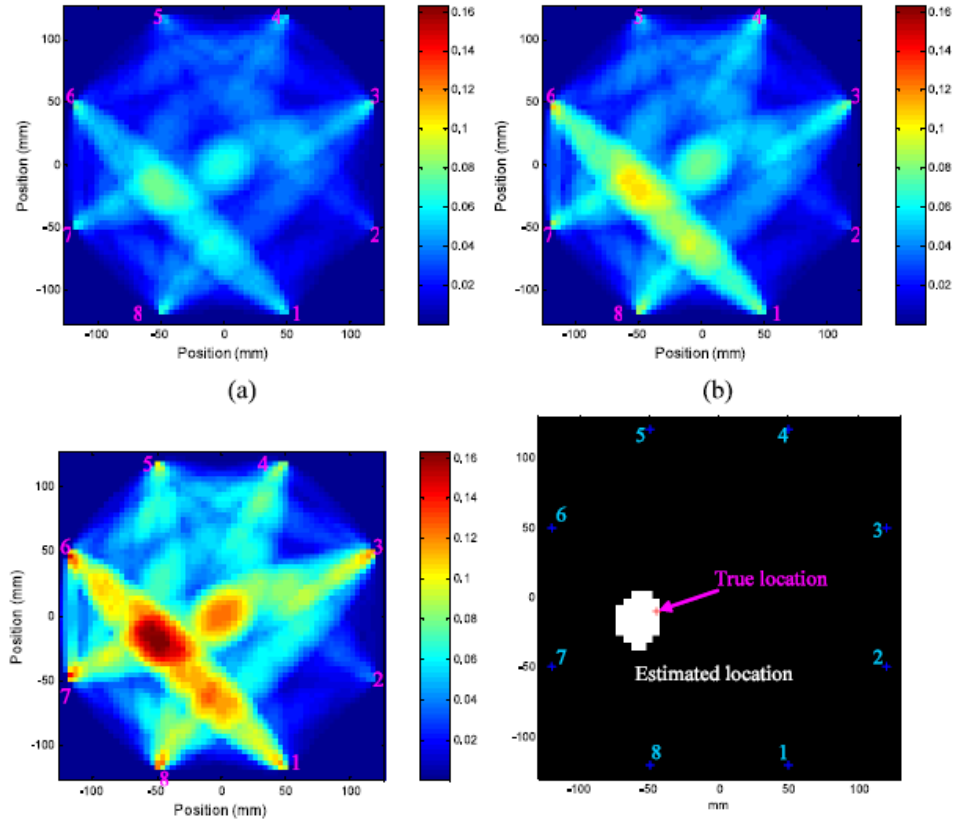

Figure 16. RAPID Detection Results.

We see from the RAPID detection results that this approach estimates the damage location accurately as long as the damage threshold is set correctly. On the top left output, we see that it's not easy to accurately say where the damage could be but on the bottom left, RAPID is able to narrow down where the damage could be located to fairly small area.

Finally, the RAPID approach was used to analyze damages to the surface of the wing to simulate corrosion. In this regard, the approach worked extremely well in finding the location of the defect in comparison to other SHM approaches. In the image reconstruction for corrosion defects, the RAPID approach correctly detected

the location of the damage but did not give much information regarding the size of the damage. Therefore, this approach may be utilized in situations where corrosion is to be expected more than direct damage (i.e. cracks or fractures).

Limitations of RAPID Approach.

Damage in this paper is detected in an area with quite a bit of background noise despite the nearly perfect experimental conditions. The correlation analysis approach seems to be very sensitive to the environment as even small disturbances can have an impact on how the wave is received. This is because the underlying assumption of this analysis is that the baseline data was run in exactly the same conditions as the real time data that it is being compared to. Even small changes in the real time data may cause serious deviations from the baseline data. If used, a possible fix for this issue is to have multiple sets of baseline data for different conditions such as when the airframe is in flight, taking off/landing, or just stationary. Additionally, changes in pressure or temperature should be taken into account as these are likely to impact the real time data. This requirement of having multiple data sets would entail that each airframe be flown under typical usage conditions multiple times for each run, a costly process both temporally and financially. Future work on this same approach should quantify at what environment thresholds cause this method to be unable to discern a crack from pure noise. A few ideas could be running this same experiment but varying temperature, pressure, or even passing a constant airflow over the system. Thus, more work is needed to ensure that this approach is robust and resilient.

As the paper acknowledges, there is still a lack of an effective algorithm to co-operatively process the PWAS network data to yield accurate defect detection, size estimation, and localization. Dong and Kim [8] similarly concluded this as extracting and processing the PWAS data from the SMART layer does take significant amounts

of time. Zhao et al. also acknowledges one of the most serious shortcomings of the PWAS as strong attenuation and scarring impeded guided waves for large-area inspection once again confirming that monitoring a large scale airframe would require enormous amounts of sensors.

Space Application Potential.

Extending this technology to spacecraft introduces a different set of considerations but has great potential for usage given how crucial integrity of systems on the spacecraft. Unlike people in airframes, astronauts do not have the option to eject or bail out of the spacecraft if critical systems fail. Therefore, the margin of error for mistakes is far narrower making endeavors to reduce the risks of problems far more important. Researchers in Romania's National Institute for Aerospace Research, Enciu, Ursu, and Toader, demonstrate in their 2016 paper how the PWAS applications on airframes can be extended to space vehicles [9]. The most critical consideration for this potential application is the extreme conditions the PWAS will need to withstand namely cosmic rays (up to 1GeV), exposure to cryogenic or high temperature variations (120 deg C to -183 deg C), and high vacuum pressures.

For their experiment, Enciu et al. imitated the conditions in outer space by subjecting the PWAS to a temperature range of -70 to 200 deg C and a integral irradiation dose of 3.71 Gy/hr [9]. A full dose estimate for a mission to Mars under minimum solar activity is 15μGy/hr which is far lower than the testing dose of 3.71Gy/hr. The experiment was divided into two different test systems: free (un-bonded) PWAS and a PWAS centrally bounded to a circular aluminum 2024 disk. Each of the systems were subjected to temperatures from -70 to 150deg C and the 3.71 Gy/hr radiation.

Analysis of the PWAS performance is quantified through the electromechanical impedance spectroscopy (EMIS) method. Essentially, change in the EMIS signature is

due to the change in the integrity of the structure due to damage. This is because the PWAS is a high-frequency modal sensor and that they assumed change is exhibited only in the real part of the electromechanical impedance. This EMIS signature was calculated analytically, numerically, and verified by experimental records.

Results from both the tests on the PWAS and the PWAS bonded to a disk demonstrated that the temperature changes translate the EMIS signature but do not significantly change the signal and radiation produces almost no significant changes. For mechanical damage analysis, the EMIS signature produces small peaks surrounding the main signal when damage is introduced. These peaks increase in amplitude the closer the mechanical damage is to the PWAS itself. Therefore, Enciu et al. concluded that environmental factors only produce shifts in the resonance peaks and variations of the amplitudes while mechanical damage induces splitting of the resonance peaks.

Enciu et al. introduces different metrics for damage detection including a statistical processing of the damaged and pristine spectral signatures. Though not explicitly stated, these may be similar to the RAPID approach above using prior data to assist in detection. The other method introduced is an entropy method given by

$$H(p, ud_k) =$$
$$-\frac{1}{(C^u + C^{d_k})\log_2 n}\left[\left(\sum_{i=1}^{n}(R_i^u + R_i^{d_k})\log_2(R_i^u + R_i^{d_k})\right) - (C^u + C^{d_k})\log_2(C^u + C^{d_k})\right]$$

where p is the probability set, ud_k is the entropy versus the EMIS signature of the damaged specimen k going from 1 to 4, C^u being the sum of our impedance values over u, and R^u being the individual impedance values themselves [9].

In conclusion, the entropy method on results from a provided results confirming that only mechanical damage leaves a permanent mark while the environmental

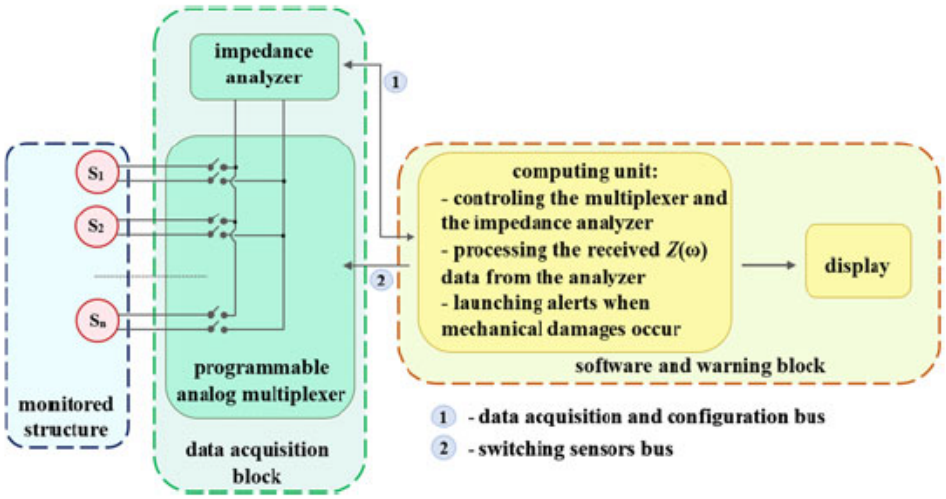

Figure 17. SHM System Implementation Scheme.

conditions did not. Like most works related to PWAS detection, the researchers noticed that the PWAS does not adequately detect the damage unless it is located at a close enough distance to the center listing 15mm as the maximum detection radius. Additionally, Enciu et al. also produced a flowchart for future SHM system implementation emphasizing a monitored array configuration, acquisition unit, and an appropriate user interface. This approach seems to correspond well with our CAFA approach earlier on in Chapter 2. Differences only seem to be in the specific tools and not the overall approach. Where Enciu et al. used the EMIS and entropy methods, we used the CAFA method. These EMIS and entropy methods testing the overall capability of the PWAS and not necessarily the specific performance of PWAS in different geometries or locations.

Limitations of Space Application.

This paper yielded that imperfections in PWAS bonding to structure and improper handling of specimens were not considered. Furthermore, the simulated harsh environmental factors tested on the PWAS were tested individually and seemed to be

tested simultaneously only once during the entropy method. Since these factors are all acting on the PWAS in space, PWAS robustness on the factors individually does not mean that the PWAS is robust to all the factors simultaneously. Future work related to this specific focus should ensure that PWAS robustness with all factors simultaneously is experimentally verified. Finally, the project that this paper stems from is supported by the Romanian Space Agency STAR Space SHM project which may have different applications that the United States Air Force given the difference in overall strategy and capability. The Air Force should verify in our own capacity that these same results for the PWAS hold for our aircraft as well.

Sensor Array Analysis and Justification.

Researchers at The Hong Kong Polytechnic University and China's Northwestern Polytechnical University Yu, Cheng, and Su created an active sensor array configuration dubbed the correlative sensor array (CSA) along with a signal processing algorithm to pinpoint thickness-holes in plate-like structures [23]. Yu et al. divides sensor array approaches into two categories: Inward accessing schemes and Outwards accessing schemes. Inward accessing schemes are identified by incident waves propagating inwards towards the inspection area where it is then received by the receivers. These schemes are similar to the ones used in Chapter 1 and various methods have been proposed to solving such a system but the core of these solvers rely on the fact that there is a significant difference between the time of flights and the wave transmitted/received. As long as there are at least two actuator-sensor paths, damage, in principle, can be triangulated. Outward accessing schemes have the sensor array in clusters centered within the inspection area. The main advantage here is that any boundary reflections will have less of an impact on the received signal. Although our assumptions for lamb waves are an infinitely long plate, the reality is that crack

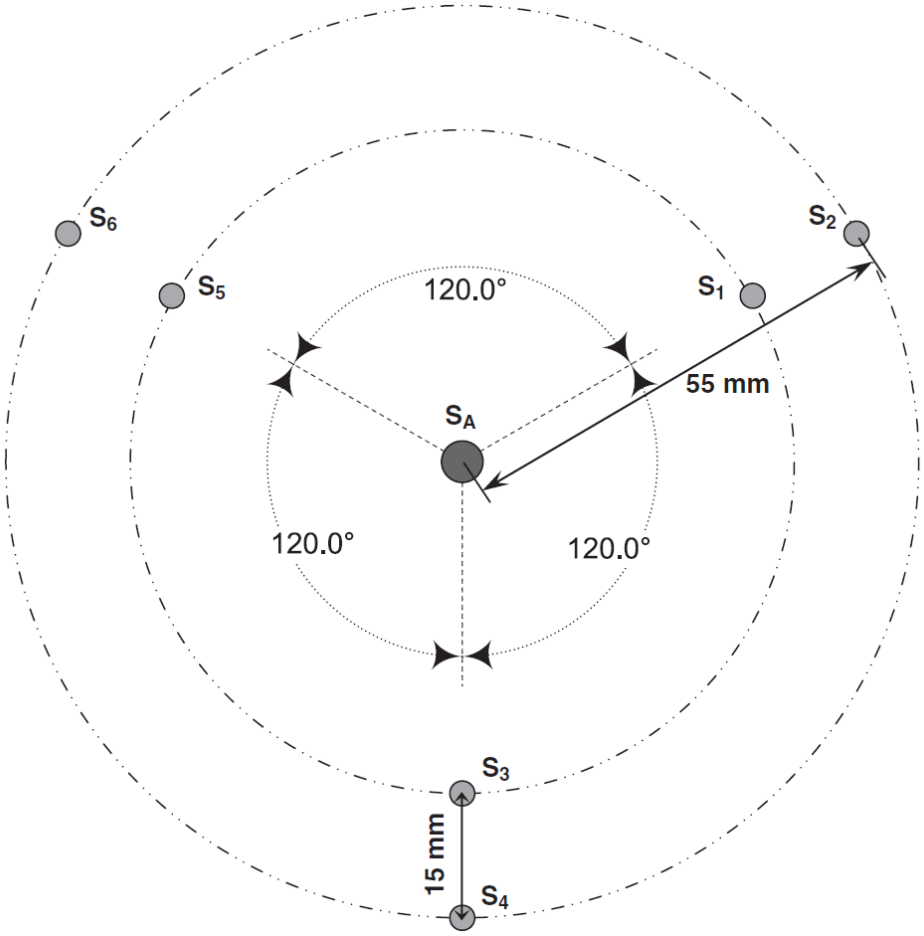

Figure 18. Correlated Sensor Array.

detection next to rivet holes may mean that there is a boundary close enough to be significant.

For their analysis, Yu et al. first used an incremental correlation coefficient comparison approach called the Moving-Window-Based Likelihood searching (MWLS) algorithm [23]. However, unlike RAPIDS, a high correlation coefficient means that there is a large chance that the damage is located at that area. This is because for this approach, the correlation coefficients are the indicator of the degree of similarity between two signals. At the extrema (damage location), this similarity would be at it's greatest since the damage signal would have overrode any other background noise

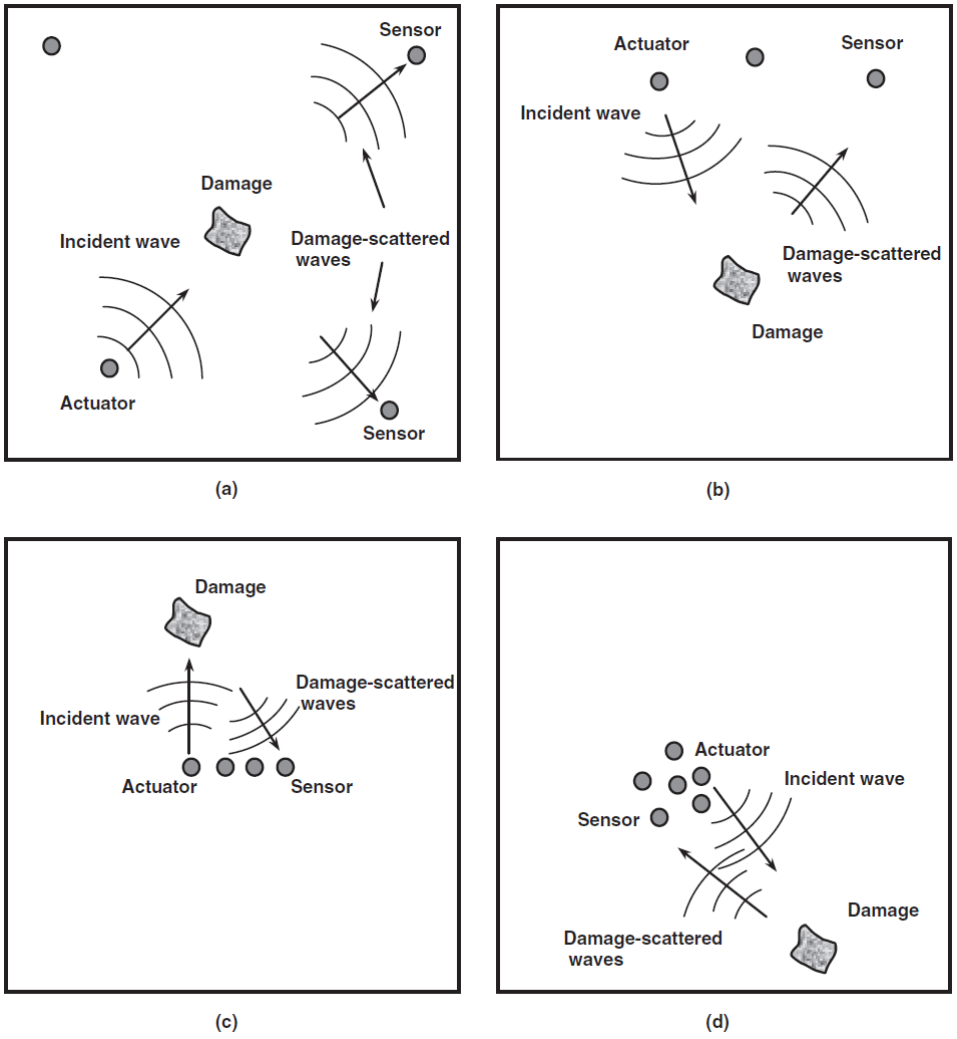

Figure 19. Sensor Array Schemes.

in the experiment.

Next, the researchers used a finite element (FE) simulation approach using ANSYS. The aluminum plate used had dimensions 600mm x 600mm x 1.5mm in size and meshed with eight-node brick solid elements with a through-thickness hole of 16mm. The location of the damage was selected randomly and the FE mesh was extremely fine near the hole similar to the CAFA approach. Also similarly to the CAFA approach in Chapter 1, in this study, the S0 mode was selected for damage identification because of, in contrast to A0, (1) its lower attenuation (the A0 mode

has the dominant outofplane movement of particles, leaking partial energy to the surrounding medium, whereas the S0 mode has mostly in-plane displacement and its energy is confined within the plate. Therefore, S0 manifests lower attenuation during propagation than A0; (2) faster propagation velocity, implying that complex wave reflection from structural boundary may be avoided; and (3) lower dispersion, facilitating signal interpretation. In addition, the S0 mode presents stronger reflection from throughthickness damage than the A0 mode [12], suitable for the CSA-based damage identification because a CSA substantially relies on the damage-reflected waves [23].

Overall, Yu et al. created a tool combining some of the previous ideas regarding correlation coefficients and time of flight for damage detection to create a new "outward accessing scheme" approach towards SHM. This lead to the creation of the CSA which was proven to be effective in detecting and locating a through thickness hole in an aluminum plate. The CSA is also robust to improper installation of individual sensors because of its clustering nature.

Limitations of Outward Accessing Schemes.

The outward accessing scheme introduces a concern that the damagereflected S0 mode may catch up with the outgoing A0 mode activated by the actuator that propagates at a lower velocity. This overlap is not so present in the inward accessing schemes because of the increased distance between the transmitter and receiver. Yu et al. did address this concern by setting up the criteria

$$\frac{L_{A-D} + L_{D-S_i}}{V_{S_0}} \geq \frac{L_{A-S_i}}{V_{A_0}} + w$$

where L_{A-D}, L_{D-S_i} and L_{A-S_i} are the distances between the damage and actuator, between the damage and sensor S_i and between the actuator and S_i, respectively. w is the length of the damage-scattered wave component in a signal, the same as that

of the incident diagnostic wave signal if wave dispersion and distortion are ignored. V_{S_0} and V_{A_0} are the propagation velocities of the S0 and A0 modes, respectively.

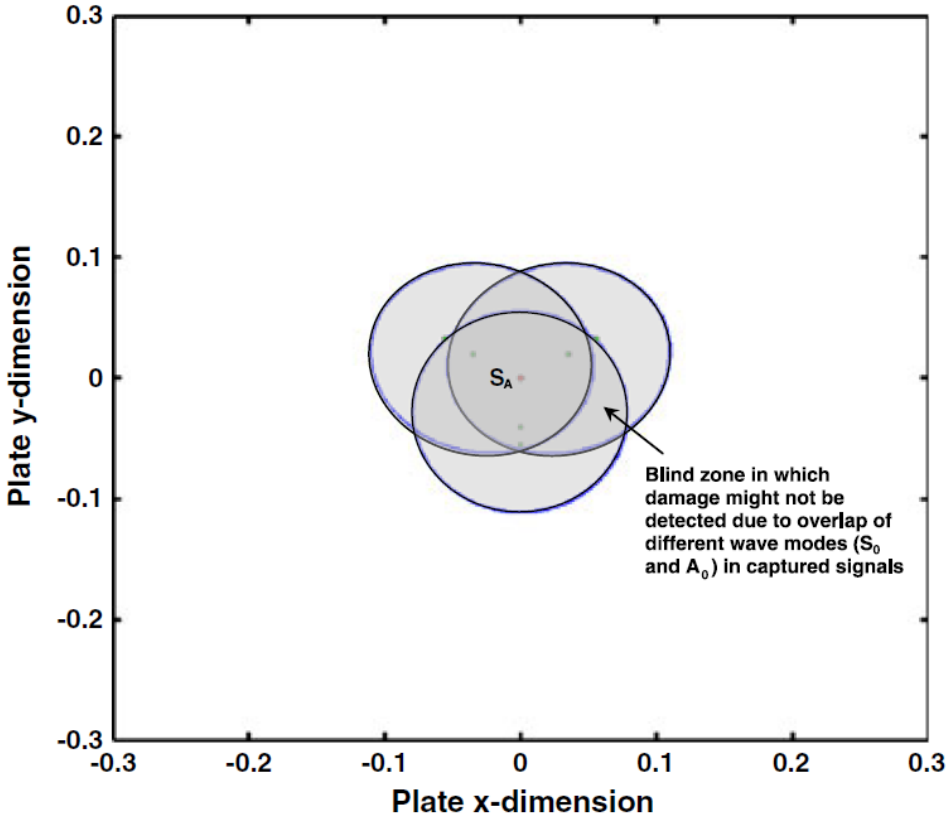

Figure 20. Blind Spots on CSA.

However, this blind zone is still a cause for concern since the PWAS already has such a limited detection range. Yu et al. stated that introducing more sets of CSA could reduce this effect [23]. However, this concession already implies that the system may not be optimized. In addition to the dull regions where the CSA is insensitive to change, the reduction in its ability to detect damage within that range impacts its overall effectiveness and utility, making improvements towards eliminating or minimizing such and effect a priority for future works.

The CSA was never truly tested in detecting through cracks on aluminum plates. In relation to the preliminary tests in Chapter 1, Yu et al. only showed that the CSA

was able to detect the hole with no crack. Given the significant geometry difference between a through-crack and a through-hole, future work should show that the CSA is actually able to detect a true example of damage and not just the hole around it.

2.4 Approach

From our literature review, we have determined that that field is still lacking in information confirming the effectiveness of a PWAS when both the transmitter angle and receiver distance are changed. Although each work has referred to the PWAS' impressive capabilities in detecting damage close to the sensor, not one of the works listed has considered comparing small changes in distances for the receiver and, with the CAFA, we are more than equipped to test this. Therefore, our next chapter will focus on this approach, filling this gap in confirmation in the SHM field.

III. Methodology

3.1 Overview

High sensitivity damage detection using piezoelectric material has been widely used in structural health monitoring (SHM) for decades. One of the main method in SHM based on using piezoelectric wafer active sensor (PWAS) are Lamb waves [18]. The Lamb wave method is used in time domain for detection and also localization of damage. An efficient numerical approach is required for fundamental understanding of the Lamb wave propagation in structure and designing of SHM network. For us to model these methods in complex geometries, the conventional finite element method (FEM) could be used. A linear FEM could be developed for modeling of Lamb wave and electromechanical impedance in structure; but to model these methods in high frequencies, a very fine mesh is needed to assure good accuracy. This very fine mesh requires a very large amount of Random-Access Memory (RAM). Therefore, this high degree of complexity leads to a significant decrease of solution speed in time and frequency domains. SHM using Lamb wave generation by PWAS attached to structure is commonly used for damage detection. In this method, a narrowband signal has been applied to actuator in order to propagate the Lamb wave in the structure where then sensor voltage is collected. Damage could appear as a wave reflection in sensor voltage. Recently, several papers have focused on decreasing of solution time for Lamb wave propagation in structures [5, 11, 16]. Ha and Chang applied hybrid spectral element method for simulation of Lamb wave in order to achieve faster computation and smaller memory requirements [11]. These theoretical models led to the development of low-cost tools for fast computer simulation of guided wave propagation.

In SHM by electromechanical impedance of PWAS, the PWAS is bonded to the

host structure using a high strength adhesive and a high frequency range (in the order of kilohertz) is applied to the PWAS. At high frequencies, the wavelength of the excitation is small, so this method becomes very sensitive and allows detecting minor changes in structure. Sepehry et al. proposed and developed theoretical model for a cantilever Euler Bernoulli beam [18]. Giurgiutiu calculated impedance of PWAS applying a continuous model of a beam and plate with PWAS [10]. In one study, 2D modeling of Kirchhoff plate with discrete singular convolution characteristic functions has been developed. Because Lamb wave generation and electromechanical impedance in high frequencies lead to a high DOF in modeling and consequently to a low speed simulation in frequency and time domains calculation, to use theses previously presented models in practice, one should apply model order reduction methods in SHM.

3.2 Prior Work

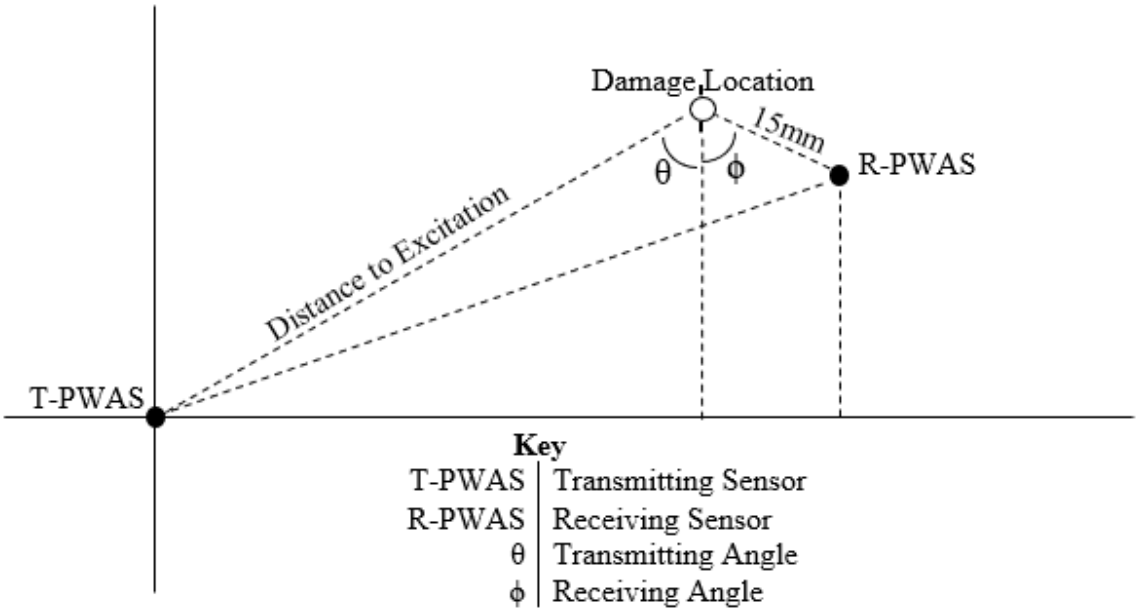

Figure 21. General Preliminary Experimental Schematic.

A preliminary project completed in relation to this effort was an application of Wave Form Revealer to generate received signals for 384 test configurations (See Figure 21). Test configurations included eleven different flaw sizes and five 2-level treatments (Receiver distance, Transmitter Angle, Receiver Angle, PWAS (Sensor) Size, Frequency). These signals were assessed for any factors that significantly impacted the signal and tested with a variety of detection algorithms to aid future SHM pursuits towards probability of detection.

Overview of Prior Work.

The transmitter and receiving sensors are PWAS which have been the subject of numerous studies. The transmitting sensor will send out a Lamb wave with a certain center frequency (200 or 550khz). When the wave hits the damage location, the damage location acts as a new wave source. The received signal at the R-PWAS is comprised of two parts: the direct incident waves from the T-PWAS and the scattered waves from the damage source. In this study, the scattered waves from the damage source are only considered.

Test Configuration.

Test configurations are combinations of the following variables:

Level	0	1	2	3	4	5	6	7	8	9	10	11
Flaw Size (mm)	0	0.32	0.64	1.28	1.92	2.56	3.2	3.84	4.48	5.12	5.76	6.4

Table 2. Flaw Sizes.

For our system, we are concerned with signal from damage on a sheet of Aluminum-2024-T3. The properties of this material are kept constant throughout the study. Sensing and damage locations are calculated from the configurations variables (Receiver Distance, Transmitter and Receiver Angles). Flaw size and transmitter angles

Factor	Recv. Dist.	Trans. Angle	Recv. Angle	PWAS Size	Freq
Low	150 mm	9°	5°	5 mm	200 khz
High	250 mm	27°	20°	7 mm	550 khz

Table 3. Factor Levels.

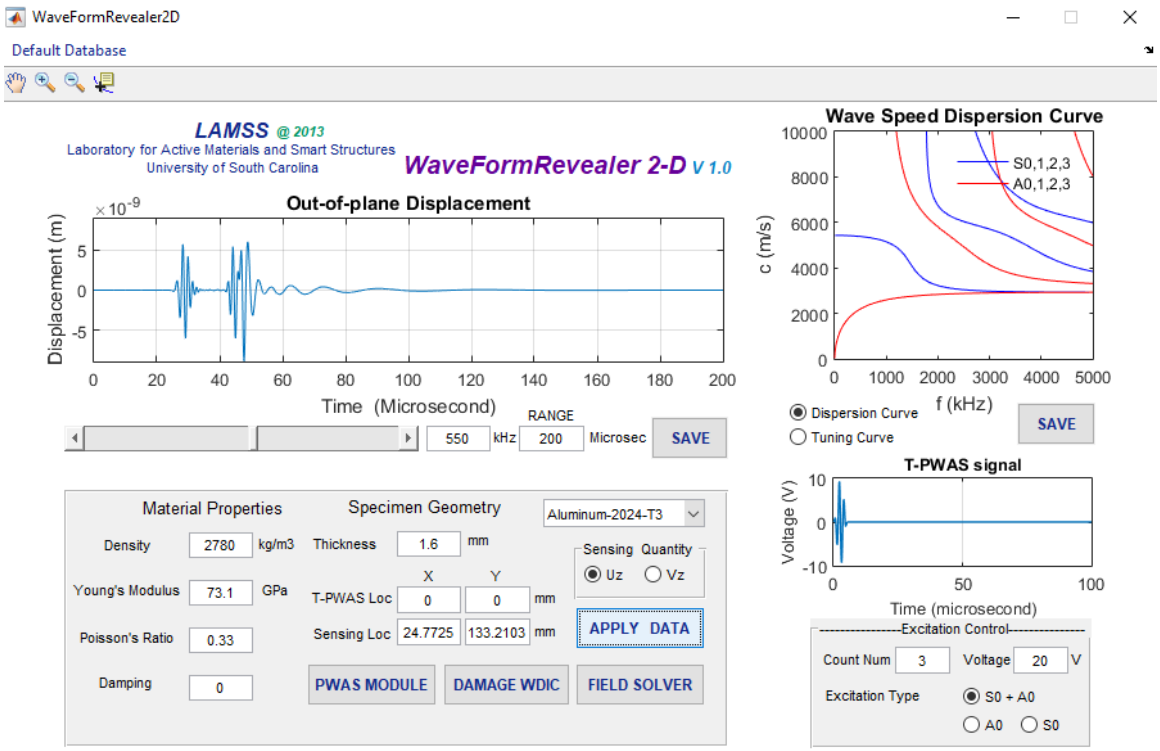

Figure 22. High Frequency Example.

are accounted for on the Damage WDIC (See Figure 24) dropdown menu which contains the WDIC generated from ANSYS in the Local FEM Harmonic Analysis stated in Chapter 2, Section 2.2. PWAS Size and Frequency are accounted by modifying the appropriate fields on the WFR2D user interface. For each configuration, the WFR2D saves the data onto an Excel file which is then manually compiled into Excel files sorted by Flaw Size and Transmitter Angle. By plotting these data points, the out-of-plane displacement graph is obtained over time (See Figures 22 and 23). Figure 22 further shows how higher frequencies create dual peaks in displacements. Addition-

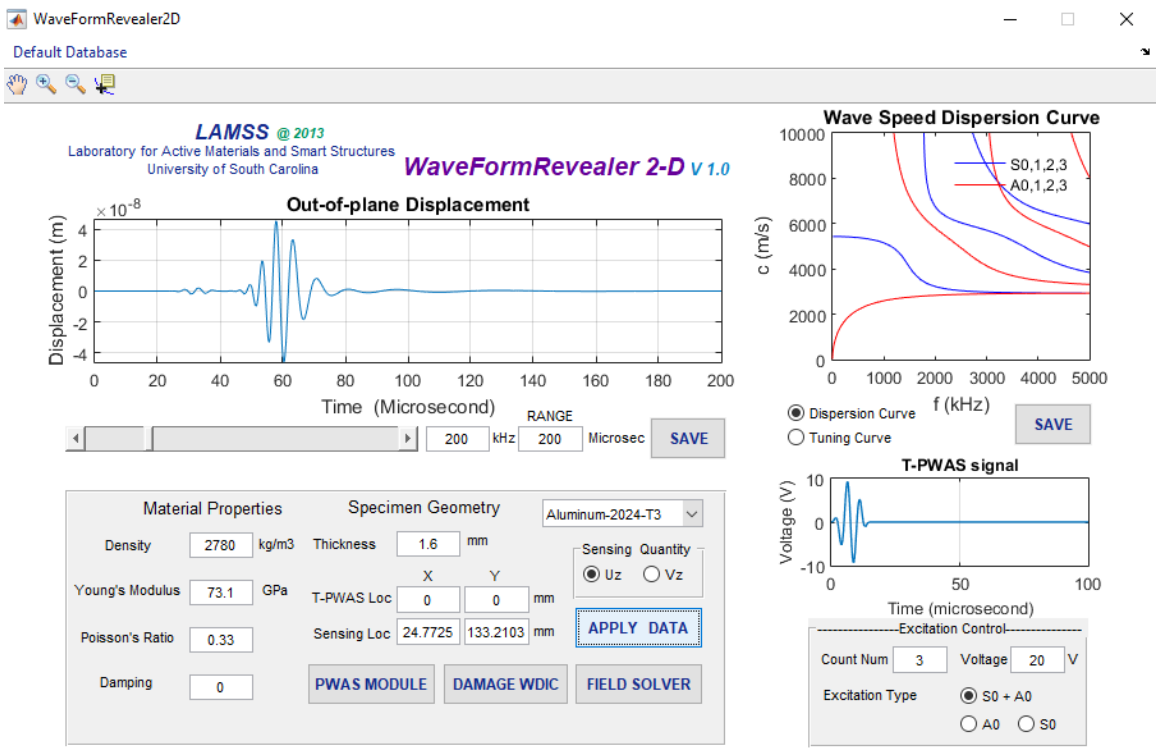

Figure 23. Low Frequency Example.

ally, the WFR2D creates a polar plot to demonstrate the scattering from the damage and rivet hole.

Research from C. Todd Owens (PhD. AFIT) [15] has shown that the reflection coefficients of real cracks are not constant over the crack length (See Figure 25). Results at the start of the crack revealed that reflection coefficients approach 1.0, indicating that a notch can accurately model this portion. As the results progressed further down the crack towards the tip, the reflection coefficients decrease significantly and approach 0, suggesting that a notch model may not be the most accurate approach. The objective of this research will build upon this potential of an improved model by utilizing variable reflection coefficients on existing numerical models. This advancement will allow models to generate more accurate representations of scattering from cracks of a certain length. This is an important cornerstone for detection systems

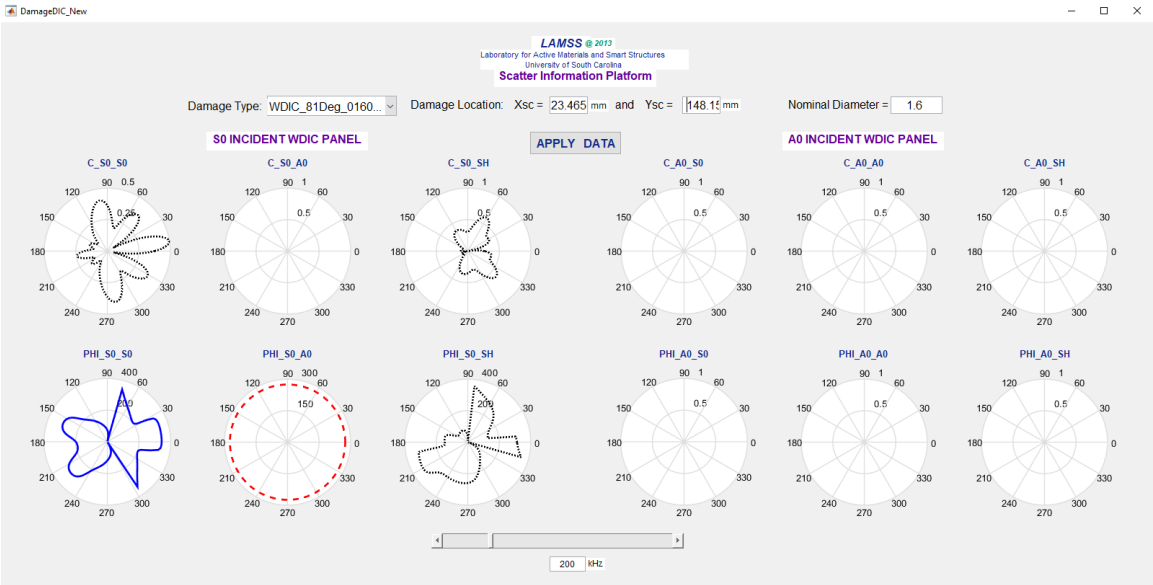

Figure 24. Sample Polar Plots from WDIC.

which compare received signals to model generated signals to characterize damage.

Additionally, from a joint paper published in [17], we used a fractional full factorial design to determine what SHM factors have a significant effect on the system. We first generated signal data for $(n+1)2^k$ test configurations where n is the number of different flaw sizes and k is the number of 2-level treatments considered. In this study, eleven flaw sizes (0-6.40mm at 0.32mm increments) and five 2-level treatments (Receiver Distance, Transmitter Angle, Receiver Angle are considered, giving 384 total configurations. For each configuration, we generate data every $1e^{-7}$seconds until $1e^{-3}$seconds, giving us 10,000 data points for each configuration. From here, we created three measures of damage index relative to the baseline signal to assist in our analysis: a correlation coefficient (DIcc), sum of squared deviation (sqdev), and the difference in peak amplitude (diffPA) [17]. The equations for these metrics are:

$$\text{DIcc} = 1 - \rho = 1 - \int_{t_{min}}^{t_{max}} f(t)g(t)\ dt \Big/ \left(\sqrt{\int_{t_{min}}^{t_{max}} f^2(t)\ dt} \sqrt{\int_{t_{min}}^{t_{max}} g^2(t)\ dt} \right),$$

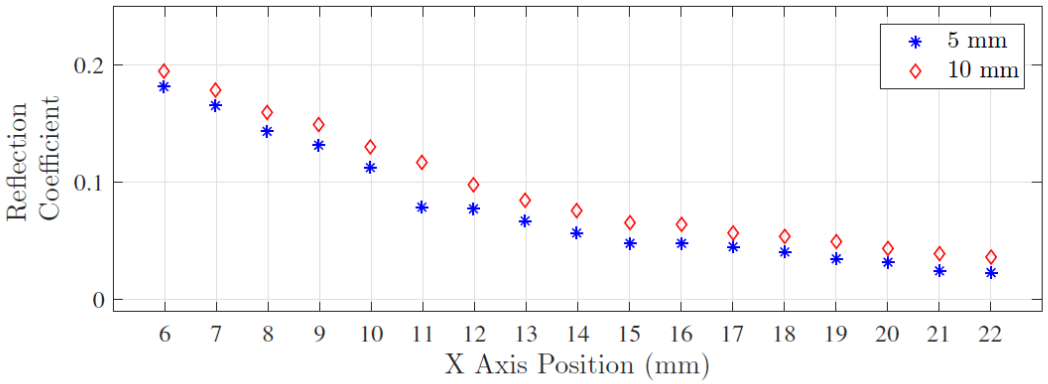

(b) RC for A_0 mode.

Figure 25. Crack Non Constant Reflection Behavior.

$$\text{sqdev} = \sum_{t_{min}}^{t_{max}} \left(g(t) - f(t)\right)^2 .$$

Finally, the difference in peak amplitude (diffPA) was computed by taking the difference in the maximum amplitudes between the two signals within the analysis window [17]. All three damage indices failed the Shapiro-Wilks test for normality so we transformed each by taking the natural logarithm. Results showed that for lnDIcc, transmitter angle (A), frequency (C), and distance to excitation (E) accounted for 97% of the total variance in the data. For lnsqdev, transmitter angle with frequency (AC) and transmitter angle with distance to excitation (AE) cross terms accounted for 98% of the total variance in the data. For lndiffPA, the three-way interaction of transmitter angle, receiver angle, and frequency (ABC) seemed to account for 78% of the total variance in the data. Variables sensor size (D) and crack size (F) did not seem to have an effect.

As a supplement to this work, we generated data for an exaggerated range of sensor sizes (1mm to 11mm in width) to observe if any of these values had a significant impact to the system. From there, we take the natural logarithm of each value to assist in data analysis. The R^2 value for generated data near 0, indicating that the

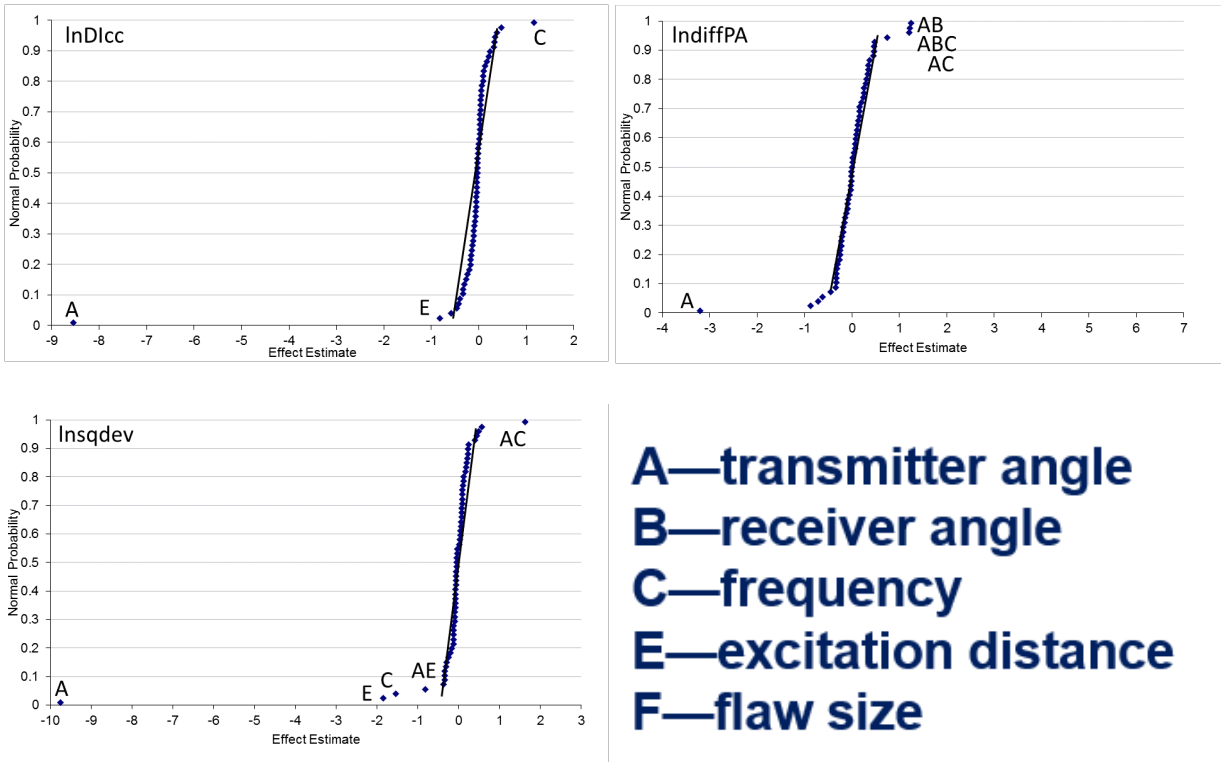

Figure 26. Lognormal Probability Plots for the damage index for the correlation coefficient ln(DIcc), difference in peak amplitude ln(diffPA) and sum of squared deviations ln(sqdev).

data from the model shows no correlation with the data generated. This means that the model does not explain any of the variability in the generated data. As a result, we concluded that sensor size has no significant impact on the accuracy of the PWAS readings. Therefore, we can safely assume in our subsequent works that we can arbitrarily choose our sensor sizes in the range 1mm to 11mm.

3.3 Limitations

In our preliminary study, we only generated data for one specific type of material. These sensors could possibly produce differing results in accuracy for different materials. Additionally, this generated data is not tested against any live observed data which leaves a question of accuracy with respect to a live model. Our test con-

figurations only factor in 2-level treatments. Higher level treatments will yield more insight as to how a treatment directly affects the output out-of-plane displacement. Additionally, a study done by the University of Florida has shown that it would take around 10,000 sensors to assess the entire fuselage areas of a Boeing 737NG totaling combined 1,000 lbs increase in weight after factoring the sensors, cables, and connections ports. This significant loss of payload would result in an average revenue loss of about $50 million per aircraft, far outweighing the potential financial benefit of $5 million from reducing maintenance cost [8]. For the Air Force, where planes often do not fly at capacity, the extra weight means that more fuel is required for the planes. This extra fuel compounds the weight issue and additionally, may impact airframe capabilities such as maneuverability and sustainability. For example, a fighter with extra weight on its wings may not be as aerodynamic, impacting its ability to perform evasive actions, creating a potentially life-threatening issue for the pilot. Additionally, there is the question of sensor reliability since we are assuming that all sensors are maintained in good condition with no degradation.

In our study, we only generated data for one specific type of material. These sensors could possibly produce differing results in accuracy for different materials. Additionally, this generated data is not tested against any live observed data which leaves a question of accuracy with respect to a live model. Our test configurations only factor in 2-level treatments. Higher level treatments will yield more insight as to how a treatment directly affects the output out-of-plane displacement.

3.4 Well Posedness

Recall the PDE for the displacement vector

$$\mu\nabla^2 u + (\lambda + \mu)\nabla(\nabla \cdot u) = \rho\ddot{u}.$$

Before we do any analysis on our system, we must first prove that a solution to our PDE exists, is unique, and continually depends on the data given.

Existence.

To show that a solution exist for our PDE, we must show that if we consider the PDE as a functional acting on our displacement vector, the functional is bounded and continuous. Our boundary conditions bound the PDE from the top and below but do not bound the displacement vector in other directions since we are working in an infinitely long plate.

Uniqueness.

Supposed that u and v are both solutions to our PDE and $w = u - v$, then we have

$$\mu\nabla^2 u + (\lambda+\mu)\nabla(\nabla\cdot u) - (\mu\nabla^2 v + (\lambda+\mu)\nabla(\nabla\cdot v)) = \rho\ddot{u} - \rho\ddot{v}$$

with $w = 0$ on the boundary,

$$\begin{aligned}
\int_V w\cdot(\mu\nabla^2 w + (\lambda+\mu)\nabla(\nabla\cdot w))\ dV &= \int_V \rho\ddot{w}w\ dV \\
\mu\int_V w\cdot(\nabla^2 w)\ dV + (\lambda+\mu)\left[\int_{\partial S} w(\nabla\cdot w)\cdot\hat{n}\ dS - \int_V (\nabla\cdot w)^2\ dV\right] &= \int_V \rho\ddot{w}w\ dV \\
\mu\int_V w\cdot(\nabla^2 w)\ dV - (\lambda+\mu)\left[\int_V (\nabla\cdot w)^2\ dV\right] &= \int_V \rho\ddot{w}w\ dV \\
\int_V \rho\ddot{w}w - \mu w\cdot(\nabla^2 w) + (\lambda+\mu)(\nabla\cdot w)^2\ dV &= 0 \quad [22] \\
\int_V \rho\ddot{w}w\ dV &= 0 \\
\therefore w &= 0
\end{aligned}$$

Continuous Dependence.

Define

$$L(u) := \mu\nabla^2 u + (\lambda+\mu)\nabla(\nabla\cdot u).$$

The energy estimate is then

$$E(L(u)) := \int_\Omega u\cdot\mu\nabla^2 + (\lambda+\mu)\nabla(\nabla\cdot u)\ dV = \int_\Omega u\cdot\vec{f}\ dV.$$

We want the energy to be continuously dependent on $\vec{f}$. Introduce vector field norm:

$$||\vec{A}||_{H^1(\vec{\nabla}\cdot+\vec{\nabla}\times,\Omega)} = \int_\Omega |\vec{A}|^2 + |\vec{\nabla}\times\vec{A}|^2 + (\vec{\nabla}\cdot\vec{A})^2\ dV$$

where $|\vec{A}| = |A_x^2 + A_y^2 + A_z^2|$

Claim: if $f=0$, then $E(L(u))=0$, and if $||\vec{f}||_{H^1(\vec{\nabla}\cdot+\vec{\nabla}\times,\Omega)} < M$ then $|E(L(u))| < kM$ for some constant $k<\infty$. Separating our integral into two parts,

$$\int_\Omega u\cdot(\mu\nabla^2 u + (\lambda+\mu)\nabla(\nabla\cdot u)\ dV = \mu\int_\Omega u\cdot(\nabla^2 u)\ dV + (\lambda+\mu)\int_\Omega u\cdot\nabla(\nabla\cdot u)\ dV.$$

Using Green's 1st Identity on the first half,

$$\mu\int_\Omega u\cdot(\nabla^2 u)\ dV = \mu\left[\int_{\partial\Omega} u\cdot\frac{\partial u}{\partial n}\ dS - \int_\Omega ||\nabla u||^2\ dV\right].$$

Integrating by parts on the second half,

$$(\lambda+\mu)\int_\Omega u\cdot\nabla(\nabla\cdot u)\ dV = (\lambda+\mu)\left[\int_{\partial\Omega} u(\nabla\cdot u)\cdot\hat{n}\ dS - \int_\Omega(\nabla\cdot U)^2\ dV\right].$$

Therefore,

$$E(L(u)) =$$
$$\mu\left[\int_{\partial\Omega} u\cdot\frac{\partial u}{\partial n}\,dS-\int_{\Omega}||\nabla u||^2\,dV\right]+(\lambda+\mu)\left[\int_{\partial\Omega}u(\nabla\cdot u)\cdot\hat{n}\,dS-\int_{\Omega}(\nabla\cdot U)^2\,dV\right].$$

Our boundary integrals for the top and bottom are "free boundaries" while the sides satisfy the Sommerfeld radiation condition since the energy scatters to infinity. Therefore, on the boundaries, the energy does continually depend on $\vec{f}$.

3.5 Experimental Setup

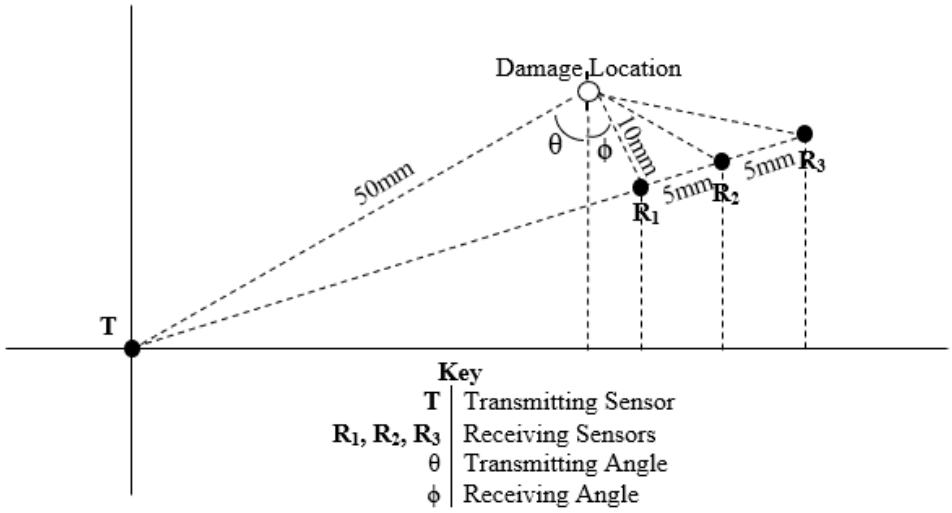

Figure 27. Test 1 Schematic.

For our analytical model we use the WaveFormRevealer2D (WFR2D) created by LAMSS at the University of Southern Carolina in order to test our system before we make any attempts to perform live tests. In our tests, we will be using a 7mm diameter 0.2mm thick circular PWAS, 100mm long 2.032mm thick aluminum 2024-T3 plate, 30mm non reflective boundary to model the infinite plate assumption. Alumninum 2024 is one of the most common alloys used in aircraft [6] so our choice in material

for our experiment directly tests a potential live application material. The rivet hole will be 1.6mm on which the damage will be a through crack of length 16mm. The signal center frequency will be set constant to 200kHz. Generated data will be the out-of-plane displacement values for the S0 mode from 0 to 1e-03 and incrementing by 1e-07 seconds giving us 10,000 data points for each configuration. From here we can see that our ωd referenced in Chapter 1, Section 1.3 is 406.4 kHz·mm which is significantly below our thresholds for higher order mode effects in the reproduced Figure 28. Thus, our choice in frequency is appropriate since it allows us to use the S0 for comparison in detection analysis without having to consider confunded signals from the A0 or higher order modes.

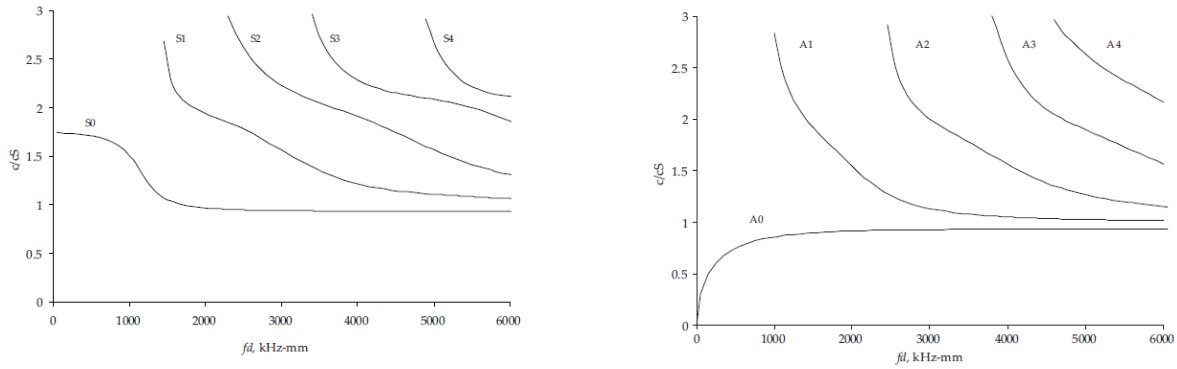

Figure 28. Symmetric and Antisymmetric Lamb wave speed dispersion curves (c_s is the shear wave speed, d is the half thickness of the plate. [10])

For our finite element meshing we use SOLID5 Coupled field element for the PWAS, COMBIN14 spring-damper element for the non-reflective boundary, and the SOLID45 structure element for the aluminum. Through the WFR2D, we will be using the CAFA approach in our analysis. For our experiment, we we will be testing two different transmitter locations and three different receiver locations. From the schematic, all the PWAS sensors are placed in a line simulating a linear array of sensors. This type of array makes the most sense near an aircraft wing where damage next to rivet holes are more likely to occur. Distances here were chosen to check to

see if small variations to the receiver distance have a significant effect on the signal and to check to see if transmitter location closer to the damage and receiver location had a significant effect.

For simplicity, we set the location of all transmitters to be at (0,0). For our distances, we set the distance from the transmitters to the damage to 50mm and the distance from the first receiver to the damage to 10mm. We also set $\theta = 9°$ and $\phi = 5°$. The locations of the other sensors are calculated through rudimentary trigonometry. The resulting locations for each sensor satisfying the initial conditions given in the the schematic are

	D_X	**D_Y**	**R1_X**	**R1_Y**	**R2_X**	**R2_Y**	**R3_X**	**R3_Y**
T1 (27°)	22.700	44.550	23.571	34.588	24.972	39.388	26.373	44.188
T2 (9°)	7.822	49.384	8.693	39.422	9.770	44.305	10.847	49.188

Table 4. Damage and PWAS Coordinates

Observe that the farthest receiving sensor is R_1 at 10mm away from the damage location.

We divide our experiment into two different test for different transmitting locations, varying the receiver locations in each test. Before each test, we do a quick check to ensure that the transmitter is able to detect the hole without the crack.

For our both transmitters, we notice that all receivers seem to detect the hole well with differing amplitudes and phases as expected shown in Figures 29 and 30. Each signal has three major peaks which is reasonable given the shape of our incident wave, which also has three major peaks.

3.6 Data Analysis

Recall the three measures of damage index relative to the baseline signal: a correlation coefficient (DIcc), sum of squared deviation (sqdev), and the difference in peak amplitude (diffPA) [17]. The equations for these metrics are:

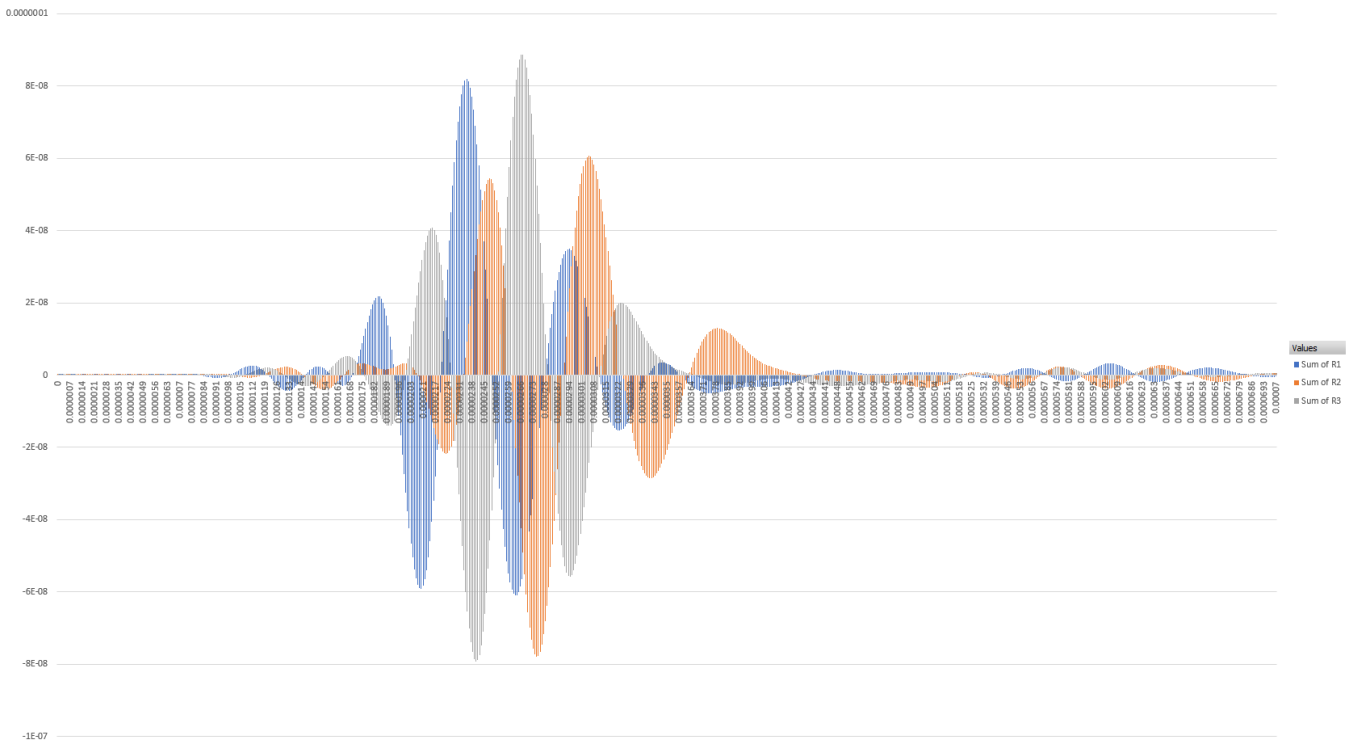

Figure 29. Test 1 with Only Rivet Hole ($\theta = 9°$).

$$\begin{aligned} \text{DIcc} = 1 - \rho &= 1 - \int_{t_{min}}^{t_{max}} f(t)g(t)\ dt \Big/ \left(\sqrt{\int_{t_{min}}^{t_{max}} f^2(t)\ dt} \sqrt{\int_{t_{min}}^{t_{max}} g^2(t)\ dt} \right) \\ &= 1 - \frac{< f, g >}{||f||||g||}, \end{aligned}$$

$$\text{sqdev} = \sum_{t_{min}}^{t_{max}} \left(g(t) - f(t) \right)^2,$$

and the difference in peak amplitude (diffPA) was computed by taking the difference in the maximum amplitudes between the two signals within the analysis window [17]. To achieve damage detection in our results, we must quantify what detection is through one or a combination of these metrics. For our experiment, detection is detected if the diffPA is more than 5% of the baseline signals peak amplitude, sqdev

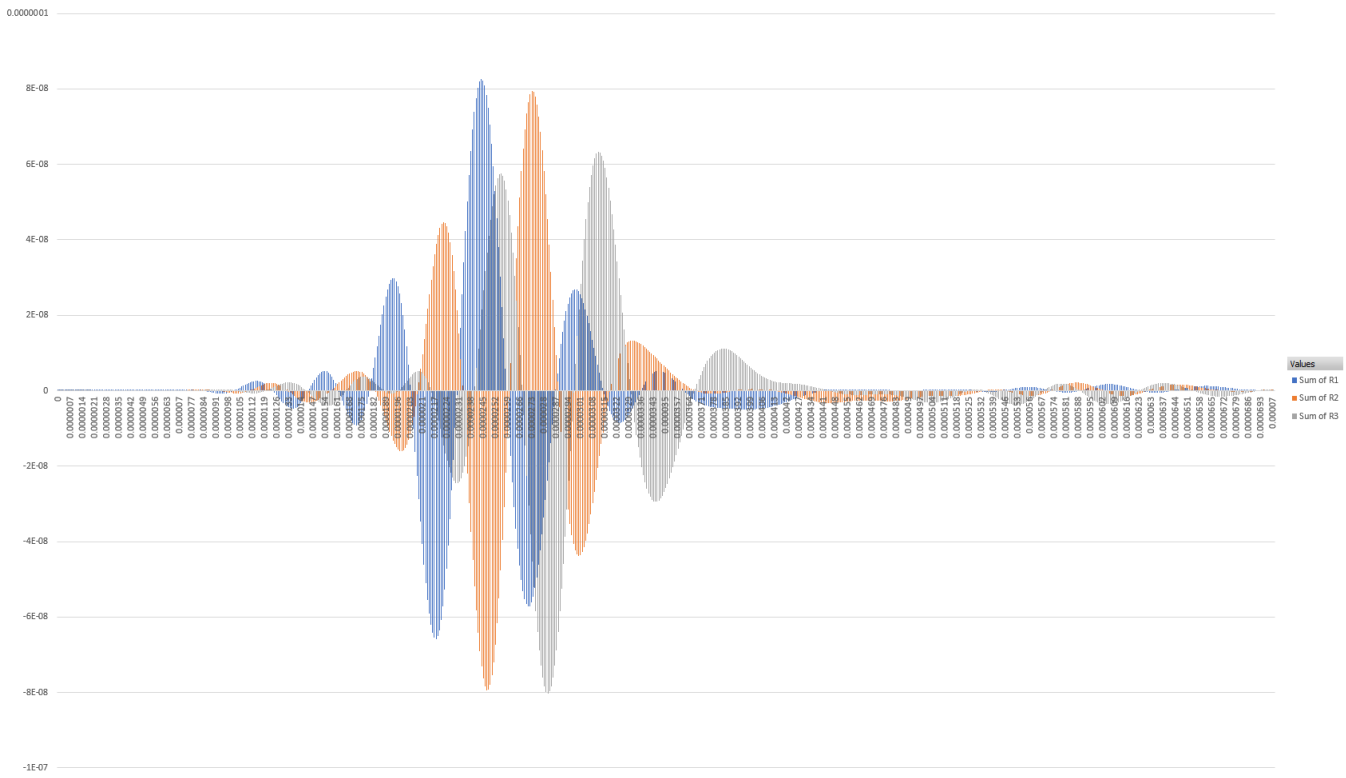

Figure 30. Test 2 With Only Rivet Hole ($\theta = 27°$).

is more than 5% of the baseline signals sum of squares, and DIcc is above 0.05.

3.7 Assumptions in Methodology

For our displacement vector, we assume that the medium (material) is homogeneous, isotropic, and linearly elastic. We assume that the crack is a through crack with constant width. A through crack here meaning that the crack is of uniform thickness passing through the material as apposed to a half-through crack that only passes halfway through. Additionally, we assume that the traveling waves travel through an infinitely long plate with no reflections. Additionally, we assume that all external physical conditions including temperature and pressure are held constant throughout our tests.

3.8 Limitations in Methodology

Much like other researchers have found, the PWAS has a very limited range in detection. Given the scope of the current field, there does not seem to be a a clear fix to address this so this limitation is reasonable for our work. However, we must ensure that the damage locations are relatively close to both the transmitting and receiving sensors. In a practical sense, this is a fairly large limitation as this is the main reason why so many sensors are needed to adequately monitor an entire airframe system. As advancements are made, future physical adjustments could improve detection radius of the PWAS but this endeavor is outside the scope of this thesis.

IV. Results

4.1 Data Scrubbing

For our experimental results, we adjust the data ranges in order to facilitate our analysis. For example, we noticed that the received wave arrives within 7×10^{-5} seconds. Compared to the received wave's signal, no other significant results are obtained past this time. This justifies us removing the data past this point in order to simplify analysis. Since our work is focused on detection capabilities, the time the received wave arrives to the sensor is not a contributing factor, only the strength of the received signal, which means that removing superfluous data does not impact our results.

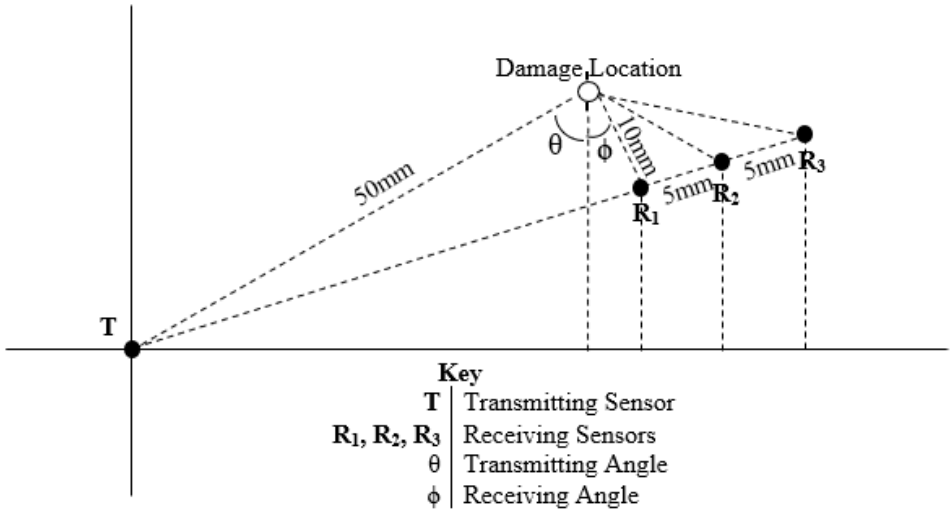

Figure 31. Test 1 Schematic.

4.2 Test One

For our first test, we narrowed down our viewing window from the 10,000 data points generated to the 702 points that actually illustrated the signal data. From

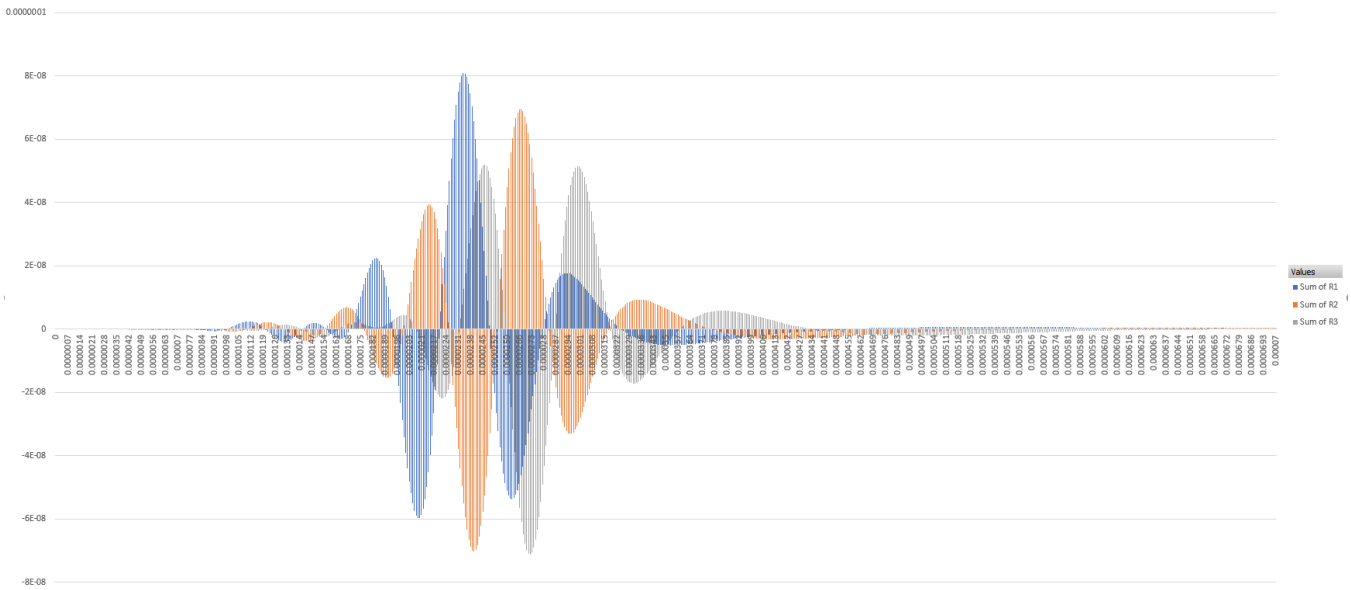

Figure 32. Test 1 Received Signals ($\theta = 9°$).

our first test results in Figures 32 to 35, the different receiver locations do make a significant difference in our results regardless of transmitter angle. Just incrementing 5mm steps provide completely different received signals. From our overall signal graph, it is difficult to see if there were any changes from the preliminary test results. Thus, we take the difference between these two data sets and obtain an appropriate metric to observe whether or not damage is being detected correctly. We see that for R_1, there is comparatively very small difference between the received signal from the damage and the received signal from just the hole. This means that at 10mm, the PWAS does detect the damage but not very strongly. This is in contrast to the the other two receiver locations of R_2 and R_3. It is important to note that these receiver locations are closer than R_1. This test confirms that the closer the damage is to the PWAS, the better the detection and that the PWAS is sensitive to small changes in damage locations. Additionally, this test reveals that the smaller the transmitter angle size, the more accurate the detection capability. However, this is mainly due to the fact that the smaller the transmitter angle the closer the

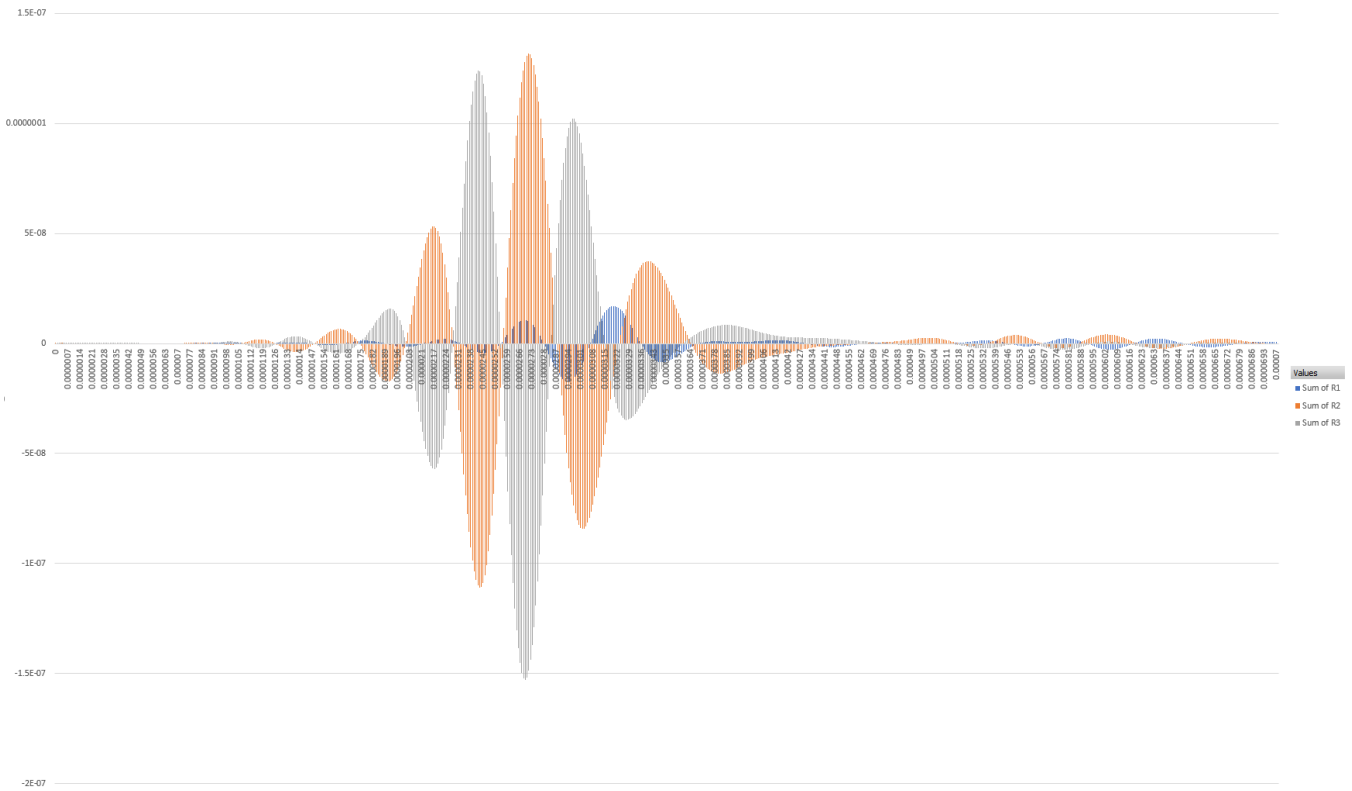

Figure 33. Test 1 Detection Analysis ($\theta = 9°$).

PWAS is to the transmitting sensor. Thus, distance is factor for both the transmitter and the receiver. Reducing either of those distances significantly increases detection capability. For the transmitters, we notice a slight difference in the signal from our change of 15mm. This is to be expected since 15mm in relation to the PWAS should produce a noticeable change. Therefore, we have confirmed that the PWAS is sensitive to transmitter location changes and will likely be effective in detecting damage even if our transmitter is not in its ideal location.

4.3 Long Distance Test

A major limitation in our first test is that the incrementing distance of 5mm is 10% of the transmitter distance and that the receiver is only at most 10mm from the damage. These conditions are ideal for a PWAS for damage detection since supporting

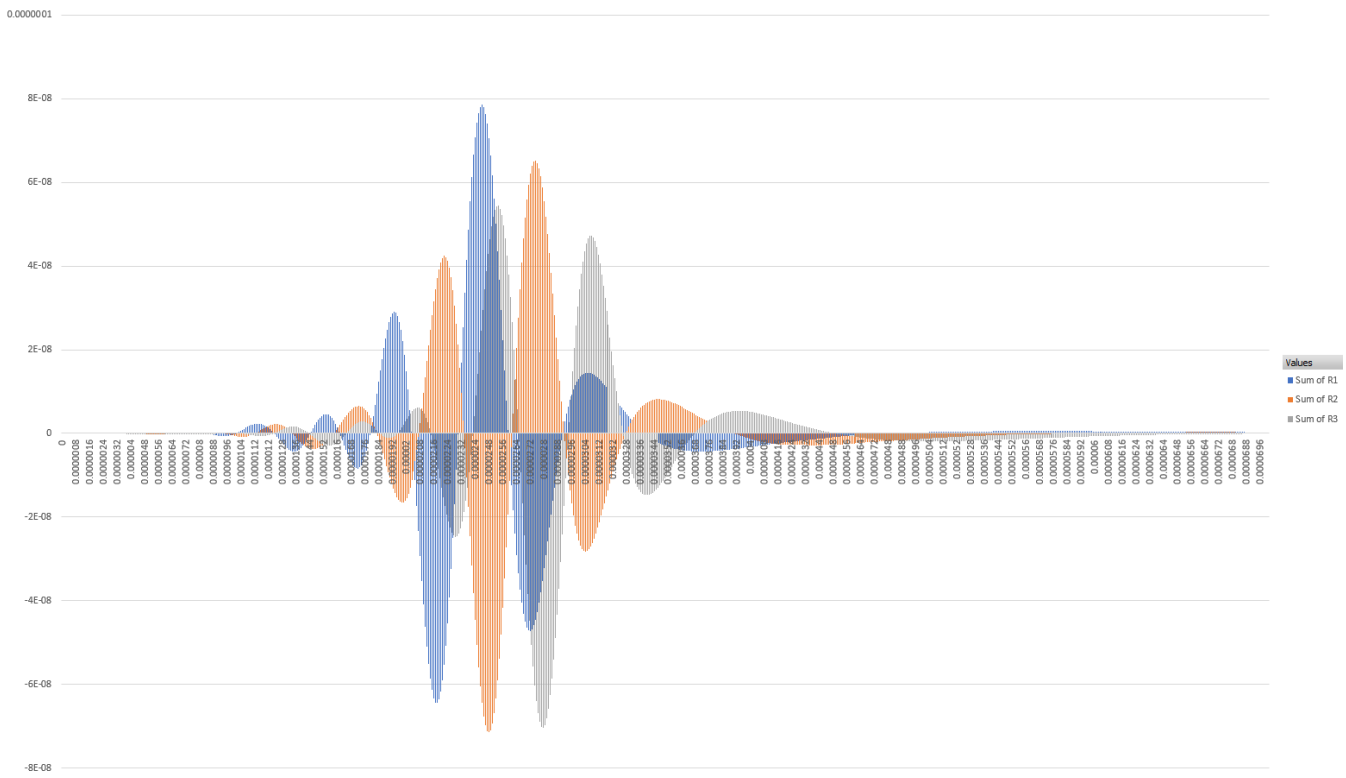

Figure 34. Test 1 Received Signals ($\theta = 27°$).

literature has stated that the PWAS is highly effective within a radius of 15mm [8]. Furthermore, being able to place the PWAS 50mm (5cm) away from the damage consistently is not a reasonable possibility. Therefore, we check an upper extrema for the PWAS sensor detection radius in order to induce more realistic conditions for a PWAS.

For this upper range, we place the transmitting PWAS 1000mm (1 meter) away from the damage source and the receiver PWAS 50mm from the damage source. Additionally, this test will provide an adequate reading of how comparatively small changes in receiver distances impact the PWAS detection capabilities. This was tested in the previous experiment, however, in this case the 1000mm distance from the transmitter to the damage is far larger than the incremental distance of 5mm. Although these values seem comparatively high in relation to our previous test and

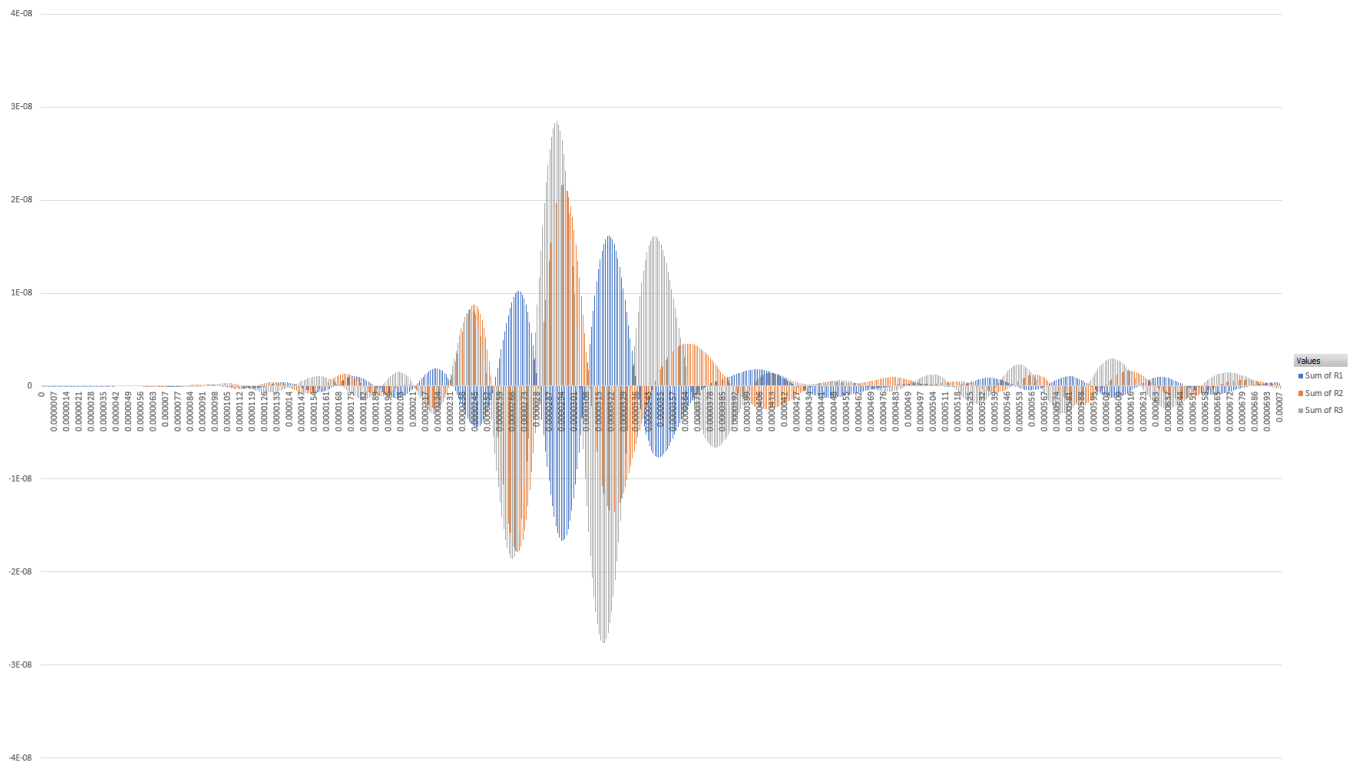

Figure 35. Test 2 Detection Analysis ($\theta = 27°$).

literature, they are not unreasonable since it is quite likely the PWAS will need to detect damage accurately from this distance in real-time applications in the future. For this test, we set our transmitter angle to be $\theta = 9°$.

In Figures 36 - 38, the received signal is overshadowed by a large signal past the signal receiving range. From these graphs, it is far more difficult to draw any conclusions about detection capability due to this overshadowing. This large value is the A0 dispersive wave. Since we are looking at the out-of-plane displacement, the A0 signal is stronger than the S0. Although we are only focused on the S0 wave, our current experimental setup does not have an equal and opposite PWAS attached directly on the opposite of the plate to cancel out the A0 mode and, thus, the A0 mode is present. The reason why we did not see the A0 mode in our other test is because our transmitter distance was comparatively low. Since we are not concerned

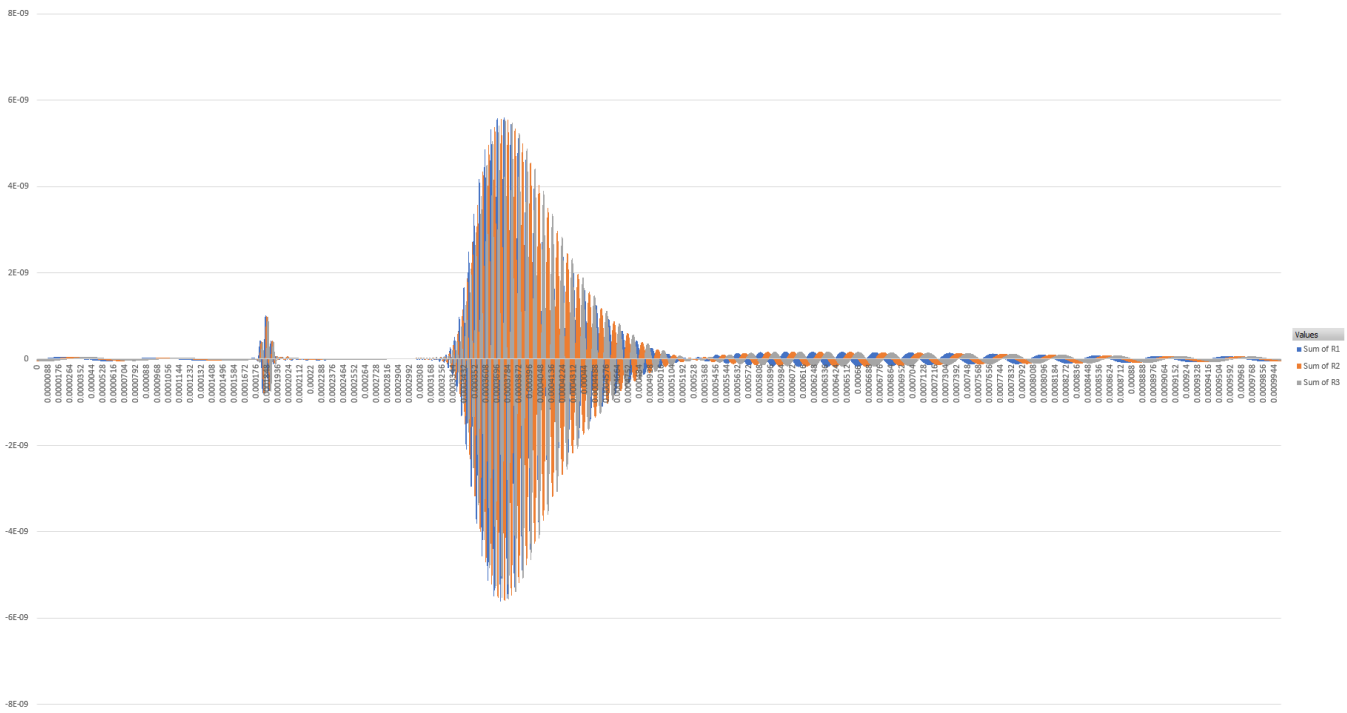

Figure 36. Long Distance Received Signals ($\theta = 9°$, D = 1000mm).

about the A0 results, we narrow our data range from the 10,000 generated data points to 352 in order to have a better idea of what our received signal, S0 actually is. Compared to our viewing window in the first test, 352 data points is about half the size of the 702 data points used before. Much like the reason why the A0 mode being present, the smaller viewing window is because of our significantly increased transmitter distance.

With our new data range shown in Figures 39 - 41, we can see that the PWAS is still able to see a slight difference between the three receiver distances. The amplitude difference here is not as pronounced but the phase difference seems to be exactly the same. Increasing the distance between the sensors and damage, therefore, seems to only impact the amplitude at this point and does not seem to have a significant effect on phase. From these results we can say that the transmitter PWAS is sensitive to receiver PWAS distance changes even with the increased distances for both the trans-

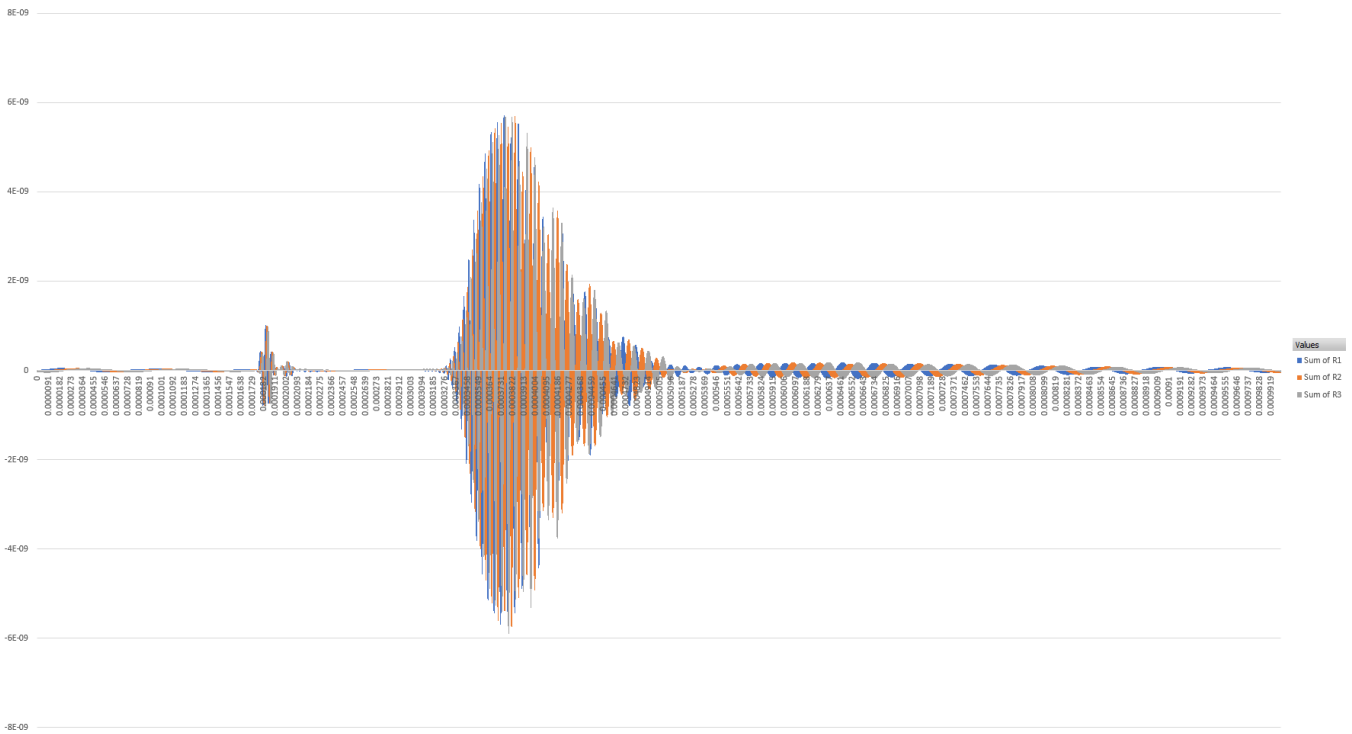

Figure 37. Long Distance Signal With Only Rivet Hole ($\theta = 9°$, D = 1000mm).

mitter and receiver. Ultimately, this confirms that the PWAS has a high potential for real-time utilization given its detection capabilities one meter away from the damage. Additionally, the PWAS used in this case was only 7mm. With a detection radius of at least 1000mm, this ratio of PWAS size to detection radius demonstrates just how useful the PWAS can be in future applications.

4.4 Damage Detection Metrics

Our three measures of damage index are: a correlation coefficient (DIcc), sum of squared deviation (sqdev), and the difference in peak amplitude (diffPA) [17]. The equations for these metrics are:

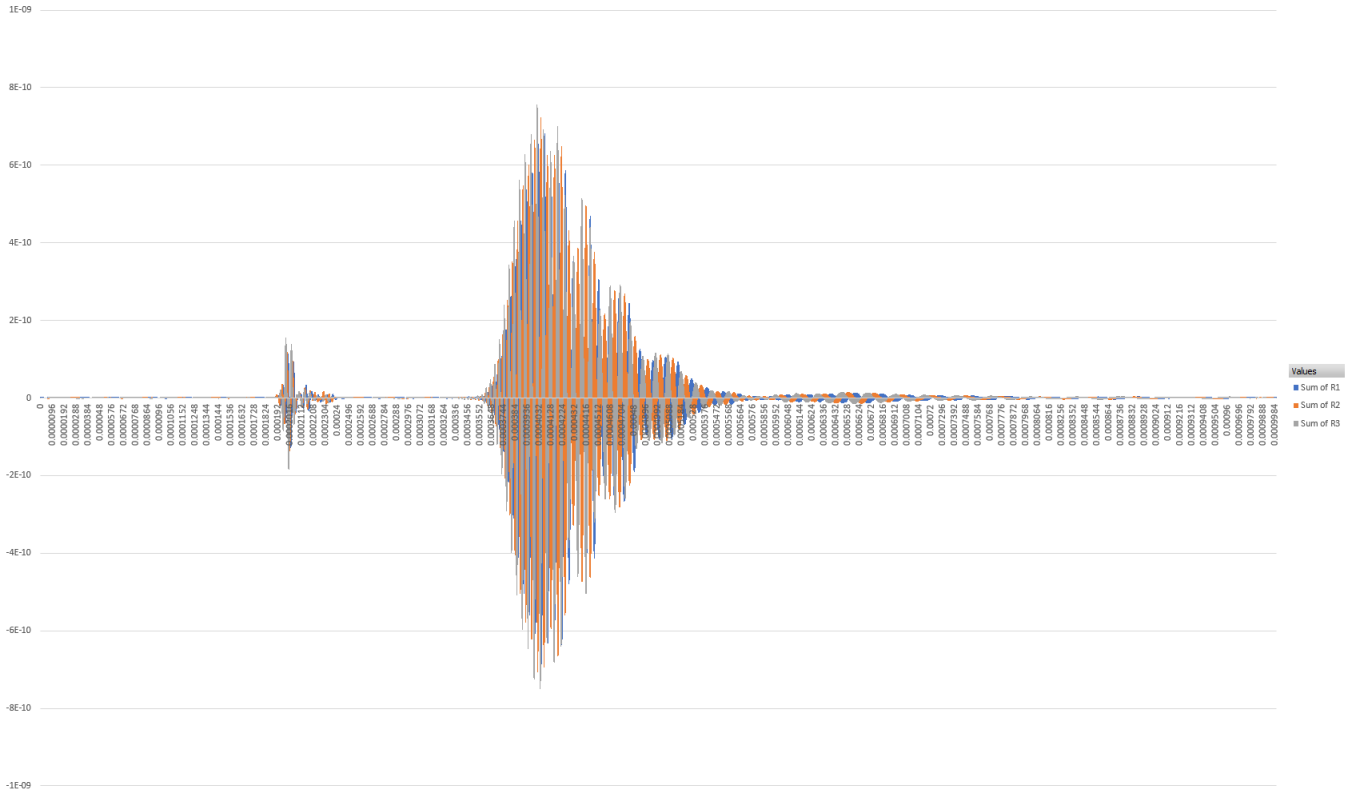

Figure 38. Long Distance Detection Analysis ($\theta = 9°$, D = 1000mm).

$$\text{DIcc} = 1 - \rho = 1 - \int_{t_{min}}^{t_{max}} f(t)g(t)\ dt / \left(\sqrt{\int_{t_{min}}^{t_{max}} f^2(t)\ dt} \sqrt{\int_{t_{min}}^{t_{max}} g^2(t)\ dt} \right),$$

$$\text{sqdev} = \sum_{t_{min}}^{t_{max}} \left(g(t) - f(t) \right)^2,$$

and the difference in peak amplitude (diffPA) was computed by taking the difference in the maximum amplitudes between the two signals within the analysis window [17]

In the following tables (Tables 5 and 6), "T1R1" means the first transmitter angle$\theta = 9°$ and the first receiver location while "LR1" means the first receiver location in the long distance test. For the tests performed, we obtain the following values for each of the damage index metrics shown in Table 5.

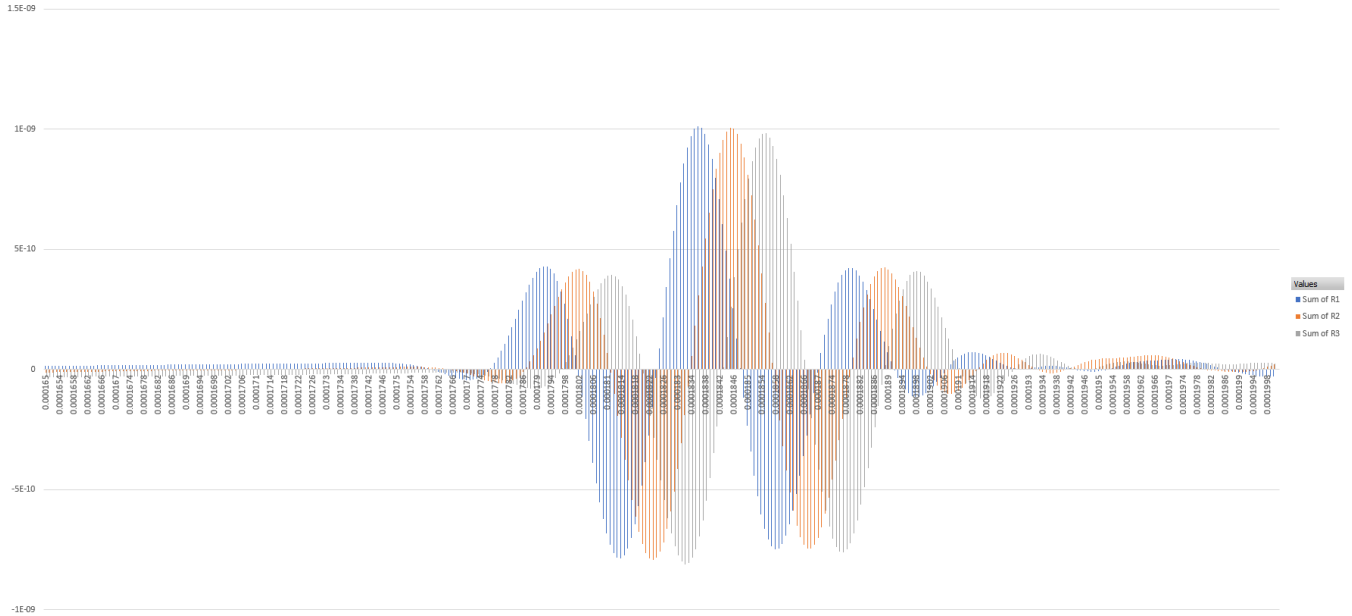

Figure 39. Long Distance Received Signals Enhanced ($\theta = 9°$, D = 1000mm).

Table 5. Damage Indices for Tests.

	T1R1	T1R2	T1R3	T2R1	T2R2	T2R3	LR1	LR2	LR3
diffPA	9.01E-12	3.71E-12	4.55E-13	4.25E-13	6.85E-12	2.64E-12	5.53E-13	-1.87E-12	7.40E-13
sqdev	1.11E-14	6.32E-13	7.58E-13	1.01E-14	1.54E-14	3.21E-14	5.42E-19	5.98E-19	1.05E-18
DIcc	2.39E-02	3.98E-01	1.97E-01	2.18E-02	2.88E-02	6.66E-02	1.80E-03	3.67E-03	6.84E-03

Now, we look at our thresholds stated in Chapter 3 Section 5: detection is detected if the diffPA is more than 5% of the baseline signals peak amplitude, sqdev is more than 5% of the baseline signals sum of squares, and DIcc is above 0.05. Converting our metric values in to percentages, gives us the following result in Table **??**.

Table 6. Detection Results.

	T1R1	T1R2	T1R3	T2R1	T2R2	T2R3	LR1	LR2	LR3
PA	29.50%	52.96%	5.86%	2.43%	168.79%	134.53%	3.78%	13.34%	2.27%
sqdev	4.95%	293.29%	282.12%	4.55%	6.71%	14.07%	1.85%	2.05%	3.62%
DIcc	0.024	0.398	0.197	0.022	0.029	0.067	0.002	0.004	0.007

In Table 6, some of the PA and sqdev percentages for $R2$ and $R3$ are greater than 100%. This is because both of these forms of measure are on differences with respect to the baseline signal. Thus, these values indicate that the PWAS is extremely capable of detection at these certain geometries since the received signal is so much

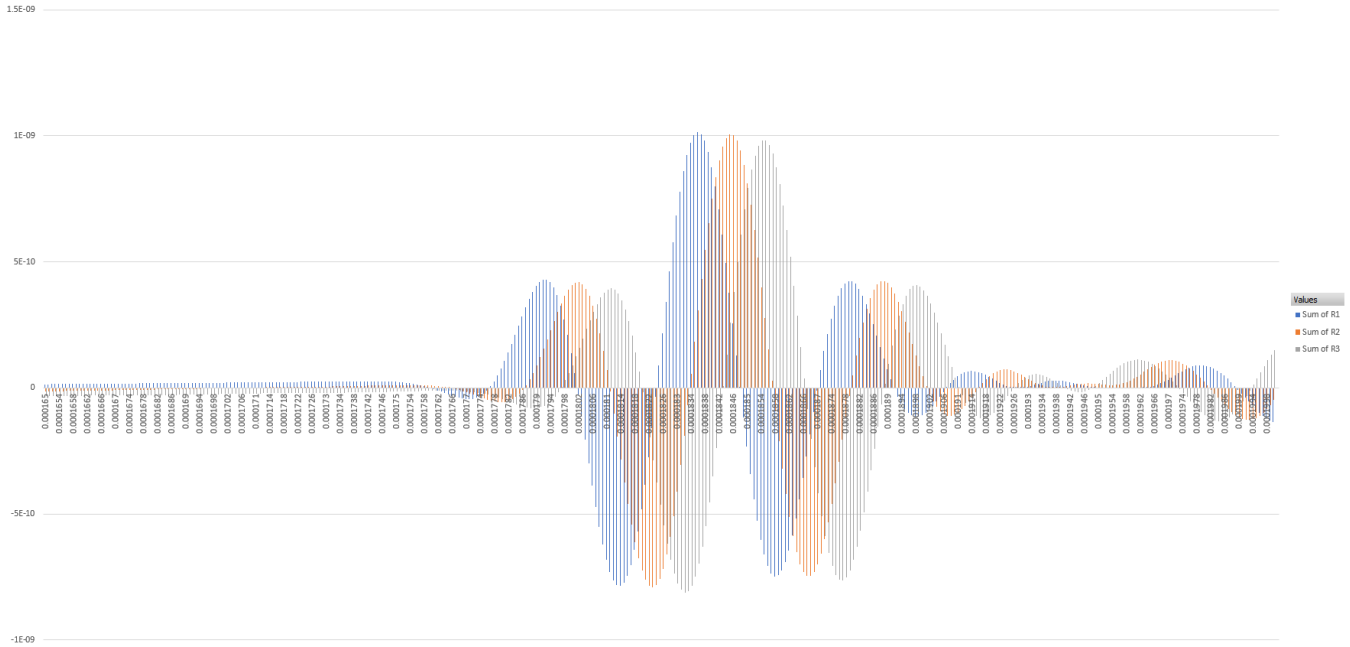

Figure 40. Long Distance Signal With Only Rivet Hole Enhanced($\theta = 9°$, D = 1000mm).

different from the transmitted signal.

Based upon our thresholds for damage detection, we see that damage is detected for $R3$ in both the $T1$ and $T2$ cases. For, $R2$ damage is generally well detected with most values above the threshold. For our long distance test of 1000mm transmitter distance. We were able to detect the damage at very specific conditions namely at $R2$ and $R3$. In all tests, $R1$ had significantly worse results for the damage metrics. Therefore, we have shown that this incrementation in receiver distance of 5mm does have a significant effect on damage detection and that there is potential for damage detection for comparatively long transmitter distances.

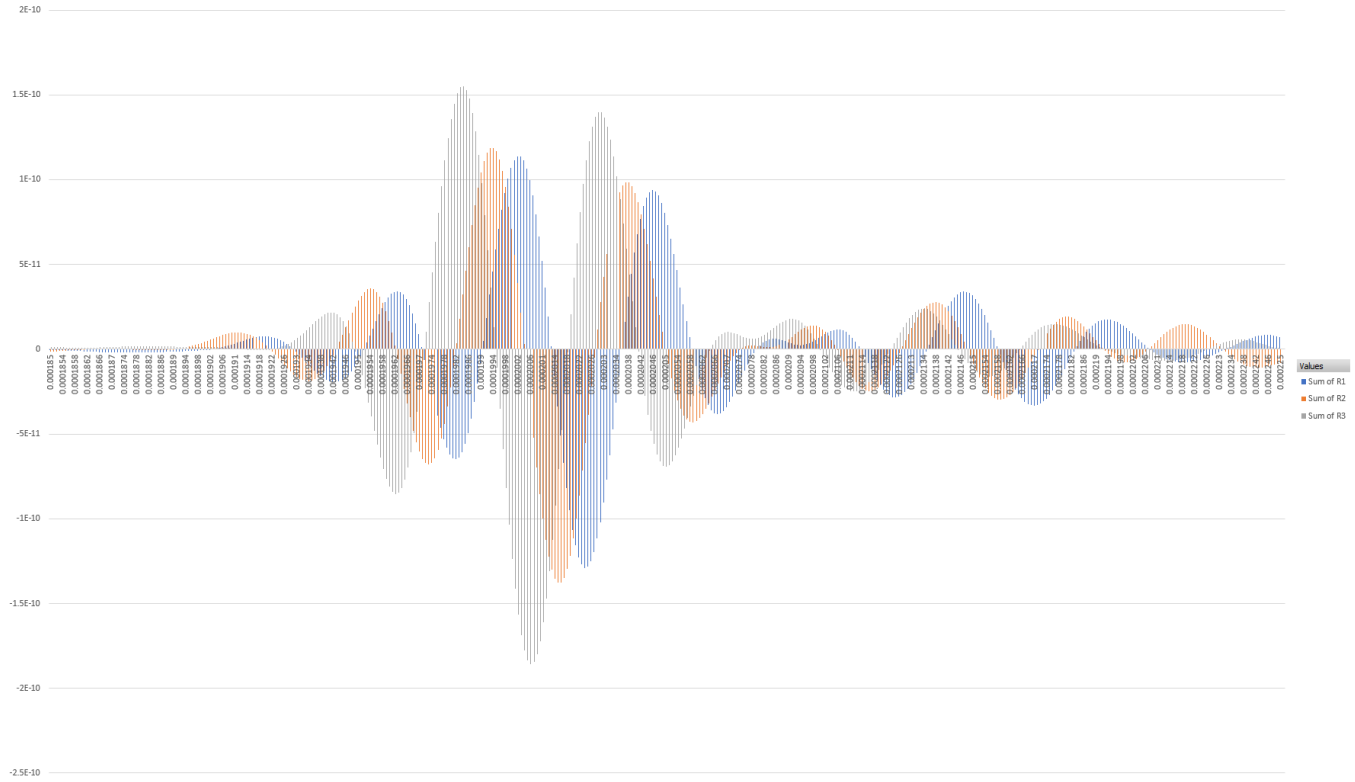

Figure 41. Long Distance Detection Analysis Enhanced($\theta = 9°$, D = 1000mm).

V. Conclusion

5.1 Overview

From our results, we see that the PWAS detection capabilities are sensitive to small changes in the transmitter and receiver sensor geometry. In our results, the damage metrics for $R1$ were far lower than the other two receiver locations, $R2$ and $R3$. Our tests have shown that the PWAS is able to not only accurately detect the presence of the damage in the near field but also able to do so at a longer distance of 1000mm for very specific geometries. Even at this longer distance, incrementing the receiver PWAS distances by 5mm produced different results in the peak amplitude, phase, and damage metrics, indicating that the PWAS is sensitive to these changes. This sensitivity is directly related to detection and establishes PWAS as an accurate detection instrument over a wide range of distances. The experiments done in this work illustrate that the PWAS can detect even slight changes in geometry regardless of how far the sensor is from the damage. Furthermore, our experiments also show that the PWAS still is able to detect the damage at a significant distance (1000mm) for certain geometries indicating that the PWAS may be more robust to farther distances than currently stated.

Given that current literature only states that the maximum detection radius for a PWAS is 15mm [8], this work provides a smoother metric that allows for more wiggle room should future researchers need it. As observed in Dong [8] any improvements however slight can make a massive dent in the millions of dollars of expected cost of using the PWAS on a real airframe. This work showing that the PWAS has a potential for detecting damage at 1000mm for certain geometries provides a potential future work to determine at what geometries is the PWAS still able to detect the damage with large transmitter and receiver sensor distances.

5.2 Scope

Much like other researchers have found, the PWAS detects damage far better when the distance is decreased. This experiment also did not take into account noise in the system which will be prevalent when applied real-time. This noise has the possibility of impacting our detection capabilities in a way which makes the damage unable to be detected since the change in the incident wave from damage may be indistinguishable from the change in the incident wave from noise. This possibility increases as the distance from the PWAS to the damage increases. Thus, we will need to keep the damage locations relatively close to both the transmitting and receiving sensors. Our tests are based upon assumptions that do not reflect real world scenarios (e.g. Lamb wave infinite plate assumption) but we believe that each are reasonable, justified, and established in the SHM field.

Although the PWAS is stated to have the potential to have real-time structural health monitoring of an airframe, this work only accounts for the PWAS's performance while completely stationary. This is mainly because the addition of air flow and other fluid dynamic factors significantly increases the complexity of this problem. Additionally, further collaboration with leading national university's aerospace departments could prove useful here to gain insights about in-flight dynamics and current engineering capabilities.

5.3 Future Works and Impact

Experimental Design.

Although we have obtained analytical solutions for our model, It would be more ideal if we could compare this to live data. With this live tests come a great deal of physical properties to consider. Table 42 has the physical properties of the PWAS. A

Property	Symbol	Value
Compliance, in plane	s_{11}^E	$15.30 \cdot 10^{-12}$ Pa^{-1}
Compliance, thickness wise	s_{33}^E	$17.30 \cdot 10^{-12}$ Pa^{-1}
Dielectric constant	ε_{33}^T	$\varepsilon_{33}^T = 1750\varepsilon_0$
Thickness-wise induced-strain coefficient	d_{33}	$400 \cdot 10^{-12}$ m/V
In-plane induced-strain coefficient	d_{31}	$-175 \cdot 10^{-12}$ m/V
Coupling factor, parallel to electric field	k_{33}Z	0.72
Coupling factor, transverse to electric field	k_{31}Z	0.36
Poisson ratio	ν	0.35
Density	ρ	7700 kg/m^3
Sound speed	c	2900 m/s

Note: $\varepsilon_0 = 8.85 \times 10^{-12}$ F/m is the permittivity of free space.

Figure 42. Physical Properties of a PWAS.

typical live experimental progression is illustrated below.

Pitch-Catch Test.

To establish a proper foundation for future works, we will start with the simplest cases. In preliminary works, we observed that the distance to excitation is a significant factor for crack detection. For pitch-catch, we place the sensors on a pristine plate 100mm away from each other, send out an propagating Lamb wave from one sensor and compare it to the received wave. Given that there are no holes or cracks, these two waves should be exactly the same[4].

Sensor Array Configuration.

When practically implementing guided wave based damage identification, a single sensor may fail to provide sufficient information for describing the damage, eroding the confidence in accepting detection results. A multitude of spatially distributed sensors are often networked to configure a sensor array/network. By communicating with

each other, a sensor array/network provides added information, increased redundancy and enhanced reliability of signal acquisition. To form a sensor array/network, one can employ an array of sensors to form a very dense configuration with the spacing between two sensors similar to or smaller than the scale of anticipated damage.

For our sensor array configuration, we place 6 sensors evenly around a semicircle radius 100mm centered around the damage source. The purpose of this separation is to see how multiple sensors react to the the damage source, observe if there is any unintended interaction, and confirm the accuracy of our process.

We use an approach very similar to Zhao et al. to set up our live experiment[25]. To attach a PZT sensor to a surface, the surface is cleaned first with alcohol, and a copper tape is attached to the cleaned surface. Then a PZT disc is glued on top of the copper tape with conductive epoxy. Finally, a lead wire is soldered or glued with conductive epoxy to the top surface of the sensor to serve as the signal wire and the copper tape is used as the electrical ground. To insulate the sensor and protect it from shock or vibration, the sensor assembly could be covered with epoxy, with only the signal and ground wires leading out. The electric mechanical impedances of the sensors were measured with an impedance analyzer (HP 4192) to check their performance. The decibel scale impedance was obtained from the reading of an impedance analyzers Z with ZdB = $20log10(|Z|)$.

For this future work, the given information would be

1. Transmitted Signal
2. Received Signal
3. Location of Rivet Hole

From this, we are trying to find

1. Crack (Y/N)

2. Angle (0- 360°)

3. Length (6.4mm - 64mm)

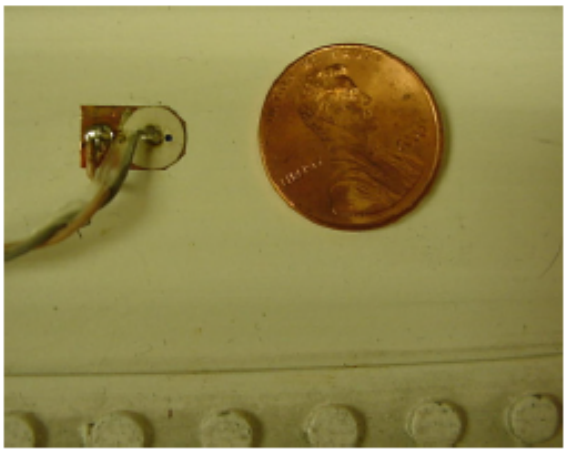

Figure 43. Live PWAS.

Due to our sensor array configuration, we already have information about how sensors detect the crack at certain angles. What remains to be done is to find the threshold where the crack can be detected. Thus, we focus on varying the crack length (starting from a comparatively large value and decreasing incrementally) in order to see at which point our methods are unable to discern the crack from a regular rivet hole. This provides a valuable metric to base all other future works.

Our next step here is to help categorize distances for the receiver. For the close distance range, the receiver should be able to predict the damage with 5% error at most. For the medium distance range, the receiver should be able to predict the damage with 15% error at most. For the long distance range, the receiver should be able to predict the damage with 25% error at most. These intervals will help assist future researchers in damage detections given that most research papers merely just state the PWAS detection capabilities as 15mm maximum.

One of the more interesting questions is how PWAS would interact with different

materials. Would plastic or other materials make PWAS approaches more or less effective? As the military turns its focuses slowly towards space and, with it, a larger focus on weight restriction on transportation, having the weight of the PWAS be offset by being able to be attached on lighter materials could prove to be important in the future. In addition, spaceframe surface materials may be significantly different than airframe materials to include heat/radioactive shielding, insulation, and other protective coatings.

5.4 Conclusion

As addressed multiple times in this thesis, one of the major considerations when using the PWAS is that it has a significantly limited detection range which means that multiple sensors are needed to monitor a system. As the size of the system increases, this limited detection range is the main cause for the increased cost and weight. Dong and Kim noted that this costs out paces the benefits by a factor of ten[8], hindering the implementation PWAS on airframe systems. The next step in this SHM field would to be to quantify at what distances the PWAS is unable to detect the crack from the noise and possibly try to increase that distance. Finally, the SMART layer requires a great deal of work to process the data so attempts to streamline this process can also reduce operational costs.

PWAS still has a long way to go to becoming a household name in the SHM field, but with each advancement, there is little doubt that its detection capability, accuracy, and flexibility make it a strong candidate for any future endeavors in SHM. Eventually, with further advancements in aerospace engineering and efficiency, PWAS can be tested in mobile situations instead of stationary ones. Given how robust the PWAS is to external factors like temperature, pressure, and radiation, these test may solidify the PWAS as the leading way to monitor structural health in not only aircraft

but possibly space and seacraft too.

In regards to the DoD, this research falls under health assessment, namely structural health. The DoD has stated that Health assessments based on condition monitoring are accomplished on the platform or operating equipment in real-time. Anonsystemhealth assessment includes sensor signal analysis, produces meaningful condition descriptors, and derives usable data from the raw sensor measurements (i.e., 35model-based reasoning combined with on-system real-time analysis of correlated sensor outputs). Health assessment facilitates the creation and maintenance of normal baseline profilesand identifies abnormalities when new data are acquired, and determines in which assessment category, if any, the data belong (e.g., alertor alarm). Health assessment software diagnoses component faults and rates the current health of the equipment or process, considering such inputs as sensor output information, technical specifications, configuration data, operating history, and historical condition data. At the operational or tactical level, on-system heath assessment helps operational commanders gauge the operating capabilities of weapons and equipment under their control. It also assists in maintenance decision making regarding appropriate repair actions and future equipment availability. The long-term health assessment goal is to provide managers with predictions about the remaining useful life of the machine before maintenance is required. There are two fundamental aspects to employing CBM+health assessment capabilities. The first relates to on-system processing and predictive maintenance (to the extent a platform is enabled with those capabilities). Generally, on-system assessment data processing is automated, and analysis is performed through the use of embedded processors. The second aspect of health assessment is the off-system processing of collected sensor data from data storage and management. Off-system analysis uses communications networks, databases, and health analysis software applications that make up the enterprise-level capability

for CBM+data collection and analysis [14]. It is clear through this statement that our current work falls within the first fundamental aspect. It's not so difficult to anticipate that this second aspect will begin to come to play once CBM+ because a mainstay for every system. On the operational side, this cutting edge technology is the future of maintenance, one of the career fields that would benefit greatly from progress. By implementing these ideas early and coordinating with companies supporting these works, the Air Force maintains a strong position in keeping our pilots in the air. As we develop more advance craft, this damage detecting technology only becomes more important as each airframe suddenly increases in value both in the checkbook but also on the battlefield.

VI. Appendix

0.1 Coordinates Code

```
T = [27, 9];
T2 = 9;
D = 1000;
R1 = 5;
R1_D = 50;
Inc = 5;
TCoord = zeros(2, 8);
for i=1:2
    TCoord(i, 1) = D*sind(T(i));
    TCoord(i, 2) = D*cosd(T(i));
    TCoord(i, 3) = TCoord(i, 1) + R1_D*sind(R1);
    TCoord(i, 4) = TCoord(i, 2) - R1_D*cosd(R1);
    TR1 = sqrt(D^2 + R1_D^2 - 2*D*R1_D*cosd(T(i) + R1));
    T_angle = 180 - (99 + asind(10/(TR1/(sind(T(i)+R1)))));
    TCoord(i, 5) = TCoord(i, 3) + Inc*cosd(T_angle);
    TCoord(i, 6) = TCoord(i, 4) + Inc*sind(T_angle);
    TCoord(i, 7) = TCoord(i, 3) + 2*Inc*cosd(T_angle);
    TCoord(i, 8) = TCoord(i, 4) + 2*Inc*sind(T_angle);
end
```

0.2 Data Tables

1.6mm Crack Data (T = transmitter, L = Long Distance Test).

Time	T1R1	T1R2	T1R3	T2R1	T2R2	T2R3
0	2.15E-11	1.07E-11	7.31E-12	1.79E-11	1.09E-11	4.6E-12
1E-07	2.14E-11	1.07E-11	7.41E-12	1.78E-11	1.06E-11	4.92E-12
2E-07	2.13E-11	1.07E-11	7.51E-12	1.77E-11	1.03E-11	5.3E-12
3E-07	2.13E-11	1.07E-11	7.62E-12	1.76E-11	1E-11	5.71E-12
4E-07	2.12E-11	1.07E-11	7.75E-12	1.75E-11	9.78E-12	6.12E-12
5E-07	2.11E-11	1.08E-11	7.91E-12	1.73E-11	9.56E-12	6.52E-12
6E-07	2.1E-11	1.08E-11	8.09E-12	1.72E-11	9.35E-12	6.88E-12
7E-07	2.09E-11	1.08E-11	8.31E-12	1.71E-11	9.18E-12	7.17E-12
8E-07	2.09E-11	1.09E-11	8.53E-12	1.7E-11	9.04E-12	7.36E-12
9E-07	2.08E-11	1.09E-11	8.76E-12	1.69E-11	8.94E-12	7.46E-12
0.000001	2.07E-11	1.09E-11	8.97E-12	1.68E-11	8.88E-12	7.46E-12
1.1E-06	2.07E-11	1.09E-11	9.15E-12	1.68E-11	8.86E-12	7.36E-12
1.2E-06	2.06E-11	1.09E-11	9.29E-12	1.67E-11	8.87E-12	7.16E-12
1.3E-06	2.06E-11	1.09E-11	9.37E-12	1.66E-11	8.92E-12	6.88E-12
1.4E-06	2.05E-11	1.08E-11	9.37E-12	1.66E-11	9E-12	6.55E-12
1.5E-06	2.05E-11	1.08E-11	9.29E-12	1.65E-11	9.11E-12	6.18E-12
1.6E-06	2.05E-11	1.07E-11	9.15E-12	1.65E-11	9.22E-12	5.82E-12
1.7E-06	2.05E-11	1.06E-11	8.93E-12	1.64E-11	9.35E-12	5.47E-12
1.8E-06	2.05E-11	1.05E-11	8.66E-12	1.64E-11	9.48E-12	5.16E-12
1.9E-06	2.05E-11	1.04E-11	8.35E-12	1.64E-11	9.61E-12	4.91E-12
0.000002	2.05E-11	1.02E-11	8.01E-12	1.64E-11	9.73E-12	4.74E-12
2.1E-06	2.06E-11	1.01E-11	7.66E-12	1.65E-11	9.82E-12	4.64E-12
2.2E-06	2.07E-11	9.97E-12	7.33E-12	1.65E-11	9.9E-12	4.61E-12
2.3E-06	2.08E-11	9.83E-12	7.01E-12	1.66E-11	9.97E-12	4.62E-12
2.4E-06	2.09E-11	9.71E-12	6.72E-12	1.67E-11	1E-11	4.66E-12

2.5E-06	2.1E-11	9.61E-12	6.45E-12	1.68E-11	1E-11	4.7E-12
2.6E-06	2.11E-11	9.51E-12	6.21E-12	1.69E-11	1.01E-11	4.7E-12
2.7E-06	2.13E-11	9.41E-12	5.99E-12	1.7E-11	1.01E-11	4.65E-12
2.8E-06	2.15E-11	9.32E-12	5.79E-12	1.72E-11	1E-11	4.51E-12
2.9E-06	2.17E-11	9.23E-12	5.58E-12	1.73E-11	1E-11	4.25E-12
0.000003	2.18E-11	9.13E-12	5.35E-12	1.75E-11	9.97E-12	3.89E-12
3.1E-06	2.2E-11	9.02E-12	5.1E-12	1.77E-11	9.89E-12	3.42E-12
3.2E-06	2.23E-11	8.87E-12	4.8E-12	1.79E-11	9.78E-12	2.84E-12
3.3E-06	2.25E-11	8.7E-12	4.46E-12	1.81E-11	9.63E-12	2.19E-12
3.4E-06	2.27E-11	8.5E-12	4.07E-12	1.83E-11	9.44E-12	1.49E-12
3.5E-06	2.29E-11	8.28E-12	3.61E-12	1.85E-11	9.19E-12	7.74E-13
3.6E-06	2.31E-11	8.02E-12	3.11E-12	1.87E-11	8.87E-12	8.85E-14
3.7E-06	2.34E-11	7.74E-12	2.57E-12	1.89E-11	8.48E-12	-5.4E-13
3.8E-06	2.36E-11	7.45E-12	2E-12	1.91E-11	8.02E-12	-1.1E-12
3.9E-06	2.38E-11	7.16E-12	1.42E-12	1.93E-11	7.49E-12	-1.6E-12
0.000004	2.4E-11	6.87E-12	8.3E-13	1.95E-11	6.89E-12	-1.9E-12
4.1E-06	2.43E-11	6.59E-12	2.68E-13	1.97E-11	6.22E-12	-2.1E-12
4.2E-06	2.45E-11	6.33E-12	-2.5E-13	1.99E-11	5.48E-12	-2.3E-12
4.3E-06	2.47E-11	6.08E-12	-7.2E-13	2.01E-11	4.7E-12	-2.4E-12
4.4E-06	2.49E-11	5.85E-12	-1.1E-12	2.03E-11	3.87E-12	-2.4E-12
4.5E-06	2.51E-11	5.63E-12	-1.5E-12	2.04E-11	3.01E-12	-2.4E-12
4.6E-06	2.53E-11	5.41E-12	-1.8E-12	2.06E-11	2.1E-12	-2.4E-12
4.7E-06	2.56E-11	5.15E-12	-2E-12	2.08E-11	1.16E-12	-2.5E-12
4.8E-06	2.58E-11	4.84E-12	-2.2E-12	2.1E-11	1.92E-13	-2.6E-12
4.9E-06	2.6E-11	4.46E-12	-2.4E-12	2.11E-11	-8.1E-13	-2.8E-12
0.000005	2.62E-11	3.97E-12	-2.5E-12	2.13E-11	-1.9E-12	-3.1E-12

5.1E-06	2.64E-11	3.34E-12	-2.7E-12	2.14E-11	-3E-12	-3.4E-12
5.2E-06	2.67E-11	2.53E-12	-2.9E-12	2.16E-11	-4.2E-12	-3.9E-12
5.3E-06	2.68E-11	1.52E-12	-3.1E-12	2.17E-11	-5.5E-12	-4.3E-12
5.4E-06	2.7E-11	3.05E-13	-3.3E-12	2.17E-11	-7E-12	-4.9E-12
5.5E-06	2.71E-11	-1.1E-12	-3.6E-12	2.17E-11	-8.5E-12	-5.4E-12
5.6E-06	2.72E-11	-2.8E-12	-3.9E-12	2.16E-11	-1E-11	-5.9E-12
5.7E-06	2.72E-11	-4.6E-12	-4.2E-12	2.15E-11	-1.2E-11	-6.3E-12
5.8E-06	2.72E-11	-6.6E-12	-4.5E-12	2.12E-11	-1.4E-11	-6.6E-12
5.9E-06	2.71E-11	-8.7E-12	-4.7E-12	2.08E-11	-1.6E-11	-6.8E-12
0.000006	2.69E-11	-1.1E-11	-4.9E-12	2.04E-11	-1.8E-11	-6.9E-12
6.1E-06	2.67E-11	-1.3E-11	-5.1E-12	1.98E-11	-2E-11	-6.8E-12
6.2E-06	2.65E-11	-1.5E-11	-5.2E-12	1.91E-11	-2.2E-11	-6.6E-12
6.3E-06	2.65E-11	-1.6E-11	-5.2E-12	1.84E-11	-2.4E-11	-6.3E-12
6.4E-06	2.66E-11	-1.7E-11	-5.2E-12	1.77E-11	-2.5E-11	-5.9E-12
6.5E-06	2.71E-11	-1.7E-11	-5.1E-12	1.71E-11	-2.6E-11	-5.5E-12
6.6E-06	2.82E-11	-1.7E-11	-5.1E-12	1.68E-11	-2.6E-11	-5.2E-12
6.7E-06	3.01E-11	-1.6E-11	-5E-12	1.68E-11	-2.5E-11	-4.9E-12
6.8E-06	3.31E-11	-1.3E-11	-5.1E-12	1.75E-11	-2.4E-11	-4.9E-12
6.9E-06	3.73E-11	-9.9E-12	-5.4E-12	1.89E-11	-2.2E-11	-5.1E-12
0.000007	4.3E-11	-5.1E-12	-6E-12	2.15E-11	-1.8E-11	-5.7E-12
7.1E-06	5.01E-11	1.09E-12	-7.1E-12	2.54E-11	-1.3E-11	-6.7E-12
7.2E-06	5.82E-11	8.83E-12	-8.6E-12	3.09E-11	-7E-12	-8.3E-12
7.3E-06	6.67E-11	1.82E-11	-1.1E-11	3.81E-11	5.71E-13	-1E-11
7.4E-06	7.44E-11	2.93E-11	-1.4E-11	4.68E-11	9.7E-12	-1.3E-11
7.5E-06	8E-11	4.22E-11	-1.7E-11	5.67E-11	2.04E-11	-1.6E-11
7.6E-06	8.14E-11	5.69E-11	-2.2E-11	6.69E-11	3.27E-11	-2E-11

7.7E-06	7.67E-11	7.35E-11	-2.7E-11	7.63E-11	4.67E-11	-2.5E-11
7.8E-06	6.38E-11	9.19E-11	-3.2E-11	8.33E-11	6.23E-11	-3E-11
7.9E-06	4.07E-11	1.12E-10	-3.7E-11	8.58E-11	7.96E-11	-3.4E-11
0.000008	6.27E-12	1.33E-10	-4.3E-11	8.19E-11	9.85E-11	-3.9E-11
8.1E-06	-4E-11	1.55E-10	-4.7E-11	6.95E-11	1.19E-10	-4.3E-11
8.2E-06	-9.8E-11	1.77E-10	-5.1E-11	4.67E-11	1.4E-10	-4.7E-11
8.3E-06	-1.7E-10	1.98E-10	-5.3E-11	1.25E-11	1.62E-10	-4.9E-11
8.4E-06	-2.4E-10	2.15E-10	-5.2E-11	-3.4E-11	1.83E-10	-4.9E-11
8.5E-06	-3.2E-10	2.26E-10	-4.9E-11	-9.1E-11	2.03E-10	-4.7E-11
8.6E-06	-4.1E-10	2.3E-10	-4.1E-11	-1.6E-10	2.2E-10	-4.2E-11
8.7E-06	-4.8E-10	2.25E-10	-3E-11	-2.3E-10	2.31E-10	-3.4E-11
8.8E-06	-5.6E-10	2.07E-10	-1.4E-11	-3.1E-10	2.36E-10	-2.1E-11
8.9E-06	-6.2E-10	1.75E-10	6.83E-12	-3.9E-10	2.31E-10	-4.9E-12
0.000009	-6.6E-10	1.29E-10	3.22E-11	-4.7E-10	2.14E-10	1.58E-11
9.1E-06	-6.8E-10	6.82E-11	6.17E-11	-5.4E-10	1.84E-10	4.08E-11
9.2E-06	-6.8E-10	-6.9E-12	9.43E-11	-6E-10	1.4E-10	6.96E-11
9.3E-06	-6.5E-10	-9.4E-11	1.28E-10	-6.4E-10	7.99E-11	1.02E-10
9.4E-06	-5.9E-10	-1.9E-10	1.62E-10	-6.5E-10	5.83E-12	1.36E-10
9.5E-06	-5E-10	-2.9E-10	1.93E-10	-6.5E-10	-8.1E-11	1.7E-10
9.6E-06	-3.7E-10	-4E-10	2.19E-10	-6.2E-10	-1.8E-10	2.02E-10
9.7E-06	-2.2E-10	-5E-10	2.36E-10	-5.6E-10	-2.8E-10	2.3E-10
9.8E-06	-4.7E-11	-5.9E-10	2.43E-10	-4.6E-10	-3.9E-10	2.52E-10
9.9E-06	1.54E-10	-6.7E-10	2.38E-10	-3.4E-10	-4.9E-10	2.63E-10
0.00001	3.76E-10	-7.3E-10	2.18E-10	-2E-10	-5.9E-10	2.63E-10
1.01E-05	6.15E-10	-7.8E-10	1.85E-10	-2.3E-11	-6.8E-10	2.49E-10
1.02E-05	8.64E-10	-7.9E-10	1.38E-10	1.74E-10	-7.5E-10	2.19E-10

1.03E-05	1.12E-09	-7.8E-10	7.84E-11	3.91E-10	-8E-10	1.74E-10
1.04E-05	1.37E-09	-7.4E-10	8.62E-12	6.22E-10	-8.3E-10	1.15E-10
1.05E-05	1.61E-09	-6.7E-10	-6.9E-11	8.62E-10	-8.3E-10	4.16E-11
1.06E-05	1.84E-09	-5.7E-10	-1.5E-10	1.11E-09	-8E-10	-4.2E-11
1.07E-05	2.04E-09	-4.3E-10	-2.3E-10	1.35E-09	-7.3E-10	-1.3E-10
1.08E-05	2.21E-09	-2.7E-10	-3.1E-10	1.58E-09	-6.4E-10	-2.3E-10
1.09E-05	2.34E-09	-8.7E-11	-3.8E-10	1.79E-09	-5.1E-10	-3.3E-10
0.000011	2.42E-09	1.21E-10	-4.4E-10	1.98E-09	-3.6E-10	-4.2E-10
1.11E-05	2.46E-09	3.46E-10	-4.9E-10	2.13E-09	-1.8E-10	-5E-10
1.12E-05	2.45E-09	5.83E-10	-5.2E-10	2.25E-09	2.78E-11	-5.7E-10
1.13E-05	2.37E-09	8.27E-10	-5.3E-10	2.32E-09	2.53E-10	-6.2E-10
1.14E-05	2.24E-09	1.07E-09	-5.2E-10	2.35E-09	4.92E-10	-6.6E-10
1.15E-05	2.06E-09	1.31E-09	-4.8E-10	2.32E-09	7.4E-10	-6.7E-10
1.16E-05	1.81E-09	1.53E-09	-4.3E-10	2.24E-09	9.9E-10	-6.6E-10
1.17E-05	1.5E-09	1.73E-09	-3.5E-10	2.1E-09	1.24E-09	-6.2E-10
1.18E-05	1.14E-09	1.9E-09	-2.5E-10	1.91E-09	1.47E-09	-5.6E-10
1.19E-05	7.3E-10	2.04E-09	-1.4E-10	1.67E-09	1.68E-09	-4.7E-10
0.000012	2.76E-10	2.13E-09	-3.5E-12	1.37E-09	1.87E-09	-3.6E-10
1.21E-05	-2.1E-10	2.18E-09	1.44E-10	1.02E-09	2.03E-09	-2.2E-10
1.22E-05	-7.2E-10	2.18E-09	3.01E-10	6.35E-10	2.14E-09	-6.5E-11
1.23E-05	-1.2E-09	2.13E-09	4.65E-10	2.09E-10	2.21E-09	1.07E-10
1.24E-05	-1.8E-09	2.03E-09	6.29E-10	-2.5E-10	2.24E-09	2.92E-10
1.25E-05	-2.3E-09	1.88E-09	7.9E-10	-7.3E-10	2.21E-09	4.84E-10
1.26E-05	-2.7E-09	1.67E-09	9.41E-10	-1.2E-09	2.13E-09	6.79E-10
1.27E-05	-3.1E-09	1.41E-09	1.08E-09	-1.7E-09	1.99E-09	8.7E-10
1.28E-05	-3.5E-09	1.1E-09	1.19E-09	-2.2E-09	1.8E-09	1.05E-09

1.29E-05	-3.7E-09	7.56E-10	1.29E-09	-2.7E-09	1.56E-09	1.22E-09
0.000013	-3.9E-09	3.78E-10	1.35E-09	-3.1E-09	1.27E-09	1.36E-09
1.31E-05	-4E-09	-2.6E-11	1.39E-09	-3.5E-09	9.29E-10	1.48E-09
1.32E-05	-4E-09	-4.4E-10	1.39E-09	-3.9E-09	5.56E-10	1.57E-09
1.33E-05	-3.9E-09	-8.7E-10	1.35E-09	-4.1E-09	1.52E-10	1.63E-09
1.34E-05	-3.7E-09	-1.3E-09	1.28E-09	-4.3E-09	-2.7E-10	1.64E-09
1.35E-05	-3.4E-09	-1.7E-09	1.17E-09	-4.3E-09	-7.1E-10	1.62E-09
1.36E-05	-3E-09	-2.1E-09	1.02E-09	-4.3E-09	-1.2E-09	1.55E-09
1.37E-05	-2.6E-09	-2.5E-09	8.36E-10	-4.1E-09	-1.6E-09	1.44E-09
1.38E-05	-2.1E-09	-2.8E-09	6.22E-10	-3.8E-09	-2E-09	1.29E-09
1.39E-05	-1.5E-09	-3.1E-09	3.79E-10	-3.5E-09	-2.4E-09	1.1E-09
0.000014	-1E-09	-3.3E-09	1.14E-10	-3E-09	-2.7E-09	8.69E-10
1.41E-05	-4.7E-10	-3.5E-09	-1.7E-10	-2.4E-09	-3E-09	6.07E-10
1.42E-05	5.12E-11	-3.7E-09	-4.6E-10	-1.7E-09	-3.3E-09	3.17E-10
1.43E-05	5.37E-10	-3.8E-09	-7.7E-10	-1E-09	-3.4E-09	4.72E-12
1.44E-05	9.74E-10	-3.8E-09	-1.1E-09	-2.8E-10	-3.6E-09	-3.2E-10
1.45E-05	1.35E-09	-3.8E-09	-1.4E-09	4.85E-10	-3.7E-09	-6.6E-10
1.46E-05	1.64E-09	-3.7E-09	-1.6E-09	1.24E-09	-3.7E-09	-1E-09
1.47E-05	1.85E-09	-3.5E-09	-1.9E-09	1.98E-09	-3.6E-09	-1.3E-09
1.48E-05	1.97E-09	-3.3E-09	-2.1E-09	2.65E-09	-3.5E-09	-1.6E-09
1.49E-05	1.99E-09	-3E-09	-2.3E-09	3.26E-09	-3.4E-09	-1.9E-09
0.000015	1.9E-09	-2.6E-09	-2.5E-09	3.78E-09	-3.2E-09	-2.2E-09
1.51E-05	1.72E-09	-2.1E-09	-2.6E-09	4.18E-09	-2.9E-09	-2.4E-09
1.52E-05	1.44E-09	-1.6E-09	-2.6E-09	4.46E-09	-2.6E-09	-2.6E-09
1.53E-05	1.08E-09	-9.7E-10	-2.6E-09	4.61E-09	-2.2E-09	-2.8E-09
1.54E-05	6.45E-10	-3.1E-10	-2.5E-09	4.6E-09	-1.8E-09	-2.9E-09

1.55E-05	1.52E-10	3.87E-10	-2.4E-09	4.44E-09	-1.4E-09	-2.9E-09
1.56E-05	-3.8E-10	1.12E-09	-2.2E-09	4.12E-09	-8.8E-10	-2.9E-09
1.57E-05	-9.3E-10	1.88E-09	-1.9E-09	3.65E-09	-3.6E-10	-2.8E-09
1.58E-05	-1.5E-09	2.64E-09	-1.6E-09	3.03E-09	1.98E-10	-2.6E-09
1.59E-05	-2E-09	3.39E-09	-1.3E-09	2.28E-09	7.81E-10	-2.4E-09
0.000016	-2.4E-09	4.11E-09	-8.8E-10	1.4E-09	1.38E-09	-2.1E-09
1.61E-05	-2.8E-09	4.78E-09	-4.8E-10	4.26E-10	2E-09	-1.7E-09
1.62E-05	-3E-09	5.39E-09	-7.6E-11	-6.3E-10	2.62E-09	-1.3E-09
1.63E-05	-3.2E-09	5.92E-09	3.26E-10	-1.7E-09	3.23E-09	-8.8E-10
1.64E-05	-3.1E-09	6.35E-09	7.1E-10	-2.9E-09	3.81E-09	-4.1E-10
1.65E-05	-2.9E-09	6.68E-09	1.07E-09	-4E-09	4.37E-09	7.38E-11
1.66E-05	-2.5E-09	6.88E-09	1.38E-09	-5E-09	4.89E-09	5.62E-10
1.67E-05	-1.8E-09	6.94E-09	1.65E-09	-6E-09	5.35E-09	1.04E-09
1.68E-05	-9.6E-10	6.86E-09	1.86E-09	-6.9E-09	5.76E-09	1.48E-09
1.69E-05	1.04E-10	6.64E-09	2.02E-09	-7.6E-09	6.08E-09	1.89E-09
0.000017	1.38E-09	6.25E-09	2.11E-09	-8.1E-09	6.33E-09	2.24E-09
1.71E-05	2.85E-09	5.71E-09	2.14E-09	-8.3E-09	6.48E-09	2.52E-09
1.72E-05	4.49E-09	5.02E-09	2.12E-09	-8.4E-09	6.53E-09	2.73E-09
1.73E-05	6.28E-09	4.17E-09	2.05E-09	-8.1E-09	6.48E-09	2.86E-09
1.74E-05	8.18E-09	3.17E-09	1.94E-09	-7.6E-09	6.31E-09	2.9E-09
1.75E-05	1.02E-08	2.05E-09	1.79E-09	-6.8E-09	6.02E-09	2.87E-09
1.76E-05	1.22E-08	7.97E-10	1.61E-09	-5.6E-09	5.61E-09	2.75E-09
1.77E-05	1.41E-08	-5.6E-10	1.42E-09	-4.2E-09	5.07E-09	2.56E-09
1.78E-05	1.6E-08	-2E-09	1.23E-09	-2.5E-09	4.41E-09	2.3E-09
1.79E-05	1.78E-08	-3.5E-09	1.03E-09	-4.8E-10	3.62E-09	1.99E-09
0.000018	1.93E-08	-5E-09	8.57E-10	1.76E-09	2.72E-09	1.64E-09

1.81E-05	2.07E-08	-6.6E-09	7.06E-10	4.21E-09	1.69E-09	1.26E-09
1.82E-05	2.17E-08	-8.1E-09	5.91E-10	6.82E-09	5.61E-10	8.62E-10
1.83E-05	2.23E-08	-9.6E-09	5.19E-10	9.54E-09	-6.7E-10	4.65E-10
1.84E-05	2.26E-08	-1.1E-08	4.98E-10	1.23E-08	-2E-09	8.31E-11
1.85E-05	2.23E-08	-1.2E-08	5.34E-10	1.51E-08	-3.4E-09	-2.7E-10
1.86E-05	2.16E-08	-1.3E-08	6.3E-10	1.78E-08	-4.8E-09	-5.8E-10
1.87E-05	2.04E-08	-1.4E-08	7.87E-10	2.04E-08	-6.3E-09	-8.3E-10
1.88E-05	1.87E-08	-1.5E-08	1E-09	2.27E-08	-7.7E-09	-1E-09
1.89E-05	1.64E-08	-1.5E-08	1.28E-09	2.48E-08	-9.2E-09	-1.1E-09
0.000019	1.36E-08	-1.6E-08	1.6E-09	2.66E-08	-1.1E-08	-1.1E-09
1.91E-05	1.02E-08	-1.5E-08	1.96E-09	2.79E-08	-1.2E-08	-1E-09
1.92E-05	6.43E-09	-1.5E-08	2.35E-09	2.88E-08	-1.3E-08	-8.3E-10
1.93E-05	2.18E-09	-1.4E-08	2.76E-09	2.91E-08	-1.4E-08	-5.5E-10
1.94E-05	-2.5E-09	-1.3E-08	3.16E-09	2.89E-08	-1.5E-08	-1.7E-10
1.95E-05	-7.4E-09	-1.1E-08	3.53E-09	2.81E-08	-1.6E-08	3.02E-10
1.96E-05	-1.3E-08	-9.5E-09	3.87E-09	2.67E-08	-1.6E-08	8.48E-10
1.97E-05	-1.8E-08	-7.3E-09	4.14E-09	2.47E-08	-1.7E-08	1.46E-09
1.98E-05	-2.3E-08	-4.8E-09	4.32E-09	2.2E-08	-1.7E-08	2.11E-09
1.99E-05	-2.9E-08	-2E-09	4.4E-09	1.87E-08	-1.6E-08	2.79E-09
0.00002	-3.4E-08	1.07E-09	4.34E-09	1.49E-08	-1.5E-08	3.47E-09
2.01E-05	-3.9E-08	4.36E-09	4.14E-09	1.05E-08	-1.4E-08	4.13E-09
2.02E-05	-4.4E-08	7.81E-09	3.78E-09	5.63E-09	-1.3E-08	4.74E-09
2.03E-05	-4.8E-08	1.14E-08	3.24E-09	3.45E-10	-1.1E-08	5.28E-09
2.04E-05	-5.2E-08	1.5E-08	2.52E-09	-5.3E-09	-9.1E-09	5.7E-09
2.05E-05	-5.5E-08	1.86E-08	1.61E-09	-1.1E-08	-6.6E-09	6E-09
2.06E-05	-5.7E-08	2.21E-08	5.05E-10	-1.7E-08	-3.9E-09	6.14E-09

2.07E-05	-5.9E-08	2.55E-08	-7.8E-10	-2.3E-08	-8.4E-10	6.09E-09
2.08E-05	-6E-08	2.87E-08	-2.2E-09	-2.9E-08	2.46E-09	5.84E-09
2.09E-05	-6E-08	3.16E-08	-3.8E-09	-3.5E-08	5.97E-09	5.38E-09
0.000021	-5.9E-08	3.41E-08	-5.6E-09	-4.1E-08	9.63E-09	4.68E-09
2.11E-05	-5.7E-08	3.62E-08	-7.4E-09	-4.6E-08	1.34E-08	3.75E-09
2.12E-05	-5.4E-08	3.78E-08	-9.3E-09	-5.1E-08	1.72E-08	2.59E-09
2.13E-05	-5E-08	3.89E-08	-1.1E-08	-5.5E-08	2.1E-08	1.19E-09
2.14E-05	-4.5E-08	3.93E-08	-1.3E-08	-5.9E-08	2.47E-08	-4.2E-10
2.15E-05	-4E-08	3.92E-08	-1.5E-08	-6.1E-08	2.82E-08	-2.2E-09
2.16E-05	-3.4E-08	3.84E-08	-1.7E-08	-6.3E-08	3.15E-08	-4.2E-09
2.17E-05	-2.7E-08	3.69E-08	-1.8E-08	-6.4E-08	3.45E-08	-6.3E-09
2.18E-05	-1.9E-08	3.47E-08	-2E-08	-6.4E-08	3.71E-08	-8.5E-09
2.19E-05	-1.1E-08	3.18E-08	-2.1E-08	-6.4E-08	3.92E-08	-1.1E-08
0.000022	-2.9E-09	2.83E-08	-2.1E-08	-6.2E-08	4.09E-08	-1.3E-08
2.21E-05	5.61E-09	2.41E-08	-2.2E-08	-5.9E-08	4.19E-08	-1.5E-08
2.22E-05	1.42E-08	1.94E-08	-2.2E-08	-5.5E-08	4.24E-08	-1.7E-08
2.23E-05	2.28E-08	1.41E-08	-2.1E-08	-5.1E-08	4.22E-08	-1.9E-08
2.24E-05	3.11E-08	8.31E-09	-2E-08	-4.5E-08	4.13E-08	-2.1E-08
2.25E-05	3.92E-08	2.15E-09	-1.9E-08	-3.9E-08	3.96E-08	-2.3E-08
2.26E-05	4.69E-08	-4.3E-09	-1.7E-08	-3.2E-08	3.73E-08	-2.4E-08
2.27E-05	5.4E-08	-1.1E-08	-1.5E-08	-2.5E-08	3.43E-08	-2.4E-08
2.28E-05	6.04E-08	-1.8E-08	-1.2E-08	-1.7E-08	3.05E-08	-2.5E-08
2.29E-05	6.61E-08	-2.5E-08	-8.8E-09	-8.7E-09	2.62E-08	-2.5E-08
0.000023	7.09E-08	-3.1E-08	-5.1E-09	-2E-10	2.12E-08	-2.4E-08
2.31E-05	7.49E-08	-3.8E-08	-1.1E-09	8.41E-09	1.56E-08	-2.3E-08
2.32E-05	7.79E-08	-4.4E-08	3.27E-09	1.7E-08	9.61E-09	-2.1E-08

2.33E-05	7.98E-08	-5E-08	7.87E-09	2.55E-08	3.18E-09	-1.9E-08
2.34E-05	8.08E-08	-5.5E-08	1.26E-08	3.36E-08	-3.6E-09	-1.6E-08
2.35E-05	8.07E-08	-5.9E-08	1.75E-08	4.14E-08	-1.1E-08	-1.3E-08
2.36E-05	7.96E-08	-6.3E-08	2.24E-08	4.87E-08	-1.8E-08	-9.2E-09
2.37E-05	7.75E-08	-6.6E-08	2.72E-08	5.54E-08	-2.5E-08	-5.1E-09
2.38E-05	7.44E-08	-6.9E-08	3.18E-08	6.13E-08	-3.2E-08	-6.4E-10
2.39E-05	7.04E-08	-7E-08	3.61E-08	6.65E-08	-3.8E-08	4.13E-09
0.000024	6.56E-08	-7E-08	4.01E-08	7.08E-08	-4.5E-08	9.11E-09
2.41E-05	6.01E-08	-7E-08	4.36E-08	7.42E-08	-5E-08	1.42E-08
2.42E-05	5.39E-08	-6.8E-08	4.66E-08	7.66E-08	-5.6E-08	1.94E-08
2.43E-05	4.71E-08	-6.6E-08	4.9E-08	7.8E-08	-6E-08	2.46E-08
2.44E-05	3.99E-08	-6.2E-08	5.07E-08	7.85E-08	-6.4E-08	2.96E-08
2.45E-05	3.24E-08	-5.8E-08	5.17E-08	7.79E-08	-6.8E-08	3.44E-08
2.46E-05	2.47E-08	-5.3E-08	5.2E-08	7.64E-08	-7E-08	3.88E-08
2.47E-05	1.68E-08	-4.7E-08	5.14E-08	7.39E-08	-7.1E-08	4.29E-08
2.48E-05	8.95E-09	-4E-08	5E-08	7.06E-08	-7.1E-08	4.64E-08
2.49E-05	1.22E-09	-3.3E-08	4.78E-08	6.65E-08	-7.1E-08	4.94E-08
0.000025	-6.3E-09	-2.5E-08	4.48E-08	6.16E-08	-6.9E-08	5.18E-08
2.51E-05	-1.3E-08	-1.7E-08	4.11E-08	5.61E-08	-6.7E-08	5.34E-08
2.52E-05	-2E-08	-9E-09	3.65E-08	5E-08	-6.3E-08	5.43E-08
2.53E-05	-2.7E-08	-7.1E-10	3.13E-08	4.35E-08	-5.9E-08	5.44E-08
2.54E-05	-3.2E-08	7.6E-09	2.55E-08	3.66E-08	-5.4E-08	5.37E-08
2.55E-05	-3.7E-08	1.58E-08	1.92E-08	2.95E-08	-4.8E-08	5.21E-08
2.56E-05	-4.2E-08	2.37E-08	1.24E-08	2.23E-08	-4.2E-08	4.97E-08
2.57E-05	-4.6E-08	3.13E-08	5.27E-09	1.5E-08	-3.5E-08	4.65E-08
2.58E-05	-4.9E-08	3.84E-08	-2.1E-09	7.81E-09	-2.7E-08	4.26E-08

2.59E-05	-5.1E-08	4.49E-08	-9.6E-09	7.79E-10	-1.9E-08	3.79E-08
0.000026	-5.3E-08	5.08E-08	-1.7E-08	-6E-09	-1.1E-08	3.25E-08
2.61E-05	-5.4E-08	5.6E-08	-2.5E-08	-1.2E-08	-3.3E-09	2.65E-08
2.62E-05	-5.4E-08	6.04E-08	-3.2E-08	-1.8E-08	4.77E-09	2E-08
2.63E-05	-5.3E-08	6.39E-08	-3.9E-08	-2.4E-08	1.27E-08	1.31E-08
2.64E-05	-5.2E-08	6.66E-08	-4.5E-08	-2.9E-08	2.04E-08	5.82E-09
2.65E-05	-5.1E-08	6.85E-08	-5.1E-08	-3.3E-08	2.77E-08	-1.6E-09
2.66E-05	-4.9E-08	6.94E-08	-5.6E-08	-3.7E-08	3.45E-08	-9.2E-09
2.67E-05	-4.6E-08	6.95E-08	-6.1E-08	-4E-08	4.08E-08	-1.7E-08
2.68E-05	-4.3E-08	6.88E-08	-6.5E-08	-4.3E-08	4.65E-08	-2.4E-08
2.69E-05	-4E-08	6.72E-08	-6.8E-08	-4.5E-08	5.15E-08	-3.1E-08
0.000027	-3.7E-08	6.49E-08	-7E-08	-4.6E-08	5.58E-08	-3.8E-08
2.71E-05	-3.3E-08	6.19E-08	-7.1E-08	-4.7E-08	5.93E-08	-4.5E-08
2.72E-05	-2.9E-08	5.83E-08	-7.1E-08	-4.7E-08	6.2E-08	-5.1E-08
2.73E-05	-2.5E-08	5.41E-08	-7.1E-08	-4.7E-08	6.39E-08	-5.6E-08
2.74E-05	-2.1E-08	4.94E-08	-6.9E-08	-4.6E-08	6.49E-08	-6E-08
2.75E-05	-1.7E-08	4.43E-08	-6.7E-08	-4.4E-08	6.52E-08	-6.4E-08
2.76E-05	-1.4E-08	3.89E-08	-6.3E-08	-4.3E-08	6.46E-08	-6.7E-08
2.77E-05	-9.8E-09	3.33E-08	-5.9E-08	-4E-08	6.34E-08	-6.9E-08
2.78E-05	-6.3E-09	2.76E-08	-5.5E-08	-3.8E-08	6.14E-08	-7E-08
2.79E-05	-3E-09	2.18E-08	-4.9E-08	-3.5E-08	5.88E-08	-7E-08
0.000028	1.53E-10	1.6E-08	-4.3E-08	-3.2E-08	5.56E-08	-7E-08
2.81E-05	3.01E-09	1.03E-08	-3.7E-08	-2.9E-08	5.18E-08	-6.8E-08
2.82E-05	5.61E-09	4.78E-09	-3E-08	-2.6E-08	4.77E-08	-6.6E-08
2.83E-05	7.93E-09	-5.1E-10	-2.3E-08	-2.3E-08	4.32E-08	-6.3E-08
2.84E-05	9.98E-09	-5.5E-09	-1.6E-08	-1.9E-08	3.84E-08	-5.9E-08

2.85E-05	1.18E-08	-1E-08	-9E-09	-1.6E-08	3.33E-08	-5.4E-08
2.86E-05	1.33E-08	-1.4E-08	-2E-09	-1.3E-08	2.82E-08	-4.9E-08
2.87E-05	1.45E-08	-1.8E-08	4.94E-09	-9.9E-09	2.3E-08	-4.3E-08
2.88E-05	1.56E-08	-2.2E-08	1.16E-08	-7E-09	1.78E-08	-3.7E-08
2.89E-05	1.64E-08	-2.5E-08	1.79E-08	-4.2E-09	1.26E-08	-3.1E-08
0.000029	1.7E-08	-2.7E-08	2.39E-08	-1.7E-09	7.62E-09	-2.4E-08
2.91E-05	1.74E-08	-2.9E-08	2.93E-08	6.45E-10	2.81E-09	-1.7E-08
2.92E-05	1.76E-08	-3.1E-08	3.42E-08	2.79E-09	-1.8E-09	-1.1E-08
2.93E-05	1.77E-08	-3.2E-08	3.86E-08	4.73E-09	-6E-09	-3.9E-09
2.94E-05	1.77E-08	-3.3E-08	4.23E-08	6.46E-09	-1E-08	2.6E-09
2.95E-05	1.75E-08	-3.3E-08	4.55E-08	8E-09	-1.4E-08	8.91E-09
2.96E-05	1.73E-08	-3.3E-08	4.79E-08	9.35E-09	-1.7E-08	1.49E-08
2.97E-05	1.69E-08	-3.3E-08	4.97E-08	1.05E-08	-2E-08	2.05E-08
2.98E-05	1.65E-08	-3.2E-08	5.09E-08	1.15E-08	-2.2E-08	2.57E-08
2.99E-05	1.6E-08	-3.1E-08	5.15E-08	1.23E-08	-2.4E-08	3.04E-08
0.00003	1.54E-08	-2.9E-08	5.14E-08	1.3E-08	-2.6E-08	3.45E-08
3.01E-05	1.48E-08	-2.8E-08	5.08E-08	1.36E-08	-2.7E-08	3.81E-08
3.02E-05	1.42E-08	-2.6E-08	4.96E-08	1.4E-08	-2.8E-08	4.11E-08
3.03E-05	1.35E-08	-2.5E-08	4.8E-08	1.42E-08	-2.8E-08	4.35E-08
3.04E-05	1.28E-08	-2.3E-08	4.58E-08	1.44E-08	-2.8E-08	4.53E-08
3.05E-05	1.21E-08	-2.1E-08	4.33E-08	1.45E-08	-2.8E-08	4.65E-08
3.06E-05	1.14E-08	-1.9E-08	4.05E-08	1.45E-08	-2.8E-08	4.72E-08
3.07E-05	1.07E-08	-1.7E-08	3.73E-08	1.44E-08	-2.7E-08	4.73E-08
3.08E-05	9.96E-09	-1.5E-08	3.4E-08	1.42E-08	-2.6E-08	4.68E-08
3.09E-05	9.25E-09	-1.3E-08	3.04E-08	1.4E-08	-2.5E-08	4.59E-08
0.000031	8.54E-09	-1.1E-08	2.68E-08	1.37E-08	-2.4E-08	4.45E-08

3.11E-05	7.85E-09	-9.4E-09	2.31E-08	1.33E-08	-2.3E-08	4.27E-08
3.12E-05	7.16E-09	-7.7E-09	1.94E-08	1.29E-08	-2.1E-08	4.05E-08
3.13E-05	6.49E-09	-6E-09	1.57E-08	1.25E-08	-2E-08	3.8E-08
3.14E-05	5.83E-09	-4.5E-09	1.21E-08	1.2E-08	-1.8E-08	3.53E-08
3.15E-05	5.2E-09	-3E-09	8.7E-09	1.16E-08	-1.7E-08	3.24E-08
3.16E-05	4.57E-09	-1.6E-09	5.41E-09	1.11E-08	-1.5E-08	2.93E-08
3.17E-05	3.97E-09	-2.7E-10	2.32E-09	1.05E-08	-1.4E-08	2.61E-08
3.18E-05	3.39E-09	9.38E-10	-5.7E-10	9.99E-09	-1.2E-08	2.28E-08
3.19E-05	2.82E-09	2.05E-09	-3.2E-09	9.45E-09	-1E-08	1.95E-08
0.000032	2.28E-09	3.08E-09	-5.6E-09	8.89E-09	-9E-09	1.63E-08
3.21E-05	1.76E-09	4.01E-09	-7.8E-09	8.33E-09	-7.6E-09	1.31E-08
3.22E-05	1.26E-09	4.85E-09	-9.7E-09	7.78E-09	-6.2E-09	1.01E-08
3.23E-05	7.75E-10	5.61E-09	-1.1E-08	7.22E-09	-4.9E-09	7.18E-09
3.24E-05	3.16E-10	6.28E-09	-1.3E-08	6.67E-09	-3.7E-09	4.42E-09
3.25E-05	-1.2E-10	6.88E-09	-1.4E-08	6.12E-09	-2.5E-09	1.83E-09
3.26E-05	-5.4E-10	7.4E-09	-1.5E-08	5.58E-09	-1.4E-09	-5.7E-10
3.27E-05	-9.3E-10	7.85E-09	-1.6E-08	5.06E-09	-3.1E-10	-2.8E-09
3.28E-05	-1.3E-09	8.23E-09	-1.6E-08	4.54E-09	6.71E-10	-4.8E-09
3.29E-05	-1.7E-09	8.55E-09	-1.7E-08	4.04E-09	1.58E-09	-6.6E-09
0.000033	-2E-09	8.8E-09	-1.7E-08	3.55E-09	2.42E-09	-8.2E-09
3.31E-05	-2.3E-09	9E-09	-1.7E-08	3.07E-09	3.2E-09	-9.6E-09
3.32E-05	-2.6E-09	9.15E-09	-1.7E-08	2.62E-09	3.91E-09	-1.1E-08
3.33E-05	-2.9E-09	9.25E-09	-1.7E-08	2.17E-09	4.56E-09	-1.2E-08
3.34E-05	-3.1E-09	9.31E-09	-1.7E-08	1.75E-09	5.14E-09	-1.3E-08
3.35E-05	-3.4E-09	9.33E-09	-1.6E-08	1.34E-09	5.66E-09	-1.3E-08
3.36E-05	-3.6E-09	9.31E-09	-1.6E-08	9.44E-10	6.13E-09	-1.4E-08

3.37E-05	-3.8E-09	9.25E-09	-1.5E-08	5.69E-10	6.54E-09	-1.4E-08
3.38E-05	-4E-09	9.16E-09	-1.5E-08	2.11E-10	6.9E-09	-1.5E-08
3.39E-05	-4.1E-09	9.05E-09	-1.4E-08	-1.3E-10	7.21E-09	-1.5E-08
0.000034	-4.3E-09	8.91E-09	-1.3E-08	-4.5E-10	7.47E-09	-1.5E-08
3.41E-05	-4.4E-09	8.74E-09	-1.2E-08	-7.6E-10	7.68E-09	-1.5E-08
3.42E-05	-4.5E-09	8.56E-09	-1.2E-08	-1E-09	7.86E-09	-1.4E-08
3.43E-05	-4.6E-09	8.35E-09	-1.1E-08	-1.3E-09	7.99E-09	-1.4E-08
3.44E-05	-4.7E-09	8.13E-09	-1E-08	-1.6E-09	8.09E-09	-1.4E-08
3.45E-05	-4.8E-09	7.9E-09	-9.2E-09	-1.8E-09	8.15E-09	-1.3E-08
3.46E-05	-4.9E-09	7.65E-09	-8.4E-09	-2.1E-09	8.18E-09	-1.3E-08
3.47E-05	-4.9E-09	7.39E-09	-7.6E-09	-2.3E-09	8.17E-09	-1.2E-08
3.48E-05	-5E-09	7.13E-09	-6.8E-09	-2.5E-09	8.14E-09	-1.2E-08
3.49E-05	-5E-09	6.85E-09	-6E-09	-2.6E-09	8.09E-09	-1.1E-08
0.000035	-5E-09	6.57E-09	-5.2E-09	-2.8E-09	8.01E-09	-1.1E-08
3.51E-05	-5.1E-09	6.28E-09	-4.5E-09	-3E-09	7.9E-09	-1E-08
3.52E-05	-5.1E-09	5.99E-09	-3.7E-09	-3.1E-09	7.78E-09	-9.3E-09
3.53E-05	-5.1E-09	5.7E-09	-3E-09	-3.3E-09	7.64E-09	-8.6E-09
3.54E-05	-5.1E-09	5.41E-09	-2.3E-09	-3.4E-09	7.49E-09	-8E-09
3.55E-05	-5.1E-09	5.11E-09	-1.7E-09	-3.5E-09	7.31E-09	-7.3E-09
3.56E-05	-5.1E-09	4.81E-09	-1E-09	-3.6E-09	7.13E-09	-6.6E-09
3.57E-05	-5E-09	4.52E-09	-4.3E-10	-3.7E-09	6.93E-09	-5.9E-09
3.58E-05	-5E-09	4.23E-09	1.4E-10	-3.8E-09	6.73E-09	-5.3E-09
3.59E-05	-5E-09	3.94E-09	6.8E-10	-3.9E-09	6.51E-09	-4.6E-09
0.000036	-5E-09	3.65E-09	1.19E-09	-4E-09	6.29E-09	-4E-09
3.61E-05	-4.9E-09	3.37E-09	1.67E-09	-4E-09	6.07E-09	-3.4E-09
3.62E-05	-4.9E-09	3.09E-09	2.11E-09	-4.1E-09	5.84E-09	-2.8E-09

3.63E-05	-4.8E-09	2.82E-09	2.53E-09	-4.1E-09	5.6E-09	-2.2E-09
3.64E-05	-4.8E-09	2.56E-09	2.92E-09	-4.2E-09	5.37E-09	-1.6E-09
3.65E-05	-4.7E-09	2.3E-09	3.28E-09	-4.2E-09	5.13E-09	-1.1E-09
3.66E-05	-4.7E-09	2.05E-09	3.61E-09	-4.3E-09	4.89E-09	-5.8E-10
3.67E-05	-4.6E-09	1.8E-09	3.91E-09	-4.3E-09	4.65E-09	-8.6E-11
3.68E-05	-4.6E-09	1.56E-09	4.18E-09	-4.3E-09	4.42E-09	3.82E-10
3.69E-05	-4.5E-09	1.33E-09	4.43E-09	-4.3E-09	4.18E-09	8.25E-10
0.000037	-4.5E-09	1.11E-09	4.65E-09	-4.3E-09	3.95E-09	1.25E-09
3.71E-05	-4.4E-09	9E-10	4.85E-09	-4.3E-09	3.72E-09	1.64E-09
3.72E-05	-4.3E-09	6.94E-10	5.03E-09	-4.3E-09	3.49E-09	2.02E-09
3.73E-05	-4.3E-09	4.97E-10	5.19E-09	-4.3E-09	3.27E-09	2.37E-09
3.74E-05	-4.2E-09	3.07E-10	5.32E-09	-4.3E-09	3.05E-09	2.69E-09
3.75E-05	-4.1E-09	1.25E-10	5.44E-09	-4.3E-09	2.84E-09	3E-09
3.76E-05	-4E-09	-4.9E-11	5.54E-09	-4.3E-09	2.63E-09	3.28E-09
3.77E-05	-4E-09	-2.2E-10	5.62E-09	-4.3E-09	2.42E-09	3.55E-09
3.78E-05	-3.9E-09	-3.8E-10	5.68E-09	-4.2E-09	2.22E-09	3.79E-09
3.79E-05	-3.8E-09	-5.3E-10	5.73E-09	-4.2E-09	2.03E-09	4.01E-09
0.000038	-3.8E-09	-6.8E-10	5.77E-09	-4.2E-09	1.83E-09	4.21E-09
3.81E-05	-3.7E-09	-8.2E-10	5.79E-09	-4.2E-09	1.64E-09	4.4E-09
3.82E-05	-3.6E-09	-9.6E-10	5.79E-09	-4.1E-09	1.46E-09	4.57E-09
3.83E-05	-3.5E-09	-1.1E-09	5.79E-09	-4.1E-09	1.27E-09	4.72E-09
3.84E-05	-3.5E-09	-1.2E-09	5.77E-09	-4E-09	1.09E-09	4.85E-09
3.85E-05	-3.4E-09	-1.3E-09	5.75E-09	-4E-09	9.19E-10	4.97E-09
3.86E-05	-3.3E-09	-1.5E-09	5.71E-09	-4E-09	7.47E-10	5.07E-09
3.87E-05	-3.2E-09	-1.6E-09	5.66E-09	-3.9E-09	5.77E-10	5.16E-09
3.88E-05	-3.2E-09	-1.7E-09	5.61E-09	-3.9E-09	4.1E-10	5.23E-09

3.89E-05	-3.1E-09	-1.8E-09	5.54E-09	-3.8E-09	2.46E-10	5.29E-09
0.000039	-3E-09	-1.9E-09	5.47E-09	-3.8E-09	8.5E-11	5.34E-09
3.91E-05	-2.9E-09	-2E-09	5.39E-09	-3.7E-09	-7.3E-11	5.37E-09
3.92E-05	-2.9E-09	-2.1E-09	5.3E-09	-3.7E-09	-2.3E-10	5.39E-09
3.93E-05	-2.8E-09	-2.2E-09	5.2E-09	-3.6E-09	-3.8E-10	5.39E-09
3.94E-05	-2.7E-09	-2.3E-09	5.1E-09	-3.6E-09	-5.3E-10	5.39E-09
3.95E-05	-2.7E-09	-2.4E-09	4.99E-09	-3.5E-09	-6.8E-10	5.37E-09
3.96E-05	-2.6E-09	-2.5E-09	4.87E-09	-3.5E-09	-8.2E-10	5.35E-09
3.97E-05	-2.5E-09	-2.5E-09	4.75E-09	-3.4E-09	-9.6E-10	5.31E-09
3.98E-05	-2.5E-09	-2.6E-09	4.63E-09	-3.3E-09	-1.1E-09	5.27E-09
3.99E-05	-2.4E-09	-2.7E-09	4.5E-09	-3.3E-09	-1.2E-09	5.21E-09
0.00004	-2.3E-09	-2.8E-09	4.37E-09	-3.2E-09	-1.3E-09	5.15E-09
4.01E-05	-2.3E-09	-2.8E-09	4.23E-09	-3.2E-09	-1.5E-09	5.08E-09
4.02E-05	-2.2E-09	-2.9E-09	4.09E-09	-3.1E-09	-1.6E-09	5.01E-09
4.03E-05	-2.1E-09	-3E-09	3.95E-09	-3.1E-09	-1.7E-09	4.92E-09
4.04E-05	-2.1E-09	-3E-09	3.8E-09	-3E-09	-1.8E-09	4.83E-09
4.05E-05	-2E-09	-3.1E-09	3.66E-09	-3E-09	-1.9E-09	4.74E-09
4.06E-05	-1.9E-09	-3.1E-09	3.51E-09	-2.9E-09	-2E-09	4.64E-09
4.07E-05	-1.9E-09	-3.1E-09	3.36E-09	-2.8E-09	-2.1E-09	4.53E-09
4.08E-05	-1.8E-09	-3.2E-09	3.21E-09	-2.8E-09	-2.2E-09	4.42E-09
4.09E-05	-1.8E-09	-3.2E-09	3.06E-09	-2.7E-09	-2.2E-09	4.31E-09
0.000041	-1.7E-09	-3.2E-09	2.91E-09	-2.7E-09	-2.3E-09	4.2E-09
4.11E-05	-1.7E-09	-3.2E-09	2.77E-09	-2.6E-09	-2.4E-09	4.08E-09
4.12E-05	-1.6E-09	-3.2E-09	2.62E-09	-2.6E-09	-2.4E-09	3.96E-09
4.13E-05	-1.5E-09	-3.2E-09	2.47E-09	-2.5E-09	-2.5E-09	3.84E-09
4.14E-05	-1.5E-09	-3.2E-09	2.33E-09	-2.5E-09	-2.5E-09	3.71E-09

4.15E-05	-1.4E-09	-3.2E-09	2.19E-09	-2.4E-09	-2.6E-09	3.59E-09
4.16E-05	-1.4E-09	-3.2E-09	2.05E-09	-2.4E-09	-2.6E-09	3.47E-09
4.17E-05	-1.3E-09	-3.2E-09	1.92E-09	-2.3E-09	-2.6E-09	3.34E-09
4.18E-05	-1.3E-09	-3.2E-09	1.78E-09	-2.3E-09	-2.6E-09	3.22E-09
4.19E-05	-1.3E-09	-3.2E-09	1.65E-09	-2.2E-09	-2.7E-09	3.09E-09
0.000042	-1.2E-09	-3.2E-09	1.52E-09	-2.2E-09	-2.7E-09	2.97E-09
4.21E-05	-1.2E-09	-3.2E-09	1.4E-09	-2.1E-09	-2.7E-09	2.85E-09
4.22E-05	-1.1E-09	-3.2E-09	1.28E-09	-2.1E-09	-2.7E-09	2.72E-09
4.23E-05	-1.1E-09	-3.1E-09	1.16E-09	-2E-09	-2.7E-09	2.6E-09
4.24E-05	-1E-09	-3.1E-09	1.04E-09	-2E-09	-2.7E-09	2.48E-09
4.25E-05	-1E-09	-3.1E-09	9.27E-10	-1.9E-09	-2.7E-09	2.37E-09
4.26E-05	-9.6E-10	-3.1E-09	8.17E-10	-1.9E-09	-2.8E-09	2.25E-09
4.27E-05	-9.2E-10	-3E-09	7.1E-10	-1.8E-09	-2.8E-09	2.13E-09
4.28E-05	-8.9E-10	-3E-09	6.05E-10	-1.8E-09	-2.8E-09	2.02E-09
4.29E-05	-8.5E-10	-3E-09	5.04E-10	-1.7E-09	-2.8E-09	1.91E-09
0.000043	-8.1E-10	-3E-09	4.05E-10	-1.7E-09	-2.8E-09	1.79E-09
4.31E-05	-7.8E-10	-2.9E-09	3.09E-10	-1.7E-09	-2.8E-09	1.69E-09
4.32E-05	-7.4E-10	-2.9E-09	2.15E-10	-1.6E-09	-2.8E-09	1.58E-09
4.33E-05	-7.1E-10	-2.9E-09	1.24E-10	-1.6E-09	-2.8E-09	1.47E-09
4.34E-05	-6.7E-10	-2.9E-09	3.57E-11	-1.5E-09	-2.8E-09	1.37E-09
4.35E-05	-6.4E-10	-2.9E-09	-5E-11	-1.5E-09	-2.8E-09	1.26E-09
4.36E-05	-6.1E-10	-2.8E-09	-1.3E-10	-1.4E-09	-2.8E-09	1.16E-09
4.37E-05	-5.7E-10	-2.8E-09	-2.1E-10	-1.4E-09	-2.8E-09	1.06E-09
4.38E-05	-5.4E-10	-2.8E-09	-2.9E-10	-1.4E-09	-2.8E-09	9.68E-10
4.39E-05	-5E-10	-2.8E-09	-3.7E-10	-1.3E-09	-2.8E-09	8.72E-10
0.000044	-4.7E-10	-2.7E-09	-4.4E-10	-1.3E-09	-2.8E-09	7.78E-10

4.41E-05	-4.3E-10	-2.7E-09	-5.2E-10	-1.2E-09	-2.8E-09	6.85E-10
4.42E-05	-4E-10	-2.7E-09	-5.9E-10	-1.2E-09	-2.8E-09	5.94E-10
4.43E-05	-3.6E-10	-2.7E-09	-6.6E-10	-1.1E-09	-2.8E-09	5.06E-10
4.44E-05	-3.3E-10	-2.6E-09	-7.2E-10	-1.1E-09	-2.8E-09	4.18E-10
4.45E-05	-2.9E-10	-2.6E-09	-7.9E-10	-1.1E-09	-2.8E-09	3.33E-10
4.46E-05	-2.6E-10	-2.6E-09	-8.5E-10	-1E-09	-2.7E-09	2.49E-10
4.47E-05	-2.2E-10	-2.5E-09	-9.1E-10	-9.7E-10	-2.7E-09	1.67E-10
4.48E-05	-1.9E-10	-2.5E-09	-9.7E-10	-9.3E-10	-2.7E-09	8.6E-11
4.49E-05	-1.5E-10	-2.5E-09	-1E-09	-8.8E-10	-2.7E-09	6.91E-12
0.000045	-1.2E-10	-2.4E-09	-1.1E-09	-8.4E-10	-2.7E-09	-7E-11
4.51E-05	-8.5E-11	-2.4E-09	-1.1E-09	-8E-10	-2.6E-09	-1.5E-10
4.52E-05	-5.2E-11	-2.4E-09	-1.2E-09	-7.5E-10	-2.6E-09	-2.2E-10
4.53E-05	-1.9E-11	-2.3E-09	-1.3E-09	-7.1E-10	-2.6E-09	-2.9E-10
4.54E-05	1.23E-11	-2.3E-09	-1.3E-09	-6.7E-10	-2.6E-09	-3.7E-10
4.55E-05	4.32E-11	-2.2E-09	-1.3E-09	-6.3E-10	-2.5E-09	-4.4E-10
4.56E-05	7.32E-11	-2.2E-09	-1.4E-09	-5.9E-10	-2.5E-09	-5E-10
4.57E-05	1.02E-10	-2.1E-09	-1.4E-09	-5.5E-10	-2.5E-09	-5.7E-10
4.58E-05	1.3E-10	-2.1E-09	-1.5E-09	-5.2E-10	-2.4E-09	-6.4E-10
4.59E-05	1.56E-10	-2.1E-09	-1.5E-09	-4.8E-10	-2.4E-09	-7E-10
0.000046	1.81E-10	-2E-09	-1.6E-09	-4.5E-10	-2.4E-09	-7.6E-10
4.61E-05	2.05E-10	-2E-09	-1.6E-09	-4.1E-10	-2.3E-09	-8.2E-10
4.62E-05	2.28E-10	-1.9E-09	-1.7E-09	-3.8E-10	-2.3E-09	-8.8E-10
4.63E-05	2.49E-10	-1.9E-09	-1.7E-09	-3.5E-10	-2.3E-09	-9.4E-10
4.64E-05	2.69E-10	-1.9E-09	-1.7E-09	-3.2E-10	-2.2E-09	-1E-09
4.65E-05	2.87E-10	-1.8E-09	-1.8E-09	-2.9E-10	-2.2E-09	-1.1E-09
4.66E-05	3.05E-10	-1.8E-09	-1.8E-09	-2.7E-10	-2.2E-09	-1.1E-09

4.67E-05	3.21E-10	-1.7E-09	-1.8E-09	-2.4E-10	-2.1E-09	-1.2E-09
4.68E-05	3.35E-10	-1.7E-09	-1.8E-09	-2.2E-10	-2.1E-09	-1.2E-09
4.69E-05	3.49E-10	-1.7E-09	-1.9E-09	-2E-10	-2.1E-09	-1.3E-09
0.000047	3.61E-10	-1.7E-09	-1.9E-09	-1.8E-10	-2.1E-09	-1.3E-09
4.71E-05	3.73E-10	-1.6E-09	-1.9E-09	-1.6E-10	-2E-09	-1.3E-09
4.72E-05	3.84E-10	-1.6E-09	-1.9E-09	-1.4E-10	-2E-09	-1.4E-09
4.73E-05	3.94E-10	-1.6E-09	-2E-09	-1.2E-10	-2E-09	-1.4E-09
4.74E-05	4.03E-10	-1.5E-09	-2E-09	-1E-10	-2E-09	-1.5E-09
4.75E-05	4.12E-10	-1.5E-09	-2E-09	-8.4E-11	-1.9E-09	-1.5E-09
4.76E-05	4.2E-10	-1.5E-09	-2E-09	-6.8E-11	-1.9E-09	-1.5E-09
4.77E-05	4.28E-10	-1.5E-09	-2E-09	-5.2E-11	-1.9E-09	-1.6E-09
4.78E-05	4.36E-10	-1.4E-09	-2E-09	-3.6E-11	-1.9E-09	-1.6E-09
4.79E-05	4.43E-10	-1.4E-09	-2E-09	-2E-11	-1.8E-09	-1.6E-09
0.000048	4.5E-10	-1.4E-09	-2.1E-09	-5.1E-12	-1.8E-09	-1.6E-09
4.81E-05	4.58E-10	-1.4E-09	-2.1E-09	9.99E-12	-1.8E-09	-1.7E-09
4.82E-05	4.65E-10	-1.3E-09	-2.1E-09	2.5E-11	-1.8E-09	-1.7E-09
4.83E-05	4.72E-10	-1.3E-09	-2.1E-09	3.99E-11	-1.8E-09	-1.7E-09
4.84E-05	4.79E-10	-1.3E-09	-2.1E-09	5.47E-11	-1.7E-09	-1.7E-09
4.85E-05	4.87E-10	-1.3E-09	-2.1E-09	6.95E-11	-1.7E-09	-1.8E-09
4.86E-05	4.94E-10	-1.2E-09	-2.1E-09	8.42E-11	-1.7E-09	-1.8E-09
4.87E-05	5.01E-10	-1.2E-09	-2.1E-09	9.88E-11	-1.7E-09	-1.8E-09
4.88E-05	5.09E-10	-1.2E-09	-2.1E-09	1.13E-10	-1.6E-09	-1.8E-09
4.89E-05	5.16E-10	-1.2E-09	-2.1E-09	1.28E-10	-1.6E-09	-1.8E-09
0.000049	5.23E-10	-1.1E-09	-2.1E-09	1.42E-10	-1.6E-09	-1.8E-09
4.91E-05	5.3E-10	-1.1E-09	-2.1E-09	1.56E-10	-1.6E-09	-1.8E-09
4.92E-05	5.37E-10	-1.1E-09	-2E-09	1.7E-10	-1.5E-09	-1.8E-09

4.93E-05	5.44E-10	-1.1E-09	-2E-09	1.84E-10	-1.5E-09	-1.8E-09
4.94E-05	5.5E-10	-1E-09	-2E-09	1.97E-10	-1.5E-09	-1.8E-09
4.95E-05	5.57E-10	-1E-09	-2E-09	2.1E-10	-1.4E-09	-1.8E-09
4.96E-05	5.63E-10	-9.7E-10	-2E-09	2.23E-10	-1.4E-09	-1.9E-09
4.97E-05	5.69E-10	-9.4E-10	-2E-09	2.36E-10	-1.4E-09	-1.9E-09
4.98E-05	5.75E-10	-9.1E-10	-2E-09	2.48E-10	-1.4E-09	-1.9E-09
4.99E-05	5.81E-10	-8.8E-10	-2E-09	2.6E-10	-1.3E-09	-1.9E-09
0.00005	5.86E-10	-8.6E-10	-2E-09	2.72E-10	-1.3E-09	-1.9E-09
5.01E-05	5.92E-10	-8.3E-10	-2E-09	2.84E-10	-1.3E-09	-1.9E-09
5.02E-05	5.97E-10	-8E-10	-2E-09	2.95E-10	-1.2E-09	-1.9E-09
5.03E-05	6.02E-10	-7.8E-10	-1.9E-09	3.06E-10	-1.2E-09	-1.9E-09
5.04E-05	6.07E-10	-7.5E-10	-1.9E-09	3.17E-10	-1.2E-09	-1.9E-09
5.05E-05	6.11E-10	-7.3E-10	-1.9E-09	3.28E-10	-1.2E-09	-1.9E-09
5.06E-05	6.16E-10	-7E-10	-1.9E-09	3.38E-10	-1.1E-09	-1.9E-09
5.07E-05	6.2E-10	-6.8E-10	-1.9E-09	3.48E-10	-1.1E-09	-1.9E-09
5.08E-05	6.25E-10	-6.6E-10	-1.9E-09	3.58E-10	-1.1E-09	-1.9E-09
5.09E-05	6.28E-10	-6.3E-10	-1.9E-09	3.68E-10	-1.1E-09	-1.9E-09
0.000051	6.32E-10	-6.1E-10	-1.9E-09	3.77E-10	-1E-09	-1.9E-09
5.11E-05	6.36E-10	-5.9E-10	-1.9E-09	3.86E-10	-1E-09	-1.8E-09
5.12E-05	6.39E-10	-5.7E-10	-1.8E-09	3.94E-10	-9.8E-10	-1.8E-09
5.13E-05	6.42E-10	-5.5E-10	-1.8E-09	4.02E-10	-9.5E-10	-1.8E-09
5.14E-05	6.44E-10	-5.3E-10	-1.8E-09	4.1E-10	-9.3E-10	-1.8E-09
5.15E-05	6.47E-10	-5.1E-10	-1.8E-09	4.17E-10	-9.1E-10	-1.8E-09
5.16E-05	6.49E-10	-4.9E-10	-1.8E-09	4.24E-10	-8.9E-10	-1.8E-09
5.17E-05	6.5E-10	-4.7E-10	-1.8E-09	4.31E-10	-8.7E-10	-1.8E-09
5.18E-05	6.52E-10	-4.5E-10	-1.8E-09	4.37E-10	-8.4E-10	-1.8E-09

5.19E-05	6.53E-10	-4.4E-10	-1.7E-09	4.43E-10	-8.2E-10	-1.8E-09
0.000052	6.53E-10	-4.2E-10	-1.7E-09	4.49E-10	-8E-10	-1.8E-09
5.21E-05	6.54E-10	-4E-10	-1.7E-09	4.54E-10	-7.8E-10	-1.8E-09
5.22E-05	6.54E-10	-3.8E-10	-1.7E-09	4.59E-10	-7.7E-10	-1.8E-09
5.23E-05	6.54E-10	-3.7E-10	-1.7E-09	4.63E-10	-7.5E-10	-1.8E-09
5.24E-05	6.54E-10	-3.5E-10	-1.7E-09	4.68E-10	-7.3E-10	-1.8E-09
5.25E-05	6.54E-10	-3.4E-10	-1.6E-09	4.72E-10	-7.1E-10	-1.7E-09
5.26E-05	6.53E-10	-3.2E-10	-1.6E-09	4.75E-10	-6.9E-10	-1.7E-09
5.27E-05	6.52E-10	-3.1E-10	-1.6E-09	4.79E-10	-6.7E-10	-1.7E-09
5.28E-05	6.52E-10	-2.9E-10	-1.6E-09	4.82E-10	-6.6E-10	-1.7E-09
5.29E-05	6.51E-10	-2.8E-10	-1.6E-09	4.85E-10	-6.4E-10	-1.7E-09
0.000053	6.5E-10	-2.6E-10	-1.6E-09	4.88E-10	-6.2E-10	-1.7E-09
5.31E-05	6.49E-10	-2.5E-10	-1.5E-09	4.91E-10	-6E-10	-1.7E-09
5.32E-05	6.47E-10	-2.4E-10	-1.5E-09	4.94E-10	-5.9E-10	-1.7E-09
5.33E-05	6.46E-10	-2.2E-10	-1.5E-09	4.97E-10	-5.7E-10	-1.6E-09
5.34E-05	6.45E-10	-2.1E-10	-1.5E-09	4.99E-10	-5.5E-10	-1.6E-09
5.35E-05	6.44E-10	-1.9E-10	-1.5E-09	5.02E-10	-5.4E-10	-1.6E-09
5.36E-05	6.43E-10	-1.8E-10	-1.5E-09	5.04E-10	-5.2E-10	-1.6E-09
5.37E-05	6.42E-10	-1.6E-10	-1.4E-09	5.07E-10	-5E-10	-1.6E-09
5.38E-05	6.41E-10	-1.5E-10	-1.4E-09	5.09E-10	-4.8E-10	-1.6E-09
5.39E-05	6.4E-10	-1.4E-10	-1.4E-09	5.12E-10	-4.7E-10	-1.6E-09
0.000054	6.39E-10	-1.2E-10	-1.4E-09	5.14E-10	-4.5E-10	-1.5E-09
5.41E-05	6.38E-10	-1.1E-10	-1.4E-09	5.17E-10	-4.3E-10	-1.5E-09
5.42E-05	6.37E-10	-9.4E-11	-1.4E-09	5.2E-10	-4.2E-10	-1.5E-09
5.43E-05	6.36E-10	-8E-11	-1.3E-09	5.22E-10	-4E-10	-1.5E-09
5.44E-05	6.36E-10	-6.6E-11	-1.3E-09	5.25E-10	-3.8E-10	-1.5E-09

5.45E-05	6.35E-10	-5.3E-11	-1.3E-09	5.28E-10	-3.6E-10	-1.5E-09
5.46E-05	6.35E-10	-3.9E-11	-1.3E-09	5.3E-10	-3.5E-10	-1.5E-09
5.47E-05	6.35E-10	-2.6E-11	-1.3E-09	5.33E-10	-3.3E-10	-1.5E-09
5.48E-05	6.34E-10	-1.3E-11	-1.3E-09	5.36E-10	-3.1E-10	-1.4E-09
5.49E-05	6.34E-10	4.35E-13	-1.2E-09	5.39E-10	-3E-10	-1.4E-09
0.000055	6.34E-10	1.31E-11	-1.2E-09	5.41E-10	-2.8E-10	-1.4E-09
5.51E-05	6.34E-10	2.54E-11	-1.2E-09	5.44E-10	-2.7E-10	-1.4E-09
5.52E-05	6.34E-10	3.74E-11	-1.2E-09	5.47E-10	-2.5E-10	-1.4E-09
5.53E-05	6.33E-10	4.9E-11	-1.2E-09	5.49E-10	-2.4E-10	-1.4E-09
5.54E-05	6.33E-10	6.01E-11	-1.2E-09	5.51E-10	-2.2E-10	-1.4E-09
5.55E-05	6.32E-10	7.08E-11	-1.1E-09	5.54E-10	-2.1E-10	-1.3E-09
5.56E-05	6.32E-10	8.11E-11	-1.1E-09	5.56E-10	-1.9E-10	-1.3E-09
5.57E-05	6.31E-10	9.09E-11	-1.1E-09	5.57E-10	-1.8E-10	-1.3E-09
5.58E-05	6.3E-10	1E-10	-1.1E-09	5.59E-10	-1.7E-10	-1.3E-09
5.59E-05	6.29E-10	1.09E-10	-1.1E-09	5.6E-10	-1.5E-10	-1.3E-09
0.000056	6.28E-10	1.18E-10	-1.1E-09	5.62E-10	-1.4E-10	-1.3E-09
5.61E-05	6.26E-10	1.26E-10	-1E-09	5.63E-10	-1.3E-10	-1.3E-09
5.62E-05	6.25E-10	1.33E-10	-1E-09	5.63E-10	-1.2E-10	-1.2E-09
5.63E-05	6.23E-10	1.4E-10	-1E-09	5.64E-10	-1.1E-10	-1.2E-09
5.64E-05	6.21E-10	1.47E-10	-1E-09	5.64E-10	-9.8E-11	-1.2E-09
5.65E-05	6.19E-10	1.54E-10	-9.9E-10	5.64E-10	-8.8E-11	-1.2E-09
5.66E-05	6.17E-10	1.6E-10	-9.7E-10	5.64E-10	-7.9E-11	-1.2E-09
5.67E-05	6.14E-10	1.66E-10	-9.5E-10	5.64E-10	-7E-11	-1.2E-09
5.68E-05	6.11E-10	1.72E-10	-9.4E-10	5.63E-10	-6.1E-11	-1.2E-09
5.69E-05	6.09E-10	1.78E-10	-9.2E-10	5.62E-10	-5.3E-11	-1.1E-09
0.000057	6.06E-10	1.83E-10	-9.1E-10	5.62E-10	-4.5E-11	-1.1E-09

5.71E-05	6.03E-10	1.89E-10	-8.9E-10	5.61E-10	-3.7E-11	-1.1E-09
5.72E-05	5.99E-10	1.94E-10	-8.7E-10	5.59E-10	-2.9E-11	-1.1E-09
5.73E-05	5.96E-10	1.99E-10	-8.6E-10	5.58E-10	-2.2E-11	-1.1E-09
5.74E-05	5.93E-10	2.04E-10	-8.4E-10	5.57E-10	-1.5E-11	-1.1E-09
5.75E-05	5.9E-10	2.09E-10	-8.2E-10	5.55E-10	-7.2E-12	-1E-09
5.76E-05	5.86E-10	2.14E-10	-8.1E-10	5.53E-10	1.45E-14	-1E-09
5.77E-05	5.83E-10	2.19E-10	-7.9E-10	5.52E-10	7.24E-12	-1E-09
5.78E-05	5.79E-10	2.23E-10	-7.8E-10	5.5E-10	1.44E-11	-1E-09
5.79E-05	5.76E-10	2.28E-10	-7.6E-10	5.48E-10	2.16E-11	-9.8E-10
0.000058	5.72E-10	2.33E-10	-7.4E-10	5.46E-10	2.88E-11	-9.6E-10
5.81E-05	5.69E-10	2.38E-10	-7.3E-10	5.45E-10	3.59E-11	-9.5E-10
5.82E-05	5.66E-10	2.43E-10	-7.1E-10	5.43E-10	4.31E-11	-9.3E-10
5.83E-05	5.62E-10	2.47E-10	-7E-10	5.41E-10	5.01E-11	-9.2E-10
5.84E-05	5.59E-10	2.52E-10	-6.8E-10	5.39E-10	5.72E-11	-9E-10
5.85E-05	5.56E-10	2.57E-10	-6.7E-10	5.38E-10	6.42E-11	-8.9E-10
5.86E-05	5.53E-10	2.61E-10	-6.5E-10	5.36E-10	7.11E-11	-8.7E-10
5.87E-05	5.49E-10	2.66E-10	-6.4E-10	5.34E-10	7.79E-11	-8.6E-10
5.88E-05	5.46E-10	2.7E-10	-6.3E-10	5.33E-10	8.46E-11	-8.4E-10
5.89E-05	5.43E-10	2.75E-10	-6.1E-10	5.31E-10	9.13E-11	-8.3E-10
0.000059	5.4E-10	2.79E-10	-6E-10	5.3E-10	9.77E-11	-8.1E-10
5.91E-05	5.38E-10	2.83E-10	-5.8E-10	5.28E-10	1.04E-10	-8E-10
5.92E-05	5.35E-10	2.87E-10	-5.7E-10	5.26E-10	1.1E-10	-7.9E-10
5.93E-05	5.32E-10	2.91E-10	-5.6E-10	5.25E-10	1.16E-10	-7.7E-10
5.94E-05	5.29E-10	2.95E-10	-5.5E-10	5.23E-10	1.22E-10	-7.6E-10
5.95E-05	5.26E-10	2.98E-10	-5.3E-10	5.21E-10	1.28E-10	-7.5E-10
5.96E-05	5.23E-10	3.02E-10	-5.2E-10	5.2E-10	1.34E-10	-7.3E-10

5.97E-05	5.2E-10	3.05E-10	-5.1E-10	5.18E-10	1.4E-10	-7.2E-10
5.98E-05	5.17E-10	3.08E-10	-5E-10	5.16E-10	1.45E-10	-7.1E-10
5.99E-05	5.14E-10	3.1E-10	-4.9E-10	5.14E-10	1.5E-10	-7E-10
0.00006	5.11E-10	3.13E-10	-4.8E-10	5.12E-10	1.56E-10	-6.8E-10
6.01E-05	5.08E-10	3.15E-10	-4.7E-10	5.1E-10	1.61E-10	-6.7E-10
6.02E-05	5.05E-10	3.18E-10	-4.5E-10	5.08E-10	1.66E-10	-6.6E-10
6.03E-05	5.02E-10	3.2E-10	-4.4E-10	5.06E-10	1.71E-10	-6.5E-10
6.04E-05	4.98E-10	3.22E-10	-4.3E-10	5.04E-10	1.76E-10	-6.4E-10
6.05E-05	4.95E-10	3.24E-10	-4.2E-10	5.01E-10	1.81E-10	-6.3E-10
6.06E-05	4.92E-10	3.25E-10	-4.1E-10	4.99E-10	1.86E-10	-6.2E-10
6.07E-05	4.88E-10	3.27E-10	-4E-10	4.96E-10	1.91E-10	-6E-10
6.08E-05	4.85E-10	3.29E-10	-3.9E-10	4.94E-10	1.95E-10	-5.9E-10
6.09E-05	4.81E-10	3.31E-10	-3.8E-10	4.91E-10	2E-10	-5.8E-10
0.000061	4.77E-10	3.32E-10	-3.7E-10	4.88E-10	2.04E-10	-5.7E-10
6.11E-05	4.74E-10	3.34E-10	-3.6E-10	4.86E-10	2.09E-10	-5.6E-10
6.12E-05	4.7E-10	3.35E-10	-3.5E-10	4.83E-10	2.13E-10	-5.5E-10
6.13E-05	4.67E-10	3.37E-10	-3.4E-10	4.8E-10	2.18E-10	-5.4E-10
6.14E-05	4.63E-10	3.39E-10	-3.3E-10	4.77E-10	2.22E-10	-5.3E-10
6.15E-05	4.59E-10	3.4E-10	-3.2E-10	4.75E-10	2.26E-10	-5.2E-10
6.16E-05	4.56E-10	3.42E-10	-3.1E-10	4.72E-10	2.3E-10	-5E-10
6.17E-05	4.52E-10	3.44E-10	-3E-10	4.69E-10	2.34E-10	-4.9E-10
6.18E-05	4.49E-10	3.45E-10	-2.9E-10	4.66E-10	2.37E-10	-4.8E-10
6.19E-05	4.45E-10	3.47E-10	-2.8E-10	4.63E-10	2.41E-10	-4.7E-10
0.000062	4.42E-10	3.48E-10	-2.8E-10	4.61E-10	2.45E-10	-4.6E-10
6.21E-05	4.38E-10	3.49E-10	-2.7E-10	4.58E-10	2.48E-10	-4.5E-10
6.22E-05	4.35E-10	3.51E-10	-2.6E-10	4.55E-10	2.52E-10	-4.4E-10

6.23E-05	4.32E-10	3.52E-10	-2.5E-10	4.53E-10	2.55E-10	-4.3E-10
6.24E-05	4.29E-10	3.53E-10	-2.4E-10	4.5E-10	2.58E-10	-4.2E-10
6.25E-05	4.26E-10	3.55E-10	-2.3E-10	4.48E-10	2.61E-10	-4.1E-10
6.26E-05	4.23E-10	3.56E-10	-2.2E-10	4.46E-10	2.64E-10	-4E-10
6.27E-05	4.2E-10	3.57E-10	-2.1E-10	4.43E-10	2.67E-10	-3.9E-10
6.28E-05	4.17E-10	3.58E-10	-2E-10	4.41E-10	2.7E-10	-3.8E-10
6.29E-05	4.14E-10	3.59E-10	-1.9E-10	4.39E-10	2.73E-10	-3.7E-10
0.000063	4.12E-10	3.61E-10	-1.8E-10	4.37E-10	2.75E-10	-3.6E-10
6.31E-05	4.09E-10	3.62E-10	-1.8E-10	4.35E-10	2.78E-10	-3.5E-10
6.32E-05	4.07E-10	3.63E-10	-1.7E-10	4.33E-10	2.8E-10	-3.4E-10
6.33E-05	4.04E-10	3.64E-10	-1.6E-10	4.31E-10	2.83E-10	-3.3E-10
6.34E-05	4.02E-10	3.65E-10	-1.5E-10	4.29E-10	2.85E-10	-3.2E-10
6.35E-05	4E-10	3.66E-10	-1.4E-10	4.27E-10	2.87E-10	-3.1E-10
6.36E-05	3.97E-10	3.67E-10	-1.4E-10	4.26E-10	2.89E-10	-3E-10
6.37E-05	3.95E-10	3.67E-10	-1.3E-10	4.24E-10	2.9E-10	-2.9E-10
6.38E-05	3.93E-10	3.68E-10	-1.2E-10	4.22E-10	2.92E-10	-2.9E-10
6.39E-05	3.91E-10	3.69E-10	-1.2E-10	4.21E-10	2.94E-10	-2.8E-10
0.000064	3.89E-10	3.69E-10	-1.1E-10	4.19E-10	2.95E-10	-2.7E-10
6.41E-05	3.87E-10	3.69E-10	-1E-10	4.17E-10	2.97E-10	-2.6E-10
6.42E-05	3.85E-10	3.7E-10	-9.7E-11	4.16E-10	2.98E-10	-2.5E-10
6.43E-05	3.83E-10	3.7E-10	-9.1E-11	4.14E-10	2.99E-10	-2.5E-10
6.44E-05	3.8E-10	3.7E-10	-8.5E-11	4.12E-10	3E-10	-2.4E-10
6.45E-05	3.78E-10	3.7E-10	-7.9E-11	4.1E-10	3.02E-10	-2.3E-10
6.46E-05	3.76E-10	3.7E-10	-7.3E-11	4.09E-10	3.03E-10	-2.3E-10
6.47E-05	3.74E-10	3.7E-10	-6.7E-11	4.07E-10	3.04E-10	-2.2E-10
6.48E-05	3.72E-10	3.7E-10	-6.2E-11	4.05E-10	3.05E-10	-2.1E-10

6.49E-05	3.7E-10	3.7E-10	-5.6E-11	4.03E-10	3.05E-10	-2E-10
0.000065	3.67E-10	3.69E-10	-5.1E-11	4.01E-10	3.06E-10	-2E-10
6.51E-05	3.65E-10	3.69E-10	-4.6E-11	3.99E-10	3.07E-10	-1.9E-10
6.52E-05	3.63E-10	3.68E-10	-4E-11	3.97E-10	3.08E-10	-1.8E-10
6.53E-05	3.6E-10	3.68E-10	-3.5E-11	3.95E-10	3.08E-10	-1.8E-10
6.54E-05	3.58E-10	3.67E-10	-3E-11	3.92E-10	3.09E-10	-1.7E-10
6.55E-05	3.55E-10	3.66E-10	-2.5E-11	3.9E-10	3.1E-10	-1.7E-10
6.56E-05	3.52E-10	3.65E-10	-2E-11	3.88E-10	3.1E-10	-1.6E-10
6.57E-05	3.5E-10	3.65E-10	-1.5E-11	3.86E-10	3.11E-10	-1.5E-10
6.58E-05	3.47E-10	3.64E-10	-1E-11	3.83E-10	3.11E-10	-1.5E-10
6.59E-05	3.44E-10	3.63E-10	-5.1E-12	3.81E-10	3.12E-10	-1.4E-10
0.000066	3.42E-10	3.62E-10	-2.3E-13	3.78E-10	3.12E-10	-1.3E-10
6.61E-05	3.39E-10	3.61E-10	4.55E-12	3.76E-10	3.13E-10	-1.3E-10
6.62E-05	3.36E-10	3.6E-10	9.28E-12	3.73E-10	3.13E-10	-1.2E-10
6.63E-05	3.33E-10	3.59E-10	1.39E-11	3.7E-10	3.13E-10	-1.2E-10
6.64E-05	3.3E-10	3.58E-10	1.86E-11	3.68E-10	3.14E-10	-1.1E-10
6.65E-05	3.27E-10	3.57E-10	2.31E-11	3.65E-10	3.14E-10	-1E-10
6.66E-05	3.25E-10	3.56E-10	2.76E-11	3.62E-10	3.14E-10	-9.9E-11
6.67E-05	3.22E-10	3.55E-10	3.2E-11	3.59E-10	3.14E-10	-9.3E-11
6.68E-05	3.19E-10	3.54E-10	3.64E-11	3.57E-10	3.14E-10	-8.8E-11
6.69E-05	3.16E-10	3.53E-10	4.07E-11	3.54E-10	3.14E-10	-8.2E-11
0.000067	3.13E-10	3.51E-10	4.5E-11	3.51E-10	3.14E-10	-7.7E-11
6.71E-05	3.1E-10	3.5E-10	4.93E-11	3.48E-10	3.14E-10	-7.2E-11
6.72E-05	3.07E-10	3.49E-10	5.35E-11	3.46E-10	3.14E-10	-6.6E-11
6.73E-05	3.04E-10	3.48E-10	5.77E-11	3.43E-10	3.14E-10	-6.1E-11
6.74E-05	3.02E-10	3.47E-10	6.19E-11	3.4E-10	3.13E-10	-5.6E-11

6.75E-05	2.99E-10	3.45E-10	6.6E-11	3.38E-10	3.13E-10	-5.1E-11
6.76E-05	2.96E-10	3.44E-10	7.01E-11	3.35E-10	3.12E-10	-4.5E-11
6.77E-05	2.93E-10	3.43E-10	7.42E-11	3.32E-10	3.12E-10	-4E-11
6.78E-05	2.91E-10	3.42E-10	7.83E-11	3.3E-10	3.11E-10	-3.5E-11
6.79E-05	2.88E-10	3.4E-10	8.23E-11	3.27E-10	3.11E-10	-3E-11
0.000068	2.86E-10	3.39E-10	8.63E-11	3.25E-10	3.1E-10	-2.5E-11
6.81E-05	2.83E-10	3.38E-10	9.02E-11	3.22E-10	3.09E-10	-2E-11
6.82E-05	2.81E-10	3.37E-10	9.41E-11	3.2E-10	3.08E-10	-1.5E-11
6.83E-05	2.78E-10	3.35E-10	9.8E-11	3.18E-10	3.07E-10	-1E-11
6.84E-05	2.76E-10	3.34E-10	1.02E-10	3.15E-10	3.06E-10	-5.2E-12
6.85E-05	2.73E-10	3.33E-10	1.06E-10	3.13E-10	3.06E-10	-4.2E-13
6.86E-05	2.71E-10	3.32E-10	1.09E-10	3.11E-10	3.05E-10	4.28E-12
6.87E-05	2.69E-10	3.31E-10	1.13E-10	3.08E-10	3.04E-10	8.93E-12
6.88E-05	2.67E-10	3.3E-10	1.16E-10	3.06E-10	3.03E-10	1.35E-11
6.89E-05	2.64E-10	3.29E-10	1.2E-10	3.04E-10	3.03E-10	1.8E-11
0.000069	2.62E-10	3.28E-10	1.23E-10	3.02E-10	3.02E-10	2.25E-11
6.91E-05	2.6E-10	3.27E-10	1.27E-10	3E-10	3.01E-10	2.69E-11
6.92E-05	2.58E-10	3.27E-10	1.3E-10	2.98E-10	3.01E-10	3.13E-11
6.93E-05	2.56E-10	3.26E-10	1.34E-10	2.96E-10	3.01E-10	3.56E-11
6.94E-05	2.54E-10	3.25E-10	1.37E-10	2.94E-10	3E-10	3.99E-11
6.95E-05	2.52E-10	3.25E-10	1.4E-10	2.92E-10	3E-10	4.41E-11
6.96E-05	2.5E-10	3.24E-10	1.43E-10	2.91E-10	3E-10	4.83E-11
6.97E-05	2.49E-10	3.23E-10	1.46E-10	2.89E-10	3E-10	5.24E-11
6.98E-05	2.47E-10	3.23E-10	1.49E-10	2.87E-10	3E-10	5.64E-11
6.99E-05	2.45E-10	3.22E-10	1.52E-10	2.85E-10	3E-10	6.03E-11
0.00007	2.43E-10	3.21E-10	1.55E-10	2.83E-10	3E-10	6.42E-11

1.6mm Hole Data (T = transmitter, L = Long Distance Test).

Time	T1R1	T1R2	T1R3	T2R1	T2R2	T2R3
0	3.05E-11	7E-12	7.76E-12	1.75E-11	-4.1E-12	1.96E-12
1E-07	3.1E-11	7.72E-12	6.92E-12	1.79E-11	-3.8E-12	1.61E-12
2E-07	3.14E-11	8.45E-12	6.11E-12	1.85E-11	-3.6E-12	1.32E-12
3E-07	3.18E-11	9.19E-12	5.37E-12	1.93E-11	-3.4E-12	1.05E-12
4E-07	3.23E-11	9.91E-12	4.7E-12	2.01E-11	-3.2E-12	8.03E-13
5E-07	3.27E-11	1.06E-11	4.08E-12	2.09E-11	-2.9E-12	5.76E-13
6E-07	3.31E-11	1.13E-11	3.46E-12	2.18E-11	-2.6E-12	3.78E-13
7E-07	3.36E-11	1.19E-11	2.8E-12	2.26E-11	-2.3E-12	2.15E-13
8E-07	3.4E-11	1.24E-11	2.04E-12	2.34E-11	-2E-12	9.72E-14
9E-07	3.45E-11	1.29E-11	1.13E-12	2.4E-11	-1.7E-12	3.41E-14
0.000001	3.5E-11	1.33E-11	2.89E-14	2.46E-11	-1.5E-12	3.14E-14
1.1E-06	3.55E-11	1.36E-11	-1.3E-12	2.52E-11	-1.3E-12	8.38E-14
1.2E-06	3.6E-11	1.39E-11	-2.8E-12	2.57E-11	-1.2E-12	1.74E-13
1.3E-06	3.65E-11	1.41E-11	-4.4E-12	2.62E-11	-1.2E-12	2.81E-13
1.4E-06	3.7E-11	1.42E-11	-6.1E-12	2.67E-11	-1.3E-12	3.82E-13
1.5E-06	3.74E-11	1.43E-11	-7.8E-12	2.73E-11	-1.4E-12	4.55E-13
1.6E-06	3.78E-11	1.42E-11	-9.4E-12	2.79E-11	-1.5E-12	4.78E-13
1.7E-06	3.81E-11	1.42E-11	-1.1E-11	2.85E-11	-1.6E-12	4.21E-13
1.8E-06	3.82E-11	1.4E-11	-1.2E-11	2.92E-11	-1.7E-12	2.58E-13
1.9E-06	3.83E-11	1.38E-11	-1.3E-11	3E-11	-1.8E-12	-2.8E-14
0.000002	3.81E-11	1.36E-11	-1.4E-11	3.07E-11	-1.9E-12	-4.5E-13
2.1E-06	3.79E-11	1.33E-11	-1.4E-11	3.15E-11	-2E-12	-1E-12

2.2E-06	3.76E-11	1.3E-11	-1.5E-11	3.21E-11	-2.2E-12	-1.7E-12
2.3E-06	3.71E-11	1.28E-11	-1.5E-11	3.27E-11	-2.4E-12	-2.6E-12
2.4E-06	3.66E-11	1.25E-11	-1.5E-11	3.32E-11	-2.7E-12	-3.6E-12
2.5E-06	3.6E-11	1.23E-11	-1.5E-11	3.35E-11	-3E-12	-4.6E-12
2.6E-06	3.55E-11	1.21E-11	-1.5E-11	3.35E-11	-3.4E-12	-5.7E-12
2.7E-06	3.49E-11	1.2E-11	-1.6E-11	3.33E-11	-3.7E-12	-6.9E-12
2.8E-06	3.44E-11	1.18E-11	-1.6E-11	3.28E-11	-4E-12	-8E-12
2.9E-06	3.4E-11	1.18E-11	-1.6E-11	3.21E-11	-4.2E-12	-9E-12
0.000003	3.37E-11	1.18E-11	-1.6E-11	3.12E-11	-4.3E-12	-1E-11
3.1E-06	3.36E-11	1.19E-11	-1.7E-11	3.01E-11	-4.5E-12	-1.1E-11
3.2E-06	3.35E-11	1.2E-11	-1.7E-11	2.9E-11	-4.6E-12	-1.2E-11
3.3E-06	3.37E-11	1.22E-11	-1.6E-11	2.78E-11	-4.8E-12	-1.3E-11
3.4E-06	3.39E-11	1.26E-11	-1.6E-11	2.66E-11	-5E-12	-1.3E-11
3.5E-06	3.43E-11	1.3E-11	-1.5E-11	2.55E-11	-5.3E-12	-1.4E-11
3.6E-06	3.46E-11	1.34E-11	-1.4E-11	2.45E-11	-5.6E-12	-1.4E-11
3.7E-06	3.5E-11	1.4E-11	-1.3E-11	2.37E-11	-6E-12	-1.5E-11
3.8E-06	3.54E-11	1.46E-11	-1.2E-11	2.28E-11	-6.4E-12	-1.5E-11
3.9E-06	3.56E-11	1.53E-11	-1E-11	2.2E-11	-6.7E-12	-1.5E-11
0.000004	3.58E-11	1.59E-11	-8.8E-12	2.13E-11	-7E-12	-1.6E-11
4.1E-06	3.58E-11	1.67E-11	-7.4E-12	2.04E-11	-7.3E-12	-1.6E-11
4.2E-06	3.56E-11	1.74E-11	-6.1E-12	1.95E-11	-7.6E-12	-1.6E-11
4.3E-06	3.53E-11	1.82E-11	-5E-12	1.84E-11	-8E-12	-1.5E-11
4.4E-06	3.48E-11	1.9E-11	-4.1E-12	1.72E-11	-8.4E-12	-1.5E-11
4.5E-06	3.41E-11	1.98E-11	-3.3E-12	1.58E-11	-8.9E-12	-1.5E-11
4.6E-06	3.33E-11	2.06E-11	-2.8E-12	1.43E-11	-9.4E-12	-1.4E-11
4.7E-06	3.24E-11	2.14E-11	-2.3E-12	1.27E-11	-1E-11	-1.4E-11

4.8E-06	3.15E-11	2.22E-11	-1.9E-12	1.12E-11	-1.1E-11	-1.3E-11
4.9E-06	3.05E-11	2.29E-11	-1.5E-12	9.7E-12	-1.1E-11	-1.2E-11
0.000005	2.96E-11	2.36E-11	-1E-12	8.4E-12	-1.2E-11	-1.1E-11
5.1E-06	2.88E-11	2.42E-11	-5E-13	7.38E-12	-1.2E-11	-1E-11
5.2E-06	2.81E-11	2.47E-11	1.34E-13	6.69E-12	-1.3E-11	-9.2E-12
5.3E-06	2.76E-11	2.52E-11	8.61E-13	6.36E-12	-1.3E-11	-8.3E-12
5.4E-06	2.73E-11	2.57E-11	1.65E-12	6.37E-12	-1.3E-11	-7.5E-12
5.5E-06	2.72E-11	2.61E-11	2.46E-12	6.69E-12	-1.3E-11	-6.8E-12
5.6E-06	2.74E-11	2.64E-11	3.2E-12	7.27E-12	-1.4E-11	-6.1E-12
5.7E-06	2.77E-11	2.67E-11	3.81E-12	8.02E-12	-1.4E-11	-5.5E-12
5.8E-06	2.81E-11	2.69E-11	4.23E-12	8.87E-12	-1.4E-11	-5.1E-12
5.9E-06	2.88E-11	2.7E-11	4.41E-12	9.73E-12	-1.4E-11	-4.7E-12
0.000006	2.95E-11	2.7E-11	4.32E-12	1.06E-11	-1.4E-11	-4.4E-12
6.1E-06	3.05E-11	2.69E-11	3.98E-12	1.14E-11	-1.4E-11	-4.3E-12
6.2E-06	3.16E-11	2.68E-11	3.41E-12	1.22E-11	-1.4E-11	-4.2E-12
6.3E-06	3.29E-11	2.66E-11	2.7E-12	1.3E-11	-1.3E-11	-4.3E-12
6.4E-06	3.45E-11	2.64E-11	1.96E-12	1.4E-11	-1.3E-11	-4.5E-12
6.5E-06	3.65E-11	2.62E-11	1.28E-12	1.52E-11	-1.2E-11	-4.7E-12
6.6E-06	3.91E-11	2.6E-11	7.41E-13	1.69E-11	-1.1E-11	-4.9E-12
6.7E-06	4.24E-11	2.58E-11	4.21E-13	1.9E-11	-1.1E-11	-5.2E-12
6.8E-06	4.67E-11	2.55E-11	3.77E-13	2.19E-11	-9.8E-12	-5.4E-12
6.9E-06	5.2E-11	2.53E-11	6.39E-13	2.57E-11	-8.8E-12	-5.7E-12
0.000007	5.85E-11	2.5E-11	1.2E-12	3.06E-11	-7.7E-12	-5.9E-12
7.1E-06	6.61E-11	2.48E-11	2.05E-12	3.66E-11	-6.4E-12	-6.1E-12
7.2E-06	7.45E-11	2.47E-11	3.18E-12	4.39E-11	-5E-12	-6.2E-12
7.3E-06	8.28E-11	2.46E-11	4.63E-12	5.24E-11	-3.4E-12	-6.3E-12

7.4E-06	8.98E-11	2.46E-11	6.47E-12	6.17E-11	-1.5E-12	-6.4E-12
7.5E-06	9.4E-11	2.47E-11	8.77E-12	7.12E-11	6.96E-13	-6.4E-12
7.6E-06	9.35E-11	2.5E-11	1.17E-11	8.01E-11	3.22E-12	-6.4E-12
7.7E-06	8.6E-11	2.53E-11	1.54E-11	8.7E-11	6.21E-12	-6.2E-12
7.8E-06	6.95E-11	2.58E-11	1.99E-11	9.02E-11	9.78E-12	-5.9E-12
7.9E-06	4.19E-11	2.65E-11	2.55E-11	8.78E-11	1.41E-11	-5.5E-12
0.000008	2.08E-12	2.73E-11	3.21E-11	7.77E-11	1.92E-11	-4.8E-12
8.1E-06	-5.1E-11	2.84E-11	3.93E-11	5.8E-11	2.52E-11	-3.9E-12
8.2E-06	-1.2E-10	2.99E-11	4.67E-11	2.7E-11	3.21E-11	-2.8E-12
8.3E-06	-1.9E-10	3.18E-11	5.32E-11	-1.6E-11	3.96E-11	-1.2E-12
8.4E-06	-2.8E-10	3.42E-11	5.75E-11	-7.2E-11	4.72E-11	7.28E-13
8.5E-06	-3.7E-10	3.73E-11	5.8E-11	-1.4E-10	5.41E-11	3.21E-12
8.6E-06	-4.6E-10	4.12E-11	5.27E-11	-2.2E-10	5.91E-11	6.33E-12
8.7E-06	-5.5E-10	4.59E-11	3.95E-11	-3E-10	6.06E-11	1.02E-11
8.8E-06	-6.3E-10	5.15E-11	1.67E-11	-3.9E-10	5.68E-11	1.49E-11
8.9E-06	-7E-10	5.79E-11	-1.7E-11	-4.8E-10	4.57E-11	2.06E-11
0.000009	-7.6E-10	6.48E-11	-6.3E-11	-5.7E-10	2.56E-11	2.72E-11
9.1E-06	-7.9E-10	7.18E-11	-1.2E-10	-6.5E-10	-5.2E-12	3.46E-11
9.2E-06	-7.9E-10	7.8E-11	-1.9E-10	-7.1E-10	-4.7E-11	4.25E-11
9.3E-06	-7.7E-10	8.22E-11	-2.7E-10	-7.6E-10	-1E-10	5.03E-11
9.4E-06	-7.1E-10	8.31E-11	-3.5E-10	-7.8E-10	-1.7E-10	5.73E-11
9.5E-06	-6.3E-10	7.89E-11	-4.4E-10	-7.8E-10	-2.4E-10	6.23E-11
9.6E-06	-5.1E-10	6.79E-11	-5.2E-10	-7.5E-10	-3.2E-10	6.39E-11
9.7E-06	-3.6E-10	4.84E-11	-5.9E-10	-6.8E-10	-4E-10	6.05E-11
9.8E-06	-1.8E-10	1.9E-11	-6.6E-10	-5.9E-10	-4.9E-10	5.02E-11
9.9E-06	3.07E-11	-2.1E-11	-7E-10	-4.7E-10	-5.6E-10	3.14E-11

0.00001	2.61E-10	-7.2E-11	-7.3E-10	-3.1E-10	-6.3E-10	2.87E-12
1.01E-05	5.11E-10	-1.3E-10	-7.3E-10	-1.3E-10	-6.8E-10	-3.6E-11
1.02E-05	7.74E-10	-2E-10	-7E-10	8.12E-11	-7.2E-10	-8.6E-11
1.03E-05	1.04E-09	-2.8E-10	-6.4E-10	3.12E-10	-7.3E-10	-1.5E-10
1.04E-05	1.31E-09	-3.6E-10	-5.6E-10	5.61E-10	-7.1E-10	-2.2E-10
1.05E-05	1.58E-09	-4.4E-10	-4.4E-10	8.21E-10	-6.7E-10	-2.9E-10
1.06E-05	1.83E-09	-5.1E-10	-2.9E-10	1.09E-09	-6E-10	-3.7E-10
1.07E-05	2.05E-09	-5.8E-10	-1.2E-10	1.35E-09	-5E-10	-4.5E-10
1.08E-05	2.25E-09	-6.3E-10	7.63E-11	1.61E-09	-3.7E-10	-5.2E-10
1.09E-05	2.41E-09	-6.7E-10	2.88E-10	1.85E-09	-2.1E-10	-5.8E-10
0.000011	2.53E-09	-6.9E-10	5.11E-10	2.07E-09	-3.4E-11	-6.3E-10
1.11E-05	2.6E-09	-6.9E-10	7.4E-10	2.25E-09	1.63E-10	-6.7E-10
1.12E-05	2.61E-09	-6.6E-10	9.69E-10	2.4E-09	3.74E-10	-6.9E-10
1.13E-05	2.57E-09	-6.1E-10	1.19E-09	2.5E-09	5.94E-10	-6.8E-10
1.14E-05	2.47E-09	-5.3E-10	1.4E-09	2.56E-09	8.19E-10	-6.5E-10
1.15E-05	2.3E-09	-4.3E-10	1.59E-09	2.55E-09	1.04E-09	-5.9E-10
1.16E-05	2.08E-09	-2.9E-10	1.76E-09	2.49E-09	1.26E-09	-5.1E-10
1.17E-05	1.78E-09	-1.4E-10	1.89E-09	2.37E-09	1.46E-09	-4E-10
1.18E-05	1.43E-09	4.34E-11	1.99E-09	2.19E-09	1.64E-09	-2.7E-10
1.19E-05	1.01E-09	2.42E-10	2.04E-09	1.94E-09	1.8E-09	-1.1E-10
0.000012	5.46E-10	4.56E-10	2.06E-09	1.64E-09	1.92E-09	6.8E-11
1.21E-05	3.59E-11	6.82E-10	2.02E-09	1.28E-09	2.01E-09	2.63E-10
1.22E-05	-5.1E-10	9.14E-10	1.94E-09	8.62E-10	2.06E-09	4.72E-10
1.23E-05	-1.1E-09	1.15E-09	1.81E-09	4.03E-10	2.07E-09	6.91E-10
1.24E-05	-1.6E-09	1.37E-09	1.63E-09	-9.6E-11	2.03E-09	9.14E-10
1.25E-05	-2.2E-09	1.59E-09	1.41E-09	-6.3E-10	1.94E-09	1.14E-09

1.26E-05	-2.7E-09	1.79E-09	1.15E-09	-1.2E-09	1.8E-09	1.35E-09
1.27E-05	-3.2E-09	1.96E-09	8.46E-10	-1.7E-09	1.62E-09	1.56E-09
1.28E-05	-3.6E-09	2.11E-09	5.16E-10	-2.3E-09	1.4E-09	1.74E-09
1.29E-05	-3.9E-09	2.21E-09	1.63E-10	-2.8E-09	1.13E-09	1.91E-09
0.000013	-4.2E-09	2.28E-09	-2E-10	-3.3E-09	8.25E-10	2.04E-09
1.31E-05	-4.3E-09	2.3E-09	-5.8E-10	-3.8E-09	4.9E-10	2.13E-09
1.32E-05	-4.3E-09	2.28E-09	-9.5E-10	-4.1E-09	1.31E-10	2.19E-09
1.33E-05	-4.3E-09	2.2E-09	-1.3E-09	-4.4E-09	-2.4E-10	2.21E-09
1.34E-05	-4.1E-09	2.08E-09	-1.6E-09	-4.6E-09	-6.3E-10	2.17E-09
1.35E-05	-3.8E-09	1.9E-09	-2E-09	-4.7E-09	-1E-09	2.09E-09
1.36E-05	-3.5E-09	1.67E-09	-2.2E-09	-4.7E-09	-1.4E-09	1.97E-09
1.37E-05	-3E-09	1.4E-09	-2.5E-09	-4.5E-09	-1.7E-09	1.79E-09
1.38E-05	-2.5E-09	1.08E-09	-2.7E-09	-4.3E-09	-2.1E-09	1.56E-09
1.39E-05	-2E-09	7.2E-10	-2.8E-09	-3.9E-09	-2.3E-09	1.29E-09
0.000014	-1.4E-09	3.29E-10	-2.9E-09	-3.3E-09	-2.6E-09	9.74E-10
1.41E-05	-8.1E-10	-8.8E-11	-3E-09	-2.7E-09	-2.8E-09	6.23E-10
1.42E-05	-2.2E-10	-5.2E-10	-3E-09	-2E-09	-2.9E-09	2.41E-10
1.43E-05	3.49E-10	-9.7E-10	-3E-09	-1.2E-09	-3E-09	-1.7E-10
1.44E-05	8.77E-10	-1.4E-09	-2.9E-09	-4.2E-10	-3.1E-09	-5.9E-10
1.45E-05	1.35E-09	-1.9E-09	-2.8E-09	4.3E-10	-3.1E-09	-1E-09
1.46E-05	1.75E-09	-2.3E-09	-2.6E-09	1.27E-09	-3E-09	-1.5E-09
1.47E-05	2.07E-09	-2.7E-09	-2.4E-09	2.09E-09	-2.9E-09	-1.9E-09
1.48E-05	2.29E-09	-3E-09	-2.1E-09	2.86E-09	-2.8E-09	-2.3E-09
1.49E-05	2.41E-09	-3.4E-09	-1.8E-09	3.56E-09	-2.6E-09	-2.7E-09
0.000015	2.42E-09	-3.6E-09	-1.4E-09	4.16E-09	-2.4E-09	-3E-09
1.51E-05	2.33E-09	-3.8E-09	-1E-09	4.64E-09	-2.1E-09	-3.3E-09

1.52E-05	2.13E-09	-4E-09	-5.7E-10	4.99E-09	-1.8E-09	-3.6E-09
1.53E-05	1.83E-09	-4E-09	-7.9E-11	5.19E-09	-1.5E-09	-3.8E-09
1.54E-05	1.44E-09	-4E-09	4.41E-10	5.23E-09	-1.2E-09	-3.9E-09
1.55E-05	9.8E-10	-3.9E-09	9.86E-10	5.1E-09	-8.3E-10	-4E-09
1.56E-05	4.58E-10	-3.7E-09	1.55E-09	4.79E-09	-4.5E-10	-3.9E-09
1.57E-05	-1E-10	-3.4E-09	2.11E-09	4.32E-09	-4.7E-11	-3.8E-09
1.58E-05	-6.7E-10	-3.1E-09	2.66E-09	3.69E-09	3.76E-10	-3.7E-09
1.59E-05	-1.2E-09	-2.7E-09	3.19E-09	2.9E-09	8.18E-10	-3.4E-09
0.000016	-1.8E-09	-2.2E-09	3.69E-09	1.97E-09	1.27E-09	-3.1E-09
1.61E-05	-2.2E-09	-1.7E-09	4.13E-09	9.22E-10	1.73E-09	-2.7E-09
1.62E-05	-2.6E-09	-1.2E-09	4.52E-09	-2.2E-10	2.2E-09	-2.2E-09
1.63E-05	-2.8E-09	-6.6E-10	4.84E-09	-1.4E-09	2.65E-09	-1.6E-09
1.64E-05	-2.9E-09	-1.1E-10	5.07E-09	-2.7E-09	3.09E-09	-1.1E-09
1.65E-05	-2.8E-09	4.17E-10	5.22E-09	-3.9E-09	3.51E-09	-4.9E-10
1.66E-05	-2.6E-09	9.26E-10	5.26E-09	-5.1E-09	3.9E-09	1.22E-10
1.67E-05	-2.1E-09	1.4E-09	5.21E-09	-6.2E-09	4.25E-09	7.24E-10
1.68E-05	-1.4E-09	1.83E-09	5.04E-09	-7.2E-09	4.56E-09	1.31E-09
1.69E-05	-4.8E-10	2.21E-09	4.76E-09	-8E-09	4.81E-09	1.85E-09
0.000017	6.47E-10	2.53E-09	4.36E-09	-8.6E-09	5.01E-09	2.35E-09
1.71E-05	1.98E-09	2.79E-09	3.85E-09	-9E-09	5.14E-09	2.78E-09
1.72E-05	3.49E-09	2.99E-09	3.23E-09	-9.2E-09	5.2E-09	3.14E-09
1.73E-05	5.17E-09	3.13E-09	2.49E-09	-9E-09	5.18E-09	3.42E-09
1.74E-05	6.99E-09	3.21E-09	1.65E-09	-8.6E-09	5.08E-09	3.61E-09
1.75E-05	8.9E-09	3.23E-09	7.03E-10	-7.8E-09	4.89E-09	3.72E-09
1.76E-05	1.09E-08	3.2E-09	-3.3E-10	-6.7E-09	4.6E-09	3.73E-09
1.77E-05	1.28E-08	3.12E-09	-1.4E-09	-5.3E-09	4.21E-09	3.66E-09

1.78E-05	1.47E-08	3E-09	-2.6E-09	-3.5E-09	3.72E-09	3.51E-09
1.79E-05	1.65E-08	2.85E-09	-3.9E-09	-1.5E-09	3.12E-09	3.28E-09
0.000018	1.81E-08	2.67E-09	-5.1E-09	7.99E-10	2.41E-09	3E-09
1.81E-05	1.95E-08	2.48E-09	-6.4E-09	3.31E-09	1.58E-09	2.65E-09
1.82E-05	2.06E-08	2.28E-09	-7.7E-09	6.01E-09	6.54E-10	2.27E-09
1.83E-05	2.14E-08	2.09E-09	-8.9E-09	8.83E-09	-3.8E-10	1.85E-09
1.84E-05	2.18E-08	1.92E-09	-1E-08	1.17E-08	-1.5E-09	1.42E-09
1.85E-05	2.17E-08	1.77E-09	-1.1E-08	1.46E-08	-2.7E-09	9.89E-10
1.86E-05	2.12E-08	1.66E-09	-1.2E-08	1.75E-08	-4E-09	5.71E-10
1.87E-05	2.01E-08	1.59E-09	-1.3E-08	2.02E-08	-5.4E-09	1.83E-10
1.88E-05	1.85E-08	1.56E-09	-1.3E-08	2.27E-08	-6.7E-09	-1.6E-10
1.89E-05	1.64E-08	1.59E-09	-1.4E-08	2.49E-08	-8.1E-09	-4.4E-10
0.000019	1.38E-08	1.67E-09	-1.4E-08	2.68E-08	-9.5E-09	-6.6E-10
1.91E-05	1.07E-08	1.8E-09	-1.4E-08	2.83E-08	-1.1E-08	-7.9E-10
1.92E-05	7.04E-09	1.96E-09	-1.3E-08	2.93E-08	-1.2E-08	-8.3E-10
1.93E-05	2.97E-09	2.16E-09	-1.3E-08	2.98E-08	-1.3E-08	-7.7E-10
1.94E-05	-1.5E-09	2.39E-09	-1.2E-08	2.97E-08	-1.4E-08	-6.2E-10
1.95E-05	-6.3E-09	2.62E-09	-1E-08	2.9E-08	-1.5E-08	-3.7E-10
1.96E-05	-1.1E-08	2.84E-09	-8.6E-09	2.77E-08	-1.6E-08	-2.6E-11
1.97E-05	-1.7E-08	3.04E-09	-6.5E-09	2.58E-08	-1.6E-08	3.97E-10
1.98E-05	-2.2E-08	3.19E-09	-4.2E-09	2.32E-08	-1.6E-08	8.9E-10
1.99E-05	-2.7E-08	3.28E-09	-1.5E-09	2E-08	-1.6E-08	1.44E-09
0.00002	-3.3E-08	3.29E-09	1.41E-09	1.62E-08	-1.5E-08	2.02E-09
2.01E-05	-3.8E-08	3.2E-09	4.57E-09	1.18E-08	-1.4E-08	2.62E-09
2.02E-05	-4.2E-08	2.98E-09	7.91E-09	6.94E-09	-1.3E-08	3.21E-09
2.03E-05	-4.7E-08	2.63E-09	1.14E-08	1.61E-09	-1.1E-08	3.77E-09

2.04E-05	-5E-08	2.13E-09	1.5E-08	-4.1E-09	-9.2E-09	4.26E-09
2.05E-05	-5.4E-08	1.46E-09	1.86E-08	-1E-08	-6.8E-09	4.67E-09
2.06E-05	-5.6E-08	6.34E-10	2.21E-08	-1.6E-08	-4.1E-09	4.97E-09
2.07E-05	-5.8E-08	-3.6E-10	2.56E-08	-2.2E-08	-1E-09	5.13E-09
2.08E-05	-5.9E-08	-1.5E-09	2.88E-08	-2.9E-08	2.32E-09	5.14E-09
2.09E-05	-5.9E-08	-2.8E-09	3.18E-08	-3.5E-08	5.92E-09	4.96E-09
0.000021	-5.8E-08	-4.3E-09	3.45E-08	-4.1E-08	9.71E-09	4.58E-09
2.11E-05	-5.7E-08	-5.9E-09	3.68E-08	-4.6E-08	1.36E-08	3.99E-09
2.12E-05	-5.4E-08	-7.6E-09	3.86E-08	-5.1E-08	1.76E-08	3.19E-09
2.13E-05	-5E-08	-9.3E-09	3.99E-08	-5.5E-08	2.16E-08	2.16E-09
2.14E-05	-4.6E-08	-1.1E-08	4.06E-08	-5.9E-08	2.56E-08	9.18E-10
2.15E-05	-4.1E-08	-1.3E-08	4.07E-08	-6.2E-08	2.93E-08	-5.4E-10
2.16E-05	-3.5E-08	-1.5E-08	4.01E-08	-6.4E-08	3.29E-08	-2.2E-09
2.17E-05	-2.8E-08	-1.6E-08	3.88E-08	-6.5E-08	3.61E-08	-4E-09
2.18E-05	-2.1E-08	-1.8E-08	3.67E-08	-6.6E-08	3.89E-08	-6E-09
2.19E-05	-1.3E-08	-1.9E-08	3.4E-08	-6.5E-08	4.13E-08	-8E-09
0.000022	-4.7E-09	-2E-08	3.05E-08	-6.3E-08	4.31E-08	-1E-08
2.21E-05	3.68E-09	-2.1E-08	2.63E-08	-6.1E-08	4.42E-08	-1.2E-08
2.22E-05	1.22E-08	-2.2E-08	2.14E-08	-5.7E-08	4.48E-08	-1.4E-08
2.23E-05	2.08E-08	-2.2E-08	1.6E-08	-5.3E-08	4.45E-08	-1.7E-08
2.24E-05	2.92E-08	-2.2E-08	9.94E-09	-4.7E-08	4.36E-08	-1.9E-08
2.25E-05	3.73E-08	-2.1E-08	3.42E-09	-4.1E-08	4.18E-08	-2E-08
2.26E-05	4.51E-08	-2E-08	-3.5E-09	-3.4E-08	3.92E-08	-2.2E-08
2.27E-05	5.23E-08	-1.8E-08	-1.1E-08	-2.6E-08	3.59E-08	-2.3E-08
2.28E-05	5.9E-08	-1.6E-08	-1.8E-08	-1.8E-08	3.18E-08	-2.4E-08
2.29E-05	6.49E-08	-1.4E-08	-2.6E-08	-9.9E-09	2.69E-08	-2.4E-08

0.000023	7.01E-08	-1.1E-08	-3.3E-08	-1.1E-09	2.14E-08	-2.4E-08
2.31E-05	7.44E-08	-7.4E-09	-4E-08	7.77E-09	1.52E-08	-2.4E-08
2.32E-05	7.77E-08	-3.7E-09	-4.7E-08	1.67E-08	8.47E-09	-2.3E-08
2.33E-05	8.01E-08	3.91E-10	-5.4E-08	2.55E-08	1.29E-09	-2.2E-08
2.34E-05	8.15E-08	4.77E-09	-6E-08	3.41E-08	-6.2E-09	-2E-08
2.35E-05	8.19E-08	9.39E-09	-6.5E-08	4.23E-08	-1.4E-08	-1.8E-08
2.36E-05	8.12E-08	1.42E-08	-7E-08	5.01E-08	-2.2E-08	-1.5E-08
2.37E-05	7.95E-08	1.9E-08	-7.4E-08	5.72E-08	-3E-08	-1.1E-08
2.38E-05	7.69E-08	2.39E-08	-7.7E-08	6.36E-08	-3.7E-08	-7.5E-09
2.39E-05	7.34E-08	2.87E-08	-7.8E-08	6.92E-08	-4.5E-08	-3.3E-09
0.000024	6.9E-08	3.33E-08	-7.9E-08	7.39E-08	-5.2E-08	1.27E-09
2.41E-05	6.38E-08	3.76E-08	-7.9E-08	7.76E-08	-5.8E-08	6.09E-09
2.42E-05	5.79E-08	4.17E-08	-7.7E-08	8.04E-08	-6.4E-08	1.11E-08
2.43E-05	5.14E-08	4.53E-08	-7.5E-08	8.21E-08	-6.9E-08	1.63E-08
2.44E-05	4.43E-08	4.84E-08	-7.1E-08	8.27E-08	-7.3E-08	2.15E-08
2.45E-05	3.69E-08	5.09E-08	-6.6E-08	8.23E-08	-7.6E-08	2.67E-08
2.46E-05	2.91E-08	5.28E-08	-6E-08	8.08E-08	-7.8E-08	3.17E-08
2.47E-05	2.12E-08	5.4E-08	-5.3E-08	7.83E-08	-7.9E-08	3.66E-08
2.48E-05	1.31E-08	5.44E-08	-4.6E-08	7.49E-08	-7.9E-08	4.11E-08
2.49E-05	5.09E-09	5.41E-08	-3.7E-08	7.05E-08	-7.8E-08	4.52E-08
0.000025	-2.8E-09	5.3E-08	-2.8E-08	6.53E-08	-7.5E-08	4.89E-08
2.51E-05	-1E-08	5.11E-08	-1.9E-08	5.94E-08	-7.2E-08	5.2E-08
2.52E-05	-1.8E-08	4.84E-08	-9E-09	5.28E-08	-6.7E-08	5.45E-08
2.53E-05	-2.5E-08	4.5E-08	1.1E-09	4.57E-08	-6.2E-08	5.63E-08
2.54E-05	-3.1E-08	4.08E-08	1.12E-08	3.81E-08	-5.5E-08	5.73E-08
2.55E-05	-3.7E-08	3.58E-08	2.13E-08	3.03E-08	-4.8E-08	5.76E-08

2.56E-05	-4.3E-08	3.03E-08	3.11E-08	2.22E-08	-4E-08	5.7E-08
2.57E-05	-4.7E-08	2.41E-08	4.05E-08	1.4E-08	-3.1E-08	5.56E-08
2.58E-05	-5.1E-08	1.75E-08	4.93E-08	5.83E-09	-2.2E-08	5.34E-08
2.59E-05	-5.5E-08	1.04E-08	5.75E-08	-2.2E-09	-1.2E-08	5.04E-08
0.000026	-5.7E-08	2.98E-09	6.5E-08	-9.9E-09	-2.4E-09	4.65E-08
2.61E-05	-5.9E-08	-4.6E-09	7.15E-08	-1.7E-08	7.27E-09	4.19E-08
2.62E-05	-6.1E-08	-1.2E-08	7.71E-08	-2.4E-08	1.69E-08	3.65E-08
2.63E-05	-6.1E-08	-2E-08	8.16E-08	-3.1E-08	2.62E-08	3.05E-08
2.64E-05	-6.1E-08	-2.8E-08	8.51E-08	-3.7E-08	3.51E-08	2.39E-08
2.65E-05	-6E-08	-3.5E-08	8.74E-08	-4.2E-08	4.35E-08	1.68E-08
2.66E-05	-5.8E-08	-4.2E-08	8.85E-08	-4.6E-08	5.12E-08	9.35E-09
2.67E-05	-5.6E-08	-4.9E-08	8.85E-08	-5E-08	5.81E-08	1.55E-09
2.68E-05	-5.4E-08	-5.5E-08	8.74E-08	-5.3E-08	6.42E-08	-6.4E-09
2.69E-05	-5.1E-08	-6.1E-08	8.51E-08	-5.5E-08	6.94E-08	-1.5E-08
0.000027	-4.7E-08	-6.6E-08	8.18E-08	-5.7E-08	7.35E-08	-2.3E-08
2.71E-05	-4.3E-08	-7E-08	7.75E-08	-5.7E-08	7.65E-08	-3E-08
2.72E-05	-3.9E-08	-7.3E-08	7.24E-08	-5.7E-08	7.85E-08	-3.8E-08
2.73E-05	-3.4E-08	-7.6E-08	6.64E-08	-5.6E-08	7.94E-08	-4.5E-08
2.74E-05	-3E-08	-7.7E-08	5.97E-08	-5.5E-08	7.93E-08	-5.2E-08
2.75E-05	-2.5E-08	-7.8E-08	5.24E-08	-5.2E-08	7.8E-08	-5.8E-08
2.76E-05	-2E-08	-7.8E-08	4.46E-08	-5E-08	7.58E-08	-6.4E-08
2.77E-05	-1.5E-08	-7.7E-08	3.65E-08	-4.6E-08	7.26E-08	-6.9E-08
2.78E-05	-9.7E-09	-7.5E-08	2.82E-08	-4.2E-08	6.86E-08	-7.3E-08
2.79E-05	-4.8E-09	-7.2E-08	1.98E-08	-3.8E-08	6.38E-08	-7.6E-08
0.000028	-3.3E-11	-6.8E-08	1.13E-08	-3.4E-08	5.83E-08	-7.8E-08
2.81E-05	4.55E-09	-6.4E-08	3.06E-09	-2.9E-08	5.21E-08	-8E-08

2.82E-05	8.9E-09	-5.9E-08	-5E-09	-2.4E-08	4.56E-08	-8E-08
2.83E-05	1.3E-08	-5.3E-08	-1.3E-08	-1.9E-08	3.86E-08	-8E-08
2.84E-05	1.68E-08	-4.7E-08	-2E-08	-1.4E-08	3.14E-08	-7.8E-08
2.85E-05	2.03E-08	-4E-08	-2.7E-08	-9E-09	2.41E-08	-7.6E-08
2.86E-05	2.34E-08	-3.3E-08	-3.3E-08	-4.3E-09	1.68E-08	-7.3E-08
2.87E-05	2.62E-08	-2.6E-08	-3.8E-08	3.33E-10	9.5E-09	-6.9E-08
2.88E-05	2.86E-08	-1.9E-08	-4.3E-08	4.66E-09	2.42E-09	-6.4E-08
2.89E-05	3.06E-08	-1.1E-08	-4.7E-08	8.69E-09	-4.4E-09	-5.8E-08
0.000029	3.22E-08	-3.8E-09	-5E-08	1.24E-08	-1.1E-08	-5.2E-08
2.91E-05	3.35E-08	3.49E-09	-5.3E-08	1.57E-08	-1.7E-08	-4.6E-08
2.92E-05	3.43E-08	1.06E-08	-5.5E-08	1.85E-08	-2.2E-08	-3.9E-08
2.93E-05	3.48E-08	1.75E-08	-5.6E-08	2.1E-08	-2.7E-08	-3.1E-08
2.94E-05	3.49E-08	2.4E-08	-5.6E-08	2.3E-08	-3.2E-08	-2.4E-08
2.95E-05	3.46E-08	3.01E-08	-5.5E-08	2.46E-08	-3.5E-08	-1.6E-08
2.96E-05	3.4E-08	3.57E-08	-5.4E-08	2.58E-08	-3.8E-08	-8.2E-09
2.97E-05	3.3E-08	4.09E-08	-5.2E-08	2.65E-08	-4.1E-08	-4.9E-10
2.98E-05	3.17E-08	4.55E-08	-5E-08	2.69E-08	-4.2E-08	7.12E-09
2.99E-05	3.01E-08	4.95E-08	-4.7E-08	2.68E-08	-4.3E-08	1.45E-08
0.00003	2.83E-08	5.29E-08	-4.4E-08	2.64E-08	-4.4E-08	2.16E-08
3.01E-05	2.62E-08	5.57E-08	-4E-08	2.56E-08	-4.4E-08	2.83E-08
3.02E-05	2.39E-08	5.79E-08	-3.7E-08	2.45E-08	-4.3E-08	3.45E-08
3.03E-05	2.14E-08	5.94E-08	-3.3E-08	2.32E-08	-4.2E-08	4.03E-08
3.04E-05	1.88E-08	6.03E-08	-2.8E-08	2.16E-08	-4E-08	4.54E-08
3.05E-05	1.62E-08	6.06E-08	-2.4E-08	1.98E-08	-3.8E-08	5E-08
3.06E-05	1.34E-08	6.04E-08	-2E-08	1.78E-08	-3.5E-08	5.39E-08
3.07E-05	1.06E-08	5.96E-08	-1.6E-08	1.57E-08	-3.3E-08	5.72E-08

3.08E-05	7.82E-09	5.82E-08	-1.2E-08	1.36E-08	-3E-08	5.97E-08
3.09E-05	5.09E-09	5.64E-08	-7.9E-09	1.14E-08	-2.7E-08	6.16E-08
0.000031	2.42E-09	5.42E-08	-4.2E-09	9.13E-09	-2.4E-08	6.28E-08
3.11E-05	-1.3E-10	5.15E-08	-6.6E-10	6.93E-09	-2E-08	6.33E-08
3.12E-05	-2.6E-09	4.86E-08	2.61E-09	4.79E-09	-1.7E-08	6.31E-08
3.13E-05	-4.8E-09	4.53E-08	5.62E-09	2.74E-09	-1.4E-08	6.23E-08
3.14E-05	-6.9E-09	4.18E-08	8.34E-09	8.11E-10	-1.1E-08	6.1E-08
3.15E-05	-8.8E-09	3.81E-08	1.08E-08	-9.8E-10	-8.2E-09	5.9E-08
3.16E-05	-1E-08	3.42E-08	1.29E-08	-2.6E-09	-5.4E-09	5.66E-08
3.17E-05	-1.2E-08	3.02E-08	1.48E-08	-4.1E-09	-2.8E-09	5.37E-08
3.18E-05	-1.3E-08	2.62E-08	1.63E-08	-5.3E-09	-3.7E-10	5.04E-08
3.19E-05	-1.4E-08	2.21E-08	1.76E-08	-6.4E-09	1.86E-09	4.67E-08
0.000032	-1.5E-08	1.81E-08	1.85E-08	-7.2E-09	3.88E-09	4.28E-08
3.21E-05	-1.5E-08	1.41E-08	1.92E-08	-7.9E-09	5.7E-09	3.86E-08
3.22E-05	-1.5E-08	1.01E-08	1.97E-08	-8.3E-09	7.3E-09	3.43E-08
3.23E-05	-1.5E-08	6.29E-09	1.99E-08	-8.5E-09	8.69E-09	2.98E-08
3.24E-05	-1.5E-08	2.58E-09	1.99E-08	-8.6E-09	9.87E-09	2.53E-08
3.25E-05	-1.5E-08	-9.9E-10	1.97E-08	-8.5E-09	1.09E-08	2.07E-08
3.26E-05	-1.4E-08	-4.4E-09	1.93E-08	-8.2E-09	1.17E-08	1.62E-08
3.27E-05	-1.3E-08	-7.6E-09	1.88E-08	-7.7E-09	1.23E-08	1.17E-08
3.28E-05	-1.3E-08	-1.1E-08	1.82E-08	-7.2E-09	1.27E-08	7.33E-09
3.29E-05	-1.2E-08	-1.3E-08	1.75E-08	-6.5E-09	1.31E-08	3.1E-09
0.000033	-1.1E-08	-1.6E-08	1.67E-08	-5.7E-09	1.32E-08	-9.5E-10
3.31E-05	-9.4E-09	-1.8E-08	1.58E-08	-4.8E-09	1.33E-08	-4.8E-09
3.32E-05	-8.2E-09	-2E-08	1.49E-08	-3.9E-09	1.33E-08	-8.4E-09
3.33E-05	-7E-09	-2.2E-08	1.4E-08	-3E-09	1.31E-08	-1.2E-08

3.34E-05	-5.8E-09	-2.4E-08	1.31E-08	-2E-09	1.29E-08	-1.5E-08
3.35E-05	-4.6E-09	-2.5E-08	1.21E-08	-1.1E-09	1.27E-08	-1.8E-08
3.36E-05	-3.4E-09	-2.6E-08	1.12E-08	-1.5E-10	1.24E-08	-2E-08
3.37E-05	-2.3E-09	-2.7E-08	1.04E-08	7.41E-10	1.2E-08	-2.2E-08
3.38E-05	-1.3E-09	-2.8E-08	9.53E-09	1.58E-09	1.16E-08	-2.4E-08
3.39E-05	-3E-10	-2.8E-08	8.73E-09	2.35E-09	1.12E-08	-2.6E-08
0.000034	5.68E-10	-2.8E-08	7.98E-09	3.04E-09	1.08E-08	-2.7E-08
3.41E-05	1.33E-09	-2.8E-08	7.27E-09	3.64E-09	1.04E-08	-2.8E-08
3.42E-05	1.99E-09	-2.8E-08	6.61E-09	4.16E-09	9.91E-09	-2.9E-08
3.43E-05	2.53E-09	-2.8E-08	6.01E-09	4.57E-09	9.45E-09	-2.9E-08
3.44E-05	2.96E-09	-2.7E-08	5.45E-09	4.89E-09	8.99E-09	-2.9E-08
3.45E-05	3.27E-09	-2.6E-08	4.93E-09	5.1E-09	8.52E-09	-2.9E-08
3.46E-05	3.47E-09	-2.6E-08	4.47E-09	5.22E-09	8.06E-09	-2.9E-08
3.47E-05	3.57E-09	-2.5E-08	4.04E-09	5.24E-09	7.59E-09	-2.9E-08
3.48E-05	3.56E-09	-2.3E-08	3.65E-09	5.18E-09	7.13E-09	-2.8E-08
3.49E-05	3.46E-09	-2.2E-08	3.3E-09	5.03E-09	6.67E-09	-2.7E-08
0.000035	3.28E-09	-2.1E-08	2.99E-09	4.81E-09	6.21E-09	-2.6E-08
3.51E-05	3.02E-09	-1.9E-08	2.7E-09	4.52E-09	5.75E-09	-2.5E-08
3.52E-05	2.7E-09	-1.8E-08	2.43E-09	4.18E-09	5.31E-09	-2.3E-08
3.53E-05	2.32E-09	-1.6E-08	2.19E-09	3.78E-09	4.87E-09	-2.2E-08
3.54E-05	1.9E-09	-1.4E-08	1.96E-09	3.36E-09	4.43E-09	-2E-08
3.55E-05	1.44E-09	-1.3E-08	1.75E-09	2.9E-09	4.01E-09	-1.9E-08
3.56E-05	9.54E-10	-1.1E-08	1.55E-09	2.41E-09	3.59E-09	-1.7E-08
3.57E-05	4.54E-10	-9.1E-09	1.36E-09	1.92E-09	3.19E-09	-1.5E-08
3.58E-05	-5.5E-11	-7.4E-09	1.18E-09	1.42E-09	2.8E-09	-1.4E-08
3.59E-05	-5.6E-10	-5.7E-09	1E-09	9.2E-10	2.43E-09	-1.2E-08

0.000036	-1.1E-09	-4E-09	8.29E-10	4.28E-10	2.07E-09	-1E-08
3.61E-05	-1.5E-09	-2.4E-09	6.56E-10	-5.1E-11	1.73E-09	-8.6E-09
3.62E-05	-2E-09	-7.7E-10	4.83E-10	-5.1E-10	1.4E-09	-6.9E-09
3.63E-05	-2.5E-09	7.56E-10	3.09E-10	-9.5E-10	1.1E-09	-5.3E-09
3.64E-05	-2.9E-09	2.22E-09	1.35E-10	-1.4E-09	8.12E-10	-3.8E-09
3.65E-05	-3.2E-09	3.6E-09	-4.1E-11	-1.8E-09	5.49E-10	-2.2E-09
3.66E-05	-3.6E-09	4.9E-09	-2.2E-10	-2.1E-09	3.09E-10	-8.1E-10
3.67E-05	-3.9E-09	6.11E-09	-4E-10	-2.5E-09	9.08E-11	5.65E-10
3.68E-05	-4.2E-09	7.23E-09	-5.8E-10	-2.8E-09	-1E-10	1.86E-09
3.69E-05	-4.4E-09	8.26E-09	-7.6E-10	-3E-09	-2.7E-10	3.08E-09
0.000037	-4.6E-09	9.18E-09	-9.4E-10	-3.3E-09	-4.2E-10	4.22E-09
3.71E-05	-4.7E-09	1E-08	-1.1E-09	-3.5E-09	-5.5E-10	5.27E-09
3.72E-05	-4.8E-09	1.07E-08	-1.3E-09	-3.7E-09	-6.5E-10	6.23E-09
3.73E-05	-4.9E-09	1.13E-08	-1.5E-09	-3.9E-09	-7.3E-10	7.11E-09
3.74E-05	-5E-09	1.18E-08	-1.6E-09	-4E-09	-7.9E-10	7.9E-09
3.75E-05	-5E-09	1.23E-08	-1.8E-09	-4.2E-09	-8.2E-10	8.6E-09
3.76E-05	-5E-09	1.26E-08	-1.9E-09	-4.3E-09	-8.4E-10	9.21E-09
3.77E-05	-5E-09	1.28E-08	-2.1E-09	-4.4E-09	-8.4E-10	9.73E-09
3.78E-05	-4.9E-09	1.29E-08	-2.2E-09	-4.4E-09	-8.3E-10	1.02E-08
3.79E-05	-4.8E-09	1.3E-08	-2.3E-09	-4.5E-09	-8E-10	1.05E-08
0.000038	-4.8E-09	1.3E-08	-2.4E-09	-4.6E-09	-7.6E-10	1.08E-08
3.81E-05	-4.7E-09	1.28E-08	-2.5E-09	-4.6E-09	-7.1E-10	1.1E-08
3.82E-05	-4.6E-09	1.27E-08	-2.5E-09	-4.6E-09	-6.5E-10	1.11E-08
3.83E-05	-4.4E-09	1.24E-08	-2.6E-09	-4.7E-09	-5.8E-10	1.11E-08
3.84E-05	-4.3E-09	1.21E-08	-2.6E-09	-4.7E-09	-5E-10	1.11E-08
3.85E-05	-4.2E-09	1.18E-08	-2.6E-09	-4.7E-09	-4.2E-10	1.1E-08

3.86E-05	-4.1E-09	1.14E-08	-2.7E-09	-4.8E-09	-3.4E-10	1.09E-08
3.87E-05	-4E-09	1.1E-08	-2.6E-09	-4.8E-09	-2.6E-10	1.07E-08
3.88E-05	-3.9E-09	1.05E-08	-2.6E-09	-4.8E-09	-1.8E-10	1.04E-08
3.89E-05	-3.8E-09	1.01E-08	-2.6E-09	-4.8E-09	-1E-10	1.02E-08
0.000039	-3.7E-09	9.57E-09	-2.5E-09	-4.9E-09	-2.2E-11	9.83E-09
3.91E-05	-3.6E-09	9.06E-09	-2.5E-09	-4.9E-09	5.14E-11	9.47E-09
3.92E-05	-3.5E-09	8.56E-09	-2.4E-09	-4.9E-09	1.21E-10	9.09E-09
3.93E-05	-3.4E-09	8.05E-09	-2.3E-09	-4.9E-09	1.84E-10	8.68E-09
3.94E-05	-3.4E-09	7.55E-09	-2.2E-09	-4.9E-09	2.41E-10	8.26E-09
3.95E-05	-3.3E-09	7.07E-09	-2.2E-09	-4.9E-09	2.92E-10	7.83E-09
3.96E-05	-3.3E-09	6.59E-09	-2.1E-09	-5E-09	3.36E-10	7.4E-09
3.97E-05	-3.2E-09	6.14E-09	-2E-09	-5E-09	3.72E-10	6.96E-09
3.98E-05	-3.2E-09	5.7E-09	-1.9E-09	-5E-09	4.01E-10	6.53E-09
3.99E-05	-3.2E-09	5.29E-09	-1.8E-09	-5E-09	4.23E-10	6.11E-09
0.00004	-3.2E-09	4.9E-09	-1.7E-09	-4.9E-09	4.36E-10	5.7E-09
4.01E-05	-3.2E-09	4.54E-09	-1.6E-09	-4.9E-09	4.43E-10	5.31E-09
4.02E-05	-3.2E-09	4.2E-09	-1.5E-09	-4.9E-09	4.41E-10	4.94E-09
4.03E-05	-3.2E-09	3.88E-09	-1.4E-09	-4.9E-09	4.32E-10	4.58E-09
4.04E-05	-3.2E-09	3.59E-09	-1.3E-09	-4.8E-09	4.15E-10	4.25E-09
4.05E-05	-3.2E-09	3.33E-09	-1.2E-09	-4.8E-09	3.9E-10	3.95E-09
4.06E-05	-3.2E-09	3.08E-09	-1.2E-09	-4.7E-09	3.58E-10	3.67E-09
4.07E-05	-3.2E-09	2.86E-09	-1.1E-09	-4.6E-09	3.19E-10	3.42E-09
4.08E-05	-3.2E-09	2.66E-09	-1.1E-09	-4.5E-09	2.73E-10	3.19E-09
4.09E-05	-3.2E-09	2.47E-09	-1E-09	-4.5E-09	2.19E-10	2.98E-09
0.000041	-3.1E-09	2.29E-09	-1E-09	-4.4E-09	1.59E-10	2.8E-09
4.11E-05	-3.1E-09	2.13E-09	-1E-09	-4.3E-09	9.15E-11	2.65E-09

4.12E-05	-3.1E-09	1.97E-09	-1E-09	-4.1E-09	1.75E-11	2.52E-09
4.13E-05	-3E-09	1.82E-09	-1E-09	-4E-09	-6.3E-11	2.4E-09
4.14E-05	-3E-09	1.68E-09	-1E-09	-3.9E-09	-1.5E-10	2.31E-09
4.15E-05	-2.9E-09	1.55E-09	-1.1E-09	-3.7E-09	-2.5E-10	2.23E-09
4.16E-05	-2.9E-09	1.41E-09	-1.1E-09	-3.6E-09	-3.5E-10	2.16E-09
4.17E-05	-2.8E-09	1.28E-09	-1.2E-09	-3.5E-09	-4.5E-10	2.11E-09
4.18E-05	-2.7E-09	1.14E-09	-1.2E-09	-3.3E-09	-5.6E-10	2.06E-09
4.19E-05	-2.6E-09	1.01E-09	-1.3E-09	-3.1E-09	-6.8E-10	2.03E-09
0.000042	-2.5E-09	8.73E-10	-1.4E-09	-3E-09	-8E-10	1.99E-09
4.21E-05	-2.3E-09	7.36E-10	-1.4E-09	-2.8E-09	-9.3E-10	1.96E-09
4.22E-05	-2.2E-09	5.98E-10	-1.5E-09	-2.7E-09	-1.1E-09	1.93E-09
4.23E-05	-2E-09	4.58E-10	-1.6E-09	-2.5E-09	-1.2E-09	1.9E-09
4.24E-05	-1.9E-09	3.17E-10	-1.7E-09	-2.3E-09	-1.3E-09	1.87E-09
4.25E-05	-1.7E-09	1.75E-10	-1.8E-09	-2.2E-09	-1.5E-09	1.83E-09
4.26E-05	-1.5E-09	3.42E-11	-1.9E-09	-2E-09	-1.6E-09	1.78E-09
4.27E-05	-1.4E-09	-1.1E-10	-2E-09	-1.8E-09	-1.7E-09	1.73E-09
4.28E-05	-1.2E-09	-2.4E-10	-2E-09	-1.7E-09	-1.9E-09	1.68E-09
4.29E-05	-9.9E-10	-3.8E-10	-2.1E-09	-1.5E-09	-2E-09	1.61E-09
0.000043	-8E-10	-5.1E-10	-2.2E-09	-1.4E-09	-2.1E-09	1.54E-09
4.31E-05	-6.1E-10	-6.3E-10	-2.3E-09	-1.2E-09	-2.3E-09	1.46E-09
4.32E-05	-4.2E-10	-7.5E-10	-2.4E-09	-1.1E-09	-2.4E-09	1.37E-09
4.33E-05	-2.3E-10	-8.7E-10	-2.4E-09	-9.2E-10	-2.5E-09	1.27E-09
4.34E-05	-3.9E-11	-9.8E-10	-2.5E-09	-7.9E-10	-2.6E-09	1.17E-09
4.35E-05	1.42E-10	-1.1E-09	-2.6E-09	-6.6E-10	-2.7E-09	1.06E-09
4.36E-05	3.16E-10	-1.2E-09	-2.6E-09	-5.5E-10	-2.8E-09	9.41E-10
4.37E-05	4.82E-10	-1.2E-09	-2.7E-09	-4.4E-10	-2.9E-09	8.21E-10

4.38E-05	6.37E-10	-1.3E-09	-2.7E-09	-3.3E-10	-3E-09	6.97E-10
4.39E-05	7.8E-10	-1.4E-09	-2.8E-09	-2.4E-10	-3E-09	5.71E-10
0.000044	9.1E-10	-1.5E-09	-2.8E-09	-1.5E-10	-3.1E-09	4.42E-10
4.41E-05	1.03E-09	-1.5E-09	-2.9E-09	-7.2E-11	-3.1E-09	3.13E-10
4.42E-05	1.13E-09	-1.5E-09	-2.9E-09	5.25E-13	-3.2E-09	1.85E-10
4.43E-05	1.21E-09	-1.6E-09	-2.9E-09	6.55E-11	-3.2E-09	5.84E-11
4.44E-05	1.28E-09	-1.6E-09	-2.9E-09	1.23E-10	-3.2E-09	-6.5E-11
4.45E-05	1.33E-09	-1.6E-09	-2.9E-09	1.74E-10	-3.2E-09	-1.9E-10
4.46E-05	1.36E-09	-1.7E-09	-3E-09	2.19E-10	-3.2E-09	-3E-10
4.47E-05	1.38E-09	-1.7E-09	-3E-09	2.57E-10	-3.2E-09	-4.1E-10
4.48E-05	1.38E-09	-1.7E-09	-3E-09	2.89E-10	-3.2E-09	-5.1E-10
4.49E-05	1.37E-09	-1.7E-09	-3E-09	3.15E-10	-3.1E-09	-6.1E-10
0.000045	1.34E-09	-1.7E-09	-3E-09	3.36E-10	-3.1E-09	-7E-10
4.51E-05	1.3E-09	-1.7E-09	-3E-09	3.53E-10	-3.1E-09	-7.8E-10
4.52E-05	1.25E-09	-1.7E-09	-3E-09	3.65E-10	-3E-09	-8.5E-10
4.53E-05	1.19E-09	-1.7E-09	-3E-09	3.72E-10	-3E-09	-9.1E-10
4.54E-05	1.13E-09	-1.7E-09	-3E-09	3.76E-10	-2.9E-09	-9.7E-10
4.55E-05	1.05E-09	-1.7E-09	-2.9E-09	3.77E-10	-2.9E-09	-1E-09
4.56E-05	9.75E-10	-1.7E-09	-2.9E-09	3.74E-10	-2.8E-09	-1.1E-09
4.57E-05	8.94E-10	-1.7E-09	-2.9E-09	3.68E-10	-2.8E-09	-1.1E-09
4.58E-05	8.12E-10	-1.7E-09	-2.9E-09	3.6E-10	-2.7E-09	-1.1E-09
4.59E-05	7.31E-10	-1.7E-09	-2.9E-09	3.49E-10	-2.7E-09	-1.1E-09
0.000046	6.52E-10	-1.8E-09	-2.8E-09	3.37E-10	-2.7E-09	-1.1E-09
4.61E-05	5.77E-10	-1.8E-09	-2.8E-09	3.23E-10	-2.7E-09	-1.1E-09
4.62E-05	5.07E-10	-1.8E-09	-2.8E-09	3.08E-10	-2.6E-09	-1.1E-09
4.63E-05	4.43E-10	-1.8E-09	-2.7E-09	2.92E-10	-2.6E-09	-1.1E-09

4.64E-05	3.85E-10	-1.8E-09	-2.7E-09	2.74E-10	-2.6E-09	-1.1E-09
4.65E-05	3.35E-10	-1.9E-09	-2.7E-09	2.57E-10	-2.6E-09	-1.1E-09
4.66E-05	2.93E-10	-1.9E-09	-2.6E-09	2.39E-10	-2.6E-09	-1.1E-09
4.67E-05	2.6E-10	-1.9E-09	-2.6E-09	2.2E-10	-2.6E-09	-1.1E-09
4.68E-05	2.35E-10	-1.9E-09	-2.5E-09	2.02E-10	-2.6E-09	-1E-09
4.69E-05	2.18E-10	-1.9E-09	-2.4E-09	1.83E-10	-2.6E-09	-1E-09
0.000047	2.1E-10	-2E-09	-2.4E-09	1.65E-10	-2.7E-09	-9.9E-10
4.71E-05	2.09E-10	-2E-09	-2.3E-09	1.47E-10	-2.7E-09	-9.8E-10
4.72E-05	2.16E-10	-2E-09	-2.3E-09	1.29E-10	-2.7E-09	-9.6E-10
4.73E-05	2.29E-10	-2E-09	-2.2E-09	1.11E-10	-2.7E-09	-9.5E-10
4.74E-05	2.49E-10	-2.1E-09	-2.1E-09	9.31E-11	-2.8E-09	-9.5E-10
4.75E-05	2.73E-10	-2.1E-09	-2E-09	7.54E-11	-2.8E-09	-9.5E-10
4.76E-05	3.02E-10	-2.1E-09	-2E-09	5.78E-11	-2.8E-09	-9.6E-10
4.77E-05	3.34E-10	-2.2E-09	-1.9E-09	4.04E-11	-2.8E-09	-9.8E-10
4.78E-05	3.68E-10	-2.2E-09	-1.8E-09	2.31E-11	-2.8E-09	-1E-09
4.79E-05	4.04E-10	-2.2E-09	-1.7E-09	5.98E-12	-2.8E-09	-1E-09
0.000048	4.4E-10	-2.3E-09	-1.7E-09	-1.1E-11	-2.8E-09	-1.1E-09
4.81E-05	4.76E-10	-2.3E-09	-1.6E-09	-2.7E-11	-2.8E-09	-1.1E-09
4.82E-05	5.12E-10	-2.4E-09	-1.5E-09	-4.3E-11	-2.7E-09	-1.2E-09
4.83E-05	5.45E-10	-2.4E-09	-1.5E-09	-5.7E-11	-2.7E-09	-1.3E-09
4.84E-05	5.76E-10	-2.5E-09	-1.4E-09	-7.1E-11	-2.7E-09	-1.3E-09
4.85E-05	6.04E-10	-2.5E-09	-1.4E-09	-8.4E-11	-2.6E-09	-1.4E-09
4.86E-05	6.29E-10	-2.6E-09	-1.4E-09	-9.5E-11	-2.6E-09	-1.5E-09
4.87E-05	6.5E-10	-2.7E-09	-1.3E-09	-1E-10	-2.5E-09	-1.6E-09
4.88E-05	6.68E-10	-2.8E-09	-1.3E-09	-1.1E-10	-2.4E-09	-1.7E-09
4.89E-05	6.83E-10	-2.8E-09	-1.3E-09	-1.2E-10	-2.4E-09	-1.8E-09

0.000049	6.94E-10	-2.9E-09	-1.3E-09	-1.2E-10	-2.3E-09	-2E-09
4.91E-05	7.02E-10	-3E-09	-1.3E-09	-1.2E-10	-2.2E-09	-2.1E-09
4.92E-05	7.08E-10	-3.1E-09	-1.3E-09	-1.1E-10	-2.1E-09	-2.2E-09
4.93E-05	7.12E-10	-3.2E-09	-1.3E-09	-1.1E-10	-2E-09	-2.3E-09
4.94E-05	7.14E-10	-3.2E-09	-1.4E-09	-9.8E-11	-2E-09	-2.5E-09
4.95E-05	7.15E-10	-3.3E-09	-1.4E-09	-8.4E-11	-1.9E-09	-2.6E-09
4.96E-05	7.15E-10	-3.4E-09	-1.4E-09	-6.6E-11	-1.8E-09	-2.7E-09
4.97E-05	7.15E-10	-3.4E-09	-1.5E-09	-4.5E-11	-1.7E-09	-2.8E-09
4.98E-05	7.16E-10	-3.4E-09	-1.5E-09	-2.1E-11	-1.7E-09	-2.9E-09
4.99E-05	7.17E-10	-3.4E-09	-1.6E-09	6.36E-12	-1.6E-09	-3E-09
0.00005	7.19E-10	-3.4E-09	-1.6E-09	3.64E-11	-1.5E-09	-3E-09
5.01E-05	7.22E-10	-3.4E-09	-1.7E-09	6.89E-11	-1.5E-09	-3.1E-09
5.02E-05	7.26E-10	-3.4E-09	-1.7E-09	1.03E-10	-1.4E-09	-3.1E-09
5.03E-05	7.3E-10	-3.3E-09	-1.8E-09	1.39E-10	-1.4E-09	-3.1E-09
5.04E-05	7.35E-10	-3.2E-09	-1.8E-09	1.75E-10	-1.4E-09	-3.1E-09
5.05E-05	7.39E-10	-3.1E-09	-1.8E-09	2.11E-10	-1.4E-09	-3.1E-09
5.06E-05	7.42E-10	-3E-09	-1.8E-09	2.47E-10	-1.4E-09	-3.1E-09
5.07E-05	7.43E-10	-2.9E-09	-1.8E-09	2.81E-10	-1.4E-09	-3E-09
5.08E-05	7.41E-10	-2.7E-09	-1.8E-09	3.14E-10	-1.4E-09	-2.9E-09
5.09E-05	7.36E-10	-2.5E-09	-1.8E-09	3.43E-10	-1.4E-09	-2.8E-09
0.000051	7.26E-10	-2.3E-09	-1.8E-09	3.69E-10	-1.4E-09	-2.7E-09
5.11E-05	7.12E-10	-2.1E-09	-1.7E-09	3.9E-10	-1.4E-09	-2.5E-09
5.12E-05	6.91E-10	-1.8E-09	-1.6E-09	4.07E-10	-1.4E-09	-2.4E-09
5.13E-05	6.63E-10	-1.6E-09	-1.6E-09	4.18E-10	-1.4E-09	-2.2E-09
5.14E-05	6.28E-10	-1.3E-09	-1.5E-09	4.23E-10	-1.4E-09	-2E-09
5.15E-05	5.85E-10	-1.1E-09	-1.4E-09	4.21E-10	-1.4E-09	-1.8E-09

5.16E-05	5.34E-10	-8E-10	-1.2E-09	4.13E-10	-1.4E-09	-1.6E-09
5.17E-05	4.75E-10	-5.5E-10	-1.1E-09	3.99E-10	-1.4E-09	-1.4E-09
5.18E-05	4.08E-10	-3.1E-10	-9.6E-10	3.77E-10	-1.4E-09	-1.2E-09
5.19E-05	3.33E-10	-8E-11	-8.1E-10	3.49E-10	-1.3E-09	-9.5E-10
0.000052	2.52E-10	1.31E-10	-6.6E-10	3.14E-10	-1.3E-09	-7.5E-10
5.21E-05	1.64E-10	3.21E-10	-5E-10	2.73E-10	-1.2E-09	-5.5E-10
5.22E-05	7.13E-11	4.86E-10	-3.5E-10	2.27E-10	-1.2E-09	-3.8E-10
5.23E-05	-2.5E-11	6.23E-10	-1.9E-10	1.76E-10	-1.1E-09	-2.2E-10
5.24E-05	-1.2E-10	7.28E-10	-4.1E-11	1.22E-10	-1E-09	-7.9E-11
5.25E-05	-2.2E-10	7.99E-10	1.02E-10	6.46E-11	-9.6E-10	3.63E-11
5.26E-05	-3.2E-10	8.34E-10	2.34E-10	5.7E-12	-8.7E-10	1.25E-10
5.27E-05	-4.1E-10	8.32E-10	3.54E-10	-5.4E-11	-7.8E-10	1.86E-10
5.28E-05	-4.9E-10	7.91E-10	4.59E-10	-1.1E-10	-6.8E-10	2.17E-10
5.29E-05	-5.7E-10	7.13E-10	5.47E-10	-1.7E-10	-5.8E-10	2.16E-10
0.000053	-6.4E-10	5.98E-10	6.17E-10	-2.2E-10	-4.7E-10	1.84E-10
5.31E-05	-6.9E-10	4.46E-10	6.66E-10	-2.7E-10	-3.7E-10	1.19E-10
5.32E-05	-7.3E-10	2.61E-10	6.95E-10	-3.1E-10	-2.7E-10	2.33E-11
5.33E-05	-7.6E-10	4.53E-11	7.03E-10	-3.5E-10	-1.7E-10	-1E-10
5.34E-05	-7.6E-10	-2E-10	6.88E-10	-3.7E-10	-8.6E-11	-2.6E-10
5.35E-05	-7.5E-10	-4.6E-10	6.53E-10	-3.9E-10	-6.2E-12	-4.4E-10
5.36E-05	-7.2E-10	-7.5E-10	5.98E-10	-4E-10	6.26E-11	-6.4E-10
5.37E-05	-6.6E-10	-1E-09	5.24E-10	-3.9E-10	1.19E-10	-8.7E-10
5.38E-05	-5.9E-10	-1.4E-09	4.33E-10	-3.8E-10	1.62E-10	-1.1E-09
5.39E-05	-5E-10	-1.7E-09	3.26E-10	-3.5E-10	1.9E-10	-1.4E-09
0.000054	-3.9E-10	-2E-09	2.07E-10	-3.1E-10	2.03E-10	-1.6E-09
5.41E-05	-2.5E-10	-2.3E-09	7.8E-11	-2.7E-10	1.99E-10	-1.9E-09

5.42E-05	-1.1E-10	-2.6E-09	-5.8E-11	-2.1E-10	1.79E-10	-2.2E-09
5.43E-05	5.27E-11	-2.8E-09	-2E-10	-1.4E-10	1.43E-10	-2.4E-09
5.44E-05	2.25E-10	-3.1E-09	-3.4E-10	-6.5E-11	9.18E-11	-2.7E-09
5.45E-05	4.05E-10	-3.3E-09	-4.8E-10	1.75E-11	2.56E-11	-2.9E-09
5.46E-05	5.91E-10	-3.5E-09	-6.1E-10	1.06E-10	-5.4E-11	-3.1E-09
5.47E-05	7.79E-10	-3.6E-09	-7.4E-10	1.99E-10	-1.5E-10	-3.3E-09
5.48E-05	9.64E-10	-3.7E-09	-8.5E-10	2.95E-10	-2.5E-10	-3.4E-09
5.49E-05	1.14E-09	-3.8E-09	-9.5E-10	3.92E-10	-3.6E-10	-3.6E-09
0.000055	1.31E-09	-3.8E-09	-1E-09	4.88E-10	-4.7E-10	-3.7E-09
5.51E-05	1.47E-09	-3.8E-09	-1.1E-09	5.81E-10	-5.9E-10	-3.7E-09
5.52E-05	1.61E-09	-3.7E-09	-1.1E-09	6.69E-10	-7.1E-10	-3.7E-09
5.53E-05	1.73E-09	-3.6E-09	-1.1E-09	7.51E-10	-8.3E-10	-3.7E-09
5.54E-05	1.82E-09	-3.4E-09	-1.1E-09	8.24E-10	-9.4E-10	-3.6E-09
5.55E-05	1.89E-09	-3.2E-09	-1.1E-09	8.87E-10	-1E-09	-3.5E-09
5.56E-05	1.93E-09	-3E-09	-1E-09	9.39E-10	-1.1E-09	-3.4E-09
5.57E-05	1.95E-09	-2.7E-09	-9.6E-10	9.78E-10	-1.2E-09	-3.2E-09
5.58E-05	1.93E-09	-2.4E-09	-8.5E-10	1E-09	-1.3E-09	-3E-09
5.59E-05	1.88E-09	-2.1E-09	-7.3E-10	1.02E-09	-1.3E-09	-2.8E-09
0.000056	1.8E-09	-1.7E-09	-5.8E-10	1.01E-09	-1.4E-09	-2.5E-09
5.61E-05	1.68E-09	-1.4E-09	-4.1E-10	9.94E-10	-1.4E-09	-2.2E-09
5.62E-05	1.54E-09	-1E-09	-2.2E-10	9.62E-10	-1.4E-09	-1.9E-09
5.63E-05	1.38E-09	-6.2E-10	-2.7E-11	9.16E-10	-1.3E-09	-1.6E-09
5.64E-05	1.18E-09	-2.4E-10	1.79E-10	8.57E-10	-1.3E-09	-1.2E-09
5.65E-05	9.71E-10	1.39E-10	3.93E-10	7.86E-10	-1.2E-09	-9.1E-10
5.66E-05	7.41E-10	5.03E-10	6.09E-10	7.05E-10	-1.1E-09	-5.6E-10
5.67E-05	4.97E-10	8.49E-10	8.24E-10	6.15E-10	-9.6E-10	-2.2E-10

5.68E-05	2.44E-10	1.17E-09	1.03E-09	5.17E-10	-8.1E-10	1.05E-10
5.69E-05	-1.2E-11	1.47E-09	1.24E-09	4.14E-10	-6.5E-10	4.17E-10
0.000057	-2.7E-10	1.73E-09	1.43E-09	3.08E-10	-4.7E-10	7.09E-10
5.71E-05	-5.2E-10	1.96E-09	1.6E-09	2E-10	-2.8E-10	9.77E-10
5.72E-05	-7.6E-10	2.15E-09	1.76E-09	9.25E-11	-8.4E-11	1.22E-09
5.73E-05	-9.8E-10	2.29E-09	1.9E-09	-1.2E-11	1.24E-10	1.42E-09
5.74E-05	-1.2E-09	2.39E-09	2.01E-09	-1.1E-10	3.36E-10	1.6E-09
5.75E-05	-1.4E-09	2.45E-09	2.1E-09	-2E-10	5.5E-10	1.73E-09
5.76E-05	-1.5E-09	2.46E-09	2.16E-09	-2.9E-10	7.61E-10	1.83E-09
5.77E-05	-1.6E-09	2.42E-09	2.19E-09	-3.6E-10	9.67E-10	1.88E-09
5.78E-05	-1.7E-09	2.34E-09	2.2E-09	-4.2E-10	1.17E-09	1.9E-09
5.79E-05	-1.8E-09	2.22E-09	2.17E-09	-4.7E-10	1.35E-09	1.87E-09
0.000058	-1.8E-09	2.05E-09	2.12E-09	-5E-10	1.52E-09	1.81E-09
5.81E-05	-1.7E-09	1.85E-09	2.04E-09	-5.2E-10	1.68E-09	1.7E-09
5.82E-05	-1.7E-09	1.61E-09	1.94E-09	-5.1E-10	1.82E-09	1.56E-09
5.83E-05	-1.6E-09	1.35E-09	1.81E-09	-4.9E-10	1.93E-09	1.38E-09
5.84E-05	-1.4E-09	1.05E-09	1.66E-09	-4.6E-10	2.02E-09	1.18E-09
5.85E-05	-1.2E-09	7.32E-10	1.49E-09	-4E-10	2.09E-09	9.42E-10
5.86E-05	-1E-09	3.96E-10	1.3E-09	-3.3E-10	2.13E-09	6.82E-10
5.87E-05	-7.8E-10	4.65E-11	1.1E-09	-2.4E-10	2.15E-09	4.01E-10
5.88E-05	-5.2E-10	-3.1E-10	8.94E-10	-1.4E-10	2.14E-09	1.04E-10
5.89E-05	-2.3E-10	-6.7E-10	6.78E-10	-3.1E-11	2.1E-09	-2.1E-10
0.000059	7.18E-11	-1E-09	4.59E-10	9.24E-11	2.04E-09	-5.2E-10
5.91E-05	3.85E-10	-1.4E-09	2.4E-10	2.24E-10	1.96E-09	-8.4E-10
5.92E-05	7.03E-10	-1.7E-09	2.49E-11	3.62E-10	1.85E-09	-1.2E-09
5.93E-05	1.02E-09	-2.1E-09	-1.8E-10	5.03E-10	1.72E-09	-1.5E-09

5.94E-05	1.34E-09	-2.4E-09	-3.8E-10	6.47E-10	1.57E-09	-1.8E-09
5.95E-05	1.64E-09	-2.6E-09	-5.7E-10	7.9E-10	1.41E-09	-2.1E-09
5.96E-05	1.94E-09	-2.9E-09	-7.4E-10	9.29E-10	1.23E-09	-2.3E-09
5.97E-05	2.21E-09	-3.1E-09	-8.9E-10	1.06E-09	1.04E-09	-2.6E-09
5.98E-05	2.46E-09	-3.3E-09	-1E-09	1.19E-09	8.42E-10	-2.8E-09
5.99E-05	2.68E-09	-3.5E-09	-1.1E-09	1.31E-09	6.38E-10	-3E-09
0.00006	2.87E-09	-3.6E-09	-1.2E-09	1.42E-09	4.3E-10	-3.2E-09
6.01E-05	3.02E-09	-3.7E-09	-1.3E-09	1.51E-09	2.22E-10	-3.3E-09
6.02E-05	3.14E-09	-3.7E-09	-1.3E-09	1.59E-09	1.73E-11	-3.4E-09
6.03E-05	3.22E-09	-3.8E-09	-1.3E-09	1.66E-09	-1.8E-10	-3.5E-09
6.04E-05	3.26E-09	-3.7E-09	-1.3E-09	1.7E-09	-3.7E-10	-3.6E-09
6.05E-05	3.26E-09	-3.7E-09	-1.3E-09	1.74E-09	-5.6E-10	-3.6E-09
6.06E-05	3.22E-09	-3.6E-09	-1.2E-09	1.75E-09	-7.2E-10	-3.6E-09
6.07E-05	3.14E-09	-3.4E-09	-1.2E-09	1.75E-09	-8.8E-10	-3.5E-09
6.08E-05	3.03E-09	-3.3E-09	-1.1E-09	1.72E-09	-1E-09	-3.4E-09
6.09E-05	2.88E-09	-3.1E-09	-9.5E-10	1.68E-09	-1.1E-09	-3.3E-09
0.000061	2.69E-09	-2.8E-09	-8.1E-10	1.63E-09	-1.2E-09	-3.2E-09
6.11E-05	2.48E-09	-2.6E-09	-6.6E-10	1.56E-09	-1.3E-09	-3E-09
6.12E-05	2.24E-09	-2.3E-09	-5E-10	1.47E-09	-1.4E-09	-2.8E-09
6.13E-05	1.98E-09	-2E-09	-3.3E-10	1.38E-09	-1.4E-09	-2.6E-09
6.14E-05	1.71E-09	-1.7E-09	-1.5E-10	1.27E-09	-1.4E-09	-2.4E-09
6.15E-05	1.42E-09	-1.4E-09	2.77E-11	1.15E-09	-1.4E-09	-2.1E-09
6.16E-05	1.12E-09	-1.1E-09	2.12E-10	1.02E-09	-1.4E-09	-1.9E-09
6.17E-05	8.16E-10	-7.6E-10	3.97E-10	8.9E-10	-1.4E-09	-1.6E-09
6.18E-05	5.13E-10	-4.3E-10	5.8E-10	7.55E-10	-1.3E-09	-1.3E-09
6.19E-05	2.14E-10	-1.1E-10	7.57E-10	6.18E-10	-1.2E-09	-1.1E-09

0.000062	-7.7E-11	2.15E-10	9.28E-10	4.81E-10	-1.1E-09	-7.8E-10
6.21E-05	-3.5E-10	5.29E-10	1.09E-09	3.46E-10	-1E-09	-5.1E-10
6.22E-05	-6.2E-10	8.3E-10	1.24E-09	2.16E-10	-9.1E-10	-2.3E-10
6.23E-05	-8.6E-10	1.12E-09	1.38E-09	9.12E-11	-7.8E-10	3.35E-11
6.24E-05	-1.1E-09	1.39E-09	1.51E-09	-2.6E-11	-6.4E-10	2.91E-10
6.25E-05	-1.3E-09	1.64E-09	1.62E-09	-1.3E-10	-4.9E-10	5.36E-10
6.26E-05	-1.4E-09	1.87E-09	1.71E-09	-2.3E-10	-3.3E-10	7.68E-10
6.27E-05	-1.6E-09	2.07E-09	1.79E-09	-3.2E-10	-1.8E-10	9.85E-10
6.28E-05	-1.7E-09	2.26E-09	1.85E-09	-4E-10	-1.4E-11	1.18E-09
6.29E-05	-1.8E-09	2.41E-09	1.9E-09	-4.6E-10	1.47E-10	1.37E-09
0.000063	-1.8E-09	2.54E-09	1.93E-09	-5.1E-10	3.07E-10	1.53E-09
6.31E-05	-1.9E-09	2.64E-09	1.94E-09	-5.4E-10	4.64E-10	1.67E-09
6.32E-05	-1.9E-09	2.72E-09	1.93E-09	-5.6E-10	6.17E-10	1.79E-09
6.33E-05	-1.8E-09	2.76E-09	1.91E-09	-5.7E-10	7.63E-10	1.89E-09
6.34E-05	-1.8E-09	2.78E-09	1.88E-09	-5.6E-10	9.02E-10	1.96E-09
6.35E-05	-1.7E-09	2.77E-09	1.83E-09	-5.5E-10	1.03E-09	2.01E-09
6.36E-05	-1.6E-09	2.74E-09	1.77E-09	-5.1E-10	1.15E-09	2.05E-09
6.37E-05	-1.4E-09	2.68E-09	1.7E-09	-4.7E-10	1.26E-09	2.06E-09
6.38E-05	-1.3E-09	2.6E-09	1.61E-09	-4.1E-10	1.36E-09	2.04E-09
6.39E-05	-1.1E-09	2.49E-09	1.52E-09	-3.5E-10	1.45E-09	2.01E-09
0.000064	-9.5E-10	2.36E-09	1.42E-09	-2.7E-10	1.52E-09	1.96E-09
6.41E-05	-7.6E-10	2.22E-09	1.31E-09	-1.9E-10	1.58E-09	1.89E-09
6.42E-05	-5.6E-10	2.05E-09	1.2E-09	-1E-10	1.63E-09	1.81E-09
6.43E-05	-3.5E-10	1.88E-09	1.08E-09	-7.5E-12	1.67E-09	1.7E-09
6.44E-05	-1.4E-10	1.69E-09	9.63E-10	8.98E-11	1.69E-09	1.59E-09
6.45E-05	6.75E-11	1.48E-09	8.42E-10	1.89E-10	1.7E-09	1.46E-09

6.46E-05	2.77E-10	1.27E-09	7.22E-10	2.9E-10	1.69E-09	1.32E-09
6.47E-05	4.83E-10	1.06E-09	6.03E-10	3.91E-10	1.68E-09	1.17E-09
6.48E-05	6.82E-10	8.35E-10	4.86E-10	4.9E-10	1.65E-09	1.01E-09
6.49E-05	8.74E-10	6.12E-10	3.73E-10	5.87E-10	1.61E-09	8.43E-10
0.000065	1.05E-09	3.89E-10	2.65E-10	6.81E-10	1.57E-09	6.74E-10
6.51E-05	1.22E-09	1.69E-10	1.62E-10	7.7E-10	1.51E-09	5.02E-10
6.52E-05	1.38E-09	-4.7E-11	6.48E-11	8.53E-10	1.44E-09	3.29E-10
6.53E-05	1.52E-09	-2.6E-10	-2.5E-11	9.31E-10	1.37E-09	1.57E-10
6.54E-05	1.65E-09	-4.6E-10	-1.1E-10	1E-09	1.29E-09	-1.3E-11
6.55E-05	1.76E-09	-6.5E-10	-1.8E-10	1.07E-09	1.21E-09	-1.8E-10
6.56E-05	1.85E-09	-8.3E-10	-2.5E-10	1.12E-09	1.12E-09	-3.4E-10
6.57E-05	1.93E-09	-1E-09	-3.1E-10	1.17E-09	1.02E-09	-5E-10
6.58E-05	1.99E-09	-1.2E-09	-3.6E-10	1.21E-09	9.29E-10	-6.4E-10
6.59E-05	2.03E-09	-1.3E-09	-4E-10	1.24E-09	8.33E-10	-7.8E-10
0.000066	2.05E-09	-1.4E-09	-4.3E-10	1.26E-09	7.35E-10	-9.1E-10
6.61E-05	2.06E-09	-1.5E-09	-4.6E-10	1.27E-09	6.38E-10	-1E-09
6.62E-05	2.06E-09	-1.6E-09	-4.8E-10	1.28E-09	5.42E-10	-1.1E-09
6.63E-05	2.03E-09	-1.7E-09	-4.9E-10	1.27E-09	4.48E-10	-1.2E-09
6.64E-05	2E-09	-1.8E-09	-4.9E-10	1.26E-09	3.57E-10	-1.3E-09
6.65E-05	1.94E-09	-1.8E-09	-4.8E-10	1.24E-09	2.69E-10	-1.4E-09
6.66E-05	1.88E-09	-1.8E-09	-4.7E-10	1.22E-09	1.85E-10	-1.4E-09
6.67E-05	1.81E-09	-1.8E-09	-4.5E-10	1.18E-09	1.06E-10	-1.5E-09
6.68E-05	1.72E-09	-1.8E-09	-4.3E-10	1.15E-09	3.25E-11	-1.5E-09
6.69E-05	1.63E-09	-1.8E-09	-4E-10	1.1E-09	-3.6E-11	-1.5E-09
0.000067	1.52E-09	-1.8E-09	-3.6E-10	1.05E-09	-9.8E-11	-1.5E-09
6.71E-05	1.42E-09	-1.7E-09	-3.2E-10	1E-09	-1.5E-10	-1.5E-09

6.72E-05	1.3E-09	-1.7E-09	-2.8E-10	9.47E-10	-2E-10	-1.5E-09
6.73E-05	1.18E-09	-1.6E-09	-2.4E-10	8.89E-10	-2.5E-10	-1.5E-09
6.74E-05	1.06E-09	-1.5E-09	-1.9E-10	8.29E-10	-2.9E-10	-1.5E-09
6.75E-05	9.37E-10	-1.5E-09	-1.4E-10	7.67E-10	-3.2E-10	-1.4E-09
6.76E-05	8.13E-10	-1.4E-09	-9E-11	7.05E-10	-3.4E-10	-1.4E-09
6.77E-05	6.9E-10	-1.3E-09	-3.9E-11	6.42E-10	-3.6E-10	-1.3E-09
6.78E-05	5.68E-10	-1.2E-09	1.25E-11	5.8E-10	-3.7E-10	-1.2E-09
6.79E-05	4.49E-10	-1.1E-09	6.41E-11	5.18E-10	-3.8E-10	-1.2E-09
0.000068	3.34E-10	-9.6E-10	1.15E-10	4.58E-10	-3.8E-10	-1.1E-09
6.81E-05	2.24E-10	-8.5E-10	1.66E-10	4E-10	-3.8E-10	-9.9E-10
6.82E-05	1.2E-10	-7.4E-10	2.15E-10	3.44E-10	-3.7E-10	-9E-10
6.83E-05	2.15E-11	-6.3E-10	2.62E-10	2.9E-10	-3.6E-10	-8.1E-10
6.84E-05	-7E-11	-5.2E-10	3.08E-10	2.39E-10	-3.4E-10	-7.2E-10
6.85E-05	-1.5E-10	-4.2E-10	3.52E-10	1.92E-10	-3.2E-10	-6.3E-10
6.86E-05	-2.3E-10	-3.2E-10	3.94E-10	1.48E-10	-2.9E-10	-5.4E-10
6.87E-05	-3E-10	-2.2E-10	4.33E-10	1.07E-10	-2.7E-10	-4.5E-10
6.88E-05	-3.5E-10	-1.3E-10	4.69E-10	7.02E-11	-2.4E-10	-3.7E-10
6.89E-05	-4E-10	-3.7E-11	5.02E-10	3.71E-11	-2.1E-10	-2.8E-10
0.000069	-4.5E-10	4.71E-11	5.32E-10	7.86E-12	-1.8E-10	-2E-10
6.91E-05	-4.8E-10	1.26E-10	5.59E-10	-1.8E-11	-1.4E-10	-1.2E-10
6.92E-05	-5E-10	2E-10	5.83E-10	-3.9E-11	-1.1E-10	-5E-11
6.93E-05	-5.2E-10	2.68E-10	6.03E-10	-5.7E-11	-7.1E-11	1.92E-11
6.94E-05	-5.3E-10	3.31E-10	6.2E-10	-7.1E-11	-3.5E-11	8.41E-11
6.95E-05	-5.3E-10	3.89E-10	6.34E-10	-8.2E-11	2.8E-13	1.44E-10
6.96E-05	-5.2E-10	4.41E-10	6.45E-10	-8.9E-11	3.58E-11	2E-10
6.97E-05	-5.1E-10	4.88E-10	6.52E-10	-9.2E-11	7.09E-11	2.5E-10

6.98E-05	-4.9E-10	5.3E-10	6.57E-10	-9.3E-11	1.05E-10	2.95E-10
6.99E-05	-4.7E-10	5.67E-10	6.59E-10	-9E-11	1.39E-10	3.36E-10
0.00007	-4.4E-10	6E-10	6.59E-10	-8.5E-11	1.72E-10	3.72E-10

Difference between Crack and Hole Data (T = transmitter, L = Long Distance Test).

Time	T1R1	T1R2	T1R3	T2R1	T2R2	T2R3
0	-9E-12	3.71E-12	-4.5E-13	4.25E-13	1.5E-11	2.64E-12
1E-07	-9.5E-12	2.98E-12	4.86E-13	-1.3E-13	1.44E-11	3.31E-12
2E-07	-1E-11	2.26E-12	1.39E-12	-8.5E-13	1.39E-11	3.99E-12
3E-07	-1.1E-11	1.54E-12	2.25E-12	-1.7E-12	1.34E-11	4.66E-12
4E-07	-1.1E-11	8.44E-13	3.05E-12	-2.6E-12	1.29E-11	5.32E-12
5E-07	-1.2E-11	1.75E-13	3.83E-12	-3.6E-12	1.25E-11	5.94E-12
6E-07	-1.2E-11	-4.6E-13	4.63E-12	-4.6E-12	1.2E-11	6.5E-12
7E-07	-1.3E-11	-1.1E-12	5.51E-12	-5.5E-12	1.15E-11	6.95E-12
8E-07	-1.3E-11	-1.6E-12	6.49E-12	-6.3E-12	1.11E-11	7.27E-12
9E-07	-1.4E-11	-2E-12	7.63E-12	-7.1E-12	1.07E-11	7.43E-12
0.000001	-1.4E-11	-2.4E-12	8.94E-12	-7.8E-12	1.04E-11	7.43E-12
1.1E-06	-1.5E-11	-2.7E-12	1.04E-11	-8.4E-12	1.02E-11	7.27E-12
1.2E-06	-1.5E-11	-3E-12	1.21E-11	-9E-12	1.01E-11	6.99E-12
1.3E-06	-1.6E-11	-3.2E-12	1.38E-11	-9.6E-12	1.01E-11	6.6E-12
1.4E-06	-1.6E-11	-3.4E-12	1.55E-11	-1E-11	1.03E-11	6.17E-12
1.5E-06	-1.7E-11	-3.5E-12	1.71E-11	-1.1E-11	1.05E-11	5.73E-12
1.6E-06	-1.7E-11	-3.5E-12	1.85E-11	-1.1E-11	1.07E-11	5.34E-12

1.7E-06	-1.8E-11	-3.5E-12	1.98E-11	-1.2E-11	1.1E-11	5.05E-12
1.8E-06	-1.8E-11	-3.5E-12	2.07E-11	-1.3E-11	1.12E-11	4.9E-12
1.9E-06	-1.8E-11	-3.4E-12	2.14E-11	-1.4E-11	1.14E-11	4.94E-12
0.000002	-1.8E-11	-3.3E-12	2.18E-11	-1.4E-11	1.16E-11	5.19E-12
2.1E-06	-1.7E-11	-3.2E-12	2.2E-11	-1.5E-11	1.19E-11	5.66E-12
2.2E-06	-1.7E-11	-3.1E-12	2.2E-11	-1.6E-11	1.21E-11	6.34E-12
2.3E-06	-1.6E-11	-2.9E-12	2.19E-11	-1.6E-11	1.24E-11	7.2E-12
2.4E-06	-1.6E-11	-2.8E-12	2.18E-11	-1.6E-11	1.27E-11	8.22E-12
2.5E-06	-1.5E-11	-2.7E-12	2.16E-11	-1.7E-11	1.31E-11	9.31E-12
2.6E-06	-1.4E-11	-2.6E-12	2.15E-11	-1.7E-11	1.34E-11	1.04E-11
2.7E-06	-1.4E-11	-2.5E-12	2.15E-11	-1.6E-11	1.38E-11	1.15E-11
2.8E-06	-1.3E-11	-2.5E-12	2.16E-11	-1.6E-11	1.4E-11	1.25E-11
2.9E-06	-1.2E-11	-2.6E-12	2.16E-11	-1.5E-11	1.42E-11	1.33E-11
0.000003	-1.2E-11	-2.7E-12	2.17E-11	-1.4E-11	1.43E-11	1.39E-11
3.1E-06	-1.2E-11	-2.8E-12	2.16E-11	-1.2E-11	1.44E-11	1.44E-11
3.2E-06	-1.1E-11	-3.1E-12	2.14E-11	-1.1E-11	1.44E-11	1.47E-11
3.3E-06	-1.1E-11	-3.5E-12	2.09E-11	-9.7E-12	1.44E-11	1.48E-11
3.4E-06	-1.1E-11	-4.1E-12	2.01E-11	-8.3E-12	1.45E-11	1.48E-11
3.5E-06	-1.1E-11	-4.7E-12	1.9E-11	-7E-12	1.45E-11	1.47E-11
3.6E-06	-1.1E-11	-5.4E-12	1.76E-11	-5.8E-12	1.45E-11	1.45E-11
3.7E-06	-1.2E-11	-6.3E-12	1.58E-11	-4.7E-12	1.45E-11	1.43E-11
3.8E-06	-1.2E-11	-7.2E-12	1.39E-11	-3.7E-12	1.44E-11	1.41E-11
3.9E-06	-1.2E-11	-8.1E-12	1.18E-11	-2.7E-12	1.42E-11	1.39E-11
0.000004	-1.2E-11	-9.1E-12	9.66E-12	-1.7E-12	1.39E-11	1.37E-11
4.1E-06	-1.1E-11	-1E-11	7.65E-12	-7E-13	1.35E-11	1.35E-11
4.2E-06	-1.1E-11	-1.1E-11	5.83E-12	4.28E-13	1.31E-11	1.32E-11

4.3E-06	-1.1E-11	-1.2E-11	4.25E-12	1.69E-12	1.27E-11	1.3E-11
4.4E-06	-9.8E-12	-1.3E-11	2.92E-12	3.1E-12	1.23E-11	1.27E-11
4.5E-06	-9E-12	-1.4E-11	1.84E-12	4.65E-12	1.19E-11	1.22E-11
4.6E-06	-8E-12	-1.5E-11	9.87E-13	6.33E-12	1.15E-11	1.17E-11
4.7E-06	-6.8E-12	-1.6E-11	3.06E-13	8.08E-12	1.12E-11	1.1E-11
4.8E-06	-5.7E-12	-1.7E-11	-2.9E-13	9.81E-12	1.08E-11	1.02E-11
4.9E-06	-4.5E-12	-1.8E-11	-8.7E-13	1.15E-11	1.04E-11	9.17E-12
0.000005	-3.4E-12	-2E-11	-1.5E-12	1.29E-11	9.82E-12	8.01E-12
5.1E-06	-2.3E-12	-2.1E-11	-2.2E-12	1.41E-11	9.15E-12	6.73E-12
5.2E-06	-1.5E-12	-2.2E-11	-3E-12	1.49E-11	8.33E-12	5.38E-12
5.3E-06	-7.9E-13	-2.4E-11	-4E-12	1.53E-11	7.35E-12	4E-12
5.4E-06	-3.3E-13	-2.5E-11	-5E-12	1.54E-11	6.2E-12	2.65E-12
5.5E-06	-1.3E-13	-2.7E-11	-6.1E-12	1.5E-11	4.9E-12	1.37E-12
5.6E-06	-1.6E-13	-2.9E-11	-7.1E-12	1.44E-11	3.43E-12	2.18E-13
5.7E-06	-4.5E-13	-3.1E-11	-8E-12	1.35E-11	1.8E-12	-7.7E-13
5.8E-06	-9.7E-13	-3.3E-11	-8.7E-12	1.24E-11	2.13E-14	-1.6E-12
5.9E-06	-1.7E-12	-3.6E-11	-9.1E-12	1.11E-11	-1.9E-12	-2.1E-12
0.000006	-2.7E-12	-3.8E-11	-9.3E-12	9.8E-12	-3.9E-12	-2.4E-12
6.1E-06	-3.8E-12	-4E-11	-9.1E-12	8.4E-12	-6.1E-12	-2.5E-12
6.2E-06	-5.1E-12	-4.1E-11	-8.6E-12	6.94E-12	-8.2E-12	-2.3E-12
6.3E-06	-6.5E-12	-4.3E-11	-7.9E-12	5.39E-12	-1E-11	-2E-12
6.4E-06	-7.9E-12	-4.3E-11	-7.1E-12	3.72E-12	-1.2E-11	-1.5E-12
6.5E-06	-9.4E-12	-4.4E-11	-6.4E-12	1.9E-12	-1.3E-11	-8.5E-13
6.6E-06	-1.1E-11	-4.3E-11	-5.8E-12	-7.7E-14	-1.4E-11	-2.5E-13
6.7E-06	-1.2E-11	-4.2E-11	-5.4E-12	-2.2E-12	-1.5E-11	2.56E-13
6.8E-06	-1.4E-11	-3.9E-11	-5.5E-12	-4.5E-12	-1.4E-11	5.6E-13

6.9E-06	-1.5E-11	-3.5E-11	-6.1E-12	-6.8E-12	-1.3E-11	5.68E-13
0.000007	-1.6E-11	-3E-11	-7.2E-12	-9.1E-12	-1E-11	1.87E-13
7.1E-06	-1.6E-11	-2.4E-11	-9.1E-12	-1.1E-11	-6.8E-12	-6.7E-13
7.2E-06	-1.6E-11	-1.6E-11	-1.2E-11	-1.3E-11	-2E-12	-2.1E-12
7.3E-06	-1.6E-11	-6.4E-12	-1.5E-11	-1.4E-11	3.93E-12	-4.1E-12
7.4E-06	-1.5E-11	4.67E-12	-2E-11	-1.5E-11	1.12E-11	-6.7E-12
7.5E-06	-1.4E-11	1.74E-11	-2.6E-11	-1.5E-11	1.97E-11	-1E-11
7.6E-06	-1.2E-11	3.19E-11	-3.3E-11	-1.3E-11	2.95E-11	-1.4E-11
7.7E-06	-9.3E-12	4.81E-11	-4.2E-11	-1.1E-11	4.05E-11	-1.9E-11
7.8E-06	-5.7E-12	6.61E-11	-5.2E-11	-7E-12	5.26E-11	-2.4E-11
7.9E-06	-1.2E-12	8.55E-11	-6.3E-11	-2E-12	6.56E-11	-2.9E-11
0.000008	4.19E-12	1.06E-10	-7.5E-11	4.19E-12	7.93E-11	-3.4E-11
8.1E-06	1.06E-11	1.27E-10	-8.7E-11	1.15E-11	9.35E-11	-4E-11
8.2E-06	1.79E-11	1.47E-10	-9.8E-11	1.97E-11	1.08E-10	-4.4E-11
8.3E-06	2.61E-11	1.66E-10	-1.1E-10	2.88E-11	1.22E-10	-4.8E-11
8.4E-06	3.51E-11	1.8E-10	-1.1E-10	3.84E-11	1.36E-10	-5E-11
8.5E-06	4.49E-11	1.89E-10	-1.1E-10	4.85E-11	1.49E-10	-5E-11
8.6E-06	5.53E-11	1.89E-10	-9.4E-11	5.87E-11	1.61E-10	-4.8E-11
8.7E-06	6.6E-11	1.79E-10	-7E-11	6.9E-11	1.71E-10	-4.4E-11
8.8E-06	7.68E-11	1.55E-10	-3.1E-11	7.91E-11	1.79E-10	-3.6E-11
8.9E-06	8.76E-11	1.17E-10	2.41E-11	8.88E-11	1.85E-10	-2.6E-11
0.000009	9.79E-11	6.43E-11	9.54E-11	9.79E-11	1.89E-10	-1.1E-11
9.1E-06	1.07E-10	-3.6E-12	1.83E-10	1.06E-10	1.89E-10	6.2E-12
9.2E-06	1.16E-10	-8.5E-11	2.84E-10	1.14E-10	1.87E-10	2.72E-11
9.3E-06	1.23E-10	-1.8E-10	3.95E-10	1.2E-10	1.81E-10	5.13E-11
9.4E-06	1.29E-10	-2.7E-10	5.12E-10	1.25E-10	1.72E-10	7.82E-11

9.5E-06	1.32E-10	-3.7E-10	6.28E-10	1.28E-10	1.59E-10	1.07E-10
9.6E-06	1.34E-10	-4.6E-10	7.36E-10	1.3E-10	1.43E-10	1.38E-10
9.7E-06	1.33E-10	-5.5E-10	8.29E-10	1.29E-10	1.22E-10	1.7E-10
9.8E-06	1.3E-10	-6.1E-10	9E-10	1.27E-10	9.8E-11	2.01E-10
9.9E-06	1.24E-10	-6.5E-10	9.41E-10	1.22E-10	6.98E-11	2.32E-10
0.00001	1.15E-10	-6.6E-10	9.47E-10	1.15E-10	3.8E-11	2.6E-10
1.01E-05	1.04E-10	-6.4E-10	9.14E-10	1.05E-10	2.9E-12	2.85E-10
1.02E-05	9.02E-11	-5.9E-10	8.39E-10	9.31E-11	-3.5E-11	3.06E-10
1.03E-05	7.38E-11	-5E-10	7.22E-10	7.82E-11	-7.5E-11	3.21E-10
1.04E-05	5.49E-11	-3.8E-10	5.64E-10	6.08E-11	-1.2E-10	3.3E-10
1.05E-05	3.36E-11	-2.3E-10	3.68E-10	4.07E-11	-1.6E-10	3.32E-10
1.06E-05	9.86E-12	-5.5E-11	1.4E-10	1.82E-11	-2E-10	3.26E-10
1.07E-05	-1.6E-11	1.45E-10	-1.1E-10	-6.5E-12	-2.4E-10	3.11E-10
1.08E-05	-4.4E-11	3.6E-10	-3.9E-10	-3.3E-11	-2.7E-10	2.88E-10
1.09E-05	-7.4E-11	5.85E-10	-6.7E-10	-6.2E-11	-3E-10	2.57E-10
0.000011	-1E-10	8.12E-10	-9.5E-10	-9.2E-11	-3.3E-10	2.17E-10
1.11E-05	-1.4E-10	1.04E-09	-1.2E-09	-1.2E-10	-3.4E-10	1.69E-10
1.12E-05	-1.7E-10	1.25E-09	-1.5E-09	-1.5E-10	-3.5E-10	1.15E-10
1.13E-05	-2E-10	1.44E-09	-1.7E-09	-1.8E-10	-3.4E-10	5.44E-11
1.14E-05	-2.3E-10	1.6E-09	-1.9E-09	-2.1E-10	-3.3E-10	-1.1E-11
1.15E-05	-2.5E-10	1.73E-09	-2.1E-09	-2.3E-10	-3E-10	-7.9E-11
1.16E-05	-2.7E-10	1.82E-09	-2.2E-09	-2.5E-10	-2.7E-10	-1.5E-10
1.17E-05	-2.8E-10	1.86E-09	-2.2E-09	-2.7E-10	-2.2E-10	-2.2E-10
1.18E-05	-2.9E-10	1.86E-09	-2.2E-09	-2.8E-10	-1.7E-10	-2.9E-10
1.19E-05	-2.8E-10	1.79E-09	-2.2E-09	-2.8E-10	-1.1E-10	-3.6E-10
0.000012	-2.7E-10	1.68E-09	-2.1E-09	-2.7E-10	-5.2E-11	-4.2E-10

1.21E-05	-2.5E-10	1.5E-09	-1.9E-09	-2.5E-10	1.35E-11	-4.8E-10
1.22E-05	-2.2E-10	1.27E-09	-1.6E-09	-2.3E-10	8.06E-11	-5.4E-10
1.23E-05	-1.8E-10	9.88E-10	-1.3E-09	-1.9E-10	1.47E-10	-5.8E-10
1.24E-05	-1.3E-10	6.57E-10	-1E-09	-1.5E-10	2.11E-10	-6.2E-10
1.25E-05	-7.6E-11	2.85E-10	-6.2E-10	-1.1E-10	2.7E-10	-6.5E-10
1.26E-05	-1.5E-11	-1.2E-10	-2E-10	-5.4E-11	3.24E-10	-6.7E-10
1.27E-05	4.87E-11	-5.6E-10	2.32E-10	2.52E-12	3.69E-10	-6.9E-10
1.28E-05	1.15E-10	-1E-09	6.79E-10	6.18E-11	4.04E-10	-6.9E-10
1.29E-05	1.81E-10	-1.5E-09	1.12E-09	1.22E-10	4.28E-10	-6.9E-10
0.000013	2.46E-10	-1.9E-09	1.56E-09	1.81E-10	4.4E-10	-6.7E-10
1.31E-05	3.06E-10	-2.3E-09	1.96E-09	2.38E-10	4.39E-10	-6.5E-10
1.32E-05	3.61E-10	-2.7E-09	2.33E-09	2.9E-10	4.24E-10	-6.2E-10
1.33E-05	4.08E-10	-3.1E-09	2.66E-09	3.36E-10	3.96E-10	-5.8E-10
1.34E-05	4.45E-10	-3.4E-09	2.92E-09	3.73E-10	3.53E-10	-5.3E-10
1.35E-05	4.71E-10	-3.6E-09	3.12E-09	4.02E-10	2.98E-10	-4.8E-10
1.36E-05	4.84E-10	-3.8E-09	3.25E-09	4.2E-10	2.31E-10	-4.2E-10
1.37E-05	4.84E-10	-3.9E-09	3.31E-09	4.26E-10	1.54E-10	-3.5E-10
1.38E-05	4.7E-10	-3.9E-09	3.29E-09	4.2E-10	6.7E-11	-2.7E-10
1.39E-05	4.41E-10	-3.8E-09	3.2E-09	4.02E-10	-2.6E-11	-1.9E-10
0.000014	3.97E-10	-3.7E-09	3.05E-09	3.71E-10	-1.2E-10	-1.1E-10
1.41E-05	3.4E-10	-3.5E-09	2.83E-09	3.28E-10	-2.2E-10	-1.6E-11
1.42E-05	2.7E-10	-3.2E-09	2.55E-09	2.74E-10	-3.2E-10	7.63E-11
1.43E-05	1.88E-10	-2.8E-09	2.22E-09	2.09E-10	-4.2E-10	1.71E-10
1.44E-05	9.64E-11	-2.4E-09	1.84E-09	1.36E-10	-5.1E-10	2.67E-10
1.45E-05	-2.8E-12	-1.9E-09	1.43E-09	5.52E-11	-5.9E-10	3.63E-10
1.46E-05	-1.1E-10	-1.4E-09	9.73E-10	-3E-11	-6.6E-10	4.57E-10

1.47E-05	-2.1E-10	-8.4E-10	4.95E-10	-1.2E-10	-7.2E-10	5.5E-10
1.48E-05	-3.2E-10	-2.3E-10	-3.4E-12	-2.1E-10	-7.6E-10	6.38E-10
1.49E-05	-4.2E-10	4.04E-10	-5.1E-10	-2.9E-10	-7.8E-10	7.22E-10
0.000015	-5.2E-10	1.06E-09	-1E-09	-3.8E-10	-7.9E-10	7.99E-10
1.51E-05	-6.1E-10	1.73E-09	-1.5E-09	-4.5E-10	-7.8E-10	8.69E-10
1.52E-05	-6.9E-10	2.39E-09	-2E-09	-5.2E-10	-7.5E-10	9.29E-10
1.53E-05	-7.5E-10	3.04E-09	-2.5E-09	-5.8E-10	-6.9E-10	9.8E-10
1.54E-05	-8E-10	3.67E-09	-2.9E-09	-6.3E-10	-6.2E-10	1.02E-09
1.55E-05	-8.3E-10	4.26E-09	-3.4E-09	-6.6E-10	-5.3E-10	1.05E-09
1.56E-05	-8.4E-10	4.81E-09	-3.7E-09	-6.7E-10	-4.3E-10	1.06E-09
1.57E-05	-8.3E-10	5.3E-09	-4E-09	-6.7E-10	-3.1E-10	1.06E-09
1.58E-05	-8E-10	5.72E-09	-4.3E-09	-6.5E-10	-1.8E-10	1.05E-09
1.59E-05	-7.4E-10	6.07E-09	-4.5E-09	-6.2E-10	-3.7E-11	1.02E-09
0.000016	-6.7E-10	6.33E-09	-4.6E-09	-5.7E-10	1.12E-10	9.8E-10
1.61E-05	-5.8E-10	6.51E-09	-4.6E-09	-5E-10	2.64E-10	9.22E-10
1.62E-05	-4.7E-10	6.59E-09	-4.6E-09	-4.1E-10	4.19E-10	8.5E-10
1.63E-05	-3.4E-10	6.58E-09	-4.5E-09	-3.1E-10	5.72E-10	7.65E-10
1.64E-05	-2E-10	6.47E-09	-4.4E-09	-2E-10	7.19E-10	6.68E-10
1.65E-05	-5.5E-11	6.26E-09	-4.2E-09	-8E-11	8.59E-10	5.59E-10
1.66E-05	1.01E-10	5.95E-09	-3.9E-09	4.79E-11	9.88E-10	4.4E-10
1.67E-05	2.62E-10	5.54E-09	-3.6E-09	1.8E-10	1.1E-09	3.13E-10
1.68E-05	4.24E-10	5.03E-09	-3.2E-09	3.13E-10	1.2E-09	1.77E-10
1.69E-05	5.81E-10	4.42E-09	-2.7E-09	4.44E-10	1.27E-09	3.58E-11
0.000017	7.32E-10	3.72E-09	-2.3E-09	5.69E-10	1.32E-09	-1.1E-10
1.71E-05	8.71E-10	2.92E-09	-1.7E-09	6.85E-10	1.34E-09	-2.6E-10
1.72E-05	9.96E-10	2.02E-09	-1.1E-09	7.89E-10	1.33E-09	-4.1E-10

1.73E-05	1.1E-09	1.04E-09	-4.4E-10	8.79E-10	1.29E-09	-5.6E-10
1.74E-05	1.19E-09	-3.7E-11	2.91E-10	9.51E-10	1.23E-09	-7.1E-10
1.75E-05	1.25E-09	-1.2E-09	1.09E-09	1E-09	1.13E-09	-8.5E-10
1.76E-05	1.3E-09	-2.4E-09	1.94E-09	1.04E-09	1.01E-09	-9.8E-10
1.77E-05	1.31E-09	-3.7E-09	2.87E-09	1.05E-09	8.58E-10	-1.1E-09
1.78E-05	1.3E-09	-5E-09	3.85E-09	1.04E-09	6.89E-10	-1.2E-09
1.79E-05	1.27E-09	-6.3E-09	4.89E-09	1.01E-09	5.05E-10	-1.3E-09
0.000018	1.21E-09	-7.7E-09	5.98E-09	9.62E-10	3.09E-10	-1.4E-09
1.81E-05	1.14E-09	-9.1E-09	7.11E-09	8.96E-10	1.08E-10	-1.4E-09
1.82E-05	1.04E-09	-1E-08	8.26E-09	8.13E-10	-9.3E-11	-1.4E-09
1.83E-05	9.2E-10	-1.2E-08	9.42E-09	7.16E-10	-2.9E-10	-1.4E-09
1.84E-05	7.86E-10	-1.3E-08	1.06E-08	6.05E-10	-4.7E-10	-1.3E-09
1.85E-05	6.38E-10	-1.4E-08	1.17E-08	4.83E-10	-6.4E-10	-1.3E-09
1.86E-05	4.77E-10	-1.5E-08	1.27E-08	3.51E-10	-7.8E-10	-1.1E-09
1.87E-05	3.05E-10	-1.6E-08	1.37E-08	2.12E-10	-9.1E-10	-1E-09
1.88E-05	1.26E-10	-1.6E-08	1.45E-08	6.72E-11	-1E-09	-8.4E-10
1.89E-05	-5.9E-11	-1.7E-08	1.51E-08	-8.2E-11	-1.1E-09	-6.6E-10
0.000019	-2.5E-10	-1.7E-08	1.56E-08	-2.3E-10	-1.1E-09	-4.5E-10
1.91E-05	-4.3E-10	-1.7E-08	1.58E-08	-3.8E-10	-1.1E-09	-2.3E-10
1.92E-05	-6.2E-10	-1.7E-08	1.58E-08	-5.3E-10	-1.1E-09	-7.6E-12
1.93E-05	-7.9E-10	-1.6E-08	1.55E-08	-6.7E-10	-1E-09	2.22E-10
1.94E-05	-9.6E-10	-1.5E-08	1.48E-08	-8.1E-10	-9.7E-10	4.49E-10
1.95E-05	-1.1E-09	-1.4E-08	1.38E-08	-9.3E-10	-8.8E-10	6.68E-10
1.96E-05	-1.2E-09	-1.2E-08	1.24E-08	-1E-09	-7.7E-10	8.73E-10
1.97E-05	-1.4E-09	-1E-08	1.07E-08	-1.1E-09	-6.5E-10	1.06E-09
1.98E-05	-1.5E-09	-8E-09	8.48E-09	-1.2E-09	-5.2E-10	1.22E-09

1.99E-05	-1.5E-09	-5.3E-09	5.9E-09	-1.3E-09	-3.8E-10	1.35E-09
0.00002	-1.6E-09	-2.2E-09	2.93E-09	-1.3E-09	-2.5E-10	1.45E-09
2.01E-05	-1.6E-09	1.16E-09	-4.2E-10	-1.3E-09	-1.2E-10	1.51E-09
2.02E-05	-1.6E-09	4.83E-09	-4.1E-09	-1.3E-09	-9.1E-12	1.53E-09
2.03E-05	-1.5E-09	8.75E-09	-8.1E-09	-1.3E-09	8.54E-11	1.51E-09
2.04E-05	-1.4E-09	1.29E-08	-1.2E-08	-1.2E-09	1.57E-10	1.44E-09
2.05E-05	-1.3E-09	1.71E-08	-1.7E-08	-1.1E-09	2.01E-10	1.33E-09
2.06E-05	-1.2E-09	2.15E-08	-2.2E-08	-9.8E-10	2.15E-10	1.16E-09
2.07E-05	-9.9E-10	2.59E-08	-2.6E-08	-8.4E-10	1.95E-10	9.57E-10
2.08E-05	-7.9E-10	3.02E-08	-3.1E-08	-6.7E-10	1.4E-10	7.08E-10
2.09E-05	-5.8E-10	3.44E-08	-3.6E-08	-4.9E-10	5.03E-11	4.22E-10
0.000021	-3.5E-10	3.84E-08	-4E-08	-2.9E-10	-7.4E-11	1.04E-10
2.11E-05	-1.1E-10	4.21E-08	-4.4E-08	-8.4E-11	-2.3E-10	-2.4E-10
2.12E-05	1.34E-10	4.54E-08	-4.8E-08	1.35E-10	-4.2E-10	-6E-10
2.13E-05	3.86E-10	4.82E-08	-5.1E-08	3.6E-10	-6.3E-10	-9.7E-10
2.14E-05	6.36E-10	5.05E-08	-5.4E-08	5.85E-10	-8.6E-10	-1.3E-09
2.15E-05	8.79E-10	5.21E-08	-5.6E-08	8.06E-10	-1.1E-09	-1.7E-09
2.16E-05	1.11E-09	5.3E-08	-5.7E-08	1.02E-09	-1.4E-09	-2E-09
2.17E-05	1.33E-09	5.32E-08	-5.7E-08	1.22E-09	-1.6E-09	-2.3E-09
2.18E-05	1.52E-09	5.25E-08	-5.6E-08	1.4E-09	-1.8E-09	-2.6E-09
2.19E-05	1.69E-09	5.1E-08	-5.5E-08	1.56E-09	-2E-09	-2.8E-09
0.000022	1.83E-09	4.86E-08	-5.2E-08	1.7E-09	-2.2E-09	-2.9E-09
2.21E-05	1.93E-09	4.53E-08	-4.8E-08	1.81E-09	-2.3E-09	-2.9E-09
2.22E-05	1.99E-09	4.1E-08	-4.3E-08	1.88E-09	-2.4E-09	-2.9E-09
2.23E-05	2.01E-09	3.59E-08	-3.7E-08	1.91E-09	-2.4E-09	-2.8E-09
2.24E-05	1.99E-09	2.99E-08	-3E-08	1.91E-09	-2.3E-09	-2.6E-09

2.25E-05	1.92E-09	2.31E-08	-2.3E-08	1.86E-09	-2.2E-09	-2.3E-09
2.26E-05	1.8E-09	1.55E-08	-1.4E-08	1.76E-09	-1.9E-09	-1.9E-09
2.27E-05	1.64E-09	7.26E-09	-4.2E-09	1.63E-09	-1.6E-09	-1.4E-09
2.28E-05	1.42E-09	-1.6E-09	6.05E-09	1.45E-09	-1.2E-09	-8.2E-10
2.29E-05	1.16E-09	-1.1E-08	1.68E-08	1.22E-09	-7.4E-10	-1.6E-10
0.000023	8.58E-10	-2E-08	2.79E-08	9.49E-10	-1.8E-10	5.57E-10
2.31E-05	5.12E-10	-3E-08	3.92E-08	6.39E-10	4.49E-10	1.33E-09
2.32E-05	1.31E-10	-4E-08	5.06E-08	2.93E-10	1.14E-09	2.15E-09
2.33E-05	-2.8E-10	-5E-08	6.18E-08	-8.6E-11	1.89E-09	2.99E-09
2.34E-05	-7.2E-10	-6E-08	7.26E-08	-4.9E-10	2.68E-09	3.83E-09
2.35E-05	-1.2E-09	-6.9E-08	8.29E-08	-9.2E-10	3.49E-09	4.66E-09
2.36E-05	-1.6E-09	-7.8E-08	9.24E-08	-1.4E-09	4.3E-09	5.46E-09
2.37E-05	-2.1E-09	-8.5E-08	1.01E-07	-1.8E-09	5.11E-09	6.19E-09
2.38E-05	-2.5E-09	-9.3E-08	1.08E-07	-2.2E-09	5.88E-09	6.85E-09
2.39E-05	-3E-09	-9.9E-08	1.15E-07	-2.7E-09	6.6E-09	7.41E-09
0.000024	-3.3E-09	-1E-07	1.19E-07	-3.1E-09	7.25E-09	7.85E-09
2.41E-05	-3.7E-09	-1.1E-07	1.22E-07	-3.4E-09	7.81E-09	8.14E-09
2.42E-05	-4E-09	-1.1E-07	1.24E-07	-3.8E-09	8.25E-09	8.29E-09
2.43E-05	-4.2E-09	-1.1E-07	1.24E-07	-4E-09	8.57E-09	8.26E-09
2.44E-05	-4.4E-09	-1.1E-07	1.22E-07	-4.2E-09	8.75E-09	8.06E-09
2.45E-05	-4.5E-09	-1.1E-07	1.18E-07	-4.4E-09	8.76E-09	7.66E-09
2.46E-05	-4.5E-09	-1.1E-07	1.12E-07	-4.4E-09	8.61E-09	7.08E-09
2.47E-05	-4.4E-09	-1E-07	1.05E-07	-4.4E-09	8.28E-09	6.3E-09
2.48E-05	-4.2E-09	-9.4E-08	9.58E-08	-4.3E-09	7.78E-09	5.33E-09
2.49E-05	-3.9E-09	-8.7E-08	8.52E-08	-4.1E-09	7.09E-09	4.19E-09
0.000025	-3.5E-09	-7.8E-08	7.32E-08	-3.7E-09	6.22E-09	2.87E-09

2.51E-05	-3E-09	-6.8E-08	5.99E-08	-3.3E-09	5.19E-09	1.41E-09
2.52E-05	-2.4E-09	-5.7E-08	4.55E-08	-2.8E-09	3.99E-09	-1.8E-10
2.53E-05	-1.7E-09	-4.6E-08	3.03E-08	-2.2E-09	2.65E-09	-1.9E-09
2.54E-05	-9E-10	-3.3E-08	1.43E-08	-1.5E-09	1.18E-09	-3.7E-09
2.55E-05	-5.2E-11	-2E-08	-2.1E-09	-7.2E-10	-3.9E-10	-5.5E-09
2.56E-05	8.58E-10	-6.6E-09	-1.9E-08	1.24E-10	-2E-09	-7.3E-09
2.57E-05	1.82E-09	7.16E-09	-3.5E-08	1.03E-09	-3.8E-09	-9.1E-09
2.58E-05	2.81E-09	2.09E-08	-5.1E-08	1.98E-09	-5.5E-09	-1.1E-08
2.59E-05	3.81E-09	3.45E-08	-6.7E-08	2.96E-09	-7.2E-09	-1.3E-08
0.000026	4.82E-09	4.78E-08	-8.2E-08	3.94E-09	-8.9E-09	-1.4E-08
2.61E-05	5.8E-09	6.06E-08	-9.6E-08	4.93E-09	-1.1E-08	-1.5E-08
2.62E-05	6.74E-09	7.28E-08	-1.1E-07	5.88E-09	-1.2E-08	-1.7E-08
2.63E-05	7.62E-09	8.41E-08	-1.2E-07	6.79E-09	-1.4E-08	-1.7E-08
2.64E-05	8.42E-09	9.44E-08	-1.3E-07	7.63E-09	-1.5E-08	-1.8E-08
2.65E-05	9.11E-09	1.04E-07	-1.4E-07	8.39E-09	-1.6E-08	-1.8E-08
2.66E-05	9.69E-09	1.12E-07	-1.4E-07	9.04E-09	-1.7E-08	-1.9E-08
2.67E-05	1.01E-08	1.19E-07	-1.5E-07	9.57E-09	-1.7E-08	-1.8E-08
2.68E-05	1.04E-08	1.24E-07	-1.5E-07	9.96E-09	-1.8E-08	-1.8E-08
2.69E-05	1.05E-08	1.28E-07	-1.5E-07	1.02E-08	-1.8E-08	-1.7E-08
0.000027	1.04E-08	1.31E-07	-1.5E-07	1.03E-08	-1.8E-08	-1.6E-08
2.71E-05	1.02E-08	1.32E-07	-1.5E-07	1.02E-08	-1.7E-08	-1.4E-08
2.72E-05	9.76E-09	1.31E-07	-1.4E-07	9.87E-09	-1.7E-08	-1.2E-08
2.73E-05	9.13E-09	1.3E-07	-1.4E-07	9.39E-09	-1.6E-08	-1E-08
2.74E-05	8.32E-09	1.27E-07	-1.3E-07	8.74E-09	-1.4E-08	-8.1E-09
2.75E-05	7.33E-09	1.22E-07	-1.2E-07	7.9E-09	-1.3E-08	-5.6E-09
2.76E-05	6.17E-09	1.17E-07	-1.1E-07	6.89E-09	-1.1E-08	-2.9E-09

2.77E-05	4.85E-09	1.1E-07	-9.6E-08	5.72E-09	-9.3E-09	-7.6E-11
2.78E-05	3.41E-09	1.02E-07	-8.3E-08	4.41E-09	-7.2E-09	2.85E-09
2.79E-05	1.84E-09	9.35E-08	-6.9E-08	2.97E-09	-5E-09	5.81E-09
0.000028	1.86E-10	8.41E-08	-5.5E-08	1.42E-09	-2.7E-09	8.78E-09
2.81E-05	-1.5E-09	7.4E-08	-4E-08	-2.1E-10	-3E-10	1.17E-08
2.82E-05	-3.3E-09	6.35E-08	-2.5E-08	-1.9E-09	2.12E-09	1.45E-08
2.83E-05	-5.1E-09	5.25E-08	-1.1E-08	-3.6E-09	4.54E-09	1.72E-08
2.84E-05	-6.8E-09	4.13E-08	3.77E-09	-5.3E-09	6.93E-09	1.96E-08
2.85E-05	-8.5E-09	3.01E-08	1.76E-08	-7E-09	9.23E-09	2.19E-08
2.86E-05	-1E-08	1.88E-08	3.08E-08	-8.7E-09	1.14E-08	2.38E-08
2.87E-05	-1.2E-08	7.71E-09	4.32E-08	-1E-08	1.35E-08	2.55E-08
2.88E-05	-1.3E-08	-3.1E-09	5.47E-08	-1.2E-08	1.53E-08	2.68E-08
2.89E-05	-1.4E-08	-1.4E-08	6.51E-08	-1.3E-08	1.7E-08	2.77E-08
0.000029	-1.5E-08	-2.3E-08	7.43E-08	-1.4E-08	1.84E-08	2.83E-08
2.91E-05	-1.6E-08	-3.3E-08	8.22E-08	-1.5E-08	1.96E-08	2.84E-08
2.92E-05	-1.7E-08	-4.2E-08	8.88E-08	-1.6E-08	2.06E-08	2.81E-08
2.93E-05	-1.7E-08	-5E-08	9.41E-08	-1.6E-08	2.12E-08	2.75E-08
2.94E-05	-1.7E-08	-5.7E-08	9.81E-08	-1.7E-08	2.16E-08	2.64E-08
2.95E-05	-1.7E-08	-6.3E-08	1.01E-07	-1.7E-08	2.17E-08	2.5E-08
2.96E-05	-1.7E-08	-6.9E-08	1.02E-07	-1.6E-08	2.15E-08	2.32E-08
2.97E-05	-1.6E-08	-7.3E-08	1.02E-07	-1.6E-08	2.1E-08	2.1E-08
2.98E-05	-1.5E-08	-7.7E-08	1.01E-07	-1.5E-08	2.03E-08	1.86E-08
2.99E-05	-1.4E-08	-8E-08	9.86E-08	-1.4E-08	1.93E-08	1.58E-08
0.00003	-1.3E-08	-8.2E-08	9.54E-08	-1.3E-08	1.81E-08	1.29E-08
3.01E-05	-1.1E-08	-8.4E-08	9.12E-08	-1.2E-08	1.68E-08	9.8E-09
3.02E-05	-9.7E-09	-8.4E-08	8.62E-08	-1.1E-08	1.52E-08	6.56E-09

3.03E-05	-8E-09	-8.4E-08	8.05E-08	-8.9E-09	1.35E-08	3.23E-09
3.04E-05	-6E-09	-8.3E-08	7.43E-08	-7.2E-09	1.16E-08	-1.3E-10
3.05E-05	-4E-09	-8.1E-08	6.75E-08	-5.3E-09	9.71E-09	-3.5E-09
3.06E-05	-2E-09	-7.9E-08	6.05E-08	-3.4E-09	7.72E-09	-6.7E-09
3.07E-05	7.1E-11	-7.7E-08	5.32E-08	-1.4E-09	5.71E-09	-9.9E-09
3.08E-05	2.14E-09	-7.3E-08	4.58E-08	6.23E-10	3.69E-09	-1.3E-08
3.09E-05	4.16E-09	-7E-08	3.83E-08	2.6E-09	1.69E-09	-1.6E-08
0.000031	6.12E-09	-6.5E-08	3.1E-08	4.53E-09	-2.5E-10	-1.8E-08
3.11E-05	7.98E-09	-6.1E-08	2.38E-08	6.39E-09	-2.1E-09	-2.1E-08
3.12E-05	9.72E-09	-5.6E-08	1.68E-08	8.14E-09	-3.9E-09	-2.3E-08
3.13E-05	1.13E-08	-5.1E-08	1.01E-08	9.76E-09	-5.5E-09	-2.4E-08
3.14E-05	1.27E-08	-4.6E-08	3.81E-09	1.12E-08	-7.1E-09	-2.6E-08
3.15E-05	1.4E-08	-4.1E-08	-2.1E-09	1.25E-08	-8.4E-09	-2.7E-08
3.16E-05	1.5E-08	-3.6E-08	-7.5E-09	1.37E-08	-9.7E-09	-2.7E-08
3.17E-05	1.58E-08	-3.1E-08	-1.2E-08	1.46E-08	-1.1E-08	-2.8E-08
3.18E-05	1.64E-08	-2.5E-08	-1.7E-08	1.53E-08	-1.2E-08	-2.8E-08
3.19E-05	1.68E-08	-2E-08	-2.1E-08	1.58E-08	-1.2E-08	-2.7E-08
0.000032	1.69E-08	-1.5E-08	-2.4E-08	1.61E-08	-1.3E-08	-2.6E-08
3.21E-05	1.69E-08	-1E-08	-2.7E-08	1.62E-08	-1.3E-08	-2.5E-08
3.22E-05	1.66E-08	-5.3E-09	-2.9E-08	1.61E-08	-1.4E-08	-2.4E-08
3.23E-05	1.61E-08	-6.8E-10	-3.1E-08	1.58E-08	-1.4E-08	-2.3E-08
3.24E-05	1.55E-08	3.71E-09	-3.3E-08	1.52E-08	-1.4E-08	-2.1E-08
3.25E-05	1.46E-08	7.87E-09	-3.4E-08	1.46E-08	-1.3E-08	-1.9E-08
3.26E-05	1.37E-08	1.18E-08	-3.4E-08	1.37E-08	-1.3E-08	-1.7E-08
3.27E-05	1.25E-08	1.55E-08	-3.5E-08	1.28E-08	-1.3E-08	-1.4E-08
3.28E-05	1.13E-08	1.89E-08	-3.5E-08	1.17E-08	-1.2E-08	-1.2E-08

3.29E-05	9.96E-09	2.2E-08	-3.4E-08	1.05E-08	-1.1E-08	-9.7E-09
0.000033	8.56E-09	2.48E-08	-3.4E-08	9.24E-09	-1.1E-08	-7.2E-09
3.31E-05	7.1E-09	2.73E-08	-3.3E-08	7.91E-09	-1E-08	-4.8E-09
3.32E-05	5.62E-09	2.96E-08	-3.2E-08	6.54E-09	-9.4E-09	-2.4E-09
3.33E-05	4.14E-09	3.15E-08	-3.1E-08	5.16E-09	-8.6E-09	-8.3E-11
3.34E-05	2.66E-09	3.32E-08	-3E-08	3.78E-09	-7.8E-09	2.15E-09
3.35E-05	1.23E-09	3.46E-08	-2.8E-08	2.41E-09	-7E-09	4.26E-09
3.36E-05	-1.5E-10	3.56E-08	-2.7E-08	1.09E-09	-6.2E-09	6.23E-09
3.37E-05	-1.5E-09	3.65E-08	-2.6E-08	-1.7E-10	-5.5E-09	8.05E-09
3.38E-05	-2.7E-09	3.7E-08	-2.4E-08	-1.4E-09	-4.7E-09	9.69E-09
3.39E-05	-3.8E-09	3.73E-08	-2.3E-08	-2.5E-09	-4E-09	1.12E-08
0.000034	-4.8E-09	3.74E-08	-2.1E-08	-3.5E-09	-3.3E-09	1.24E-08
3.41E-05	-5.7E-09	3.72E-08	-2E-08	-4.4E-09	-2.7E-09	1.35E-08
3.42E-05	-6.5E-09	3.68E-08	-1.8E-08	-5.2E-09	-2.1E-09	1.44E-08
3.43E-05	-7.2E-09	3.62E-08	-1.7E-08	-5.9E-09	-1.5E-09	1.51E-08
3.44E-05	-7.7E-09	3.54E-08	-1.6E-08	-6.5E-09	-9E-10	1.56E-08
3.45E-05	-8.1E-09	3.44E-08	-1.4E-08	-6.9E-09	-3.8E-10	1.6E-08
3.46E-05	-8.3E-09	3.32E-08	-1.3E-08	-7.3E-09	1.19E-10	1.61E-08
3.47E-05	-8.5E-09	3.19E-08	-1.2E-08	-7.5E-09	5.82E-10	1.61E-08
3.48E-05	-8.5E-09	3.05E-08	-1E-08	-7.6E-09	1.02E-09	1.6E-08
3.49E-05	-8.5E-09	2.89E-08	-9.3E-09	-7.7E-09	1.42E-09	1.56E-08
0.000035	-8.3E-09	2.72E-08	-8.2E-09	-7.6E-09	1.8E-09	1.52E-08
3.51E-05	-8.1E-09	2.54E-08	-7.2E-09	-7.5E-09	2.15E-09	1.46E-08
3.52E-05	-7.8E-09	2.36E-08	-6.2E-09	-7.3E-09	2.48E-09	1.4E-08
3.53E-05	-7.4E-09	2.17E-08	-5.2E-09	-7.1E-09	2.78E-09	1.32E-08
3.54E-05	-7E-09	1.97E-08	-4.3E-09	-6.8E-09	3.05E-09	1.23E-08

3.55E-05	-6.5E-09	1.77E-08	-3.4E-09	-6.4E-09	3.31E-09	1.14E-08
3.56E-05	-6E-09	1.57E-08	-2.6E-09	-6E-09	3.54E-09	1.05E-08
3.57E-05	-5.5E-09	1.36E-08	-1.8E-09	-5.6E-09	3.74E-09	9.44E-09
3.58E-05	-5E-09	1.16E-08	-1E-09	-5.2E-09	3.93E-09	8.4E-09
3.59E-05	-4.4E-09	9.62E-09	-3.2E-10	-4.8E-09	4.09E-09	7.34E-09
0.000036	-3.9E-09	7.65E-09	3.6E-10	-4.4E-09	4.23E-09	6.27E-09
3.61E-05	-3.4E-09	5.73E-09	1.01E-09	-4E-09	4.34E-09	5.21E-09
3.62E-05	-2.9E-09	3.87E-09	1.63E-09	-3.6E-09	4.43E-09	4.15E-09
3.63E-05	-2.4E-09	2.07E-09	2.22E-09	-3.2E-09	4.5E-09	3.12E-09
3.64E-05	-1.9E-09	3.41E-10	2.78E-09	-2.8E-09	4.55E-09	2.12E-09
3.65E-05	-1.5E-09	-1.3E-09	3.32E-09	-2.5E-09	4.58E-09	1.16E-09
3.66E-05	-1.1E-09	-2.9E-09	3.82E-09	-2.1E-09	4.58E-09	2.29E-10
3.67E-05	-7.4E-10	-4.3E-09	4.3E-09	-1.8E-09	4.56E-09	-6.5E-10
3.68E-05	-4.1E-10	-5.7E-09	4.76E-09	-1.5E-09	4.52E-09	-1.5E-09
3.69E-05	-1.2E-10	-6.9E-09	5.19E-09	-1.3E-09	4.46E-09	-2.3E-09
0.000037	1.29E-10	-8.1E-09	5.59E-09	-1E-09	4.37E-09	-3E-09
3.71E-05	3.44E-10	-9.1E-09	5.97E-09	-8.1E-10	4.27E-09	-3.6E-09
3.72E-05	5.26E-10	-1E-08	6.32E-09	-6.2E-10	4.14E-09	-4.2E-09
3.73E-05	6.74E-10	-1.1E-08	6.64E-09	-4.4E-10	4E-09	-4.7E-09
3.74E-05	7.91E-10	-1.2E-08	6.94E-09	-2.8E-10	3.84E-09	-5.2E-09
3.75E-05	8.8E-10	-1.2E-08	7.21E-09	-1.4E-10	3.66E-09	-5.6E-09
3.76E-05	9.43E-10	-1.3E-08	7.46E-09	-1.5E-11	3.47E-09	-5.9E-09
3.77E-05	9.83E-10	-1.3E-08	7.67E-09	9.85E-11	3.27E-09	-6.2E-09
3.78E-05	1E-09	-1.3E-08	7.86E-09	2.01E-10	3.05E-09	-6.4E-09
3.79E-05	1.01E-09	-1.4E-08	8.02E-09	2.94E-10	2.83E-09	-6.5E-09
0.000038	9.94E-10	-1.4E-08	8.15E-09	3.79E-10	2.59E-09	-6.6E-09

3.81E-05	9.71E-10	-1.4E-08	8.26E-09	4.58E-10	2.35E-09	-6.6E-09
3.82E-05	9.4E-10	-1.4E-08	8.33E-09	5.33E-10	2.1E-09	-6.5E-09
3.83E-05	9.02E-10	-1.4E-08	8.38E-09	6.05E-10	1.85E-09	-6.4E-09
3.84E-05	8.6E-10	-1.3E-08	8.4E-09	6.74E-10	1.6E-09	-6.3E-09
3.85E-05	8.18E-10	-1.3E-08	8.4E-09	7.43E-10	1.34E-09	-6.1E-09
3.86E-05	7.75E-10	-1.3E-08	8.37E-09	8.12E-10	1.09E-09	-5.8E-09
3.87E-05	7.36E-10	-1.3E-08	8.31E-09	8.81E-10	8.39E-10	-5.5E-09
3.88E-05	7.01E-10	-1.2E-08	8.23E-09	9.51E-10	5.9E-10	-5.2E-09
3.89E-05	6.71E-10	-1.2E-08	8.13E-09	1.02E-09	3.46E-10	-4.9E-09
0.000039	6.48E-10	-1.1E-08	8.01E-09	1.09E-09	1.07E-10	-4.5E-09
3.91E-05	6.32E-10	-1.1E-08	7.87E-09	1.16E-09	-1.2E-10	-4.1E-09
3.92E-05	6.25E-10	-1.1E-08	7.71E-09	1.24E-09	-3.5E-10	-3.7E-09
3.93E-05	6.26E-10	-1E-08	7.53E-09	1.31E-09	-5.7E-10	-3.3E-09
3.94E-05	6.36E-10	-9.8E-09	7.34E-09	1.37E-09	-7.7E-10	-2.9E-09
3.95E-05	6.55E-10	-9.4E-09	7.14E-09	1.44E-09	-9.7E-10	-2.5E-09
3.96E-05	6.81E-10	-9.1E-09	6.93E-09	1.5E-09	-1.2E-09	-2E-09
3.97E-05	7.16E-10	-8.7E-09	6.71E-09	1.56E-09	-1.3E-09	-1.6E-09
3.98E-05	7.57E-10	-8.3E-09	6.49E-09	1.62E-09	-1.5E-09	-1.3E-09
3.99E-05	8.05E-10	-8E-09	6.26E-09	1.67E-09	-1.6E-09	-9E-10
0.00004	8.58E-10	-7.7E-09	6.02E-09	1.71E-09	-1.8E-09	-5.5E-10
4.01E-05	9.16E-10	-7.4E-09	5.79E-09	1.75E-09	-1.9E-09	-2.3E-10
4.02E-05	9.77E-10	-7.1E-09	5.56E-09	1.77E-09	-2E-09	6.9E-11
4.03E-05	1.04E-09	-6.8E-09	5.33E-09	1.8E-09	-2.1E-09	3.38E-10
4.04E-05	1.1E-09	-6.6E-09	5.11E-09	1.81E-09	-2.2E-09	5.78E-10
4.05E-05	1.17E-09	-6.4E-09	4.89E-09	1.81E-09	-2.3E-09	7.88E-10
4.06E-05	1.23E-09	-6.2E-09	4.68E-09	1.8E-09	-2.3E-09	9.68E-10

4.07E-05	1.28E-09	-6E-09	4.48E-09	1.79E-09	-2.4E-09	1.12E-09
4.08E-05	1.34E-09	-5.8E-09	4.28E-09	1.76E-09	-2.4E-09	1.24E-09
4.09E-05	1.38E-09	-5.7E-09	4.1E-09	1.73E-09	-2.4E-09	1.33E-09
0.000041	1.42E-09	-5.5E-09	3.93E-09	1.69E-09	-2.5E-09	1.39E-09
4.11E-05	1.46E-09	-5.4E-09	3.77E-09	1.63E-09	-2.5E-09	1.43E-09
4.12E-05	1.48E-09	-5.2E-09	3.63E-09	1.57E-09	-2.4E-09	1.44E-09
4.13E-05	1.49E-09	-5.1E-09	3.49E-09	1.5E-09	-2.4E-09	1.43E-09
4.14E-05	1.49E-09	-4.9E-09	3.37E-09	1.43E-09	-2.4E-09	1.41E-09
4.15E-05	1.48E-09	-4.8E-09	3.26E-09	1.34E-09	-2.3E-09	1.36E-09
4.16E-05	1.46E-09	-4.7E-09	3.16E-09	1.25E-09	-2.2E-09	1.3E-09
4.17E-05	1.43E-09	-4.5E-09	3.08E-09	1.15E-09	-2.2E-09	1.23E-09
4.18E-05	1.38E-09	-4.4E-09	3E-09	1.05E-09	-2.1E-09	1.15E-09
4.19E-05	1.32E-09	-4.2E-09	2.94E-09	9.41E-10	-2E-09	1.07E-09
0.000042	1.25E-09	-4.1E-09	2.88E-09	8.29E-10	-1.9E-09	9.76E-10
4.21E-05	1.16E-09	-3.9E-09	2.84E-09	7.13E-10	-1.8E-09	8.83E-10
4.22E-05	1.07E-09	-3.7E-09	2.79E-09	5.95E-10	-1.7E-09	7.91E-10
4.23E-05	9.62E-10	-3.6E-09	2.76E-09	4.75E-10	-1.5E-09	7.01E-10
4.24E-05	8.45E-10	-3.4E-09	2.73E-09	3.54E-10	-1.4E-09	6.16E-10
4.25E-05	7.19E-10	-3.3E-09	2.7E-09	2.32E-10	-1.3E-09	5.36E-10
4.26E-05	5.85E-10	-3.1E-09	2.68E-09	1.11E-10	-1.2E-09	4.63E-10
4.27E-05	4.43E-10	-2.9E-09	2.66E-09	-8.5E-12	-1E-09	3.98E-10
4.28E-05	2.95E-10	-2.8E-09	2.65E-09	-1.3E-10	-8.9E-10	3.42E-10
4.29E-05	1.42E-10	-2.6E-09	2.63E-09	-2.4E-10	-7.6E-10	2.95E-10
0.000043	-1.3E-11	-2.5E-09	2.61E-09	-3.5E-10	-6.3E-10	2.57E-10
4.31E-05	-1.7E-10	-2.3E-09	2.6E-09	-4.6E-10	-5.1E-10	2.29E-10
4.32E-05	-3.3E-10	-2.2E-09	2.58E-09	-5.6E-10	-3.9E-10	2.11E-10

4.33E-05	-4.8E-10	-2E-09	2.56E-09	-6.6E-10	-2.7E-10	2.01E-10
4.34E-05	-6.4E-10	-1.9E-09	2.54E-09	-7.4E-10	-1.7E-10	2.01E-10
4.35E-05	-7.8E-10	-1.8E-09	2.52E-09	-8.3E-10	-6.5E-11	2.08E-10
4.36E-05	-9.2E-10	-1.7E-09	2.5E-09	-9E-10	2.81E-11	2.23E-10
4.37E-05	-1.1E-09	-1.6E-09	2.47E-09	-9.7E-10	1.13E-10	2.44E-10
4.38E-05	-1.2E-09	-1.5E-09	2.44E-09	-1E-09	1.89E-10	2.7E-10
4.39E-05	-1.3E-09	-1.4E-09	2.41E-09	-1.1E-09	2.56E-10	3.01E-10
0.000044	-1.4E-09	-1.3E-09	2.37E-09	-1.1E-09	3.14E-10	3.35E-10
4.41E-05	-1.5E-09	-1.2E-09	2.33E-09	-1.2E-09	3.63E-10	3.72E-10
4.42E-05	-1.5E-09	-1.1E-09	2.29E-09	-1.2E-09	4.02E-10	4.1E-10
4.43E-05	-1.6E-09	-1.1E-09	2.25E-09	-1.2E-09	4.32E-10	4.47E-10
4.44E-05	-1.6E-09	-1E-09	2.21E-09	-1.2E-09	4.54E-10	4.84E-10
4.45E-05	-1.6E-09	-9.7E-10	2.16E-09	-1.2E-09	4.67E-10	5.18E-10
4.46E-05	-1.6E-09	-9.2E-10	2.11E-09	-1.2E-09	4.73E-10	5.49E-10
4.47E-05	-1.6E-09	-8.8E-10	2.06E-09	-1.2E-09	4.72E-10	5.77E-10
4.48E-05	-1.6E-09	-8.3E-10	2.01E-09	-1.2E-09	4.66E-10	5.99E-10
4.49E-05	-1.5E-09	-7.9E-10	1.96E-09	-1.2E-09	4.55E-10	6.16E-10
0.000045	-1.5E-09	-7.5E-10	1.9E-09	-1.2E-09	4.4E-10	6.27E-10
4.51E-05	-1.4E-09	-7.1E-10	1.84E-09	-1.1E-09	4.22E-10	6.31E-10
4.52E-05	-1.3E-09	-6.7E-10	1.78E-09	-1.1E-09	4.03E-10	6.29E-10
4.53E-05	-1.2E-09	-6.2E-10	1.72E-09	-1.1E-09	3.83E-10	6.19E-10
4.54E-05	-1.1E-09	-5.8E-10	1.66E-09	-1E-09	3.63E-10	6.02E-10
4.55E-05	-1E-09	-5.3E-10	1.6E-09	-1E-09	3.45E-10	5.78E-10
4.56E-05	-9E-10	-4.8E-10	1.53E-09	-9.6E-10	3.3E-10	5.47E-10
4.57E-05	-7.9E-10	-4.3E-10	1.47E-09	-9.2E-10	3.18E-10	5.1E-10
4.58E-05	-6.8E-10	-3.8E-10	1.4E-09	-8.8E-10	3.1E-10	4.66E-10

4.59E-05	-5.7E-10	-3.2E-10	1.33E-09	-8.3E-10	3.07E-10	4.17E-10
0.000046	-4.7E-10	-2.7E-10	1.26E-09	-7.8E-10	3.09E-10	3.62E-10
4.61E-05	-3.7E-10	-2.1E-10	1.19E-09	-7.4E-10	3.16E-10	3.03E-10
4.62E-05	-2.8E-10	-1.5E-10	1.12E-09	-6.9E-10	3.3E-10	2.4E-10
4.63E-05	-1.9E-10	-8.6E-11	1.05E-09	-6.4E-10	3.49E-10	1.74E-10
4.64E-05	-1.2E-10	-2.6E-11	9.74E-10	-6E-10	3.73E-10	1.06E-10
4.65E-05	-4.8E-11	3.46E-11	8.98E-10	-5.5E-10	4.02E-10	3.62E-11
4.66E-05	1.16E-11	9.41E-11	8.2E-10	-5.1E-10	4.37E-10	-3.4E-11
4.67E-05	6.1E-11	1.53E-10	7.39E-10	-4.6E-10	4.75E-10	-1E-10
4.68E-05	1.01E-10	2.1E-10	6.57E-10	-4.2E-10	5.17E-10	-1.7E-10
4.69E-05	1.31E-10	2.66E-10	5.72E-10	-3.8E-10	5.61E-10	-2.4E-10
0.000047	1.52E-10	3.21E-10	4.86E-10	-3.4E-10	6.07E-10	-3E-10
4.71E-05	1.64E-10	3.75E-10	3.97E-10	-3E-10	6.54E-10	-3.6E-10
4.72E-05	1.68E-10	4.27E-10	3.08E-10	-2.7E-10	7.01E-10	-4.2E-10
4.73E-05	1.64E-10	4.79E-10	2.18E-10	-2.3E-10	7.47E-10	-4.7E-10
4.74E-05	1.54E-10	5.31E-10	1.27E-10	-1.9E-10	7.91E-10	-5.1E-10
4.75E-05	1.39E-10	5.84E-10	3.62E-11	-1.6E-10	8.32E-10	-5.5E-10
4.76E-05	1.18E-10	6.37E-10	-5.3E-11	-1.3E-10	8.69E-10	-5.7E-10
4.77E-05	9.43E-11	6.92E-10	-1.4E-10	-9.2E-11	9E-10	-5.9E-10
4.78E-05	6.76E-11	7.5E-10	-2.3E-10	-5.9E-11	9.26E-10	-5.9E-10
4.79E-05	3.93E-11	8.11E-10	-3.1E-10	-2.6E-11	9.46E-10	-5.9E-10
0.000048	1.02E-11	8.75E-10	-3.9E-10	5.67E-12	9.59E-10	-5.8E-10
4.81E-05	-1.9E-11	9.44E-10	-4.6E-10	3.7E-11	9.64E-10	-5.5E-10
4.82E-05	-4.7E-11	1.02E-09	-5.2E-10	6.76E-11	9.62E-10	-5.1E-10
4.83E-05	-7.3E-11	1.1E-09	-5.8E-10	9.73E-11	9.52E-10	-4.6E-10
4.84E-05	-9.6E-11	1.18E-09	-6.3E-10	1.26E-10	9.35E-10	-4E-10

4.85E-05	-1.2E-10	1.27E-09	-6.8E-10	1.53E-10	9.11E-10	-3.3E-10
4.86E-05	-1.3E-10	1.37E-09	-7.1E-10	1.79E-10	8.79E-10	-2.5E-10
4.87E-05	-1.5E-10	1.47E-09	-7.4E-10	2.03E-10	8.41E-10	-1.6E-10
4.88E-05	-1.6E-10	1.57E-09	-7.5E-10	2.25E-10	7.98E-10	-6.4E-11
4.89E-05	-1.7E-10	1.68E-09	-7.6E-10	2.44E-10	7.5E-10	4.13E-11
0.000049	-1.7E-10	1.78E-09	-7.6E-10	2.61E-10	6.98E-10	1.52E-10
4.91E-05	-1.7E-10	1.89E-09	-7.5E-10	2.75E-10	6.43E-10	2.67E-10
4.92E-05	-1.7E-10	2E-09	-7.3E-10	2.85E-10	5.87E-10	3.84E-10
4.93E-05	-1.7E-10	2.11E-09	-7E-10	2.92E-10	5.31E-10	5.02E-10
4.94E-05	-1.6E-10	2.21E-09	-6.6E-10	2.95E-10	4.76E-10	6.18E-10
4.95E-05	-1.6E-10	2.3E-09	-6.2E-10	2.94E-10	4.23E-10	7.32E-10
4.96E-05	-1.5E-10	2.38E-09	-5.7E-10	2.89E-10	3.74E-10	8.4E-10
4.97E-05	-1.5E-10	2.46E-09	-5.1E-10	2.81E-10	3.29E-10	9.41E-10
4.98E-05	-1.4E-10	2.52E-09	-4.5E-10	2.69E-10	2.9E-10	1.03E-09
4.99E-05	-1.4E-10	2.56E-09	-3.9E-10	2.54E-10	2.56E-10	1.11E-09
0.00005	-1.3E-10	2.59E-09	-3.3E-10	2.36E-10	2.29E-10	1.18E-09
5.01E-05	-1.3E-10	2.59E-09	-2.8E-10	2.15E-10	2.1E-10	1.23E-09
5.02E-05	-1.3E-10	2.58E-09	-2.2E-10	1.92E-10	1.98E-10	1.26E-09
5.03E-05	-1.3E-10	2.55E-09	-1.7E-10	1.67E-10	1.93E-10	1.28E-09
5.04E-05	-1.3E-10	2.49E-09	-1.3E-10	1.42E-10	1.96E-10	1.28E-09
5.05E-05	-1.3E-10	2.41E-09	-9.4E-11	1.16E-10	2.06E-10	1.25E-09
5.06E-05	-1.3E-10	2.3E-09	-7E-11	9.1E-11	2.23E-10	1.21E-09
5.07E-05	-1.2E-10	2.18E-09	-5.7E-11	6.68E-11	2.45E-10	1.14E-09
5.08E-05	-1.2E-10	2.03E-09	-5.7E-11	4.44E-11	2.71E-10	1.06E-09
5.09E-05	-1.1E-10	1.86E-09	-7E-11	2.46E-11	3.01E-10	9.49E-10
0.000051	-9.4E-11	1.67E-09	-9.8E-11	8.09E-12	3.33E-10	8.22E-10

5.11E-05	-7.6E-11	1.47E-09	-1.4E-10	-4.5E-12	3.66E-10	6.78E-10
5.12E-05	-5.2E-11	1.25E-09	-1.9E-10	-1.3E-11	3.98E-10	5.17E-10
5.13E-05	-2.2E-11	1.02E-09	-2.6E-10	-1.5E-11	4.29E-10	3.41E-10
5.14E-05	1.6E-11	7.89E-10	-3.5E-10	-1.3E-11	4.56E-10	1.54E-10
5.15E-05	6.12E-11	5.51E-10	-4.4E-10	-4E-12	4.78E-10	-4.2E-11
5.16E-05	1.14E-10	3.13E-10	-5.5E-10	1.1E-11	4.95E-10	-2.4E-10
5.17E-05	1.75E-10	8.05E-11	-6.7E-10	3.24E-11	5.04E-10	-4.5E-10
5.18E-05	2.43E-10	-1.4E-10	-7.9E-10	6.03E-11	5.06E-10	-6.5E-10
5.19E-05	3.19E-10	-3.5E-10	-9.3E-10	9.46E-11	4.98E-10	-8.6E-10
0.000052	4.02E-10	-5.5E-10	-1.1E-09	1.35E-10	4.81E-10	-1E-09
5.21E-05	4.9E-10	-7.2E-10	-1.2E-09	1.81E-10	4.55E-10	-1.2E-09
5.22E-05	5.83E-10	-8.7E-10	-1.3E-09	2.32E-10	4.18E-10	-1.4E-09
5.23E-05	6.79E-10	-9.9E-10	-1.5E-09	2.87E-10	3.72E-10	-1.5E-09
5.24E-05	7.77E-10	-1.1E-09	-1.6E-09	3.46E-10	3.17E-10	-1.7E-09
5.25E-05	8.74E-10	-1.1E-09	-1.7E-09	4.07E-10	2.53E-10	-1.8E-09
5.26E-05	9.69E-10	-1.2E-09	-1.9E-09	4.7E-10	1.81E-10	-1.9E-09
5.27E-05	1.06E-09	-1.1E-09	-2E-09	5.32E-10	1.04E-10	-1.9E-09
5.28E-05	1.15E-09	-1.1E-09	-2.1E-09	5.94E-10	2.19E-11	-1.9E-09
5.29E-05	1.22E-09	-9.9E-10	-2.1E-09	6.54E-10	-6.3E-11	-1.9E-09
0.000053	1.29E-09	-8.6E-10	-2.2E-09	7.09E-10	-1.5E-10	-1.9E-09
5.31E-05	1.34E-09	-7E-10	-2.2E-09	7.6E-10	-2.4E-10	-1.8E-09
5.32E-05	1.38E-09	-5E-10	-2.2E-09	8.05E-10	-3.2E-10	-1.7E-09
5.33E-05	1.4E-09	-2.7E-10	-2.2E-09	8.42E-10	-4E-10	-1.5E-09
5.34E-05	1.41E-09	-9E-12	-2.2E-09	8.71E-10	-4.7E-10	-1.4E-09
5.35E-05	1.39E-09	2.71E-10	-2.1E-09	8.9E-10	-5.3E-10	-1.2E-09
5.36E-05	1.36E-09	5.71E-10	-2E-09	9E-10	-5.8E-10	-9.6E-10

5.37E-05	1.31E-09	8.83E-10	-2E-09	8.98E-10	-6.2E-10	-7.2E-10
5.38E-05	1.23E-09	1.2E-09	-1.8E-09	8.86E-10	-6.5E-10	-4.7E-10
5.39E-05	1.14E-09	1.53E-09	-1.7E-09	8.63E-10	-6.6E-10	-2E-10
0.000054	1.02E-09	1.85E-09	-1.6E-09	8.28E-10	-6.5E-10	7.59E-11
5.41E-05	8.92E-10	2.16E-09	-1.4E-09	7.83E-10	-6.3E-10	3.54E-10
5.42E-05	7.45E-10	2.46E-09	-1.3E-09	7.28E-10	-5.9E-10	6.3E-10
5.43E-05	5.84E-10	2.74E-09	-1.1E-09	6.63E-10	-5.4E-10	9E-10
5.44E-05	4.11E-10	3E-09	-9.8E-10	5.9E-10	-4.7E-10	1.16E-09
5.45E-05	2.3E-10	3.22E-09	-8.2E-10	5.1E-10	-3.9E-10	1.4E-09
5.46E-05	4.39E-11	3.42E-09	-6.7E-10	4.24E-10	-2.9E-10	1.62E-09
5.47E-05	-1.4E-10	3.58E-09	-5.3E-10	3.34E-10	-1.9E-10	1.82E-09
5.48E-05	-3.3E-10	3.7E-09	-4.1E-10	2.41E-10	-6.7E-11	1.99E-09
5.49E-05	-5.1E-10	3.77E-09	-2.9E-10	1.47E-10	5.92E-11	2.13E-09
0.000055	-6.8E-10	3.81E-09	-2E-10	5.35E-11	1.91E-10	2.24E-09
5.51E-05	-8.4E-10	3.79E-09	-1.2E-10	-3.7E-11	3.26E-10	2.31E-09
5.52E-05	-9.8E-10	3.74E-09	-6.4E-11	-1.2E-10	4.6E-10	2.34E-09
5.53E-05	-1.1E-09	3.64E-09	-3.3E-11	-2E-10	5.93E-10	2.33E-09
5.54E-05	-1.2E-09	3.49E-09	-2.5E-11	-2.7E-10	7.2E-10	2.28E-09
5.55E-05	-1.3E-09	3.31E-09	-4.2E-11	-3.3E-10	8.38E-10	2.2E-09
5.56E-05	-1.3E-09	3.08E-09	-8.4E-11	-3.8E-10	9.46E-10	2.08E-09
5.57E-05	-1.3E-09	2.82E-09	-1.5E-10	-4.2E-10	1.04E-09	1.92E-09
5.58E-05	-1.3E-09	2.53E-09	-2.4E-10	-4.4E-10	1.12E-09	1.72E-09
5.59E-05	-1.2E-09	2.21E-09	-3.5E-10	-4.5E-10	1.18E-09	1.5E-09
0.000056	-1.2E-09	1.87E-09	-4.9E-10	-4.5E-10	1.22E-09	1.25E-09
5.61E-05	-1.1E-09	1.51E-09	-6.4E-10	-4.3E-10	1.24E-09	9.68E-10
5.62E-05	-9.2E-10	1.14E-09	-8.1E-10	-4E-10	1.24E-09	6.7E-10

5.63E-05	-7.5E-10	7.61E-10	-9.9E-10	-3.5E-10	1.21E-09	3.57E-10
5.64E-05	-5.6E-10	3.85E-10	-1.2E-09	-2.9E-10	1.17E-09	3.39E-11
5.65E-05	-3.5E-10	1.53E-11	-1.4E-09	-2.2E-10	1.1E-09	-2.9E-10
5.66E-05	-1.2E-10	-3.4E-10	-1.6E-09	-1.4E-10	1E-09	-6.2E-10
5.67E-05	1.17E-10	-6.8E-10	-1.8E-09	-5.1E-11	8.87E-10	-9.5E-10
5.68E-05	3.67E-10	-1E-09	-2E-09	4.59E-11	7.52E-10	-1.3E-09
5.69E-05	6.21E-10	-1.3E-09	-2.2E-09	1.48E-10	5.99E-10	-1.6E-09
0.000057	8.74E-10	-1.5E-09	-2.3E-09	2.54E-10	4.3E-10	-1.8E-09
5.71E-05	1.12E-09	-1.8E-09	-2.5E-09	3.61E-10	2.48E-10	-2.1E-09
5.72E-05	1.36E-09	-2E-09	-2.6E-09	4.67E-10	5.48E-11	-2.3E-09
5.73E-05	1.58E-09	-2.1E-09	-2.8E-09	5.7E-10	-1.5E-10	-2.5E-09
5.74E-05	1.77E-09	-2.2E-09	-2.9E-09	6.69E-10	-3.5E-10	-2.7E-09
5.75E-05	1.95E-09	-2.2E-09	-2.9E-09	7.6E-10	-5.6E-10	-2.8E-09
5.76E-05	2.09E-09	-2.2E-09	-3E-09	8.42E-10	-7.6E-10	-2.9E-09
5.77E-05	2.21E-09	-2.2E-09	-3E-09	9.14E-10	-9.6E-10	-2.9E-09
5.78E-05	2.29E-09	-2.1E-09	-3E-09	9.73E-10	-1.2E-09	-2.9E-09
5.79E-05	2.33E-09	-2E-09	-2.9E-09	1.02E-09	-1.3E-09	-2.9E-09
0.000058	2.33E-09	-1.8E-09	-2.9E-09	1.05E-09	-1.5E-09	-2.8E-09
5.81E-05	2.3E-09	-1.6E-09	-2.8E-09	1.06E-09	-1.6E-09	-2.6E-09
5.82E-05	2.23E-09	-1.4E-09	-2.7E-09	1.06E-09	-1.8E-09	-2.5E-09
5.83E-05	2.12E-09	-1.1E-09	-2.5E-09	1.03E-09	-1.9E-09	-2.3E-09
5.84E-05	1.97E-09	-8E-10	-2.3E-09	9.95E-10	-2E-09	-2.1E-09
5.85E-05	1.79E-09	-4.8E-10	-2.2E-09	9.38E-10	-2E-09	-1.8E-09
5.86E-05	1.57E-09	-1.3E-10	-2E-09	8.66E-10	-2.1E-09	-1.6E-09
5.87E-05	1.33E-09	2.19E-10	-1.7E-09	7.78E-10	-2.1E-09	-1.3E-09
5.88E-05	1.06E-09	5.81E-10	-1.5E-09	6.76E-10	-2.1E-09	-9.5E-10

5.89E-05	7.73E-10	9.47E-10	-1.3E-09	5.62E-10	-2E-09	-6.2E-10
0.000059	4.69E-10	1.31E-09	-1.1E-09	4.37E-10	-1.9E-09	-2.9E-10
5.91E-05	1.53E-10	1.67E-09	-8.2E-10	3.04E-10	-1.9E-09	4.22E-11
5.92E-05	-1.7E-10	2.01E-09	-6E-10	1.65E-10	-1.7E-09	3.74E-10
5.93E-05	-4.9E-10	2.34E-09	-3.7E-10	2.14E-11	-1.6E-09	7.01E-10
5.94E-05	-8.1E-10	2.65E-09	-1.6E-10	-1.2E-10	-1.5E-09	1.02E-09
5.95E-05	-1.1E-09	2.94E-09	3.51E-11	-2.7E-10	-1.3E-09	1.32E-09
5.96E-05	-1.4E-09	3.2E-09	2.18E-10	-4.1E-10	-1.1E-09	1.61E-09
5.97E-05	-1.7E-09	3.43E-09	3.82E-10	-5.5E-10	-9E-10	1.87E-09
5.98E-05	-1.9E-09	3.63E-09	5.27E-10	-6.8E-10	-7E-10	2.11E-09
5.99E-05	-2.2E-09	3.79E-09	6.5E-10	-8E-10	-4.9E-10	2.32E-09
0.00006	-2.4E-09	3.92E-09	7.49E-10	-9E-10	-2.7E-10	2.51E-09
6.01E-05	-2.5E-09	4.01E-09	8.24E-10	-1E-09	-6.2E-11	2.66E-09
6.02E-05	-2.6E-09	4.06E-09	8.74E-10	-1.1E-09	1.49E-10	2.79E-09
6.03E-05	-2.7E-09	4.07E-09	8.99E-10	-1.2E-09	3.53E-10	2.88E-09
6.04E-05	-2.8E-09	4.05E-09	9E-10	-1.2E-09	5.5E-10	2.94E-09
6.05E-05	-2.8E-09	3.99E-09	8.76E-10	-1.2E-09	7.37E-10	2.96E-09
6.06E-05	-2.7E-09	3.89E-09	8.29E-10	-1.3E-09	9.1E-10	2.95E-09
6.07E-05	-2.7E-09	3.76E-09	7.6E-10	-1.2E-09	1.07E-09	2.91E-09
6.08E-05	-2.5E-09	3.59E-09	6.71E-10	-1.2E-09	1.21E-09	2.84E-09
6.09E-05	-2.4E-09	3.4E-09	5.63E-10	-1.2E-09	1.34E-09	2.74E-09
0.000061	-2.2E-09	3.18E-09	4.39E-10	-1.1E-09	1.44E-09	2.61E-09
6.11E-05	-2E-09	2.93E-09	3E-10	-1.1E-09	1.53E-09	2.45E-09
6.12E-05	-1.8E-09	2.66E-09	1.49E-10	-9.9E-10	1.59E-09	2.28E-09
6.13E-05	-1.5E-09	2.37E-09	-1.1E-11	-9E-10	1.64E-09	2.08E-09
6.14E-05	-1.2E-09	2.07E-09	-1.8E-10	-7.9E-10	1.66E-09	1.86E-09

6.15E-05	-9.6E-10	1.76E-09	-3.5E-10	-6.7E-10	1.66E-09	1.63E-09
6.16E-05	-6.6E-10	1.44E-09	-5.3E-10	-5.5E-10	1.64E-09	1.38E-09
6.17E-05	-3.6E-10	1.11E-09	-7E-10	-4.2E-10	1.61E-09	1.12E-09
6.18E-05	-6.4E-11	7.8E-10	-8.7E-10	-2.9E-10	1.55E-09	8.59E-10
6.19E-05	2.31E-10	4.53E-10	-1E-09	-1.5E-10	1.48E-09	5.92E-10
0.000062	5.18E-10	1.33E-10	-1.2E-09	-2E-11	1.39E-09	3.24E-10
6.21E-05	7.93E-10	-1.8E-10	-1.4E-09	1.12E-10	1.28E-09	5.68E-11
6.22E-05	1.05E-09	-4.8E-10	-1.5E-09	2.4E-10	1.16E-09	-2.1E-10
6.23E-05	1.29E-09	-7.7E-10	-1.6E-09	3.62E-10	1.04E-09	-4.6E-10
6.24E-05	1.51E-09	-1E-09	-1.7E-09	4.77E-10	8.97E-10	-7.1E-10
6.25E-05	1.7E-09	-1.3E-09	-1.8E-09	5.83E-10	7.51E-10	-9.4E-10
6.26E-05	1.87E-09	-1.5E-09	-1.9E-09	6.79E-10	5.99E-10	-1.2E-09
6.27E-05	2.01E-09	-1.7E-09	-2E-09	7.64E-10	4.42E-10	-1.4E-09
6.28E-05	2.12E-09	-1.9E-09	-2.1E-09	8.37E-10	2.84E-10	-1.6E-09
6.29E-05	2.2E-09	-2.1E-09	-2.1E-09	8.98E-10	1.25E-10	-1.7E-09
0.000063	2.25E-09	-2.2E-09	-2.1E-09	9.45E-10	-3.2E-11	-1.9E-09
6.31E-05	2.28E-09	-2.3E-09	-2.1E-09	9.78E-10	-1.9E-10	-2E-09
6.32E-05	2.27E-09	-2.4E-09	-2.1E-09	9.97E-10	-3.4E-10	-2.1E-09
6.33E-05	2.23E-09	-2.4E-09	-2.1E-09	1E-09	-4.8E-10	-2.2E-09
6.34E-05	2.17E-09	-2.4E-09	-2E-09	9.94E-10	-6.2E-10	-2.3E-09
6.35E-05	2.09E-09	-2.4E-09	-2E-09	9.72E-10	-7.5E-10	-2.3E-09
6.36E-05	1.97E-09	-2.4E-09	-1.9E-09	9.38E-10	-8.6E-10	-2.3E-09
6.37E-05	1.84E-09	-2.3E-09	-1.8E-09	8.92E-10	-9.7E-10	-2.4E-09
6.38E-05	1.69E-09	-2.2E-09	-1.7E-09	8.34E-10	-1.1E-09	-2.3E-09
6.39E-05	1.52E-09	-2.1E-09	-1.6E-09	7.67E-10	-1.2E-09	-2.3E-09
0.000064	1.34E-09	-2E-09	-1.5E-09	6.91E-10	-1.2E-09	-2.2E-09

6.41E-05	1.15E-09	-1.8E-09	-1.4E-09	6.07E-10	-1.3E-09	-2.2E-09
6.42E-05	9.45E-10	-1.7E-09	-1.3E-09	5.17E-10	-1.3E-09	-2.1E-09
6.43E-05	7.36E-10	-1.5E-09	-1.2E-09	4.21E-10	-1.4E-09	-2E-09
6.44E-05	5.24E-10	-1.3E-09	-1E-09	3.22E-10	-1.4E-09	-1.8E-09
6.45E-05	3.11E-10	-1.1E-09	-9.2E-10	2.21E-10	-1.4E-09	-1.7E-09
6.46E-05	9.9E-11	-9E-10	-7.9E-10	1.18E-10	-1.4E-09	-1.5E-09
6.47E-05	-1.1E-10	-6.9E-10	-6.7E-10	1.58E-11	-1.4E-09	-1.4E-09
6.48E-05	-3.1E-10	-4.7E-10	-5.5E-10	-8.5E-11	-1.3E-09	-1.2E-09
6.49E-05	-5E-10	-2.4E-10	-4.3E-10	-1.8E-10	-1.3E-09	-1E-09
0.000065	-6.9E-10	-2E-11	-3.2E-10	-2.8E-10	-1.3E-09	-8.7E-10
6.51E-05	-8.6E-10	2E-10	-2.1E-10	-3.7E-10	-1.2E-09	-6.9E-10
6.52E-05	-1E-09	4.15E-10	-1.1E-10	-4.6E-10	-1.1E-09	-5.1E-10
6.53E-05	-1.2E-09	6.24E-10	-1E-11	-5.4E-10	-1.1E-09	-3.4E-10
6.54E-05	-1.3E-09	8.25E-10	7.77E-11	-6.1E-10	-9.8E-10	-1.6E-10
6.55E-05	-1.4E-09	1.02E-09	1.58E-10	-6.8E-10	-9E-10	1.46E-11
6.56E-05	-1.5E-09	1.2E-09	2.29E-10	-7.3E-10	-8.1E-10	1.83E-10
6.57E-05	-1.6E-09	1.36E-09	2.93E-10	-7.8E-10	-7.1E-10	3.44E-10
6.58E-05	-1.6E-09	1.52E-09	3.48E-10	-8.2E-10	-6.2E-10	4.98E-10
6.59E-05	-1.7E-09	1.66E-09	3.95E-10	-8.6E-10	-5.2E-10	6.43E-10
0.000066	-1.7E-09	1.78E-09	4.33E-10	-8.8E-10	-4.2E-10	7.79E-10
6.61E-05	-1.7E-09	1.89E-09	4.63E-10	-9E-10	-3.3E-10	9.03E-10
6.62E-05	-1.7E-09	1.98E-09	4.85E-10	-9E-10	-2.3E-10	1.02E-09
6.63E-05	-1.7E-09	2.05E-09	4.99E-10	-9E-10	-1.3E-10	1.12E-09
6.64E-05	-1.7E-09	2.11E-09	5.06E-10	-8.9E-10	-4.3E-11	1.21E-09
6.65E-05	-1.6E-09	2.15E-09	5.05E-10	-8.8E-10	4.49E-11	1.28E-09
6.66E-05	-1.6E-09	2.18E-09	4.97E-10	-8.5E-10	1.29E-10	1.35E-09

6.67E-05	-1.5E-09	2.19E-09	4.83E-10	-8.2E-10	2.08E-10	1.4E-09
6.68E-05	-1.4E-09	2.18E-09	4.63E-10	-7.9E-10	2.82E-10	1.43E-09
6.69E-05	-1.3E-09	2.17E-09	4.38E-10	-7.5E-10	3.5E-10	1.46E-09
0.000067	-1.2E-09	2.13E-09	4.08E-10	-7E-10	4.12E-10	1.47E-09
6.71E-05	-1.1E-09	2.09E-09	3.74E-10	-6.5E-10	4.69E-10	1.47E-09
6.72E-05	-9.9E-10	2.03E-09	3.36E-10	-6E-10	5.19E-10	1.46E-09
6.73E-05	-8.8E-10	1.96E-09	2.95E-10	-5.5E-10	5.62E-10	1.44E-09
6.74E-05	-7.6E-10	1.89E-09	2.52E-10	-4.9E-10	5.99E-10	1.41E-09
6.75E-05	-6.4E-10	1.8E-09	2.07E-10	-4.3E-10	6.3E-10	1.36E-09
6.76E-05	-5.2E-10	1.71E-09	1.61E-10	-3.7E-10	6.54E-10	1.32E-09
6.77E-05	-4E-10	1.61E-09	1.13E-10	-3.1E-10	6.72E-10	1.26E-09
6.78E-05	-2.8E-10	1.51E-09	6.58E-11	-2.5E-10	6.84E-10	1.19E-09
6.79E-05	-1.6E-10	1.4E-09	1.82E-11	-1.9E-10	6.9E-10	1.12E-09
0.000068	-4.9E-11	1.29E-09	-2.9E-11	-1.3E-10	6.9E-10	1.05E-09
6.81E-05	5.89E-11	1.18E-09	-7.5E-11	-7.7E-11	6.86E-10	9.71E-10
6.82E-05	1.61E-10	1.07E-09	-1.2E-10	-2.4E-11	6.76E-10	8.89E-10
6.83E-05	2.57E-10	9.65E-10	-1.6E-10	2.76E-11	6.63E-10	8.05E-10
6.84E-05	3.45E-10	8.57E-10	-2.1E-10	7.6E-11	6.45E-10	7.19E-10
6.85E-05	4.27E-10	7.52E-10	-2.5E-10	1.21E-10	6.24E-10	6.34E-10
6.86E-05	5E-10	6.49E-10	-2.8E-10	1.63E-10	5.99E-10	5.48E-10
6.87E-05	5.65E-10	5.51E-10	-3.2E-10	2.01E-10	5.72E-10	4.64E-10
6.88E-05	6.21E-10	4.56E-10	-3.5E-10	2.36E-10	5.42E-10	3.81E-10
6.89E-05	6.69E-10	3.66E-10	-3.8E-10	2.67E-10	5.1E-10	3.02E-10
0.000069	7.08E-10	2.81E-10	-4.1E-10	2.94E-10	4.77E-10	2.25E-10
6.91E-05	7.39E-10	2.01E-10	-4.3E-10	3.18E-10	4.43E-10	1.51E-10
6.92E-05	7.61E-10	1.27E-10	-4.5E-10	3.37E-10	4.07E-10	8.17E-11

6.93E-05	7.76E-10	5.77E-11	-4.7E-10	3.53E-10	3.72E-10	1.65E-11
6.94E-05	7.82E-10	-5.9E-12	-4.8E-10	3.65E-10	3.36E-10	-4.4E-11
6.95E-05	7.81E-10	-6.4E-11	-4.9E-10	3.74E-10	3E-10	-1E-10
6.96E-05	7.74E-10	-1.2E-10	-5E-10	3.79E-10	2.64E-10	-1.5E-10
6.97E-05	7.6E-10	-1.6E-10	-5.1E-10	3.81E-10	2.29E-10	-2E-10
6.98E-05	7.4E-10	-2.1E-10	-5.1E-10	3.8E-10	1.94E-10	-2.4E-10
6.99E-05	7.14E-10	-2.5E-10	-5.1E-10	3.75E-10	1.61E-10	-2.8E-10
0.00007	6.84E-10	-2.8E-10	-5E-10	3.68E-10	1.28E-10	-3.1E-10

Bibliography

1. J.D. Achenbach. *Wave Propagation in Elastic Solids*. North-Holland Publishing Company, New York, NY, 16 edition, 1973.

2. Md Yeasin Bhuiyan, Yanfeng Shen, and Victor Giurgiutiu. Guided wave based crack detection in the rivet hole using global analytical with local FEM approach. *Materials*, 9(7):602, 2016.

3. Md Yeasin Bhuiyan, Yanfeng Shen, and Victor Giurgiutiu. Interaction of {L}amb waves with rivet hole cracks from multiple directions. *Proc. IMechE Part C: J. Mechanical Engineering Science*, 231(16):2974–2987, 2017.

4. G Chen and J Zhou. *Boundary Element Methods*. Academic Press, New York, NY, 1992.

5. Jeffrey Crider II. Damage Detection Using Lamb Waves for Structural Health Monitoring. page 97, 2007.

6. M. M. Derriso, C. D. McCurry, and C. M. Schubert Kabban. A novel approach for implementing structural health monitoring systems for aerospace structures. *Structural Health Monitoring (SHM) in Aerospace Structures*, pages 33–56, 2016.

7. DoD. Condition based Maintenance plus (CBM+). (January), 2013.

8. Ting Dong and Nam Kim. Cost-Effectiveness of Structural Health Monitoring in Fuselage Maintenance of the Civil Aviation Industry . *Aerospace*, 5(3):87, 2018.

9. Daniela Enciu, Ioan Ursu, and Adrian Toader. New results concerning structural health monitoring technology qualification for transfer to space vehicles. *Structural Control and Health Monitoring*, 24(10):1–14, 2017.

10. Victor Giurgiutiu. *Wave Propagation SHM with PWAS Transducers*. 2014.

11. Sungwon Ha and Fu K. Chang. Optimizing a spectral element for modeling PZT-induced Lamb wave propagation in thin plates. *Smart Materials and Structures*, 19(1), 2010.

12. J M Jin. *The Finite Element Method in Electromagnetics*. Wiley & Sons, Hoboken, NJ, 3rd edition, 2014.

13. Seth S Kessler. Certifying a structural health monitoring system: Characterizing durability, reliability and longevity (2005). In *Proceedings of the 1st International A Design of Experiments Approach 73 Forum on Integrated Systems Health Engineering and Management in Aerospace*, pages 7–10, Napa, CA, 2005.

14. Department of Defense, Deputy Under Secretary of Defense for Logistics Material, and Material. Condition Based Maintenance Plus DoD Guidebook. (May), 2008.

15. C. Todd Owens. *EFFECTS OF MECHANICAL LOAD HISTORY ON LAMB WAVE INTERACTIONS WITH FATIGUE CRACKS IN ALUMINUM PLATES*. Dissertation, Air Force Institute of Technology, 2017.

16. J.L. Rose. *Ultrasonic Waves in Solid Media*. Cainbridge University Press, New York, NY, 2004.

17. Christine Schubert Kabban, Richard Uber, Kevin Lin, Bin Lin, Md Bhuiyan, and Victor Giurgiutiu. Uncertainty Evaluation in the Design of Structural Health Monitoring Systems for Damage Detection. *Aerospace*, 5(2):45, 2018.

18. N. Sepehry, M. Shamshirsaz, and F. Bakhtiari Nejad. Low-cost simulation using model order reduction in structural health monitoring: Application of balanced proper orthogonal decomposition. *Structural Control and Health Monitoring*, 24(11):1–10, 2017.

19. Yanfeng Shen. Structural health monitoring using linear and nonlinear ultrasonic guided waves. *PhD Dissertation*, page 224, 2014.

20. Yanfeng Shen and Victor Giurgiutiu. Effective non-reflecting boundary for {L}amb waves: Theory, finite element implementation, and applications. *Wave Motion*, 58:22–41, 2015.

21. Yanfeng Shen and Victor Giurgiutiu. Combined analytical FEM approach for efficient simulation of Lamb wave damage detection. *Ultrasonics*, 69:116–128, 2016.

22. I Stakgold and M Holst. *Green's Functions and Boundary Value Problems*. Wiley & Sons, Hoboken, NJ, 3rd edition, 2011.

23. Zhoufei Yu, Yanli Lei, and Tiegang Li. Mean proloculus size as a salinity index in benthic floraminifera Ammonia aomoriensis: Based on culture and seasonal studies. *Journal of the Palaeontological Society of India*, 61(2):215–223, 2016.

24. Meiling Zhao, Zhonghua Qiao, and Tao Tang. A fast high order method for electromagnetic scattering by large open cavities. *J. Comput. Math.*, 29(3):287–304, 2011.

25. Xiaoliang Zhao, Huidong Gao, Guangfan Zhang, Bulent Ayhan, Fei Yan, Chiman Kwan, and Joseph L. Rose. Active health monitoring of an aircraft wing with embedded piezoelectric sensor/actuator network: I. Defect detection, localization and growth monitoring. *Smart Materials and Structures*, 16(4):1208–1217, 2007.

REPORT DOCUMENTATION PAGE

Form Approved
OMB No. 0704–0188

1. REPORT DATE *(DD–MM–YYYY)*	2. REPORT TYPE	3. DATES COVERED *(From — To)*
21–03–2019	Master's Thesis	Sept 2017 — Mar 2019

4. TITLE AND SUBTITLE

Piezoelectric Sensor Crack Detection on Airframe Systems

5a. CONTRACT NUMBER

5b. GRANT NUMBER

AFOSR- F4FGA07187J001

5c. PROGRAM ELEMENT NUMBER

6. AUTHOR(S)

Lin, Kevin J, 2d Lt, USAF

5d. PROJECT NUMBER

18C358B, 19C909

5e. TASK NUMBER

5f. WORK UNIT NUMBER

7. PERFORMING ORGANIZATION NAME(S) AND ADDRESS(ES)

Air Force Institute of Technology
Graduate School of Engineering and Management (AFIT/EN)
2950 Hobson Way
WPAFB OH 45433-7765

8. PERFORMING ORGANIZATION REPORT NUMBER

AFIT-ENC-MS-19-M-001

9. SPONSORING / MONITORING AGENCY NAME(S) AND ADDRESS(ES)

10. SPONSOR/MONITOR'S ACRONYM(S)

AFOSR

11. SPONSOR/MONITOR'S REPORT NUMBER(S)

12. DISTRIBUTION / AVAILABILITY STATEMENT

Distribution Statement A:
Approved for Public Release; distribution unlimited.

13. SUPPLEMENTARY NOTES

14. ABSTRACT

In 2008, the Department of Defense published a guidebook for a methodology named Condition-Based Maintenance Plus (CBM+) which capabilities include improving productivity, shortening maintenance cycles, lowering costs, and increasing availability and reliability. This push replaces existing inspection criteria, often conducted as non-destructive testing (NDT), with structural health monitoring (SHM) systems. The SHM system addressed utilizes guided Lamb waves generated by piezoelectric wafer active sensors (PWAS) to detect the existence, size, and location of damage from through-thickness cracks around a rivet hole. The SHM field lacks an experiment testing how small changes in receiver sensor distances affect damage detection. In addition, prior research has shown that transmitter and receiver PWAS angles significantly affected the received signal. Experiments here used existing damage detection metrics to establish thresholds for detection. Tests with two transmitter angles $\theta = 9^\circ, 27^\circ$ and three receiver distances, linearly incremented by 5mm, illustrated that damage detection capabilities significantly changed as the receiver distances were incremented at both 50mm and 1000mm transmitter distances. For 1000mm, the PWAS was able to detect the damage at certain geometries. This work validates of the PWAS detection capabilities for small changes and motivates further pursuits for varying PWAS geometries for long distances.

15. SUBJECT TERMS

Structural Health Monitoring, Acoustic Wave Propagation, Finite Element Method, Non-Destructive Testing

16. SECURITY CLASSIFICATION OF:			17. LIMITATION OF ABSTRACT	18. NUMBER OF PAGES	19a. NAME OF RESPONSIBLE PERSON
a. REPORT	b. ABSTRACT	c. THIS PAGE			Capt Richard Uber, AFIT/ENC
U	U	U	UU	173	19b. TELEPHONE NUMBER *(include area code)* (312) 785-3636, x4450; richard.uber@afit.edu